PHYTOCHEMICAL STUDIES OF *Mesua lepidota* AND *Garcinia griffithii* WITH THE AID OF ^{13}C-NMR DEREPLICATION AND THEIR ANTICHOLINESTERASE ACTIVITIES

LEONG SOW TEIN

FACULTY OF SCIENCE
UNIVERSITI MALAYA
KUALA LUMPUR

2024

PHYTOCHEMICAL STUDIES OF *Mesua lepidota* AND *Garcinia griffithii* WITH THE AID OF ^{13}C-NMR DEREPLICATION AND THEIR ANTICHOLINESTERASE ACTIVITIES

LEONG SOW TEIN

THESIS SUBMITTED IN FULFILMENT OF THE REQUIREMENTS FOR THE DEGREE OF DOCTOR OF PHILOSOPHY

DEPARTMENT OF CHEMISTRY
FACULTY OF SCIENCE
UNIVERSITI MALAYA
KUALA LUMPUR

2024

UNIVERSITI MALAYA

ORIGINAL LITERARY WORK DECLARATION

Name of Candidate: **LEONG SOW TEIN**

Matric No: **17010927/3 (new) SHC 140100 (old)**

Name of Degree: DOCTOR OF PHILOSOPHY

Title of Project Paper/Research Report/Dissertation/Thesis ("this Work"):

PHYTOCHEMICAL STUDIES OF *Mesua lepidota* AND *Garcinia griffithii* WITH THE AID OF ^{13}C-NMR DEREPLICATION AND THEIR ANTICHOLINESTERASE ACTIVITIES

Field of Study: **ORGANIC CHEMISTRY**

I do solemnly and sincerely declare that:

(1) I am the sole author/writer of this Work;
(2) This Work is original;
(3) Any use of any work in which copyright exists was done by way of fair dealing and for permitted purposes and any excerpt or extract from, or reference to or reproduction of any copyright work has been disclosed expressly and sufficiently and the title of the Work and its authorship have been acknowledged in this Work;
(4) I do not have any actual knowledge nor do I ought reasonably to know that the making of this work constitutes an infringement of any copyright work;
(5) I hereby assign all and every right in the copyright to this Work to the Universiti Malaya ("UM"), who henceforth shall be owner of the copyright in this Work and that any reproduction or use in any form or by any means whatsoever is prohibited without the written consent of UM having been first had and obtained;
(6) I am fully aware that if in the course of making this Work I have infringed any copyright whether intentionally or otherwise, I may be subject to legal action or any other action as may be determined by UM.

ture

Date: 08-02-2024

Subscribed and solemnly declared before,

Witness's Signature

Date: 08-02-2024

Name:

Designation:

PHYTOCHEMICAL STUDIES OF *Mesua lepidota* AND *Garcinia griffithii* WITH THE AID OF ^{13}C-NMR DEREPLICATION AND THEIR ANTICHOLINESTERASE ACTIVITIES

ABSTRACT

Phytochemical studies on *Mesua lepidota* and *Garcinia griffithii*, using a ^{13}C-NMR dereplication tool, MixONat were carried out. From the bark hexane extract of *M. lepidota*, a total of sixteen (16) compounds were identified; of these, eight (8) were identified using the MixONat, while thirteen (13) isolated and purified. Five (5) of these compounds were identified through both the isolation and ^{13}C-NMR dereplication technique. Fifteen (15) of these compounds were already known; sitosterol **174**, stigmasterol **173**, α-amyrin **194**, friedelin **186**, friedelinol **189**, betulinic acid **177**, glutinol **491**, lepidotol A **70**, B **71** & E **86**, lepidotin A **88** and B **89**, mammea A/BB cylco F **77**, ochrocarpin E **76**, pyranojacareubin **164**, and one, lepidotin C **490**, was new. In addition, the ^{13}C-NMR dereplication (MixONat) on the dichloromethane extract of *G. griffithii* leaves revealed six (6) compounds, three (3) were isolated. The identified metabolites were (+)-camboginol **253**, isoxanthochymol **248**, xanthochymol **270** and (+)-cycloxanthochymol **252**, garcimultiflorone D **262** and parvifoliol F **492**. Three (3) *Mammea* coumarins exhibited potent inhibition on butyryl cholinesterase (BChE); lepidotin C **490**, lepidotin B **89** and mammea A/BB cyclo F **77** with the IC_{50} values of 1.79±0.07 µM, 1.60±0.26 µM, and 2.24±0.12 µM respectively. Lepidotin B **89** was the most potent inhibitor of BChE, which demonstrated a threefold increase in potency compared to the drug galantamine. It showed a mix-mode inhibition profile, with the inhibition constant, K_i value of 1.03 µM. Molecular docking and molecular dynamics simulations revealed stable interations of lepidotin B **89** with key residues within five critical regions of BChE, which include both active binding sites and allosteric binding

sites. This analysis predicted a favourable binding affinity for lepidotin B **89** and facilitated the identification of significant residues crucial for the binding interaction.

Keywords: Dereplication, MixONat, lepidotin B, BChE inhibitor, *Mesua*, *Garcinia*

PHYTOCHEMICAL STUDIES OF *Mesua lepidota* AND *Garcinia griffithii* WITH THE AID OF ^{13}C-NMR DEREPLICATION AND THEIR ANTICHOLINESTERASE ACTIVITIES

ABSTRAK

Kajian fitokimia terhadap *Mesua lepidota* dan *Garcinia griffithii*, menggunakan alat dereplikasi ^{13}C-NMR, MixONat telah dilaksanakan. Daripada ekstrak heksana kulit *M. lepidota*, sebanyak enam belas (16) sebatian telah dikenalpasti; lapan (8) daripadanya dikenal pasti dengan MixONat, tiga belas (13) didapati melalui teknik pengasingan manakala lima (5) sebatian dikenal pasti daripada kedua-dua pengasingan dan teknik dereplikasi ^{13}C-NMR. Lima belas (15) sebatian telah diketahui; sitosterol **174**, stigmasterol **173**, α-amyrin **194**, friedelin **186**, friedelinol **189**, asid betulinik **177**, glutinol **491**, lepidotol A **70**, B **71** & E **86**, lepidotin A **88**, B **89** mammea A/BB cyclo F **77**, ochrocarpin E **76,** pyranojacareubin **164**, dan satu sebatian baru iaitu lepidotin C **490**. Selain itu, dereplikasi ^{13}C-NMR terhadap ekstrak diklorometana daun *G. griffithii* mendedahkan enam (6) sebatian, dan tiga (3) daripadanya telah berjaya diasingkan. Metabolit yang dikenal pasti adalah (+)-camboginol **253**, isoxanthochymol **248**, xanthochymol **270**, (+)-cycloxanthochymol **252**, garcimultiflorone D **262** dan parvifoliol F **492**. Tiga (3) *Mammea* coumarin mempamerkan perencatan signifikasi terhadap butiril kolinesterase (BChE); lepidotin C **490**, lepidotin B **89** dan mammea A/BB cyclo F **77** dengan nilai IC_{50} masing-masing ialah 1.79±0.07 µM, 1.60±0.26 µM dan 2.24±0.12 µM. Lepidotin B **89** merupakan perencat BChE yang terkuat dengan menunjukkan potensi tiga kali ganda lebih tinggi berbanding galantamine. Ia menunjukkan profil perencatan mod campuran, dengan pemalar perencatan, K_i 1.03 µM. Simulasi dok molekul dan dinamik molekul mendedahkan interaksi stabil lepidotin B **89** dengan sisa utama kawasan kritikal BChE, yang merangkumi tapak pengikatan aktif dan alosterik. Analisis ini meramalkan

pertalian pengikatan yang menggalakkan untuk lepidotin B **89** dan memudahkan pengenalpastian sisa penting yang penting untuk interaksi pengikatan.

Kata kunci: Dereplikasi, MixONat, lepidotin B, perencat BChE, *Mesua*, *Garcinia*

ACKNOWLEDGEMENTS

Foremost, I would like to express my deep and sincere gratitude to my supervisor, Professor Dr. Khalijah Awang for her continued support on my PhD study. Her patience, motivation, immense knowledge, and guidance help me all the time in the research.

Besides, I am also thankful to my fellow lab mates in phytolab: Afiq, Aimi, Aqmal, Azeana, Azrul, Chong, Faizah, Hafiz, Haslinda, Hazlina, Hazrina, Norsita, Rosalind, Shelly, and Sook Yee, for the stimulating discussion, suggestion, and help. It is a great honour to work with them.

I had the pleasure of working with Dr. Severine and members of SONAS lab. Thank you for the comprehensive advice, kind support and guidance especially during the training period.

I would like to acknowledge the technical support from the staff of Chemistry Department, Faculty of Science, Universiti Malaya.

A special thanks to my parents and family members, the work cannot be done without their love, encouragement, and endless support. Thank you for always been there for me whenever I needed and everything that they helped me to achieve.

Last but not least, I would like to thank you for the effort of each and everybody who has helped me in this study at any stage, but the name does not find a place in this acknowledgement. It would not have been possible to complete the thesis without them.

TABLE OF CONTENTS

LIST OF SCHEMES

LIST OF FIGURES

LIST OF TABLES

LIST OF SYMBOLS AND ABBREVIATIONS

α	:	Alpha
β	:	Beta
γ	:	Gamma
λ	:	Maximum wavelength
δ	:	Chemical shift
Å	:	Angstrom
s	:	Singlet
d	:	Doublet
m	:	Multiplet
q	:	Quartet
t	:	Triplet
dd	:	Doublet of doublets
dt	:	Doublet of triplets
br s	:	Broad singlet
hept	:	Heptet
sext	:	Sextet
*h*BChE	:	Human butyrylcholinesterase
m/z	:	Mass per charge
ACN	:	Acetonitrile
AD	:	Alzheimer's disease
ADT	:	AutoDock tools
ATCh	:	Acetylthiocholine
ATCI	:	Acetylthiocholine iodide
ACh	:	Acetylcholine

AChE	:	Acetylcholinesterase enzyme
BChE	:	Butyrylcholinesterase enzyme
BTCh	:	Butyrylthiocholine
CC	:	Column chromatography
$CDCl_3$	:	Deuterated chloroform
CD_3OD	:	Deuterated methanol
CH_3	:	Methyl group
$CHCl_3$		Chloroform
COSY	:	^1H-^1H Correlation Spectroscopy
DB	:	Database
DCM	:	Dichloromethane
DEPT	:	Distortionless Enhancement by Polarization Transfer
DGG	:	Dichloromethane extract of *G. griffithii*
DNP	:	Dictionary of Natural Products
DPPH	:	2,2-diphenylpucrylhydrazyl
DTNB	:	5,5'-dithiobis (2-nitrobenzoic acid)
ESIMS	:	Electrospray Ionization Mass Spectrometry
FA	:	Formic acid
G.	:	*Garcinia*
HMBC	:	Heteronuclear Multiple Bond Coherence
HML	:	Hexane extract of *M. lepidota*
HPLC	:	High Performance Liquid Chromatography
HREIMS	:	High-Resolution Electron Ionization Mass Spectrometry
HSQC	:	Heteronuclear Single Quantum Coherence
IC_{50}	:	Concentration required to inhibit 50% of activity
IR	:	Infrared spectroscopy

K_i	:	Inhibition constant
LB plot	:	Lineweaver-Burk plot
LCMS	:	Liquid Chromatography Mass Spectrometry
M.	:	*Mesua*
MeOH	:	Methanol
MCI	:	Mild cognitive impairment
NMR	:	Nuclear magnetic resonance
NPs	:	Natural products
OCH_3	:	Methoxy group
OD	:	Optical density
OH	:	Hydroxy group
OSC	:	Oxidosqualene cyclase
PDB	:	Protein data bank
PPAPs	:	Polyprenylated acyl phloroglucinols
PTLC	:	Preparative thin layer chromatography
SD	:	Standard deviation
TFA	:	Trifluoroacetic acid
TLC	:	Thin layer chromatography
UV	:	Ultraviolet spectroscopy
1D-NMR	:	One dimensional nuclear magnetic resonance
2D-NMR	:	Two-dimensional nuclear magnetic resonance
^{1}H	:	Proton NMR
^{13}C	:	13-carbon NMR
cm	:	Centimeter
cm^{-1}	:	Per centimeter
°C	:	Degree Celsius

g	:	Gram
Hz	:	Hertz
J	:	Coupling constant
kg	:	Kilogram
M	:	Molar
MHz	:	Mega Hertz
m	:	Meter
min	:	Minute
mL	:	Milliliter
mM	:	Millimolar
mg/mL	:	Milligram per milliliter
nm	:	Nanometer
µg/mL	:	Microgram per milliliter
µM	:	Micromolar
µL	:	Microliter
ppm	:	Parts per million
U/mL	:	Unit per milliliter

LIST OF APPENDICES

CHAPTER 1: INTRODUCTION

1.1 General

Humans are associated with matters from nature every day such as food, flavoring agents, furniture, essential oils, skincare and cosmetic items, traditional medicines, sanitary products, and luggage. Nature is in fact, the source of everything from daily necessity goods to extravagant items. The biodiversity of nature has evolved over time to produce a bewildering range of secondary metabolites (Dar et al., 2017) including alkaloid, flavonoid, and terpene. Furthermore, plant products containing these secondary metabolites have played a leading medical role in most cultures since ancient times (Beutler, 2009).

Medicinal plants and microorganisms were the major source of medicines over many centuries (Calixto, 2019). The oldest records for the usage of medicinal plants dates back to 2400 B.C. on clay tablets in Mesopotamia (Attinger, 2008). The Chinese Materia Medica was compiled by Li Shizhen in 1578 (David et al., 2015; Zheng, 1988). Most of the medicines or remedies were in the form of mixtures of various natural sources such as plants and minerals. Only in 1806, Friederich Serturner known as German pharmacist and a pioneer of alkaloid chemistry has identified the pure form of morphine **1**, an alkaloid produced from poppy. Hence, prompting a further search for alternative plant-derived medicines that are pure (WHO, 2019). Furthermore, aspirin **2** (Alfonso et al., 2014), a well-known natural products (NPs) medicine that is still used today, is an inspirational discovery for all NPs researchers.

NPs such as morphine **1** and aspirin **2** (Figure 1.1) have been employed in medicine to treat a variety of conditions, including neurodegenerative disorders. As global life expectancy is increasing and the estimated global population (≥ 65 years) will reach 1 billion (approximately 12% of the total global population) by 2030 (He et al., 2016),

neurodegenerative diseases become a globally concerned issue. *Ginkgo biloba* (Barbalho et al., 2022), *Panax ginseng* (Kim et al., 2018) , and *Curcuma longa* were some examples of plants with beneficial effects in the therapy of neurodegenerative diseases like Alzheimer's disease (AD), Parkinson's disease, and Huntington's disease. Galantamine **3**, an alkaloid extract from *Galanthus* species is a prescribed acetyl cholinesterase (AChE) inhibitor drug for dementia and AD until today. Other than that, secondary metabolites like curcumin **4** (Bertoncello et al., 2018; Seo et al., 2018), resveratrol **5** (Wightman, 2017), quercetin **6** (de Andrade Teles et al., 2018), berberine **7** (Figure 1.1) (Kaufmann et al., 2016; Zanforlin et al., 2017), showed promising effects in biological activities related to neurodegenerative diseases (Sharifi-Rad et al., 2020). As a result, NPs research until today is critical for novel medication discoveries for the treatment of a variety of maladies, notably neurodegenerative diseases.

Malaysia has the most biologically diversified terrestrial ecosystems, including tropical rainforest due to its unique location in the equatorial region. Apart from it, Malaysia is regarded as one of the twelve mega-biodiversity countries of the world which having established a National Biodiversity Policy in 1998 to guide the country's biodiversity conservation efforts. Until 2016, there are more than 17,631 species of plants were found in Malaysian forests (*Flora and Fauna*, 2016) with 2700 endemic species (*Biodiversity of flora in Malaysia*). Hence, the diversification of plant species offers an excellent opportunity to search for local NPs with the potential to be developed as leads and therapeutics in drug discovery programs.

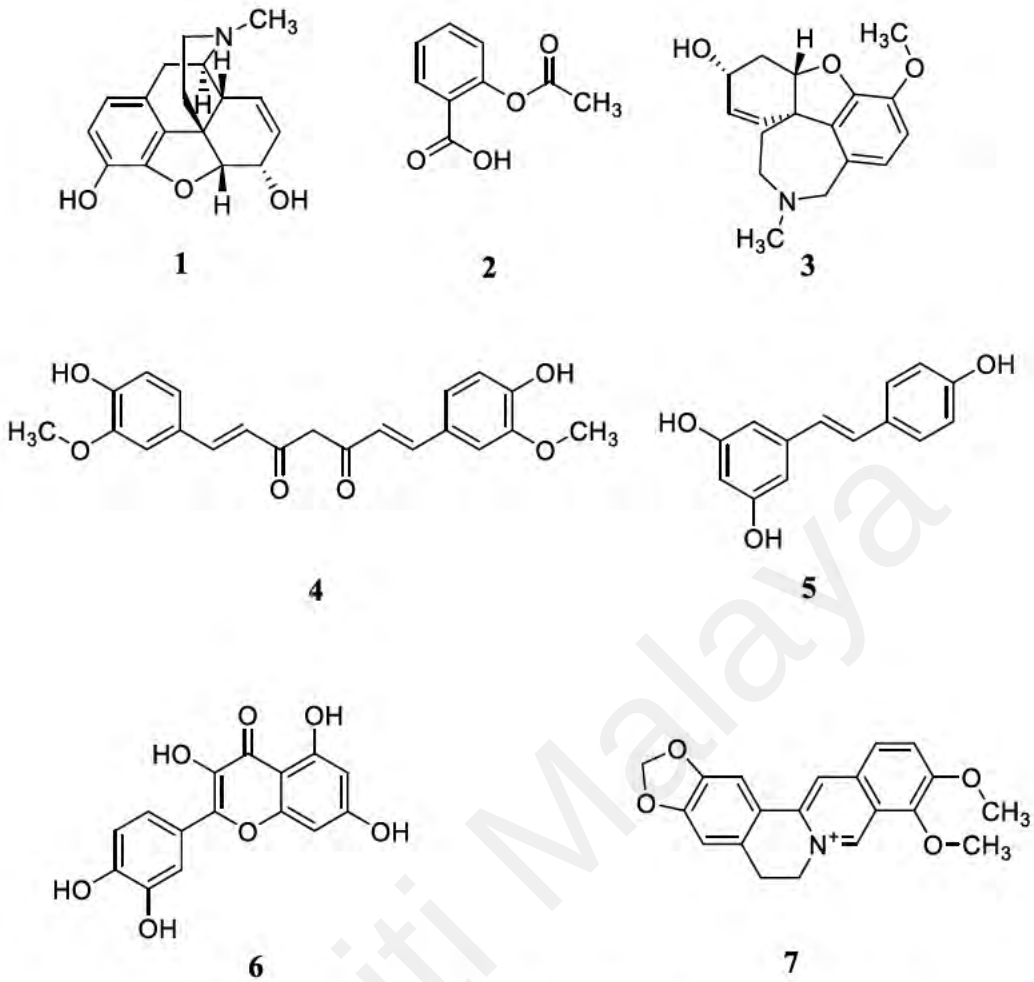

Figure 1.1: Examples of some active structures and drugs.

A lot of phytochemical research on Malaysian flora and fauna were carried out and some promising outcomes were obtained. Several examples of plants with bioactive metabolites were *Calophyllum flavoramulum*, *Endiandra kingiana*, and *Tabernaemontana corymbosa*. Amentoflavone **8** and 3-methoxy-2-hydroxyxanthone **9** (Figure 1.2) derived from *Calophyllum flavoramulum* were natural inhibitors of advanced glycation end-products (AGEs) (Ferchichi et al., 2012). In 2015, the study on the bark extract of *Endiandra kingiana* showed that Kingianins G **10** and H **11** (Figure 1.2) were potent inhibitors of Mcl-1/Bid interaction (Azmi et al., 2016). Furthermore, a novel alkaloid, Jerantinine A **12** (Figure 1.2) isolated from *Tabernaemontana corymbosa*

potently inhibits proliferation and colony formation of human-derived carcinoma cell lines, appear as potential antitumor agent (Raja et al., 2014).

Although research in NPs is very important for drug development, it is both time-consuming and costly due to the necessity for many chemicals and high precision instrumentation. Additionally, utilizing chemicals has negative environmental consequences. As a result, various computational tools have been developed to expedite the process of NPs research, such as molecular networking by using LC-MS and ^{13}C-NMR dereplication. These techniques can assist identify compounds with high certainty in the studied plant without the need to isolate them.

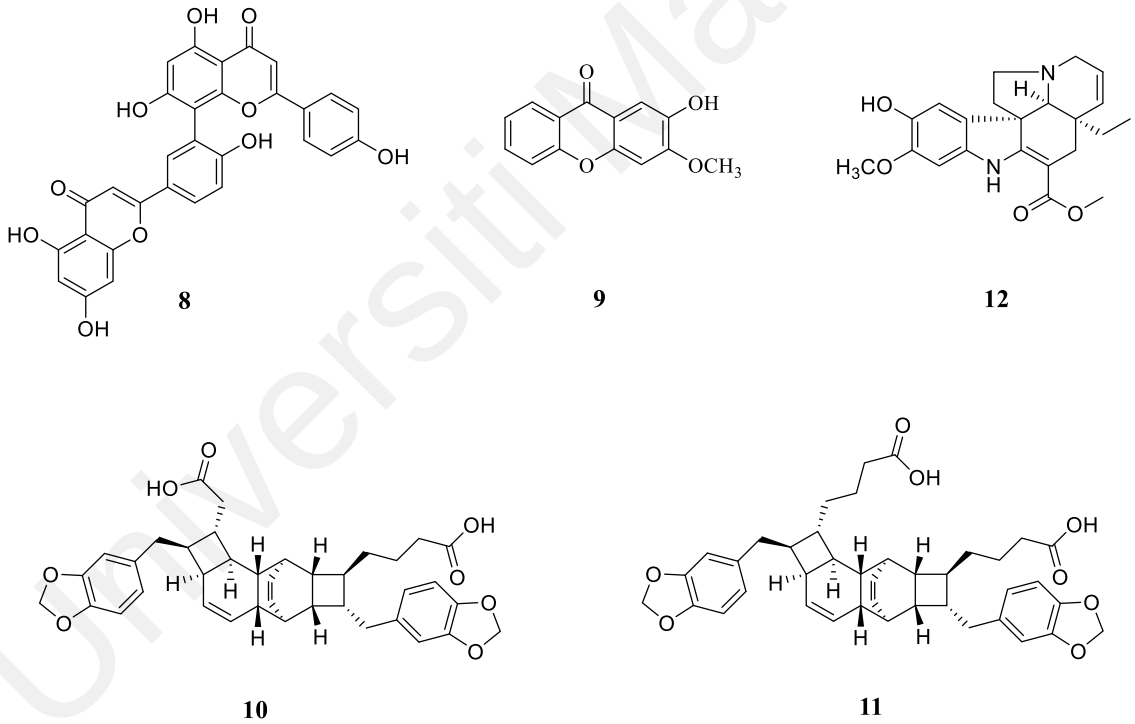

Figure 1.2: Examples of compounds isolated from Malaysia plant species.

For this study, *Mesua lepidota* (*M. lepidota*) and *Garcinia griffithii* (*G. griffithii*) from the clusioids clade were selected based on their positive screening activity against cholinesterase enzymes. Both plants demonstrated strong butyrylcholinesterase (BChE) inhibition, with extracts from *M. lepidota* and *G. griffithii* plants inhibiting the enzyme

by 91.25% and 94.07%, respectively. Both plants were then subjected to the MixONat (^{13}C-NMR dereplication) analysis. Selected compounds were isolated to validate the efficacy of MixONat and also for anticholinesterase testing.

1.2 *Clusiaceae* alliance (Malpighiales) / The clusioids

The clusioids are a clade of flowering plants in the large rosid order Malpighiales (Wurdack & Davis, 2009). The clade comprised of Bonnetiaceae, Calophyllaceae, Clusiaceae s.s., Hypericaceae, and Podostemaceae, representing 94 genera and about 1900 species (Ruhfel et al., 2011). Species in this clade are morphologically heterogeneous and ecologically diverse, Growth forms include large tropical rainforest trees, temperate and high-altitude tropical herbs, and shrubs, as well as aquatic plants of swift-flowing river and streams. Although the distribution is practically worldwide, its greatest species diversity lies inside the tropics (Byrne et al., 2018; Ruhfel et al., 2011).

The terrestrial members of the clade (*i.e.*, Bonnetiaceae, Calophyllaceae, Clusiaceae s. s., and Hypericaceae) have long been considered closely related, and the name *Clusiaceae nom. cons.* or the *Guttiferae* Juss. *nom. cons.*, *nom. alt.* has historically been applied to various combinations of taxa now found in these four families (Ruhfel et al., 2011). As the family is quite ancient (the fossil record date trace back about 90 Myr (Crepet & Nixon, 1998)) and the species undergo rapid molecular evolution (Adams et al., 2002; Davis et al., 2007), the family circumscriptions and interfamilial relationships of the clade have been hard to certain (Wurdack & Davis, 2009). Furthermore, the phylogenetic relationships within the Malpighiales that are not fully resolved (Stevens, 2001 onwards; Davis *et al.*, 2004; APG II, 2003; Tokuoka & Tobe, 2006; APG III, 2009, Wurdack & Davis, 2009; Sun *et al.* 2016) and the limits of the clades in the Bonnetiaceae-Podostemaceae caused the removal of Calophyllaceae from Clusiaceae in APG III, 2009 (GROUP, 2009).

The knowledge on interfamily relationships is improved later (APG IV, 2016). Hence, recent phylogenetic studies which based on molecular analyses, using plastid and nuclear gene regions (Savolainen *et al.*, 2000a, 2000b; Soltis *et al.*, 2000; Stevens, 2001 onwards; APG II, 2003; Davis *et al.* 2004, 2005; Tokuoka & Tobe, 2006; Wurdack & Davis, 2009; APG III, 2009; APG IV, 2016; Sun *et al.* 2016). Wurdack & Davis (2009) showed that the Clusiaceae are polyphyletic, with the two commonly recognized subfamilies of the Clusiaceae *s.l.* not forming a clade: So as to ensure monophyletic family circumscriptions, Wurdack & Davis (2009) reinstated the Calophyllaceae, a decision repeatedly and re-confirmed in year 2016 (APG IV, 2016) (Byrne et al., 2018; Chase et al., 2016)).

1.3 Distribution and habitat of genus *Mesua* and *Garcinia*

According to the World Flora Online, Calophyllaceae consists of twelve (12) plant genera and 774 species (WFO, 2022a), and Clusiaceae contains nineteen (19) genera and 1694 species (WFO, 2022b). Both families were distributed over tropical regions. A genus was selected from each of the aforementioned families for this research, where *Mesua* from family Calophyllaceae and *Garcinia* from Clusiaceae were selected.

As Stevens (2006) indicates Calophyllaceae (as Clusiaceae) are found mainly in moist, tropical, lowland, or lower montane forests. Most genera are found in primary forests, while others grow in peat swamp forests or black-water floodplains (Byrne et al., 2018; Stevens, 2007).

1.3.1 Genus *Mesua*

The genus *Mesua* are evergreen woody shrubs or small to medium-sized trees with hard and heavy wood. It is called as “penaga” in Malaysia (Chan, 2015). *Mesua ferrea*, or commonly known as Ceylon iron wood is the best-known species within the genus (Rouger et al., 2018).

Genus *Mesua* is a tiny genus that has 97 species (WFO, 2022d). The genus is mainly distributed in Southeast Asia, especially Indo-Malaysian region. It is instinctive to Bangladesh, Borneo, Cambodia, India, Jawa, Laos, Malaya, Myanmar, the Philippines, Sri Lanka, Thailand, and Vietnam. The genus is further introduced into China South-Central, China Southeast and Trinidad-Tobago (*Garcinia L.*). Some of the species, *i.e. M. stylosa* in Sri Lankan forest (Gunatilleke et al., 2017) and *M. catharinae* in Siberut Island (Suhandi et al., 2002) were endemic (Rouger et al., 2018).

1.3.2 Genus *Garcinia* Linn.

Garcinia L. is the second biggest genus among Clusiaceae. It consisted of 789 species (WFO, 2022c) that dispersed throughout tropical regions with the highest concentration in the Paleotropics (Sweeney 2008).

Garcinia L. (Clusiaceae), generally known as mangosteen plant, is a genus of evergreen polygamous trees or shrubs. *Garcinia* species are widely distributed in tropical Asia, Southern Africa (Raina et al., 2016) and Northern Australia. Many species are locally used, and the edible fruits are of interest worldwide, as well as having potential implication on the economy of local communities (Seethapathy et al., 2018). As *Mesua*, *Garcinia* is most commonly found in the Indo-Malaysian area too.

1.4 Appearance and morphology of *Mesua lepidota* and *Garcinia griffithii*

Mesua lepidota T. Anderson and *Garcinia griffithii* T. Anderson were the chosen species for the study. The appearance and morphology of the two species were discussed in the next sub-chapter, 1.4.1 and 1.4.2, respectively.

1.4.1 *Mesua lepidota*

Mesua lepidota, locally known as “penaga bayan” or “penaga tikus” in Sumatra and Malaya, is a majestic tree that can reach a height of up to 20 meters (m) and possesses a

trunk diameter of 40 centimeters (cm). The bole of the tree is fluted at the base, while the bark is characterized by its adherent and scaly texture. The outer bark exhibits a smooth texture with a reddish-brown color, while the inner bark showcases a pinkish-brown hue, accompanied by translucent to clear, yellow, and varnish-like exudate.

The leaves of *M. lepidota* are arranged oppositely on the stem and are simple in structure, featuring entire margins. The petiole, which connects the leaf blade to the stem, measures approximately 5 millimeters (mm) in length. The blade itself takes on an oblong-elliptical shape, measuring around 8 to 15 cm in length and 3 to 5 cm in width. It possesses a wedge-shaped base, slightly recurved margin, and an acuminate apex (Figure 1.3).

The inflorescence of *M. lepidota* is found in terminal or axillary umbels, consisting of 1 to 3-flowered racemes, extending to a length of approximately 6 cm. The flowers are bisexual and appear on pedicels accompanied by small, paired bracts. The flower structure consists of four (4) decussate sepals that are rounded and have a diameter of 5 mm. Additionally, the flowers feature four (4) petals, which are narrowed at the base and exhibit a roundish apical part measuring about 8 mm in diameter. The color of the petals can range from white to pink (Figure 1.3).

The fruit of *M. lepidota* takes on a spherical capsule shape with a diameter of approximately 2.5 cm. It possesses a thick and woody structure and is seated on persistent sepals, which are usually reflexed and also thick and woody (Figure 1.3).

These details provide a comprehensive description of *M. lepidota*, highlighting its physical characteristics such as its size, bark texture and color, leaf structure, inflorescence, and fruit morphology.

Figure 1.3: *Mesua lepidota* T. Anderson.

1.4.2 *Garcinia griffithii* T. Anders

Garcinia griffithii is a tree with 15 m height and 18 cm stem diameter. It had smooth and reddish-brown color bark. The inner part of the bark was pale yellow to brown color with the present of yellow latex (Figure 1.4).

The leaves are oppositely simple and thinly coriaceous. Its shape from oblong to ovate oblong with the apex of broadly pointed to rounded and obtuse base. Large leaves with the size of 26-38 cm × 12-16 cm. The upper surface of the leaves was bright green color, and the lower surface was pale green (Figure 1.4).

There are more than 20 pairs of secondary nerves distantly apart and raised on both sides. The midrib sunken above and raised beneath. In addition, the tertiary nerves faint on both surfaces of the leaves.

The petioles were 1.5-2.0 cm in length. The fruit was depressed globose in shape with the size of 5.5 × 4 cm. It was ribbed, subsessile, stigma disc-like, and sunken centrally.

Figure 1.4: *Garcinia griffithii* T. Anderson.

1.5 Problem statement

The prevalence estimates of mild cognitive impairment (MCI) among adults aged 65 or older owing to any cause ranged from 15 to 20 percent (Roberts & Knopman, 2013). While patients with MCI, particularly amnestic MCI, have an increased chance of developing AD or dementia (Kantarci et al., 2009; Lopez, 2013). A recent investigation indicated that after two years of follow-up, 15 percent of individuals older than 65 with MCI acquired dementia (Association, 2019). Four drugs have been approved as the cholinesterase inhibitors (ChEIs) for the treatment of MCI. These drugs include donepezil, galantamine, tacrine and rivastigmine (de Souza et al., 2016). However, the drug's adverse effects were severe, and the medicine's efficacy was not promising. As the individual ChEIs have different pharmacological mechanism of action (Hogan & Patterson, 2002), the search for more ChEIs from natural resources may aid in the understanding of the efficacy of ChEIs in the treatment of MCI. The chemical constituents of *M. lepidota* and *G. griffithii* were of interest in this study since both plants

showed strong potent activities against BChE with 91.25% and 94.07% inhibition at 200 µg/mL, respectively.

Garcinia is a large genus consists of nearly 400 species (*Garcinia L.*, n.d.). There were only three polyprenylated acyl phloroglucinols (PPAPs) reported from *G. griffithii*, including isoxanthochymol **248** (Elfita et al., 2009), isogarcinol/cambogin **310** and guttiferone I **284** (Nguyen et al., 2005). The enolic beta-diketone system and 3,4-dihydroxybenzoyl substituents have been identified as crucial elements in the structures of type B PPAPs, which contribute considerably to their anticancer activities (Ciochina & Grossman, 2006; Yang et al., 2018). The peculiar structure and bioactivities of PPAPs make them ideal pharmacological leads. Hence, the search for other PPAPs from *G. griffithii* became an interest in the study.

After several decades, NPs are still playing a vital role as a source of drug leads. However, the traditional chromatographic and spectroscopic methods are tedious, time consuming, and the organic solvents used are not environmentally friendly. Various dereplication techniques have been used in accelerating NPs isolation. Hence, MixONat, a recently developed tool by SONAS researchers, will be used in research to determine the compounds that could be present in *M. lepidota* and *G. griffithii.*

1.6 Objectives

The objectives of the study are as follows:

i. To execute the chemical constituents' profiles of *M. lepidota* and *G. griffithii* extracts with the MixONat software.

ii. To isolate secondary metabolites from the active fractions of *M. lepidota* through different chromatographic methods, *i.e.*, column chromatography (CC), thin layer chromatography (TLC) and high performance liquid chromatography (HPLC) and elucidate the chemical structures of the isolated compounds through 1D and 2D nuclear magnetic resonance spectroscopy (NMR), Infrared spectroscopy (IR) and mass spectroscopy (MS).

iii. To isolate PPAPs from *the G. griffithii* extract through different chromatographic methods, *i.e.*, CC, TLC, and HPLC and elucidate the chemical structures of the isolated compounds through 1D and 2D NMR, IR and MS.

iv. To analyze the acetyl (AChE) and butyryl (BChE) cholinesterase inhibitory activities of the isolated compounds through Ellman's method with modification.

v. To evaluate the type of inhibition and binding interactions on the most potent compound with cholinesterase through enzyme kinetic studies, molecular docking, and molecular dynamics simulations.

CHAPTER 2: LITERATURE REVIEW

The literature review was divided into three parts, *i.e.*, the general chemical aspects, the ^{13}C-NMR dereplication and the cholinesterase inhibitory activities. The chemical aspects of both *Mesua* and *Garcinia* genus will be deliberate in sub-chapter 2.1. As mentioned in the preceding chapter, the *Mesua* genus is rather small in comparison to the *Garcinia* genus. Consequently, the *Mesua* genus has received far less attention in the literature than *Garcinia*. As a result of the extensive research on *Garcinia*, the discussion of the genus will be confined to the last two decades of literatures (publication 2010 - 2023).

2.1 General chemical aspects

The reported secondary metabolites isolated from *Mesua* and *Garcinia* species are greatly represented by polyphenolic compounds (Rouger et al., 2018). For *Mesua*, most of the isolated metabolites are coumarins and xanthones bearing one or several prenyl groups (Rouger et al., 2018), while xanthones and PPAPs were commonly found in genus *Garcinia*. Such prenylated polyphenols are rather nonpolar and thus seldom found in aqueous or hydro-alcoholic traditional preparations.

2.1.1 *Mesua*

Various types of compounds had been isolated from different species of *Mesua*, including coumarins, triterpenes, xanthones, flavonoids, PPAPs, phenolic compounds *etc.*

2.1.1.1 Coumarins

Coumarins are aromatic oxygenated molecules constructed by the fusion of benzene and α-pyrone rings. Following IUPAC systematic nomenclature, the coumarin nucleus corresponds to 2*H*-chromen-2one (2*H*-1-benzopyran-2-one or benzo-α-pyrone) ring

(Ortiz Villamizar et al., 2018). It is a fragrant colorless compound isolated from the tonka bean (Dipteryx odorata; family Fabaceae; Plate) by Vogel in 1820, which was the initial member of this class of compounds (Chatterji, 1968; Murray, 1978; Sarker & Nahar, 2017).

Coumarins belong to a large class of phenolic substances found in many plants. In plants, coumarins act as phytoalexins, which are defense metabolites produced especially in response to a menace from other organisms (Gutiérrez-Mellado et al., 1996). The distribution of coumarins in a wide range of plants is correlated with their ability to respond to traumatic injuries caused by plant diseases or drying, and with the inhibitory growth of fungal plant pathogens, acting as potent repellents against insects (Soine, 1964). Furthermore, the coumarins are involved in plant metabolism, through taking part in growth regulation of plants (Matern, 2010; Ortiz Villamizar et al., 2018)

Coumarins from *Mesua* genus are mainly 4-substituted type of coumarin (Chatterji, 1968). Crombie *et al.* categorized this type of coumarins as *Mammea* coumarin (Crombie et al., 1987).

(a) ***Mammea coumarins***

Mammea coumarins are NPs commonly isolated from plants of genera *Mammea*, *Mesua* and *Calophyllum* (Dang et al., 2015). With a 5,7-dioxygenated coumarinic skeleton, *Mammea* coumarins are substituted with a prenyl or an acyl at C-6 or C-8 together with an alkyl or phenyl group at C-4 position (Cechinel Filho et al., 2009; Dang et al., 2015).

From a biogenetic point of view, *Mammea* type coumarins belong to a homogeneous group of naturally occurring heterocycles with a biosynthetic scheme related to that of neoflavonoids (Raad et al., 2006). From the literature review, the 4-phenyl coumarins are

the most isolated *Mammea* coumarins. It was hypothesized that 4-phenylcoumarins could result from the S_N2' reaction of a prenylated acylphloroglucinol (polyketide pathway) with the α-carbon of the side chain of a phenylpropanoyl unit (*e.g.* a cinnamic acid) followed by lactonization (Jean, 2008; Ramiandrasoa et al., 1983). The specific nomenclature assigned by Crombie *et al.* to these compounds also takes into account the various cyclization which often occur between the prenyl side chain and an adjacent hydroxyl group (Crombie et al., 1966). Table 2.1 listed the coumarins isolated from *Mesua* genus and the details.

Table 2.1: Coumarins isolated from *Mesua* genus.

No.	Plant Species	Parts	Chemical Constituents	Molecular Formula	Site collection	References
1.	*M. assamica*	Bark	Theraphin A **13**	$C_{21}H_{26}O_6$	Myanmar	(Gogoi, 2018)
		Bark, flower	Theraphin B **14**	$C_{22}H_{28}O_6$		
			Theraphin C **15**	$C_{22}H_{28}O_6$		
		Bark	Theraphin D **29**	$C_{21}H_{24}O_6$		
		Root	Assamene **32**	$C_{22}H_{28}O_6$		
		Fruit peels	Mammea A/AA cyclo F or Cyclomammeisin **34**	$C_{25}H_{26}O_6$		
			Mammea A/AA or Mammeisin **40**	$C_{25}H_{26}O_5$		
		Flower	Kayeassamin A **16**	$C_{26}H_{34}O_6$		
			Kayeassamin B **17**	$C_{26}H_{34}O_6$		
			Kayeassamin C **18**	$C_{27}H_{36}O_6$		
			Kayeassamin D **19**	$C_{27}H_{36}O_6$		
			Kayeassamin E **20**	$C_{21}H_{26}O_6$		
			Kayeassamin F **21**	$C_{22}H_{28}O_6$		
			Kayeassamin G **22**	$C_{22}H_{28}O_6$		
			Kayeassamin H **30**	$C_{21}H_{24}O_5$		
			Kayeassamin I **31**	$C_{26}H_{32}O_6$		
			Mammea A/AA cyclo D **49**	$C2_5H_{24}O_5$		
			Mammea A/BC **56**	$C_{24}H_{24}O_5$		
			Mammea B/AC **65**	$C_{21}H_{26}O_5$		
			Mammea A/AC **41**	$C_{24}H_{24}O_5$		
			Mammea A/AC cyclo D **50**	$C_{24}H_{22}O_5$		
			Theraphin B **14**	$C_{22}H_{28}O_6$		
			Theraphin C **15**	$C_{22}H_{28}O_6$		
			Mammea B/AC cyclo F **66**	$C_{21}H_{26}O_6$		
			Deacetyl mammea E/ BA cyclo D **67**	$C_{22}H_{26}O_6$		

Table 2.1, continued.

No.	Plant Species	Parts	Chemical Constituents	Molecular Formula	Site collection	References
2.	*M. beccariana*	Stem bark	Mammea A/AB **42**	$C_{25}H_{26}O_5$	Sarawak, Malaysia	(Ee et al., 2011; Teh et al., 2010)
			Beccamarin **68**	$C_{24}H_{22}O_6$		(Ee et al., 2011; Teh et al., 2012)
			Beccamarin T / lepidotol A **70**	$C_{29}H_{32}O_5$	Sarawak, Malaysia	(Thiruventhan Karunakaran et al., 2016)
3.	*M. borneensis*	Stem bark	Mammea A/BA **57**	$C_{25}H_{27}O_5$	East Kalimantan, Indonesia.	(Tanjung et al., 2016)
			Mammea A/AA cyclo D **49**	$C_{25}H_{25}O_5$		
			Mammea A/AD or mesuol **43**	$C_{24}H_{25}O_5$		
4.	*M. calophylloides*	Stem bark	Mesucalophylloidin **69**	$C_{30}H_{33}O_5$	East Kalimantan, Indonesia.	(Tanjung et al., 2018)
			Mammea A/BA cyclo F **74**	$C_{25}H_{26}O_6$		
5.	*M. elegans*	Stem bark	Mesuagenin A **79**	$C_{30}H_{32}O_5$	Kedah, Malaysia	(Awang et al., 2010)
			Mesuagenin B **80**	$C_{30}H_{32}O_5$		
			Mesuagenin C **58**	$C_{29}H_{32}O_5$		
			Mesuagenin D **75**	$C_{30}H_{34}O_6$		
			Mammea A/BA cyclo D or Isomammeigin **81**	$C_{25}H_{24}O_5$		
			5,7-Dihydroxy-8-(2-methylbutanoyl)-6-[(*E*)-3,7-dimethylocta-2,6-dienyl]-4-phenyl-2*H*-chromen-2-one **59**	$C_{30}H_{34}O_5$		
			5,7-dihydroxy-8-(3-methylbutanoyl)-6-[(*E*)-3,7-dimethylocta-2,6-dienyl]-4-phenyl-2*H*-chromen-2-one **60**	$C_{30}H_{34}O_5$		
			Mammea A/BA cyclo F **74**	$C_{25}H_{26}O_6$		
			Mammea A/BA **57**	$C_{25}H_{26}O_5$		

Table 2.1, continued.

No.	Plant Species	Parts	Chemical Constituents	Molecular Formula	Site collection	References
			Mammea A/BB or isomammeisin **61**	$C_{25}H_{26}O_5$		(Chan, 2015)
			Ochrocarpin E **76**	$C_{24}H_{24}O_6$		
			Mammea A/BB cyclo F **77**	$C_{25}H_{26}O_6$		
			Mesuagenin F **78**	$C_{30}H_{34}O_6$		
			Isodisparfuran **84**	$C_{22}H_{18}O_5$		
6.	*M. hexapetala*	Stem bark	Hexapetarin **85**	$C_{22}H_{28}O_6$	Sarawak, Malaysia	(T. Karunakaran et al., 2016)
7.	*M. kunstleri*	Stem bark	Mammea A/BB or isomammeisin **61**	$C_{25}H_{26}O_5$	Kedah, Malaysia	(Chan, 2015)
			Mammea A/BA **57**	$C_{25}H_{26}O_5$		
			Mesuagenin C **58**	$C_{29}H_{32}O_5$		
			5,7-dihydroxy-8-(2-methylbutanoyl)-6-[(E)-3,7-dimethylocta-2,6-dienyl]-4-phenyl-2-chromen-2-one **59**	$C_{30}H_{34}O_5$		
			5,7-dihydroxy-8-(3-methylbutanoyl)-6-[(E)-3,7-dimethylocta-2,6-dienyl]-4-phenyl-2-chromen-2-one **60**	$C_{30}H_{34}O_5$		
			Mammea A/BB cyclo D or Ponnalide **82**	$C_{25}H_{24}O_5$		
			Mammea A/BA cyclo D or Isomammeigin **81**	$C_{25}H_{24}O_5$		
			Mesuagenin E **83**	$C_{29}H_{30}O_5$		
			Mesuagenin A **79**	$C_{30}H_{32}O_5$		
			Mesuagenin B **80**	$C_{30}H_{32}O_5$		
8.	*M. lepidota*	Fruit	lepidotol A **70**	$C_{29}H_{33}O_5$	Johor, Malaysia	(Rouger et al., 2015)
			Lepidotol B **71**	$C_{30}H_{33}O_5$		
			Lepidotol C **72**	$C_{28}H_{29}O_5$		

Table 2.1, continued.

No.	Plant Species	Parts	Chemical Constituents	Molecular Formula	Site collection	References
			Lepidotol D **73**	$C_{29}H_{31}O_5$		
			Lepidotol E **86**	$C_{29}H_{31}O_6$		
			Lepidotin A **88**	$C_{24}H_{25}O_5$		
			Lepidotin B **89**	$C_{25}H_{27}O_5$		
			Mammea A/OB **62**	$C_{20}H_{18}O_5$		
			Mammea A/OC **63**	$C_{19}H_{16}O_5$		
9.	*M. racemosa*	Leaves	Racemosol **44**	$C_{24}H_{24}O_6$	Kelantan, Malaysia	(Morel, Guilet, et al., 1999)
			Mammea A/AC cyclo F **35**	$C_{24}H_{24}O_6$		
			Mammea A/AC **41**	$C_{24}H_{24}O_5$		
			Mammea A/AC cyclo D **50**	$C_{24}H_{22}O_5$		
			Mammea A/AD cyclo D or mesuagin **51**	$C_{24}H_{22}O_5$		
			Mammea A/BB or isomammeisin **61**	$C_{25}H_{26}O_5$		
			Mammea A/AA or Mammeisin **40**	$C_{25}H_{26}O_5$		
			Racemosone **45**	$C_{21}H_{18}O_6$	Kelantan, Malaysia	(Morel, Dartiguelongue, et al., 1999)
			Furanoracemosone **90**	$C_{21}H_{16}O_5$		
			Mammea A/BC **56**	$C_{24}H_{24}O_5$		
			Isoracemosol **64**	$C_{24}H_{25}O_6$		
10.	*M. thwaitesii*	Bark	Mammea A/AA cyclo F or Cyclomammeisin **34**	$C_{25}H_{26}O_6$	-	(Bandaranayake et al., 1975)
		Seeds	Mammea A/AA or Mammeisin **40**	$C_{25}H_{26}O_5$		
		seed oil	Mammea A/AD cyclo D or mesuagin **51**	$C_{24}H_{22}O_5$		
			Mammea A/AD cyclo F **36**	$C_{24}H_{24}O_6$		
			Mammea A/AB cyclo D or mammeigin **52**	$C_{25}H_{24}O_5$		

Table 2.1, continued.

No.	Plant Species	Parts	Chemical Constituents	Molecular Formula	Site collection	References
			Mammea A/AB **42**	$C_{25}H_{26}O_5$		
			Mammea A/AB cyclo F **37**	$C_{25}H_{26}O_6$		
			Mammea A/AD or mesuol **43**	$C_{24}H_{24}O_5$		
			Mammea A/AC **41**	$C_{24}H_{24}O_5$		
11.	*M. ferrea*	Seed oil	Mesuarin **53**	$C_{25}H_{24}O_5$	-	(Bhattacharyya et al., 1988)
			Mammea A/AB cyclo D or mammeigin **52**	$C_{25}H_{24}O_5$		Bala & Seshadri, 1971)(Suresh et al., 2014) (Chakraborty & Chatterji, 1969)
			Mammea A/AD or mesuol **43**	$C_{24}H_{24}O_5$		(Bala & Seshadri, 1971) (Suresh et al., 2014)
			Mammea A/AD cyclo D or mesuagin **51**	$C_{24}H_{22}O_5$		(Chakraborty & Chatterji, 1969) (Suresh et al., 2014)
			Mammea A/AA or Mammeisin **40**	$C_{25}H_{26}O_5$		(Suresh et al., 2014)
		Seed	Mammea A/AD or mesuol **43**	$C_{24}H_{24}O_5$	Karnataka, India	(Chahar et al., 2012)
		Seed kernel	Mammea A/AD or mesuol **43**	$C_{24}H_{24}O_5$	-	(Chakraborty & Bose, 1960)
		Trunk bark	Ferruol A **92**	$C_{23}H_{30}O_5$	-	(Govindachari, Pai, Subramaniam, Ramdas Rao, et al., 1967) (Suresh et al., 2014)
			Mammea B/BA or ferruol B **93**	$C_{22}H_{28}O_5$		(Suresh et al., 2014)
		Flowering buds	5,7-dihydroxy-8-(2-methylbutanoyl)-6-[3,7-dimethylocta-2,6-dienyl]-4-phenyl-2*H*-chromen-2-one **59**	$C_{30}H_{34}O_5$	Chandigarh, India	(Roy et al., 2013)

Table 2.1, continued.

No.	Plant Species	Parts	Chemical Constituents	Molecular Formula	Site collection	References
			Surangin C **33**	$C_{27}H_{36}O_6$		
			Mammea A/AB cyclo D or mammeigin **52**	$C_{25}H_{24}O_5$		
			Mammea A/AB **42**	$C_{25}H_{26}O_5$		
			Mammea A/BB or isomammeisin **61**	$C_{25}H_{26}O_5$		
			5,7-dihydroxy-6-(2-methylbutanoyl)-4-phenyl-2H-chromen-2-one **46**	$C_{20}H_{18}O_5$		
			Mammea A/AB cyclo F **37**	$C_{25}H_{26}O_6$		
		Blossoms	Mammea A/AD or mesuol **43**	$C_{24}H_{24}O_5$	-	(Verotta et al., 2004)
			Mammea A/AB **42**	$C_{25}H_{26}O_5$		
			Mammea A/AA or Mammeisin **40**	$C_{25}H_{26}O_5$		
			5,7-Dihydroxy-6-(2-methylbutanoyl)-8-[(*E*)-3,7-dimethylocta-2,6-dienyl]-4-phenyl-2*H*-chromen-2-one **47**	$C_{30}H_{34}O_5$		
			5,7-Dihydroxy-6-(3-methylbutanoyl)-8-[(*E*)-3,7-dimethylocta-2,6-dienyl]-4-phenyl-2*H*-chromen-2-one **48**	$C_{30}H_{34}O_5$		
			Mammea A/BB or isomammeisin **61**	$C_{25}H_{26}O_5$		
			Mammea A/BA **57**	$C_{25}H_{26}O_5$		
			5,7-Dihydroxy-8-(2-methylbutanoyl)-6-[(*E*)-3,7-dimethylocta-2,6-dienyl]-4-phenyl-2*H*-chromen-2-one **59**	$C_{30}H_{34}O_5$		
			5,7-dihydroxy-8-(3-methylbutanoyl)-6-[(*E*)-3,7-dimethylocta-2,6-dienyl]-4-phenyl-2*H*-chromen-2-one **60**	$C_{30}H_{34}O_5$		
			Mammea A/AD cyclo F **36**	$C_{24}H_{24}O_6$		

Table 2.1, continued.

No.	Plant Species	Parts	Chemical Constituents	Molecular Formula	Site collection	References
			Mammea A/AB cyclo F **37**	$C_{25}H_{26}O_6$		
			Mammea A/AA cyclo F or Cyclomammeisin **34**	$C_{25}H_{26}O_6$		
			Assamene **32**	$C_{22}H_{28}O_6$		
			Surangin C **33**	$C_{27}H_{36}O_6$		
			8,9-Dihydro-5-hydroxy-6-(2-methylbutanoyl)-4-phenyl-8-(prop-1-en-2-yl)furo[2,3-h]chromen-2-one **38**	$C_{25}H_{24}O_5$		
			8,9-Dihydro-5-hydroxy-6-(3-methylbutanoyl)-4-phenyl-8-(prop-1-en-2-yl)furo[2,3-h]chromen-2-one **39**	$C_{25}H_{24}O_5$		
			Mammea A/AD cyclo D or mesuagin **51**	$C_{24}H_{22}O_5$		
			Mammea A/AB cyclo D or mammeigin **52**	$C_{25}H_{24}O_5$		
			Mammea A/AA cyclo D **49**	$C_{25}H_{24}O_5$		
			5-Hydroxy-6-isobutyryl–8-methyl-8-(4-methylpent-3-enyl)-4-phenyl-2*H*-pyrano[2,3-h]chromen-2-one **54**	$C_{29}H_{30}O_5$		
			5-Hydroxy-8-methyl-6-(2-methylbutanoyl)-8-(4-methylpent-3-enyl)-4-phenyl-2*H*-pyrano[2,3-h]chromen-2-one **55**	$C_{30}H_{32}O_5$		
		Flowering buds	Mesuaferol D **94**	$C_{27}H_{36}O_7$	Urumqi, P. R. of China	(Wang et al., 2020)
			Mesuaferol E **95**	$C_{26}H_{34}O_7$		
			Mesuaferol F **96**	$C_{27}H_{36}O_7$		

Table 2.1, continued.

No.	Plant Species	Parts	Chemical Constituents	Molecular Formula	Site collection	References
			iso-Mesuaferol F **87**	$C_{27}H_{36}O_7$		
		Flowering buds	Mesuaferol G **23**	$C_{27}H_{36}O_7$	Urumqi, P. R. of China	(S. Wang et al., 2019)
			Mesuaferol H **24**	$C_{27}H_{36}O_7$		
			Mesuaferol I **25**	$C_{27}H_{36}O_7$		
			Mesuaferol J **26**	$C_{26}H_{34}O_6$		
			Mesuaferol K **27**	$C_{21}H_{26}O_6$		
			Surangin D **28**	$C_{27}H_{36}O_6$		
			Surangin C **33**	$C_{27}H_{36}O_6$		
			Theraphin B **14**	$C_{22}H_{28}O_6$		
			Theraphin C **15**	$C_{22}H_{28}O_6$		
		twigs	Isodisparfuran **84**	$C_{22}H_{18}O_5$	Trang, Thailand	(Chakthong et al., 2020)
			Disparfuran B **91**	$C_{22}H_{18}O_5$		
			Mammea A/AA cyclo D **49**	$C_{25}H_{24}O_5$		
			Mammea A/AA cyclo F or Cyclomammeisin **34**	$C_{25}H_{26}O_6$		
		Flowerimg buds	Mesuaferol A **97**	$C_{30}H_{33}O_5$	-	(Chen et al., 2022)
			Mesuaferol B **98**	$C_{29}H_{31}O_5$		
			Mesuaferol C **99**	$C_{30}H_{33}O_5$		
		Branches and leaves	Mesuaferlinn A **100**	$C_{25}H_{24}O_6$	Gengma, Yunnan Province, People's Republic of China	(Zhou et al., 2022)
			Mesuaferlinn B **101**	$C_{24}H_{22}O_6$		
			Mesuaferlinn C **102**	$C_{24}H_{22}O_5$		
			8,9-Dihydro-5-hydroxy-6-(2-methylbutanoyl)-4-phenyl-8-(prop-1-en-2-yl)furo[2,3-h]chromen-2-one **38**	$C_{25}H_{24}O_5$		
			Mammea A/BD **103**	$C_{24}H_{24}O_5$		
			Mammea A/BB or isomammeisin **61**	$C_{25}H_{26}O_5$		

Table 2.1, continued.

No.	Plant Species	Parts	Chemical Constituents	Molecular Formula	Site collection	References
			Mammea A/AD cyclo D or mesuagin **51**	$C_{24}H_{22}O_5$		
			Mammea A/AB cyclo D or mammeigin **52**	$C_{25}H_{24}O_5$		
			Mammea A/AB cyclo E **104**	$C_{25}H_{26}O_6$		
			Mammea A/AB cyclo F **37**	$C_{25}H_{26}O_6$		
			Mammea A/AD cyclo F **36**	$C_{24}H_{24}O_6$		
			Mammea A/AB **42**	$C_{25}H_{26}O_5$		
			Mammea A/BB cyclo F **77**	$C_{25}H_{26}O_6$		

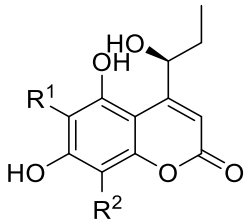

No.	R^1	R^2
13	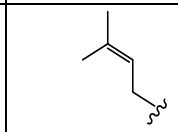	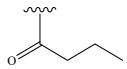
14	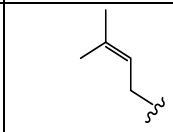	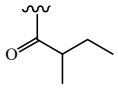
15	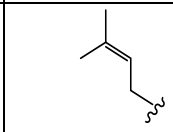	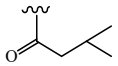
16	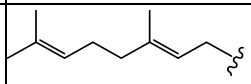	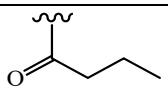
17	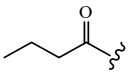	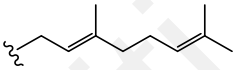
18	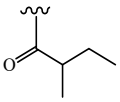	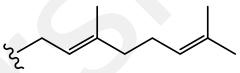
19	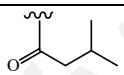	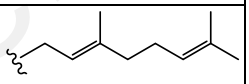
20	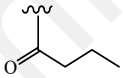	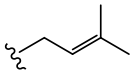

No.	R^1	R^2
21	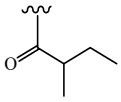	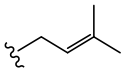
22	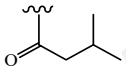	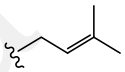
23	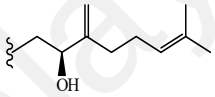	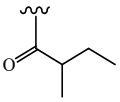
24	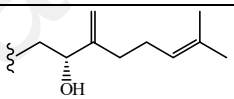	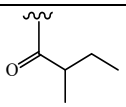
25	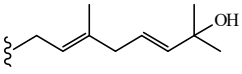	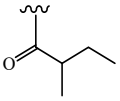
26	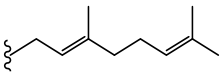	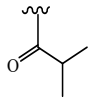
27	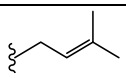	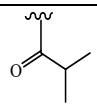
28	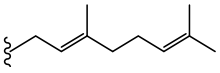	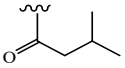

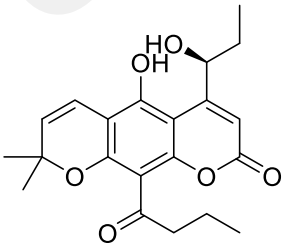

29

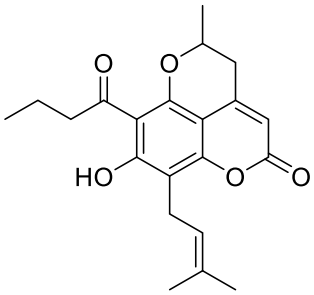

30

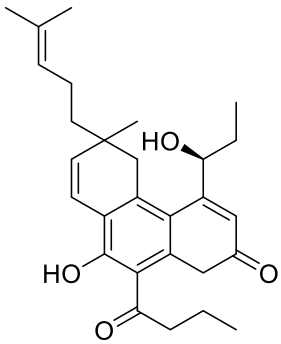

31

Figure 2.1: Structures of coumarins isolated from *Mesua* genus.

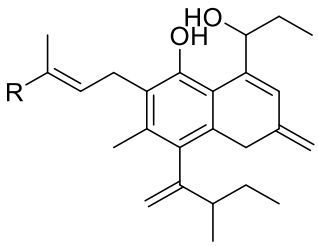

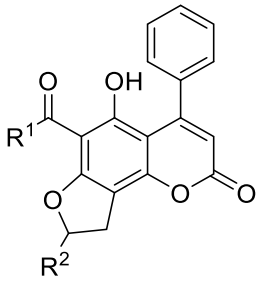

No.	R
32	CH_3
33	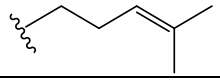

No.	R^1	R^2
34	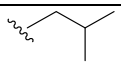	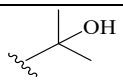
35	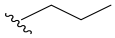	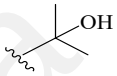
36	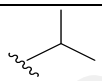	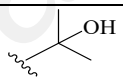
37	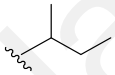	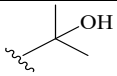
38	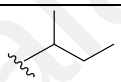	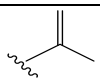
39	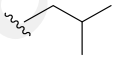	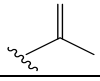
97	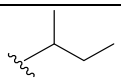	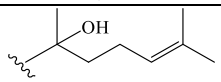
98	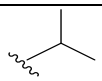	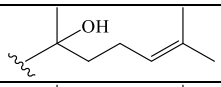
99	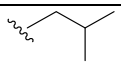	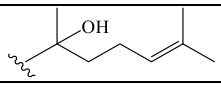
102	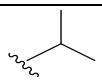	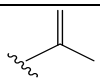

Figure 2.1, continued.

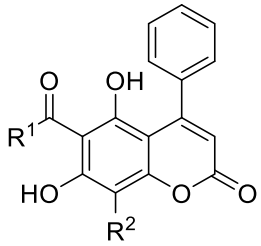

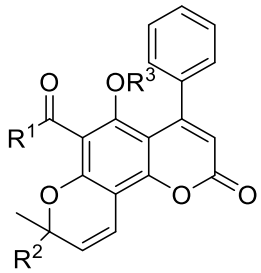

No.	R^1	R^2
40		
41		
42		
43		
44		OH
45		O
46		H
47		
48		

No.	R^1	R^2	R^3
49		CH_3	H
50		CH_3	H
51		CH_3	H
52		CH_3	H
53		CH_3	CH_3
54			H
55			H

Figure 2.1, continued.

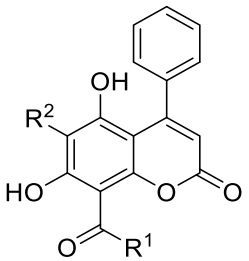

No.	R^1	R^2
56		
57		
58		
59		
60		
61		
62		H
63		H
64		OH
103		

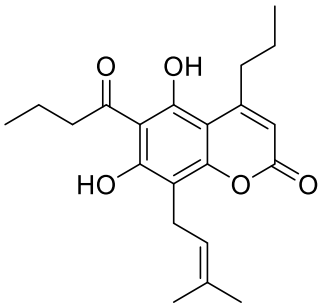

65

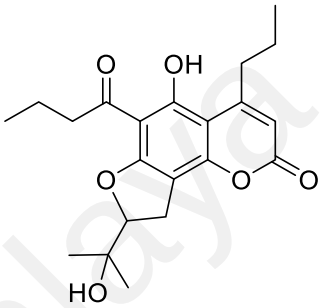

66

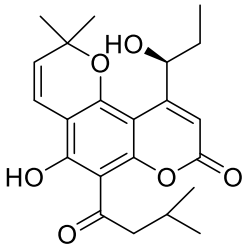

67

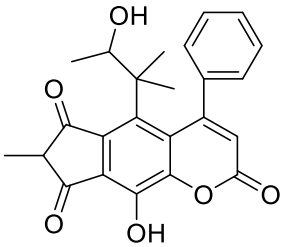

68

Figure 2.1, Continued

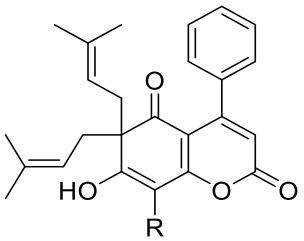

No.	R
69	
70	
71	
72	
73	

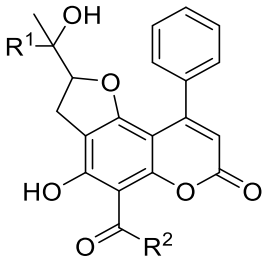

No.	R^1	R^2
74	CH_3	
75		
76	CH_3	
77	CH_3	
78		

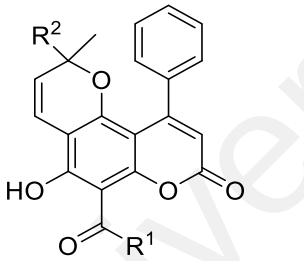

No.	R^1	R^2
79		
80		
81		CH_3
82		CH_3
83		

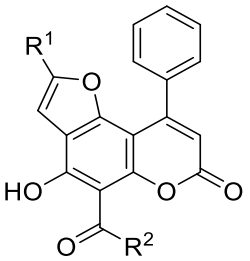

No.	R^1	R^2
84	H	
100	OH	
101	OH	

Figure 2.1, continued.

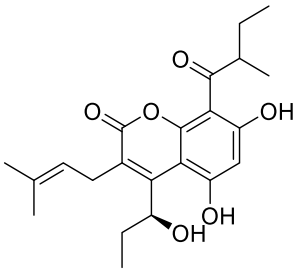

85

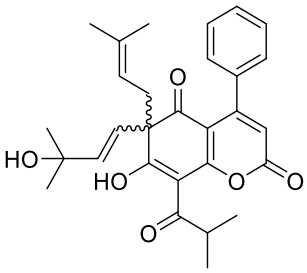

86

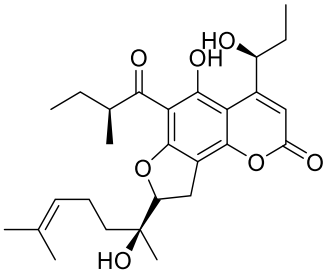

87

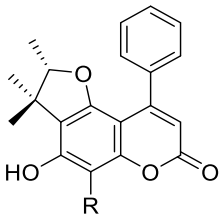

No.	R
88	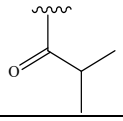
89	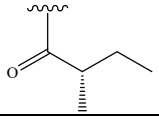

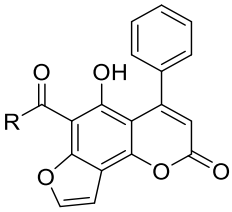

No.	R
90	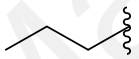
91	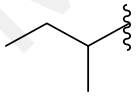

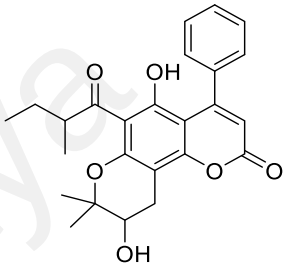

104

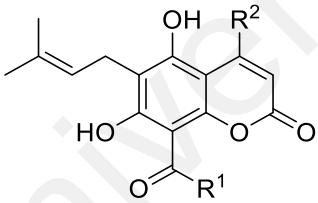

No.	R^1	R^2
92	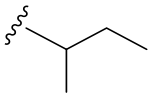	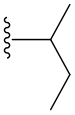
93	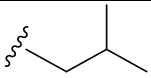	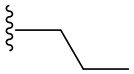

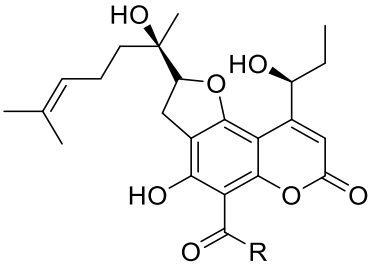

No.	R
94	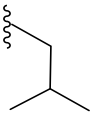
95	
96	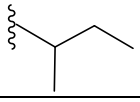

Figure 2.1, continued.

(b) ***Biosynthesis pathway of Mammea coumarins***

Biosynthetically, coumarins is derived from the shikimate pathway. However, the biosynthesis pathway of *Mammea* coumarins differs, as it is associated with the origin of neoflavonoids (Gautier et al., 1972; Raad et al., 2006).

The biosynthesis of *Mammea* coumarins take place by the interaction of a phloroglucinol unit and a unit of an acid deriving from a variable amino acid (Majumdar, 1979). An α, β-unsaturated acid (for structures in this study cinnamic acid is suggested) is then introduced and dehydrogenation of the acid intermediate leads to the formation of double bond followed by cyclization to give the core structure of *Mammea* coumarin (Scheme 2.1) (Gautier et al., 1972; Ramiandrasoa et al., 1983; Rouger, 2015).

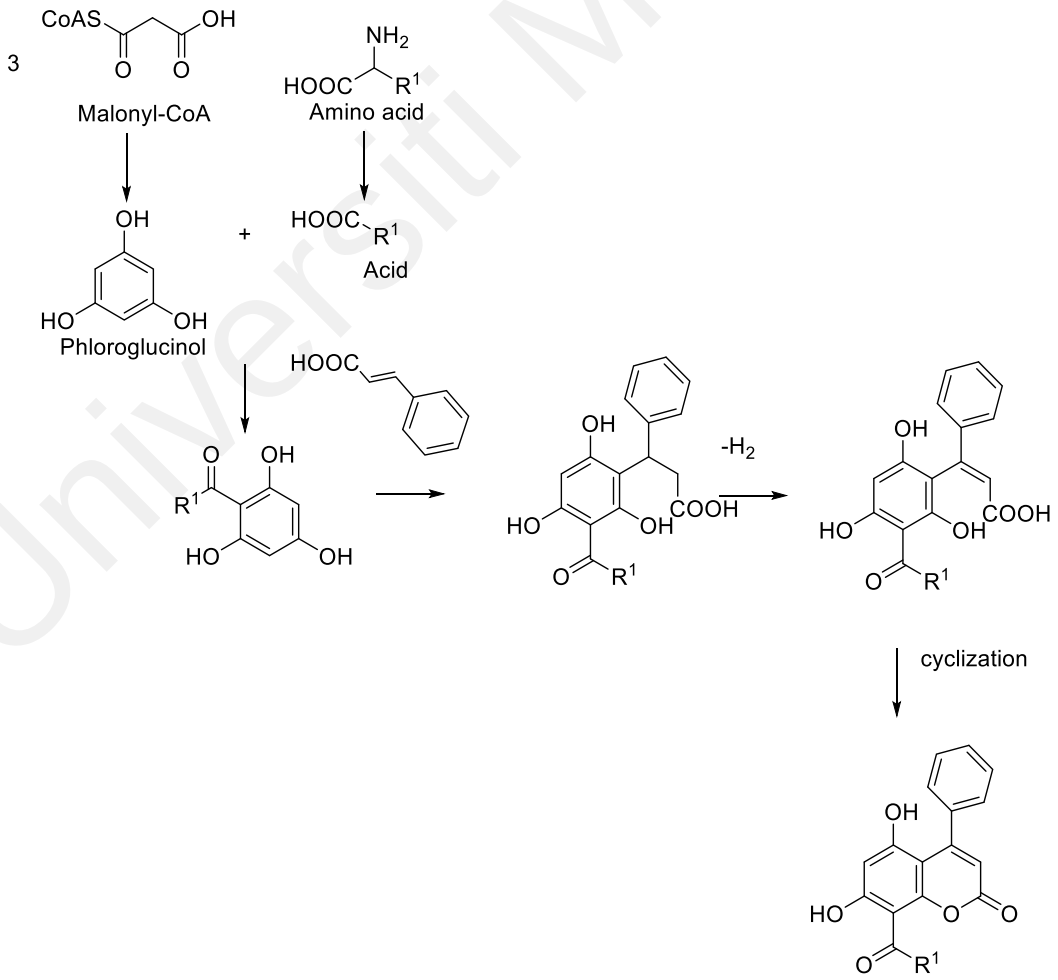

Scheme 2.1: Biosynthesis pathway of *Mammea* type coumarins (Gautier et al., 1972; Ramiandrasoa et al., 1983; Rouger, 2015).

(c) ***Naming system of Mammea coumarins***

To prevent the profusion of trivial names and grouping of the *Mammea* coumarins systematically, a nomenclature was formerly established by Crombie *et al.* (1987). Basically, "*Mammea*" is followed by a first letter that indicates the substituents at C-4. Then, a slash (/) is used to separate the first and second letter. The second letter assigns the position of the acyl group; either at C-6 or C-8. Subsequently, a third letter is designated the type of acyl substituents. If cyclisation of prenyl substituent occurred, the naming is continued by the prefix cyclo and a fourth letter that indicating the type of heterocycle involved (Table 2.2) (Crombie et al., 1987; Dang et al., 2015).

Table 2.2: Summary of the naming system for the *Mammea* type coumarins.

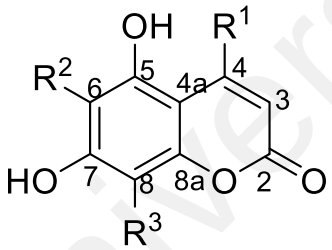	**Substitution in C-4**	**1st letter**
	R^1- phenyl	Mammea A
	R^1- propyl	Mammea B
	R^1- pentyl	Mammea C
	R^1- 1-methylpropyl	Mammea D
	R^1- 1-acetoxypropyl	Mammea E
	Position of the acyl group	**2nd letter**
	R^2- acyl	A
	R^3- acyl	B
	Substitution at C-6 or C-8	**3rd letter**
	R^2/R^3 - 3-methylbutyryl	A
	- 2-methylbutyryl	B
	- butyryl	C
	- 2-methylrpopionyl	D
	If cyclisation occurs	**Cyclo + 4th letter**
	2, 2-dimethylchromene	Cyclo D
	3-hydroxy-2, 2-dimethyldihydropyran	Cyclo E
	2-(1-hydroxy-1-methylethyl) dihydrofuran	Cyclo F

2.1.1.2 Xanthones

Chemically, xanthones (9*H*-xanthen-9-ones) are heterocyclic compounds with the dibenzo-γ-pyrone framework (Sousa & Pinto, 2005). Although the parental structure of xanthone is symmetry (Vieira & Kijjoa, 2005), it has a mixed biogenetic origin in higher plants. The carbons in xanthone are assigned numbers based on a biosynthetic convention; with the acetate-derived ring A are firstly assigned as carbons 1-4, then follow by carbons 5-8, to the shikimate-derived ring B (El-Seedi et al., 2010). Xanthones are also typically poly-substituted structure and occur as either fully aromatized (Masters & Br se, 2012) or subdivided into different degree of oxygenation (Negi et al., 2013).

Miscellaneous xanthones were described with different types of substituents in different positions, associated with their tricyclic scaffold (El-Seedi et al., 2010), leading to a wide range of pharmacological activitiy (Sousa & Pinto, 2005). Hence, Lesch and Bräse (Lesch & Braese, 2004) have described the xanthone scaffold as a "privileged structure" due to its ability to interact with a diverse range of targets biomolecules (El-Seedi et al., 2010; Masters & Br se, 2012). Xanthones have been reported to display various biological activities, including anticholinergic (Negi et al., 2011), immunomodulatory effect (Leiro et al., 2004), antimalarial (Ignatushchenko et al., 2000), anti-inflammatory (Pinto et al., 2005), and anticancer activities (Negi et al., 2013; Shan et al., 2011).

Most of the *Mesua* xanthones are simple oxygenated xanthones, prenylated and related xanthones, as well as bisxanthones. Cyclisation of the prenylated group with a vicinal hydroxyl group lead to the isolation of tetra- or pentacyclic xanthones. "Dimeric xanthones" such as mesuaferrol A and B, mesuabixanthone A and B, which exhibit a more complex structure were also isolated from *Mesua* species (Rouger et al., 2018). The details were presented in Table 2.3.

Table 2.3: Xanthones isolated from *Mesua* genus.

No.	Plant Species	Parts	Chemical Constituents	Molecular Formula	Site collection	References
1.	*M. assamica*	Bark	2-hydroxyxanthone **9**	$C_{13}H_8O_3$	Myanmar	(Gogoi, 2018)
			1,7-dihydroxyxanthone or euxanthone **105**	$C_{13}H_8O_4$		
			5-hydroxy-1-methoxyxanthone **106**	$C_{14}H_{10}O_4$		
2.	*M. beccariana*	Stem bark	6-deoxyjacareubin **152**	$C_{18}H_{14}O_5$	Sarawak, Malaysia	(Teh et al., 2012)
			Mesuarianone **159**	$C_{28}H_{28}O_6$		(Ee et al., 2011; Thiruventhan Karunakaran et al., 2016; Teh et al., 2016; Teh et al., 2010)
			Mesuasinone **160**	$C_{28}H_{30}O_5$		
			Beccarixanthone T **163**	$C_{29}H_{32}O_6$	Sarawak, Malaysia	(Thiruventhan Karunakaran et al., 2016)
			1, 5-dihydroxy xanthone **110**	$C_{13}H_8O_4$		
3.	*M. congestiflora*	Root	α-mangostin **107**	$C_{24}H_{26}O_6$	Sarawak, Malaysia	(Ee, Teh, Kwong, et al., 2012)
4.	*M. corneri*	Stem bark	Inophyllin B **161**	$C_{23}H_{22}O_6$	Pahang, Malaysia	(Ghazali & Izaddin, 2006)
			Rubraxanthone **108**	$C_{24}H_{24}O_6$		
5.	*M. daphnifolia*	Stem bark	Cudraxanthone G **109**	$C_{24}H_{26}O_5$	Pahang, Malaysia	(Ee et al., 2005)
			Ananixanthone **162**	$C_{23}H_{22}O_5$		
			1, 3, 5-trihydroxy-4-methoxyxanthone or daphnifolin **112**	$C_{14}H_{10}O_6$		
			1,7-dihydroxyxanthone or euxanthone **105**	$C_{13}H_8O_4$		
6.	*M. hexapetala*	Stem bark	Trapezifolixanthone **153**	$C_{23}H_{22}O_5$	Sarawak, Malaysia	(T. Karunakaran et al., 2016)
			Cudraxanthone G **109**	$C_{24}H_{26}O_5$		
			1, 3, 7-trihydroxy-2, 4-di (3-methyl-2-butenyl) xanthone **111**	$C_{23}H_{24}O_5$		
7.	*M. myrtifolia*	Timber	Jacareubin **154**	$C_{18}H_{14}O_6$	Sarawak, Malaysia	(Gunasekera & Sultanbawa, 1977)

Table 2.3, continued.

No.	Plant Species	Parts	Chemical Constituents	Molecular Formula	Site collection	References
8.	*M. thwaitesii*	Timber and bark	1, 5-dihydroxy xanthone **110**	$C_{13}H_8O_4$	-	(Bandaranayake et al., 1975)
			1,7-dihydroxyxanthone or euxanthone **105**	$C_{13}H_8O_4$		
			1, 3-dimethoxy-5-hydroxyxanthone **113**	$C_{15}H_{12}O_5$		
			1, 5, 6- trihydroxyxanthone or mesuaxanthone B **114**	$C_{13}H_8O_5$		
9.	*M. ferrea*	Stem bark	1,6-dihydroxyxanthone **115**	$C_{13}H_8O_4$	Pokhara, Nepal	(Singh et al., 1993)
			Pyranojacareubin **164**	$C_{23}H_{20}O_6$		
			Mesuabisxanthone-A **166**	$C_{33}H_{24}O_{12}$		
			Mesuabisxanthone-B **167**	$C_{34}H_{26}O_{12}$		
			Mesuferrol A **168**	$C_{32}H_{22}O_{12}$	East Java, Indonesia	(Iinuma et al., 1996)
			Mesuferrol B **169**	$C_{33}H_{24}O_{12}$		
			1,7-dihydroxyxanthone or euxanthone **105**	$C_{13}H_8O_4$		
			5-hydroxy-1-methoxyxanthone **106**	$C_{14}H_{10}O_4$		
		Heartwood	1,3-dimethoxy-5,6-dihydroxyxanthone or ferrxanthone **116**	$C_{15}H_{12}O_6$	Kerala, India	(Walia & Mukerjee, 1984)
			2-methoxy xanthone **117**	$C_{14}H_{10}O_3$		
			1,7-dihydroxyxanthone or euxanthone **105**	$C_{13}H_8O_4$		
			1, 5, 6- trihydroxyxanthone or mesuaxanthone B **114**	$C_{13}H_8O_5$		
			1, 5-dihydroxy xanthone **110**	$C_{13}H_8O_4$	Kerala & McRitchi Reservoir, India	(Walia & Mukerjee, 1984) (Chow & Quon, 1968)
			1,5-dihydroxy-3-methoxy xanthone or mesuaxanthone A **119**	$C_{14}H_{10}O_5$		

Table 2.3, continued.

No.	Plant Species	Parts	Chemical Constituents	Molecular Formula	Site collection	References
			1-hydroxy-7-methoxy xanthone **121**	$C_{14}H_{10}O_4$		
			1,7-dihydroxyxanthone or euxanthone **105**	$C_{13}H_8O_4$	McRitchi Reservoir, -, Shimoga, Karnataka, India	(Chow & Quon, 1968) (Govindachari, Pai, Subramaniam, Rao, et al., 1967) (Suresh et al., 2014)
			1,5-dihydroxy-3-methoxy xanthone or mesuaxanthone A **119**	$C_{14}H_{10}O_5$	Shimoga, Karnataka, India	(Govindachari, Pai, Subramaniam, Rao, et al., 1967) (Suresh et al., 2014)
			1, 5, 6- trihydroxyxanthone or mesuaxanthone B **114**	$C_{13}H_8O_5$		
		Timber	2-hydroxyxanthone **9**	$C_{13}H_8O_3$	-	(Gunasekera et al., 1975)
			2-methoxy xanthone **117**	$C_{14}H_{10}O_3$		
			4-hydroxy xanthone **118**	$C_{13}H_8O_3$		
			1-hydroxy-5-methoxy xanthone **120**	$C_{14}H_{10}O_4$		
			1-hydroxy-7-methoxy xanthone **121**	$C_{14}H_{10}O_4$		
			3-hydroxy-4-methoxy xanthone **122**	$C_{14}H_{10}O_4$		
			1, 5-dihydroxy xanthone **110**	$C_{13}H_8O_4$		
			1,7-dihydroxyxanthone or euxanthone **105**	$C_{13}H_8O_4$		
			1, 5, 6- trihydroxyxanthone or mesuaxanthone B **114**	$C_{13}H_8O_5$		
			1,3,6-trihydroxy-7,8-dimethoxy xanthone **123**	$C_{15}H_{12}O_7$		
			3,6-dihydroxy-1,7,8-trimethoxy xanthone **124**	$C_{16}H_{14}O_7$		
		Root bark	Mesuaferrin C **170**	$C_{24}H_{26}O_6$	Selangor, Malaysia	(Teh et al., 2013) (Ee, Teh, Rahmani, et al., 2012)
			Caloxanthone C **155**	$C_{23}H_{22}O_5$		
			Macluraxanthone **156**	$C_{23}H_{22}O_6$		
			Mesuaferrin A **171**	$C_{23}H_{22}O_6$	-	(Teh et al., 2013)

Table 2.3, continued.

No.	Plant Species	Parts	Chemical Constituents	Molecular Formula	Site collection	References
			Mesuaferrin B **172**	$C_{23}H_{20}O_6$		
			1, 5-dihydroxy xanthone **110**	$C_{13}H_8O_4$		
			Tovopyrifolin C **125**	$C_{14}H_{10}O_6$		
		Root	4-methoxypyranojacareubin **165**	$C_{24}H_{22}O_6$	Trang Thailand	(Chukaew et al., 2019)
			4-hydroxy-3-prenylpyranoxanthone **157**	$C_{23}H_{22}O_5$		
			1-hydroxy-5,7-dimethoxyxanthone **126**	$C_{15}H_{12}O_5$		
			5-hydroxy-1,6,7-trimethoxyxanthone **127**	$C_{16}H_{14}O_6$		
			2-hydroxy-1,5-dimethoxyxanthone **128**	$C_{15}H_{12}O_5$		
			Pyranojacareubin **164**	$C_{23}H_{20}O_6$		
			Rheediachromenoxanthone **158**	$C_{18}H_{14}O_5$		
			1,4-dihydroxyxanthone **129**	$C_{13}H_8O_4$		
			1-hydroxy-4-methoxyxanthone **130**	$C_{14}H_{10}O_4$		
			4-hydroxy xanthone **118**	$C_{13}H_8O_3$		
			1, 5-dihydroxy xanthone **110**	$C_{13}H_8O_4$		
			1-hydroxy-5-methoxy xanthone **120**	$C_{14}H_{10}O_4$		
			4-methoxyxanthone **131**	$C_{14}H_{10}O_3$		
			1,6-dihydroxyxanthone **115**	$C_{13}H_8O_4$		
			1, 5, 6- trihydroxyxanthone or mesuaxanthone B **114**	$C_{13}H_8O_5$		
			1,6-dihydroxy-5-methoxyxanthone **132**	$C_{14}H_{10}O_5$		
			6-hydroxy-1,5-dimethoxyxanthone **133**	$C_{15}H_{12}O_5$		
			2,5-dihydroxy-1-methoxyxanthone **134**	$C_{14}H_{10}O_5$		
			5-hydroxy-1,6-dimethoxyxanthone **135**	$C_{15}H_{12}O_5$		
			1,5-dihydroxy-6-methoxyxanthone **136**	$C_{14}H_{10}O_5$		
			1-hydroxy-5,6-dimethoxyxanthone **137**	$C_{15}H_{12}O_5$		

Table 2.3, continued.

No.	Plant Species	Parts	Chemical Constituents	Molecular Formula	Site collection	References
			3,4-dimethoxyxanthone **138**	$C_{15}H_{12}O_4$		
			2-hydroxyxanthone **9**	$C_{13}H_8O_3$		
			2-methoxy xanthone **117**	$C_{14}H_{10}O_3$		
			1-hydroxy-7-methoxy xanthone **121**	$C_{14}H_{10}O_4$		
			1-hydroxy-6,7-dimethoxyxanthone **139**	$C_{15}H_{12}O_5$		
			2,3,4-trimethoxyxanthone **140**	$C_{16}H_{14}O_5$		
			1,8-dihydroxy-2-methoxyxanthone **141**	$C_{14}H_{10}O_5$		
			1,3,8-trihydroxy-2-methoxyxanthone **142**	$C_{14}H_{10}O_6$		
			1-hydroxy-2,5-dimethoxyxanthone **143**	$C_{15}H_{12}O_5$		
			1-hydroxy-3,5-dimethoxyxanthone **144**	$C_{15}H_{12}O_5$		
			1,5-dihydroxy-3-methoxy xanthone or mesuaxanthone A **119**	$C_{14}H_{10}O_5$		
			2-hydroxy-1-methoxyxanthone **145**	$C_{14}H_{10}O_4$		
			1,2-dimethoxyxanthone **146**	$C_{15}H_{12}O_4$		
			1-hydroxy-7,8-dimethoxyxanthone **147**	$C_{15}H_{12}O_5$		
			5-hydroxy-1,2-dimethoxyxanthone **148**	$C_{15}H_{12}O_5$		
			5-hydroxy-1-methoxyxanthone **106**	$C_{14}H_{10}O_4$		
			1, 3-dimethoxy-5-hydroxyxanthone **113**	$C_{15}H_{12}O_5$		
		bark	Mesuaferrin A **171**	$C_{23}H_{22}O_6$	Visakhapatnam, India	(Chaithanya et al., 2018; Krishna Chaithanya et al., 2019)
		twigs	5-hydroxy-1,6-dimethoxyxanthone **135**	$C_{15}H_{12}O_5$	Trang, Thailand	(Chakthong et al., 2020)
			5-hydroxy-1,3,6,7-tetramethoxyxanthone **149**	$C_{17}H_{17}O_7$		
			1, 5, 6- trihydroxyxanthone or mesuaxanthone B **114**	$C_{13}H_8O_5$		
			1,3,7-trihydroxyxanthone **150**	$C_{13}H_8O_5$		

Table 2.3, continued.

No.	Plant Species	Parts	Chemical Constituents	Molecular Formula	Site collection	References
			1,7-dihydroxy-3-methoxyxanthone **151**	$C_{14}H_{10}O_5$		
		flowers	1,7-dihydroxyxanthone or euxanthone **105**	$C_{13}H_8O_4$	Nakhon Si Thammarat, Thailand	(Manse et al., 2022)
			1,3,7-trihydroxyxanthone **150**	$C_{13}H_8O_5$		

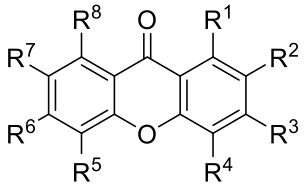

No.	R^1	R^2	R^3	R^4	R^5	R^6	R^7	R^8
9	H	OH	H	H	H	H	H	H
105	OH	H	H	H	H	H	OH	H
106	OCH_3	H	H	H	OH	H	H	H
107	OH	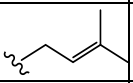	OH	H	H	OH	OCH_3	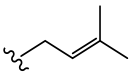
108	OH	H	OH	H	H	OH	OCH_3	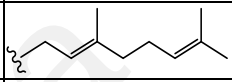
109	OH	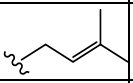	OCH_3	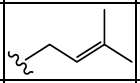	OH	H	H	H
110	OH	H	H	H	OH	H	H	H
111	OH	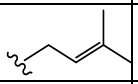	OH	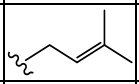	H	H	OH	H
112	OH	H	OH	OCH_3	OH	H	H	H
113	OCH_3	H	OCH_3	H	OH	H	H	H
114	OH	H	H	H	OH	OH	H	H
115	OH	H	H	H	H	OH	H	H
116	OCH_3	H	OCH_3	H	OH	OH	H	H
117	H	OCH_3	H	H	H	H	H	H
118	H	H	H	OH	H	H	H	H
119	OH	H	OCH_3	H	OH	H	H	H
120	OH	H	H	H	OCH_3	H	H	H
121	OH	H	H	H	H	H	OCH_3	H

Figure 2.2: Structures of xanthones isolated from *Mesua* genus.

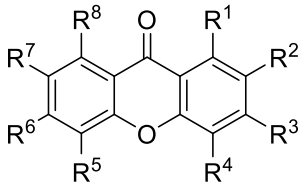

No.	R^1	R^2	R^3	R^4	R^5	R^6	R^7	R^8
122	H	H	OH	OCH_3	H	H	H	H
123	OH	H	OH	H	H	OH	OCH_3	OCH_3
124	OCH_3	H	OH	H	H	OH	OCH_3	OCH_3
125	OH	OCH_3	OH	H	OH	H	H	H
126	OH	H	H	H	OCH_3	H	OCH_3	H
127	OCH_3	H	H	H	OH	OCH_3	OCH_3	H
128	OCH_3	OH	H	H	OCH_3	H	H	H
129	OH	H	H	OH	H	H	H	H
130	OH	H	H	OCH_3	H	H	H	H
131	H	H	H	OCH_3	H	H	H	H
132	OH	H	H	H	OCH_3	OH	H	H
133	OCH_3	H	H	H	OCH_3	OH	H	H
134	OCH_3	OH	H	H	OH	H	H	H
135	OCH_3	H	H	H	OH	OCH_3	H	H
136	OH	H	H	H	OH	OCH_3	H	H
137	OH	H	H	H	OCH_3	OCH_3	H	H
138	H	H	OCH_3	OCH_3	H	H	H	H
139	OH	H	H	H	H	OCH_3	OCH_3	H
140	H	OCH_3	OCH_3	OCH_3	H	H	H	H
141	OH	OCH_3	H	H	H	H	H	OH
142	OH	OCH_3	OH	H	H	H	H	OH

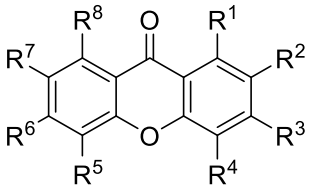

No.	R^1	R^2	R^3	R^4	R^5	R^6	R^7	R^8
143	OH	OCH_3	H	H	OCH_3	H	H	H
144	OH	H	OCH_3	H	OCH_3	H	H	H
145	OCH_3	OH	H	H	H	H	H	H
146	OCH_3	OCH_3	H	H	H	H	H	H
147	OH	H	H	H	H	H	OCH_3	OCH_3
148	OCH_3	OCH_3	H	H	OH	H	H	H
149	OCH_3	H	OCH_3	H	OH	OCH_3	OCH_3	H
150	OH	H	OH	H	H	H	OH	H
151	OH	H	OCH_3	H	H	H	OH	H

Figure 2.2, continued.

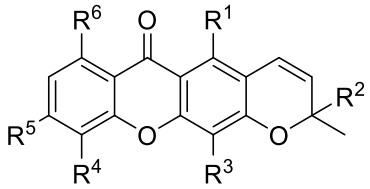

No.	R^1	R^2	R^3	R^4	R^5	R^6
152	OH	CH_3	H	OH	H	H
153	OH	CH_3	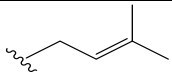	OH	H	H
154	OH	CH_3	H	OH	OH	H
155	OH	CH_3	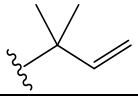	OH	H	H
156	OH	CH_3	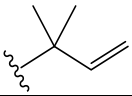	OH	OH	H
157	H	CH_3	H	OH	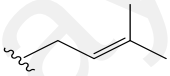	H
158	H	CH_3	OH	H	H	OH

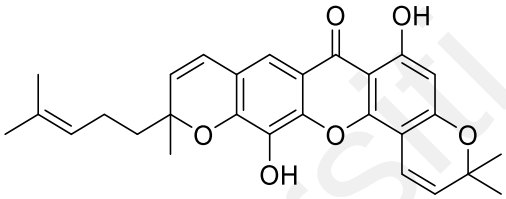

159

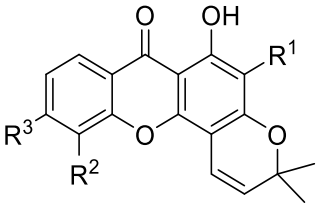

No.	R^1	R^2	R^3
160	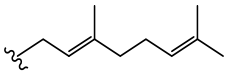	H	OH
161	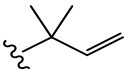	OH	OH
162	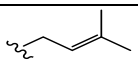	OH	H

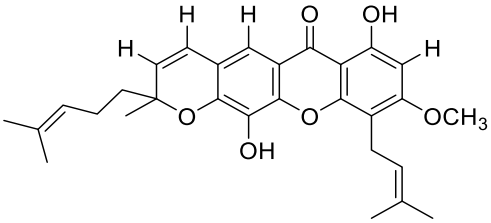

163

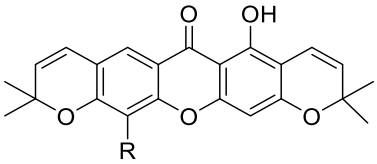

No.	R
164	OH
165	OCH_3

Figure 2.2, continued.

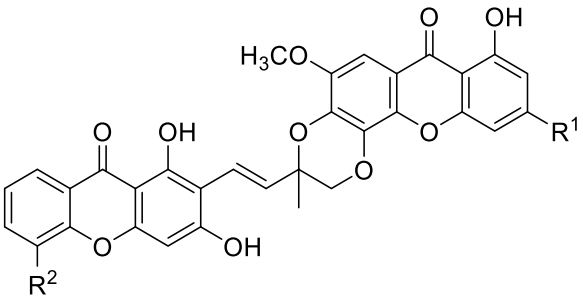

No.	R^1	R^2
166	OCH_3	OH
167	OCH_3	OCH_3
168	OH	OH
169	OH	OCH_3

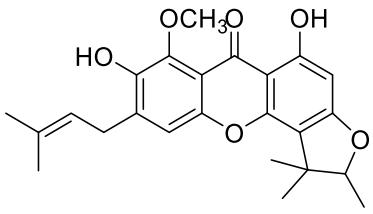

170

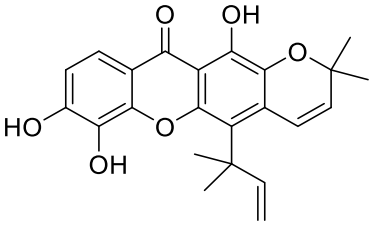

171

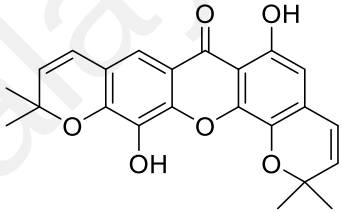

172

Figure 2.2, continued.

(a) ***Biosynthetic pathway of xanthones***

The oxygenation patterns of xanthones in higher plants suggest that the biosynthesis of xanthones origin from a mixed shikimate-acetate pathway (Peres et al., 2000). Phenylalanine, derived from shikimate, loses two carbon atoms from the side chain, and oxidized to form *m*-hydroxybenzoic acid (Negi et al., 2013). Then an intermediate is formed by adding three malonyl-CoA units to a precursor in C6–C1 of the benzoic acid (Negi et al., 2013). Cyclisation of the shikimate-acetate intermediate form a substituted benzophenone, through regioselective intermolecular oxidative phenol coupling yields the central ring of the xanthone moiety (El-Seedi et al., 2010; Peres et al., 2000). Different ways of the oxidative coupling leading to two types of folding of the benzophenone, which is in the ortho or in the para position to the hydroxyl substituent in ring B to form

1,3,5-trihydroxyxanthone or 1,3,7-trihydroxyxanthone **150**, respectively (Scheme 2.2) (Negi et al., 2013; Rouger, 2015).

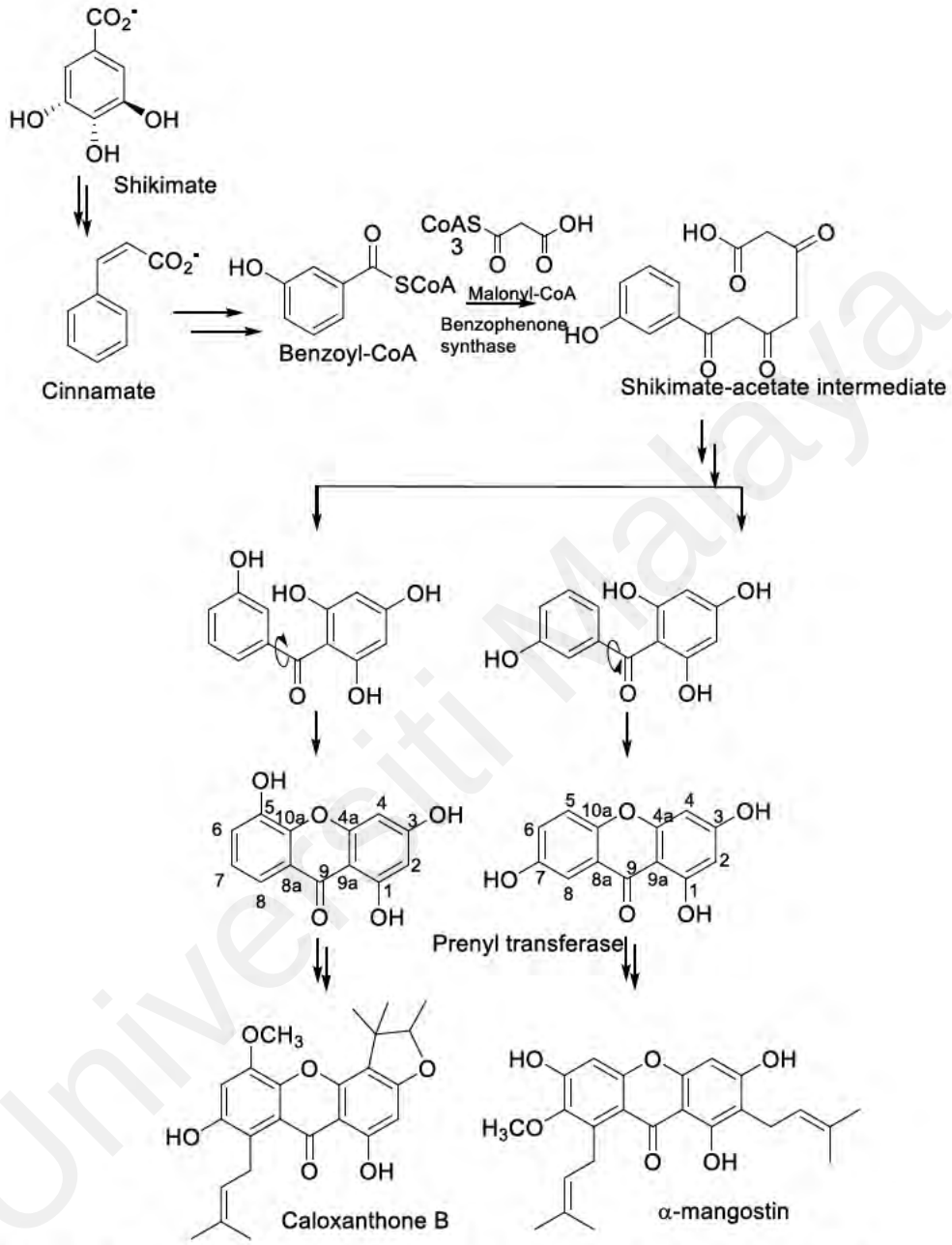

Scheme 2.2: Biosynthesis pathway of xanthones (Negi et al., 2013; Rouger, 2015).

2.1.1.3 Triterpenes and sterols isolated.

Mesua species exude essential oil and oleo-gum resin which lead to the existence of terpenoid compounds in the plant species (Rouger et al., 2018). Triterpene is a 30-carbon compound originated from the 5-carbon isoprene units (Hill & Connolly, 2017). The

triterpenes from *Mesua* are simple pentacyclic triterpenoids which play crucial functions in plant growth and organ development processes. For instance, *β*-amyrin **195** involve in root growth, root development and flowering (Ghosh, 2017).

Sterols and triterpenes are biosynthesized from mevalonate pathway (Thimmappa et al., 2014). Unlike triterpenes, sterols may serve as hormones and are involved in the structural arrangement of membrane in plants. Sitosterol **174** is the most found sterol in higher plants, apart from that, stigmasterol **173** is also very common (Grunwald, 1975). Table 2.4 recorded the isolated sterols and triterpenes from *Mesua*.

Table 2.4: Terpenes and sterols isolated from *Mesua* genus.

No.	Plant Species	part	Chemical Constituents	Molecular Formula	Site collection	References
1.	*M. beccariana*		Stigmasterol **173**	$C_{29}H_{48}O$	Sarawak, Malaysia	(Teh et al., 2012; Teh et al., 2010)
			Betulinic acid **177**	$C_{30}H_{48}O_3$		
			Friedelin **186**	$C_{30}H_{50}O$		(Teh et al., 2010)
			β-sitosterol **174**	$C_{29}H_{50}O$	Sarawak, Malaysia	(Thiruventhan Karunakaran et al., 2016)
			γ-sitosterol **175**	$C_{29}H_{50}O$		
2.	*M. corneri*		Stigmasterol **173**	$C_{29}H_{48}O$	Kuala Lumpur, Malaysia	(Ghazali & Izaddin, 2006)
			Friedelin **186**	$C_{30}H_{50}O$		
			Friedelan-1, 3-Dione **187**	$C_{30}H_{48}O_2$		
3.	*M. daphnifolia*		Friedelin **186**	$C_{30}H_{50}O$	Pahang, Malaysia	(Ee et al., 2005)
			Friedelan-1, 3-Dione **187**	$C_{30}H_{48}O_2$		
			Lupeol or Lup-20(29)-en-3*β*-ol **178**	$C_{30}H_{50}O$		
4.	*M. hexapetala*		Friedelin **186**	$C_{30}H_{50}O$	Sarawak, Malaysia	(T. Karunakaran et al., 2016)
			Stigmasterol **173**	$C_{29}H_{48}O$		
			β-sitosterol **174**	$C_{29}H_{50}O$		
			γ-sitosterol **175**	$C_{29}H_{50}O$		
5.	*M. kunstleri*	twigs	Lupeol or Lup-20(29)-en-3*β*-ol **178**	$C_{30}H_{50}O$	Songkhla, Thailand	(Panthong & Boonsri, 2018)
			Betulin **179**	$C_{30}H_{50}O_2$		
			Lup-20(29)-ene-3*β*,16*β*,28-triol **180**	$C_{30}H_{50}O_3$		
			Lupenone **181**	$C_{30}H_{48}O$		
			Lup-20(29)-ene-3*β*,16*β*-diol **182**	$C_{30}H_{50}O_2$		
			Betulinaldehyde **183**	$C_{30}H_{48}O_2$		
			Betulinic acid **177**	$C_{30}H_{48}O_3$		
			(2α,3β)-2,3-Dihydroxylup-20(29)-en-28-oic acid **184**	$C_{30}H_{48}O_4$		

Table2.4, continued.

No.	Plant Species	part	Chemical Constituents	Molecular Formula	Site collection	References
6.	*M. myrtifolia*		Simiarenone **190**	$C_{30}H_{48}O$	Sarawak, Malaysia	(Gunasekera & Sultanbawa, 1977)
			Simiarenol **191**	$C_{30}H_{50}O$		
			Taraxerol **192**	$C_{30}H_{50}O$		
			Betulinic acid **177**	$C_{30}H_{48}O_3$		
			β-sitosterol **174**	$C_{29}H_{50}O$		
			Myrtifolic acid **188**	$C_{30}H_{48}O_3$		
			Oleanolic acid **193**	$C_{30}H_{48}O_3$		
7.	*M. nagassarium*		Friedelin **186**	$C_{30}H_{50}O$	-	(Ridwan Islam, 2014)
			3*β*-friedelanol **189**	$C_{30}H_{52}O$		
			Lupeol or Lup-20(29)-en-3*β*-ol **178**	$C_{30}H_{50}O$		
			3-oxo-betulin **185**	$C_{30}H_{48}O_2$		
			Spinasterol **176**	$C_{29}H_{48}O$		
8.	*M. thwaitesii*		*β*-sitosterol **174**	$C_{29}H_{50}O$	-	(Bandaranayake et al., 1975)
9.	*M. ferrea*		Betulinic acid **177**	$C_{30}H_{48}O_3$	Pokhara, Nepal	(Singh et al., 1993)
			Friedelin **186**	$C_{30}H_{50}O$	Chiang Mai, Thailand	(Keawsa-Ard et al., 2015)
			β-sitosterol **174**	$C_{29}H_{50}O$		
			α-amyrin **194**	$C_{30}H_{50}O$		
			β-amyrin **195**	$C_{30}H_{50}O$		
			Lupeol or Lup-20(29)-en-3*β*-ol **178**	$C_{30}H_{50}O$		
			β-amyrin **195**	$C_{30}H_{50}O$	Ranikhet, & Shimoga, Karnataka, India	(Dennis et al., 1988) (Raju et al., 1976) (Suresh et al., 2014)
			β-sitosterol **174**	$C_{29}H_{50}O$		
			α-amyrin **194**	$C_{30}H_{50}O$	Ranikhet, India	(Raju et al., 1976)
			β-sitosterol **174**	$C_{29}H_{50}O$	Kerala & McRitchi Reservoir, India	(Walia & Mukerjee, 1984) (Chow & Quon, 1968)
			Stigmasterol **173**	$C_{29}H_{48}O$	Kerala, India	(Walia & Mukerjee, 1984)
			β-sitosterol **174**	$C_{29}H_{50}O$	-	(Gunasekera et al., 1975)

Table2.4, continued.

No.	Plant Species	part	Chemical Constituents	Molecular Formula	Site collection	References
			β-sitosterol **174**	$C_{29}H_{50}O$	-	(Verotta et al., 2004)
			β-sitosterol **174**	$C_{29}H_{50}O$	Selangor, Malaysia	(Ee, Teh, Rahmani, et al., 2012)
			Friedelin **186**	$C_{30}H_{50}O$		
			Betulinic acid **177**	$C_{30}H_{48}O_3$		
		flowers	Lupeol or Lup-20(29)-en-3*β*-ol **178**	$C_{30}H_{50}O$	Nakhon Si Thammarat Province of Thailand	(Manse et al., 2022)
			Betulinaldehyde **183**	$C_{30}H_{48}O_2$		
			Ursolic acid **196**	$C_{30}H_{48}O_3$		

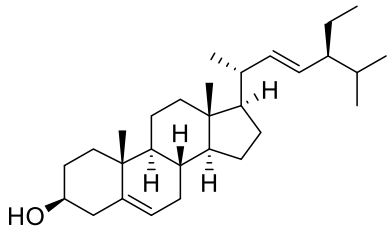

173

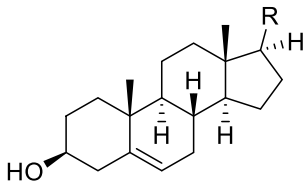

No.	R
174	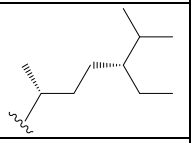
175	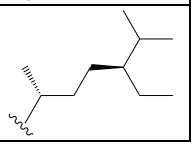

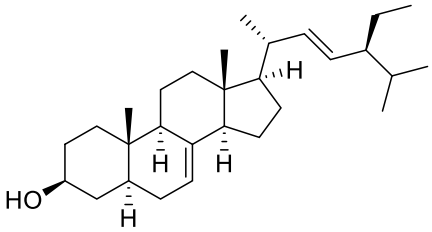

176

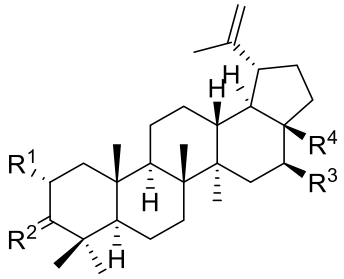

No.	R^1	R^2	R^3	R^4
177	H	OH, H	H	COOH
178	H	OH, H	H	CH_3
179	H	OH, H	H	CH_2OH
180	H	OH, H	OH	CH_2OH
181	H	OH, H	H	CH_3
182	H	OH, H	OH	CH_3
183	H	OH, H	H	CHO
184	OH	OH, H	H	COOH
185	H	O	H	CH_2OH

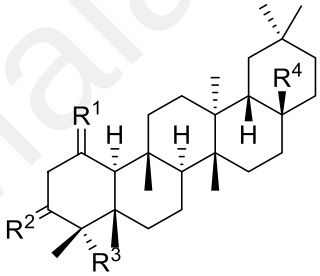

No.	R^1	R^2	R^3	R^4
186	H, H	O	H	CH_3
187	O	O	H	CH_3
188	H, H	OH, H	H	CH_3
189	H, H	OH, H	CH_3	COOH

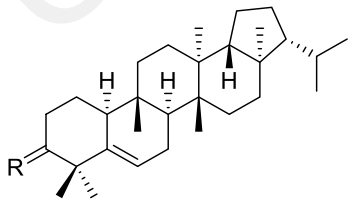

No.	R
190	O
191	OH, H

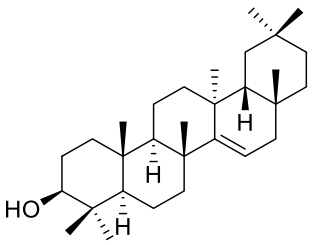

192

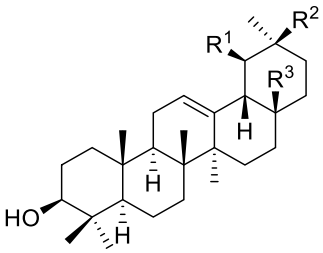

No.	R^1	R^2	R^3
193	H	CH_3	COOH
194	CH_3	H	CH_3
195	H	CH_3	CH_3
196	CH_3	H	COOH

Figure 2.3: Structures of triterpenes and sterols isolated from *Mesua* genus.

(a) ***Biosynthesis pathway of sterols and triterpenes***

Although both triterpenes and sterols are isoprenoids that are synthesized *via* the same mevalonate pathway (Thimmappa et al., 2014), there is a distinction between sterols and triterpenes in which these molecules are synthesized. The difference involved the cyclization of 2,3-oxidosqualene, the precursor, to sterol or triterpene products. Cyclization is one of the most remarkable enzymatic reactions known in terpene metabolism.

In sterol biosynthesis, 2, 3-oxidosqualene is cyclized to the sterol cycloartenol *via* the chair-boat-chair conformation. In contrast, this substrate is folded into the chair-chair-chair conformation in triterpene biosynthesis. The conformation prior to cyclization into a various triterpene skeletal, *β*-amyrin **195** is shown as an example in Scheme 2.3 (Thimmappa et al., 2014).

In the cyclization process, 2,3-oxidosqualene is catalyzed by oxidosqualene cyclases (OSCs) to a variety of cyclic triterpene scaffolds (Misra et al., 2014; Thimmappa et al., 2014; Ghosh, 2016). In most cases, the cyclic triterpene scaffolds derived from the OSC-catalyzed reactions undergo a plethora of scaffold-, regio-, and stereo-specific oxidations catalyzed by the cytochrome P450 monooxygenases (P450s), leading to triterpene scaffold decoration with various functional groups such as hydroxyl, carbonyl, carboxyl, and epoxy moieties (Ghosh, 2017).

Besides the first diversifying step of the triterpene biosynthetic pathway, the class II terpene synthases also mark the branch point for the biosynthesis of the sterols and steroid hormones (Thimmappa et al., 2014; Ghosh, 2016).

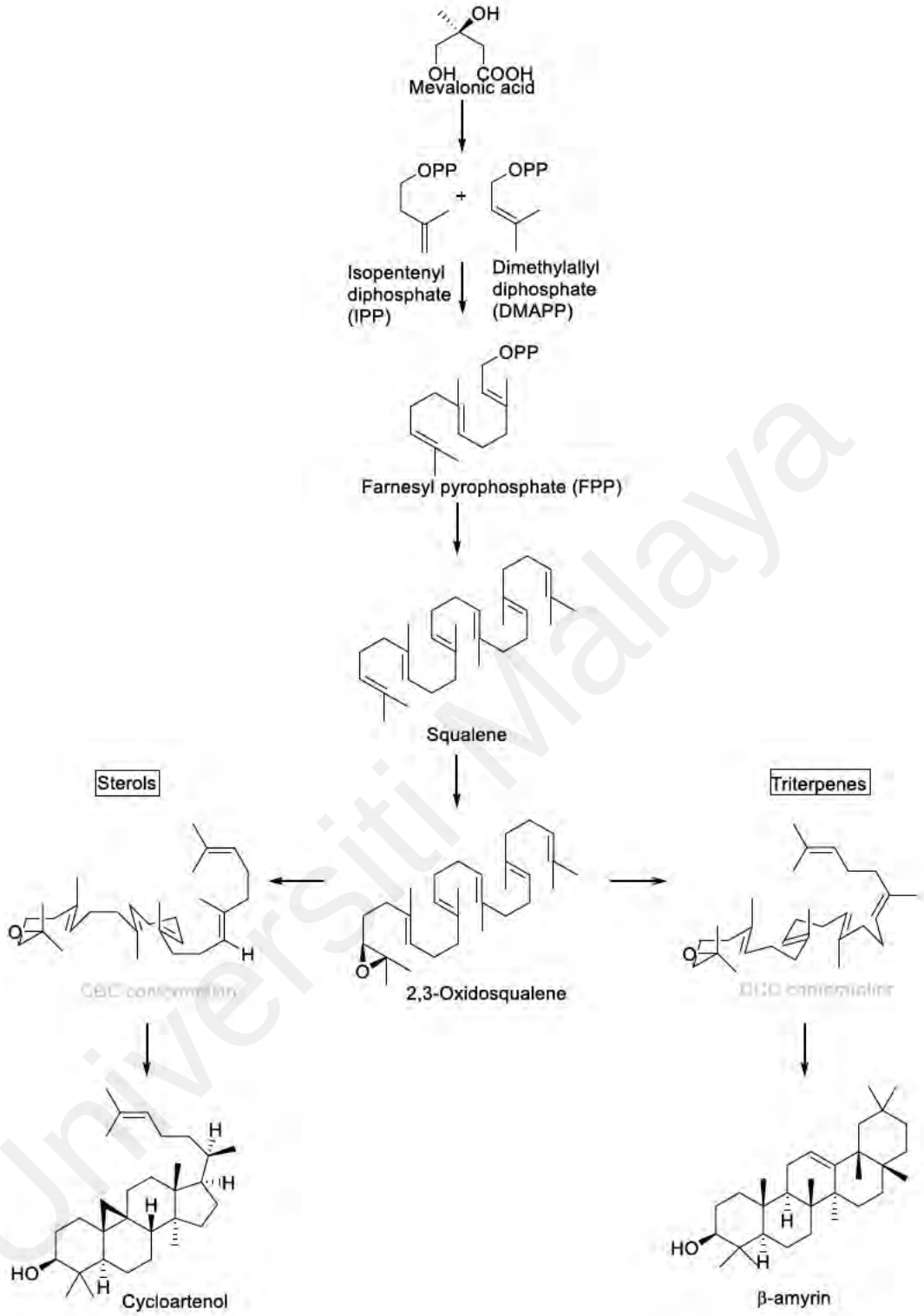

Scheme 2.3: Biosynthesis pathway of sterols and triterpenes (Thimmappa et al., 2014).

2.1.1.4 Other chemical substituents isolated from *Mesua* genus.

Besides the aforementioned types of metabolites, chromanone acids, flavones, PPAPs, *etc*. were reported too. The details of the chemical substituents were demonstrated in Table 2.5.

Table 2.5: Other chemical constituents isolated from *Mesua* genus.

No.	Plant Species	Site collection	Parts	Type	Chemical Constituents	Molecular Formula	References
1.	*M. beccariana*	Sarawak, Malaysia	Stem bark	Anthraquinone	4-methoxy-1, 3, 5-trihydroxyanthraquinone **197**	$C_{15}H_{10}O_6$	(Ee et al., 2011; Teh et al., 2012; Teh et al., 2010)
					2, 5-dihydroxy-1, 3, 4-trimethoxyanthraquinone **198**	$C_{17}H_{14}O_7$	
				Cyclodione	Mesuadione **200**	$C_{16}H_{24}O_4$	(Teh et al., 2012)
2.	*M. calophylloides*	Kalimantan, Indonesia	Stem bark	Chromanone acid	Calolongic acid **201**	$C_{22}H_{28}O_6$	(Tanjung et al., 2018)
					Isocalolongic acid **202**	$C_{22}H_{28}O_6$	
3.	*M. congestiflora*	Sarawak, Malaysia	Root	Benzophenone	Congestiflorone **215**	$C_{28}H_{32}O_4$	(Ee, Teh, Kwong, et al., 2012)
4.	*M. ferrea*	Pokhara, Nepal & East Java, Indonesia	Stem bark	Flavanols	(-)-epicatechin **205**	$C_{15}H_{14}O_6$	(Singh et al., 1993) (Iinuma et al., 1996)
		-	Leave	Flavone glycoside	Mesuein **206**	$C_{28}H_{34}O_{15}$	(Alam et al., 1987)
		-	Stamens	Cyclohexadione	Mesuaferrol **203**	$C_{35}H_{46}O_6$	(Dennis et al., 1988)
		Ranikhet, & Karnataka, India		Biflavonoid	Mesuaferrone A **212**	$C_{30}H_{22}O_{10}$	(Raju et al., 1976) (Suresh et al., 2014)
					Mesuaferrone B **213**	$C_{30}H_{20}O_{10}$	
				Chromanone acid	Mesuanic acid **204**	$C_{35}H_{46}O_6$	
		Sarawak, Malaysia	Root bark	Anthraquinone	1,8-dihydro-3-methoxy-6-methylanthraquinone **199**	$C_{16}H_{12}O_5$	(Teh et al., 2011)
		Kelantan, Malaysia	Bark	PPAP	Mesuaferroic acid A **216**	$C_{35}H_{46}O_7$	(Rasol et al., 2017)
					Mesuaferroic acid B **225**	$C_{35}H_{46}O_7$	
					Mesuaferroic acid C **217**	$C_{35}H_{46}O_7$	
					Mesuaferroic acid E **218**	$C_{35}H_{48}O_9$	
					Mesuaferroic acid F **219**	$C_{35}H_{46}O_7$	

Table2.5, continued.

No.	Plant Species	Site collection	Parts	Type	Chemical Constituents	Molecular Formula	References
		Shan, Myanmar	Flowers	PPAP	Mesuaferroic acid H **226**	$C_{36}H_{48}O_6$	(Zhang et al., 2020)
					Mesuaferroic acid I **221**	$C_{35}H_{46}O_7$.	
					Mesuaferroic acid J **220**	$C_{35}H_{46}O_8$	
					Mesuaferroic acid K **222**	$C_{35}H_{46}O_8$	
					Mesuaferroic acid L **223**	$C_{35}H_{46}O_7$	
					Mesuaferroic acid C **217**	$C_{35}H_{46}O_7$	
					Laxifloranone **224**	$C_{35}H_{46}O_6$	
		Shan, Myanmar	Flowers	Flavonoid	Kaempferol 3-*O*-rhamnoside **207**	$C_{21}H_{20}O_{10}$	(Zhang et al., 2019)
				Flavonoid	Quercitrin or quercetin 3-*O*-rhamnoside **208**	$C_{21}H_{20}O_{11}$	
				Flavonoid	Quercetin **6**	$C_{15}H_{10}O_7$	
				Biflavonoid	Rhusflavanone **214**	$C_{30}H_{22}O_{10}$	
				Biflavonoid	Mesuaferrone B **213**	$C_{30}H_{20}O_{10}$	
				Phenolic	5,6,6'-trihydroxy [1.1'-biphenyl]-3,3'- dicarboxylic acid **227**	$C_{14}H_9O_7$	
				Phenolic	3-amino-4-hydroxybenzoic acid **228**	$C_7H_7NO_3$	
				Phenolic	Protocatechuic acid **229**	$C_7H_6O_4$	
				Phenolic	Gallic acid **230**	$C_7H_6O_5$	
				Phenolic	Protocatechuic acid ethyl ester **231**	$C_9H_{10}O_4$	

Table2.5, continued.

No.	Plant Species	Site collection	Parts	Type	Chemical Constituents	Molecular Formula	References
			Stamens	Biflavonoid	Rhusflavanone **214**	$C_{30}H_{22}O_{10}$	(Zar Wynn Myint et al., 2019)
					Mesuaferrone B **213**	$C_{30}H_{20}O_{10}$	
				Phenolic	Gallic acid **230**	$C_7H_6O_5$	
				Phenolic	Benzyl-β-D-glucopyranoside **233**	$C_{13}H_{18}O_6$	
				Phenolic	Protocatechuic acid **229**	$C_7H_6O_4$	
				Phenolic	Protocatechuic acid ethyl ester **231**	$C_8H_8O_4$	
				Phenolic	*p*-Hydroxybenzoic acid **232**	$C_7H_6O_3$	
				Flavonoid	Apigenin 8-*C*-glucoside **209**	$C_{21}H_{20}O_{10}$	
					Quercitrin or quercetin 3-*O*-rhamnoside **208**	$C_{21}H_{20}O_{11}$	
					Kaempferol 3-*O*-rhamnoside **207**	$C_{21}H_{20}O_{10}$	
					Kaempferol 3-*O*-glucoside **211**	$C_{21}H_{20}O_{11}$	
					Luteolin 8-*C*-glucoside **210**	$C_{21}H_{20}O_{11}$	
		Nakhon Si Thammarat Province of Thailand	Flowers	Biflavonoid	Mesuaferrone A **212**	$C_{30}H_{22}O_{10}$	(Manse et al., 2022)
					Mesuaferrone B **213**	$C_{30}H_{20}O_{10}$	
				Flavonoid	Apigenin **234**	$C_{15}H_{10}O_5$	
					Luteolin **235**	$C_{15}H_{10}O_6$	
					Vitexin **236**	$C_{21}H_{20}O_{10}$	
					Orientin **237**	$C_{21}H_{20}O_{11}$	
					Saponaretin **238**	$C_{21}H_{20}O_{10}$	
					Homoorientin **239**	$C_{21}H_{20}O_{11}$	
					Apigenin-7-*O*-rutinoside **240**	$C_{27}H_{30}O_{14}$	
					Quercetin **6**	$C_{15}H_{10}O_7$	

Table2.5, continued.

No.	Plant Species	Site collection	Parts	Type	Chemical Constituents	Molecular Formula	References
					kaempferol-3-*O*-α-L-rhamnopyranoside **241**	$C_{21}H_{20}O_{10}$	
					Quercetin-3-*O*-α-L-rhamnopyranoside **242**	$C_{21}H_{20}O_{11}$	
				Phenylpropanoid	*Trans*-cinnamic acid **243**	$C_9H_8O_2$	
				Phenolic	*p*-Hydroxybenzoic acid **232**	$C_7H_6O_3$	
					Protocatechuic acid **229**	$C_7H_6O_4$	
					Vanillic acid **244**	$C_8H_8O_4$	
					Protocatechuic aldehyde **245**	$C_7H_6O_3$	
					Gallic acid **230**	$C_7H_6O_5$	

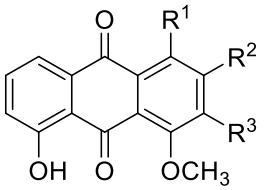

No.	R^1	R^2	R^3
197	OH	H	OH
198	OCH_3	OH	OCH_3

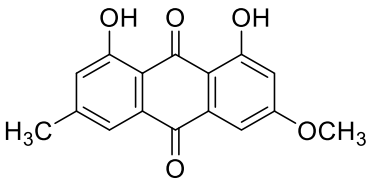

199

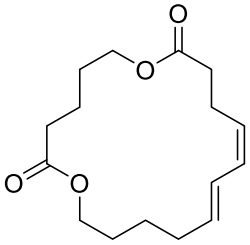

200

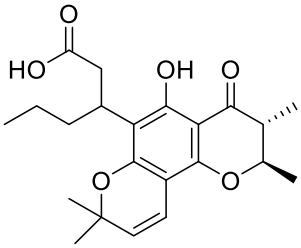

201

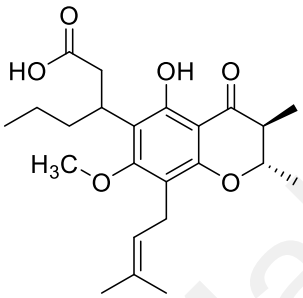

202

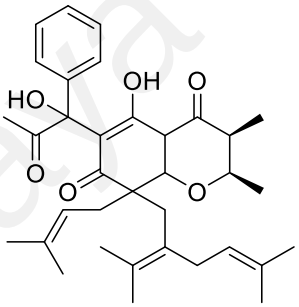

203

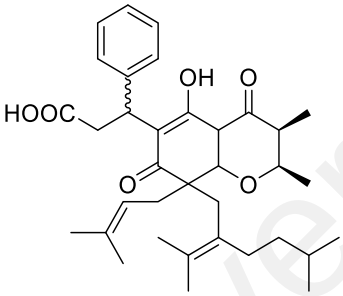

204

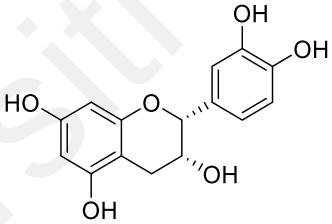

205

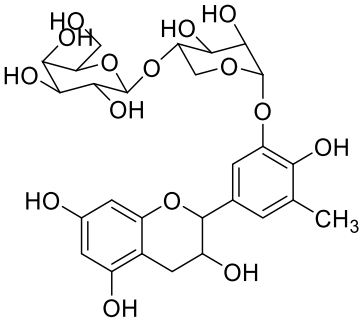

206

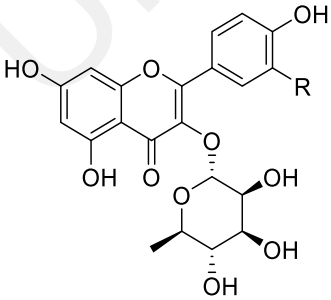

No.	R
207	H
208	OH

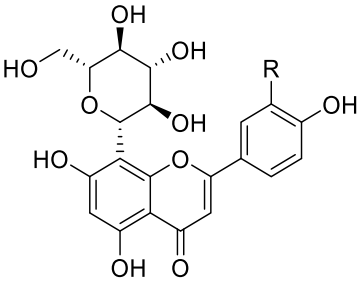

No.	R
209	H
210	OH

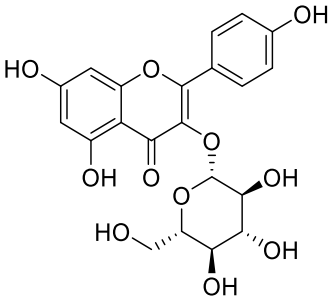

211

Figure 2.4: Structures of the chemical constituents isolated from *Mesua* genus.

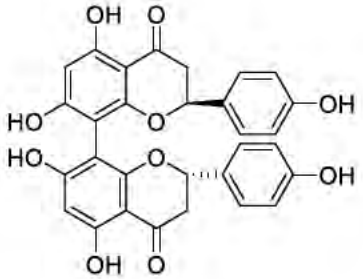

212

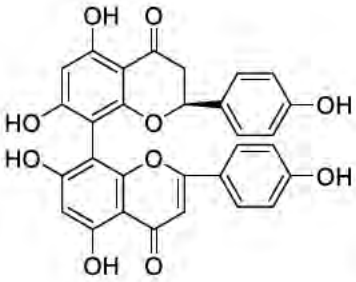

213

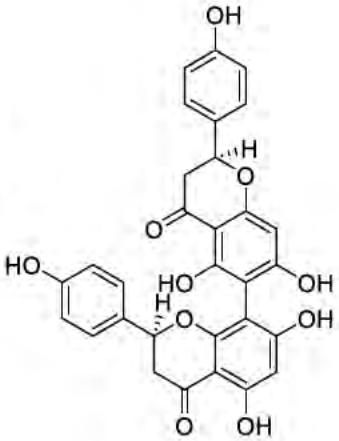

214

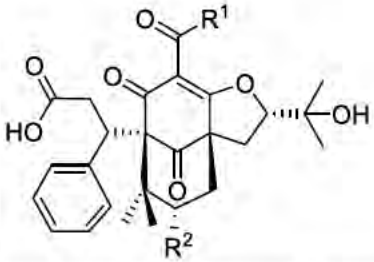

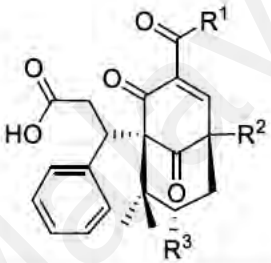

No.	R^1	R^2
216	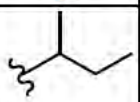	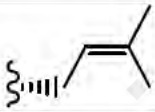
217	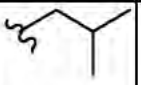	
218	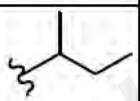	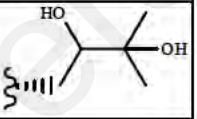
219		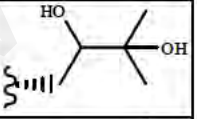
220	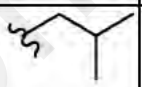	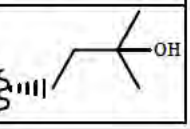

No.	R^1	R^2	R^3
221	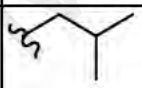	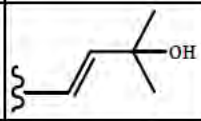	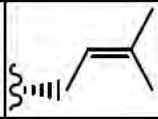
222	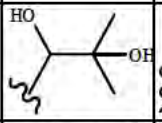	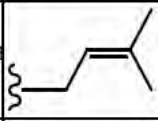	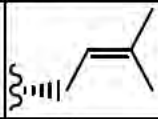
223	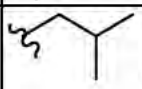	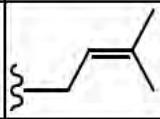	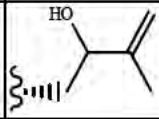
224	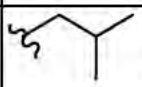	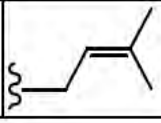	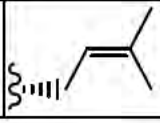

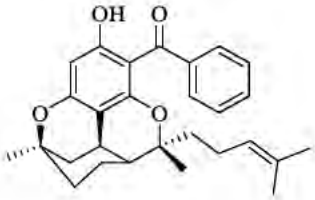

215

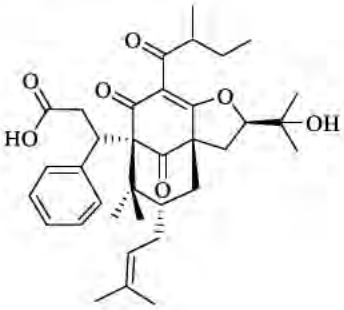

225

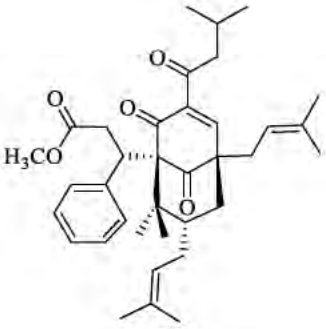

226

Figure 2.4, continued.

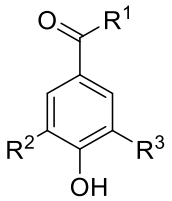

No.	R^1	R^2	R^3
227	OH	H	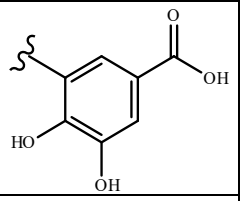
228	OH	H	NH_2
229	OH	H	OH
230	OH	OH	OH
231	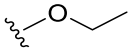	OH	OH
232	OH	H	H
244	OH	H	OCH_3
245	H	H	OH

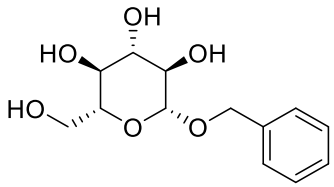

233

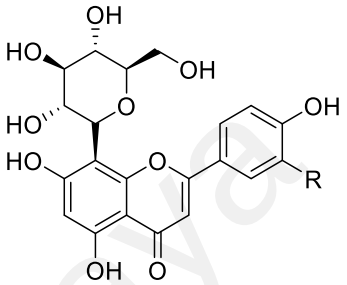

No.	R
236	H
237	OH

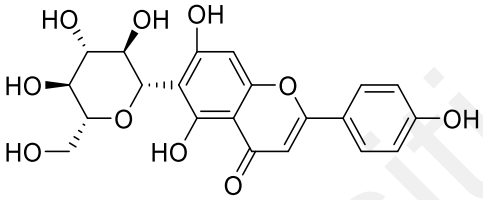

238

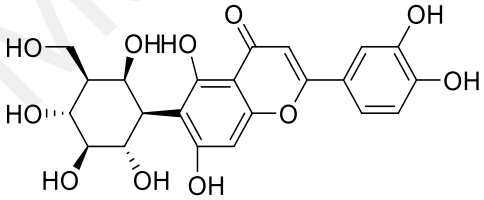

239

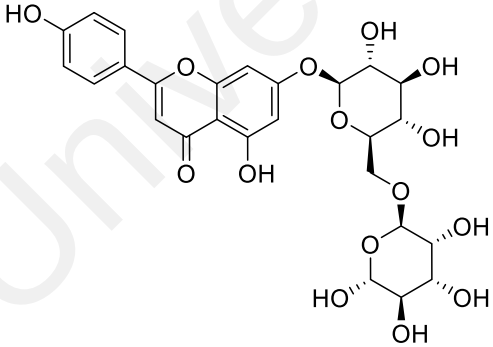

240

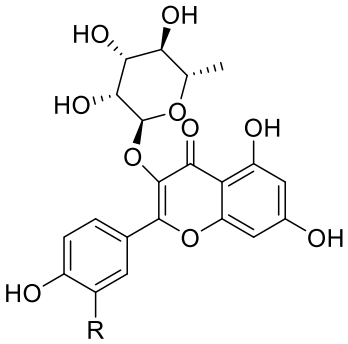

No.	R
241	H
242	OH

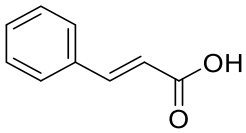

243

Figure 2.4, continued.

2.1.2 *Garcinia*

There are several types of compounds reported from *Garcinia* genus, including PPAPs, xanthones, flavonoids, and triterpenes. As the objective is to study the PPAPs from *Garcinia*, this research exclusively focuses on the reported PPAPs isolated from this genus.

2.1.2.1 Polycyclic polyprenylated acyl phloroglucinols (PPAPs)

PPAPs possessing highly oxygenated acylphloroglucinol-derived cores (a bicyclo [3.3.1] nonane - 2,4,9 - trione or bicyclo [3.2.1] octane - 2,4,8 - trione core (Richard et al., 2012)) are adorned with isoprenyl, geranyl or more highly substituted side chains. This unique class of hybrid NPs is particularly isolated from the plants of the family Guttiferae (Clusiaceae), mainly from the genera *Hypericum* and *Garcinia*.

The PPAPs have been classified into three types (A, B, or C) (Figure 2.5), depending on their isomeric forms (Ciochina & Grossman, 2006). However, Yang *et al.* 2018 revised the structures of the published type C PPAPs to type A structures. The classification of a PPAP as type A or B depends on the relative position of the acyl group: type A PPAPs have a C-1 acyl group and an adjacent C-8 quaternary center, whereas type B PPAPs have a C-3 acyl group (Ciochina & Grossman, 2006; Richard et al., 2012; Yang et al., 2018).

Yang *et al.* 2018 introduced a new classification of PPAPs; with the Cuesta-Rubio and Grossman's classification remained as subclassification. As the PPAP profiles are generated *via* three major biosynthetic pathways, it was divided into three groups (I-III) according to their different scaffolds (Yang et al., 2018).

(a) ***Type B PPAPs.***

Most of the PPAPs reported from genus *Garcinia* were type B, where the majority of them share a characteristic hydroxylated benzoyl group. The acyl groups of this class of

PPAPs are located at the C-3 position. It has been found that the enolic β-diketone system and 3,4-dihydroxybenzoyl substituents in the structures of type B PPAPs are important for their anticancer activities (Ciochina & Grossman, 2006; Yang et al., 2018).

Type B PPAPs that possess a 3,4-dihydroxybenzoyl substituent are prone to be oxidized (C-6 position of benzene) and further cyclized with O-2 or O-4 to form a fused tetracyclic system (Ciochina & Grossman, 2006; Yang et al., 2018). Table 2.6 recorded the reported PPAPs from *Garcinia* from 2010 until 2023.

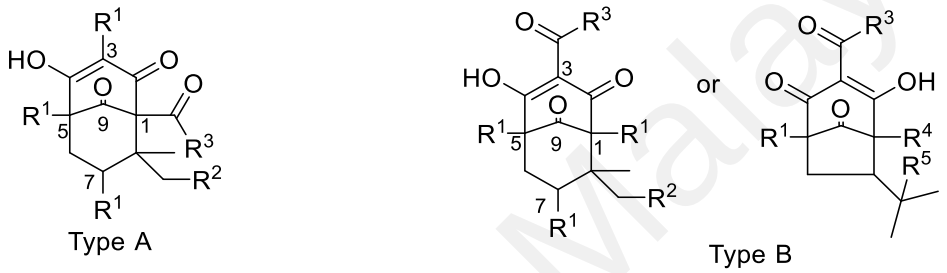

R1 = Me, C_5H_9, or $C_{10}H_{17}$
R_2 = H or prenyl
R_3 = i-Pr, i-Bu, s-Bu, Ph, 3-(HO)C_6H_4, or 3,4-$(HO)_2C_6H_3$
R_4 = Me, R_5 = OH or R_4-R_5 =CH_2CHR_6
R_6 = H, CMe=CH_2, or CMe_2OH

Figure 2.5: Type A and B PPAPs.

Table 2.6: PPAPs isolated from *Garcinia* species reported from 2010 to 2023.

No.	Plant species	Parts	Chemical constituents	Molecular formula	Site collection	References
1.	*G. afzelii*	Seeds	Guttiferone O or oxy-oblongifolin A **246**	$C_{38}H_{48}O_6$	Cameroon	(Lannang et al., 2010)
			Isoxanthochymol* **248**	$C_{38}H_{50}O_6$		
			Guttiferone E aka (+)-camboginol* **253**	$C_{38}H_{50}O_6$		
2.	*G. bracteata*	Fruits	Garcibractinone A **271**	$C_{33}H_{40}O_4$	Yunnan, P. R. of China	(Chen et al., 2020)
			Garcibractinone B **272**	$C_{33}H_{40}O_4$		
			Doitunggarcinone A **273**	$C_{33}H_{40}O_4$		
			Doitunggarcinone B **277**	$C_{33}H_{42}O_4$		
			Garcibracteatone **274**	$C_{33}H_{40}O_4$		
		Fruits	Garcibracteamone H **278**	$C_{33}H_{40}O_4$	Yunnan, P. R. of China	(Xue et al., 2020)
			Garcibracteamone I **279**	$C_{33}H_{40}O_5$		
			Garcibracteamone J **280**	$C_{33}H_{42}O_5$		
			Xerophenone A **281**	$C_{33}H_{42}O_5$		
3.	*G. cambogia*	Fruits	Guttiferone M **282**	$C_{38}H_{50}O_6$	Ceylon	(Masullo et al., 2010)
			Oxy-guttiferone I **296**	$C_{38}H_{48}O_6$		
			Oxy-guttiferone K2 **305**	$C_{38}H_{48}O_6$		
			Oxy-guttiferone M **302**	$C_{38}H_{48}O_6$		
			Oxy-guttiferone K **306**	$C_{38}H_{48}O_6$		
4.	*G. cochinchinensis*	Fruits	Guttiferone Q **283**	$C_{33}H_{42}O_4$	Dong Nai Vietnam	(Nguyen et al., 2011)
			Guttiferone R **307**	$C_{33}H_{42}O_5$		
			Guttiferone S **308**	$C_{33}H_{42}O_5$		
			Guttiferone I **284**	$C_{38}H_{50}O_5$		

Table 2.6, continued.

No.	Plant species	Parts	Chemical constituents	Molecular formula	Site collection	References
		Bark	Guttiferone T **309**	$C_{38}H_{50}O_7$	Ma Da Plantation, Vietnam	(Trinh et al., 2013)
			Isogarcinol aka cambogin aka 30-*epi*-cambogin* **310**	$C_{38}H_{50}O_6$		
			(−)-Guttiferone G **285**	$C_{43}H_{58}O_6$		
			(±)-Garcinialiptone A* **315**	$C_{38}H_{48}O_6$		
5.	*G. cowa*	Twigs	Isogarcinol aka cambogin aka 30-*epi*-cambogin* **310**	$C_{38}H_{51}O_6$	Yunnan, P. R. of China	(Xu et al., 2010)
		Ripe fruit	Cowabenzophenone A **313**	$C_{38}H_{48}O_4$	Nong Khai, Thailand	(Sriyatep et al., 2014)
			Cowabenzophenone B **314**	$C_{35}H_{44}O_5$		
		Inflorescences	Cowanone aka chamuangone **286**	$C_{33}H_{42}O_4$		(Trisuwan & Ritthiwigrom, 2012)
		Leaves	Cowanone aka chamuangone **286**	$C_{33}H_{42}O_4$		(Sakunpak & Panichayupakaranant, 2012)
		Twigs	Garcicowin A **320**	$C_{36}H_{54}O_3$	Yunnan, P. R. of China	(Xu et al., 2010)
			Garcicowin B **287**	$C_{43}H_{58}O_5$		
			Garcicowin C * **249**	$C_{38}H_{48}O_6$		
			Garcicowin D **322**	$C_{38}H_{48}O_6$		
			Isogarcinol aka cambogin aka 30-*epi*-cambogin* **310**	$C_{38}H_{50}O_6$		
			Guttiferone B **288**	$C_{43}H_{58}O_6$		
			Guttiferone K **289**	$C_{38}H_{50}O_6$		
			Garcinol aka (−)-camboginol aka guttiferone F* **254**	$C_{38}H_{50}O_6$		
			Oblongifolin A **255**	$C_{38}H_{50}O_6$		
			Oblongifolin B **290**	$C_{38}H_{50}O_6$		
			Oblongifolin C **291**	$C_{43}H_{58}O_6$		

Table 2.6, continued.

No.	Plant species	Parts	Chemical constituents	Molecular formula	Site collection	References
			Oblongifolin D **256**	$C_{43}H_{58}O_6$		
6.	*G. epunctata* Stapf	Stem bark	Epunctanone **311**	$C_{38}H_{52}O_6$	Eloumden Yaoundé in central Cameroon	(Fotso et al., 2014)
			7-*epi*-isogarcinol **312**	$C_{38}H_{50}O_6$		
7.	*G. esculenta*	Twigs	Garciesculentone A **321**	$C_{38}H_{50}O_7$	Yunnan, P. R. of China	(Zhang, Zhang, et al., 2014)
			Garciesculentone B **297**	$C_{38}H_{48}O_7$		
			Garciesculentone C **257**	$C_{39}H_{54}O_8$		
			Garciesculentone D **258**	$C_{38}H_{50}O_7$		
			Garciesculentone E **259**	$C_{38}H_{50}O_7$		
			Garciniagifolone A **316**	$C_{38}H_{48}O_6$		
			Garcimultiflorone E **260**	$C_{38}H_{50}O_7$		
			Isogarcinol aka cambogin aka 30-*epi*-cambogin* **310**	$C_{38}H_{50}O_6$		
			Garcinol aka (−)-camboginol aka guttiferone F* **254**	$C_{38}H_{50}O_6$		
			Garcicowin C * **249**	$C_{38}H_{48}O_6$		
8.	*G. indica*	Fruit rinds	14-deoxyisogarcinol **250**	$C_{38}H_{50}O_5$	Bengaluru	(Kaur et al., 2012)
			No name **323**	$C_{38}H_{48}O_6$		
			Isogarcinol aka cambogin aka 30-*epi*-cambogin* **310**	$C_{38}H_{50}O_6$		
			Garcinol aka (−)-camboginol aka guttiferone F* **254**	$C_{38}H_{50}O_6$		
9.	*G. multiflora*	Leaves & twigs	(±)-Garcimulin A* **324**	$C_{38}H_{50}O_6$	Guizhou P. R. of China	(Fan et al., 2015)
			Garcimulin B **325**	$C_{38}H_{50}O_6$		
			(±)-Garmultin A **326**	$C_{38}H_{48}O_8$		(Tian et al., 2016)
			(±)-Garmultin C **328**	$C_{38}H_{50}O_8$		
			(±)-Garmultin D **330**	$C_{38}H_{50}O_7$		

Table 2.6, continued.

No.	Plant species	Parts	Chemical constituents	Molecular formula	Site collection	References
			(±)-Garmultin F **332**	$C_{35}H_{42}O_8$		
			Garmultin B **327**	$C_{38}H_{48}O_8$		
			Garmultin E **331**	$C_{38}H_{50}O_7$		
			Garmultin G **333**	$C_{35}H_{41}O_8$		
		Twigs	18-hydroxygarcimultiflorone D **261**	$C_{38}H_{53}O_8$	Hainan, P. R. of China	(Liu et al., 2010)
			Garcimultiflorone D **262**	$C_{38}H_{51}O_7$		
			Garcimultiflorone E **260**	$C_{38}H_{52}O_8$		
			Garcimultiflorone F **263**	$C_{38}H_{52}O_8$		
			Isogarcimultiflorone F **264**	$C_{38}H_{52}O_8$		
			Guttiferone E aka (+)-camboginol* **253**	$C_{38}H_{50}O_6$		
			Garcinol aka (−)-camboginol aka guttiferone F* **254**	$C_{38}H_{50}O_6$		
			Aristophenone A **292**	$C_{33}H_{42}O_6$		
			Isoxanthochymol* **248**	$C_{38}H_{50}O_6$		
		Fruits	Garcimultiflorone D or isosampsonione J **334**	$C_{38}H_{48}O_5$	Pingtung County, Taiwan	(Ting et al., 2012)
			Garcimultiflorone G **329**	$C_{38}H_{50}O_7$		(Ting et al., 2014)
		Leaves	Garcimultiflorone H **265**	$C_{33}H_{42}O_6$	Hainan, P. R. of China	(Fu et al., 2015)
			Garcimultiflorone I **298**	$C_{33}H_{40}O_6$		
			Garcimultiflorone J **336**	$C_{38}H_{48}O_6$		
		Stems	Garcimultiflorone K **266**	$C_{38}H_{50}O_4$	Pingtung Country, Taiwan	(Cheng et al., 2018)
			Garcimultiflorone A **337**	$C_{38}H_{50}O_4$		
			Garcimultiflorone B **338**	$C_{38}H_{48}O_4$		
		Branches	Garcimultiflorone K **339**	$C_{38}H_{48}O_5$	Yunnan, P. R. of China	(Wang et al., 2018)

Table 2.6, continued.

No.	Plant species	Parts	Chemical constituents	Molecular formula	Site collection	References
			Garcimultiflorone L **340**	$C_{38}H_{50}O_4$		
			Garcimultiflorone M **341**	$C_{39}H_{52}O_6$		
			Garcimultiflorone N **342**	$C_{38}H_{48}O_4$		
			Garcimultiflorone O **343**	$C_{38}H_{50}O_6$		
			Garcimultiflorone P **344**	$C_{33}H_{40}O_5$		
			Garcimultiflorone Q **345**	$C_{38}H_{50}O_9$		
		Fruits	Garcimultine A **346**	$C_{38}H_{48}O_4$	Guangxi, P. R. of China	(Liu et al., 2017)
			Garcimultine B **347**	$C_{38}H_{48}O_4$		
			Isogarcinol aka cambogin aka 30-*epi*-cambogin* **310**	$C_{38}H_{50}O_6$		
			Garcinol aka (−)-camboginol aka guttiferone F* **254**	$C_{38}H_{50}O_6$		
			Garcicowin C * **249**	$C_{38}H_{48}O_6$		
			Garcimulin A **324**	$C_{38}H_{50}O_6$		
			Garcimulin B **325**	$C_{38}H_{50}O_6$		
		Leaves & twigs	Garcinielliptone GC **348**	$C_{38}H_{50}O_7$	Guizhou, P. R. of China	(Yang et al., 2020)
			Symphonone F **349**	$C_{38}H_{50}O_7$		
			Symphonone H **303**	$C_{38}H_{48}O_6$		
			Symphonone I **350**	$C_{38}H_{48}O_6$		
			Coccinone B **251**	$C_{38}H_{50}O_7$		
			Garciniagifolone A **316**	$C_{38}H_{48}O_6$		
		Fruits	Norgarmultinone A **351**	$C_{37}H_{52}O_3$	Guangxi, P. R. of China	(Teng et al., 2020)
			Norgarmultinone B **352**	$C_{37}H_{52}O_3$		
		Fruits	*Epi*-isosampsonione J **335**	$C_{38}H_{48}O_5$	Guangxi, P. R. of China	(Chen et al., 2019a)
			Iso-hyperisampsin C **353**	$C_{38}H_{48}O_5$		
			Iso-hypersampsonone G **354**	$C_{38}H_{50}O_5$		

Table 2.6, continued.

No.	Plant species	Parts	Chemical constituents	Molecular formula	Site collection	References
			Garcimultinone A **355**	$C_{35}H_{44}O_5$		
			Iso-hypersampsonone B **357**	$C_{35}H_{44}O_6$		
			Epi-isohypersampsonone B **358**	$C_{35}H_{44}O_6$		
			Iso-hypersampsonone C **359**	$C_{38}H_{50}O_7$		
			Iso-hyperisampsin O **361**	$C_{38}H_{50}O_8$		
			Garcimultinone B **362**	$C_{35}H_{44}O_7$		
			Garcimultiflorone D or isosampsonione J **334**	$C_{38}H_{48}O_5$		
			Sampsonione B **363**	$C_{33}H_{42}O_5$		
			Hyphenrone M **364**	$C_{33}H_{42}O_6$		
		Fruits	*Iso*-hypersampsonone F **356**	$C_{38}H_{51}O_6$	Guangxi, P. R. of China	(Teng et al., 2019)
			Iso-hookerione J **365**	$C_{38}H_{51}O_4$		
			Iso-sampsonione H **366**	$C_{35}H_{45}O_4$		
			Epi-garcimultiflorone P **360**	$C_{33}H_{41}O_5$		
			Garcimultinone C **369**	$C_{38}H_{48}O_5$		
		Fruits	Garmultinone A **367**	$C_{33}H_{42}O_5$	Guangxi, P. R. of China	(Chen et al., 2019b)
			Garmultinone B **370**	$C_{33}H_{42}O_5$		
			Garmultinone C **368**	$C_{33}H_{42}O_7$		
			Garmultinone D **371**	$C_{38}H_{51}O_4$		
		Fruits	Garcimultinone D **424**	$C_{38}H_{50}O_4$	Guangxi, P. R. of China	(Teng et al., 2021)
			Garcimultinone E **425**	$C_{38}H_{50}O_6$		
			Garcimultinone F **426**	$C_{38}H_{50}O_5$		
			Garcimultinone G **427**	$C_{34}H_{44}O_6$		
			Garcimultinone H **428**	$C_{38}H_{50}O_5$		
			Garcimultinone I **429**	$C_{38}H_{50}O_4$		
			Garcimultinone J **430**	$C_{38}H_{50}O_6$		

Table 2.6, continued.

No.	Plant species	Parts	Chemical constituents	Molecular formula	Site collection	References
			Garcimultinone K **431**	$C_{38}H_{50}O_7$		
			Garcimultinone L **432**	$C_{38}H_{50}O_5$		
			Garcimultinone M **433**	$C_{38}H_{50}O_4$		
			Garcimultinone N **434**	$C_{38}H_{50}O_7$		
			Garcimultiflorone A **337**	$C_{38}H_{50}O_4$		
			Hyperscabrone M **435**	$C_{33}H_{42}O_5$		
			13,14-didehydroxy-7-*epi*-isogarcinol **436**	$C_{38}H_{50}O_4$		
			Xerophenone C **437**	$C_{33}H_{42}O_5$		
			Garcimultiflorone G **329**	$C_{38}H_{50}O_7$		
			Garcimultiflorone P **344**	$C_{33}H_{40}O_5$		
			Garcimultiflorone N **342**	$C_{38}H_{48}O_4$		
			Garciniagifolone A **316**	$C_{38}H_{48}O_6$		
			Garcibracteatone **274**	$C_{33}H_{40}O_4$		
			Nemorosonol **438**	$C_{33}H_{42}O_4$		
10.	*G. nujiangensis*	Leaves	Nujiangefolin A **299**	$C_{38}H_{48}O_6$	Yunnan, P. R. of China	(Xia et al., 2012)
			Nujiangefolin B **247**	$C_{38}H_{48}O_6$		
			Nujiangefolin C **372**	$C_{38}H_{50}O_7$		
		Fruits	Nujiangefolin D **300**	$C_{38}H_{48}O_7$	Yunnan, P. R. of China	(Tang et al., 2020)
			Symphonone H **303**	$C_{38}H_{48}O_6$		
			Garcimultiflorone E **260**	$C_{38}H_{50}O_7$		
			(-)-Cycloxanthochymol* **453**	$C_{38}H_{50}O_6$		
			Nujiangefolin A **299**	$C_{38}H_{48}O_6$		
			Nujiangefolin B **247**	$C_{38}H_{48}O_6$		
11.	*G. nuntasaenii*	Roots	Garcinuntin A **373**	$C_{38}H_{50}O_4$	Bueng Kan, Thailand	(Chaturonrutsamee et al., 2018)
			Garcinuntin B **374**	$C_{38}H_{50}O_4$		

Table 2.6, continued.

No.	Plant species	Parts	Chemical constituents	Molecular formula	Site collection	References
			Garcinuntin C **375**	$C_{38}H_{48}O_4$		
12.	*G. oblongifolia*	Barks	Garciniagifolone A **316**	$C_{38}H_{48}O_6$	Hainan, P. R. of China	(Shan et al., 2012)
			Garcinol aka (−)-camboginol aka guttiferone F* **254**	$C_{38}H_{50}O_6$		
		Peel	Oblongifolin H **301**	$C_{38}H_{49}O_5$	Guangxi, P. R. of China	(Zhou et al., 2010)
			Oblongifolin I **304**	$C_{38}H_{49}O_5$		
		Leaves	Oblongifolin J **376**	$C_{32}H_{38}O_5$		(Zhang, Tao, et al., 2014)
			Oblongifolin C **291**	$C_{43}H_{58}O_6$		
			Oblongifolin K **317**	$C_{32}H_{38}O_7$		
			Oblongifolin L **377**	$C_{33}H_{42}O_4$		
			Oblongifolin M **381**	$C_{33}H_{42}O_5$		
			Oblongifolin N **378**	$C_{33}H_{40}O_5$		
			Oblongifolin O **379**	$C_{33}H_{40}O_5$		
			Oblongifolin P **267**	$C_{24}H_{28}O_5$		
			Oblongifolin Q **380**	$C_{33}H_{42}O_5$		
			Oblongifolin R **382**	$C_{33}H_{42}O_5$		
			Oblongifolin S **383**	$C_{33}H_{42}O_5$		
			Oblongifolin T **268**	$C_{38}H_{50}O_7$		
			Oblongifolin U **293**	$C_{38}H_{50}O_5$		
			Oblongifolin V **294**	$C_{27}H_{30}O_5$		(Zhang et al., 2016)
			Oblongifolin W **384**	$C_{27}H_{30}O_5$		
			Oblongifolin X **385**	$C_{27}H_{28}O_5$		
			Oblongifolin Y **386**	$C_{25}H_{28}O_6$		
			Oblongifolin Z **387**	$C_{33}H_{44}O_5$		
			Oblongifolin AA **295**	$C_{33}H_{42}O_4$		

Table 2.6, continued.

No.	Plant species	Parts	Chemical constituents	Molecular formula	Site collection	References
		Fruits	Garcoblone A aka Garciyunnanin F **439**	$C_{33}H_{42}O_7$	Guangxi, P. R. of China	(Wu et al., 2022)
			Garcoblone B **440**	$C_{32}H_{42}O_7$		
			Garcoblone C **441**	$C_{33}H_{42}O_8$		
			Garcoblone D **442**	$C_{38}H_{50}O_7$		
			Garcoblone E **443**	$C_{38}H_{50}O_7$		
			sampsonione P **444**	$C_{33}H_{42}O_5$		
			7-*epi*-clusianone **445**	$C_{33}H_{42}O_4$		
			Isogarcinol aka cambogin aka 30-*epi*-cambogin* **310**	$C_{38}H_{50}O_6$		
			13,14-didehydoxyisogarcinol **436**	$C_{38}H_{50}O_4$		
			Garcinol aka (−)-camboginol aka guttiferone F* **254**	$C_{38}H_{50}O_6$		
			Garcimultiflorone K **266**	$C_{38}H_{50}O_4$		
			Garcinialone **394**	$C_{38}H_{50}O_7$		
13.	*G. paucinervis*	Leaves	Paucinone A **388**	$C_{38}H_{50}O_7$	Yunnan, P. R. of China	(Gao et al., 2010)
			Paucinone B **389**	$C_{38}H_{50}O_7$		
			Paucinone C **390**	$C_{38}H_{50}O_8$		
			Paucinone D **391**	$C_{38}H_{50}O_7$		
		Fruits	Paucinochymol A **269**	$C_{38}H_{50}O_7$	Guangxi, P. R. of China	(Tan et al., 2020)
			Paucinochymol B **392**	$C_{38}H_{50}O_7$		
			Paucinochymol C **393**	$C_{38}H_{50}O_7$		
			Isogarcinol aka cambogin aka 30-*epi*-cambogin* **310**	$C_{38}H_{50}O_6$		
			7-*epi*-isogarcinol **312**	$C_{38}H_{50}O_6$		

Table 2.6, continued.

No.	Plant species	Parts	Chemical constituents	Molecular formula	Site collection	References
			Garcicowin C * **249**	$C_{38}H_{48}O_6$		
			Symphonone I **350**	$C_{38}H_{48}O_6$		
			Garcinialone **394**	$C_{38}H_{50}O_7$		
			Symphonone H **303**	$C_{38}H_{48}O_6$		
14.	*G. picrorhiza*	Stem bark	Picrorhizone A **494**	$C_{38}H_{50}O_7$	Bogor, Indonesia	(Sukandar et al., 2020)
			Picrorhizone B **495**	$C_{38}H_{50}O_5$		
			Picrorhizone C **496**	$C_{38}H_{50}O_4$		
			Picrorhizone D **497**	$C_{38}H_{52}O_7$		
			Picrorhizone E **498**	$C_{37}H_{48}O_7$		
			Picrorhizone F **499**	$C_{38}H_{50}O_7$		
			Picrorhizone G **500**	$C_{38}H_{48}O_8$		
			Picrorhizone H **493**	$C_{38}H_{48}O_6$		
			Garcinopicrobenzophenone **418**	$C_{38}H_{50}O_6$		
15.	*G. propinqua*	Stem bark	Sampsonione R **395**	$C_{30}H_{36}O_5$	Chiang Rai, Thailand	(Sriyatep et al., 2017)
			Hypersampsone M **396**	$C_{30}H_{36}O_4$		
			Sampsonione B **363**	$C_{33}H_{42}O_5$		
			Xerophenone A **281**	$C_{33}H_{42}O_5$		
			Doitunggarcinone A **273**	$C_{33}H_{40}O_4$		
			Doitunggarcinone B **277**	$C_{33}H_{42}O_4$		
		Twigs	Doitunggarcinone A **273**	$C_{33}H_{40}O_4$		(Tantapakul et al., 2012)
			Doitunggarcinone B **277**	$C_{33}H_{42}O_4$		
			Xerophenone A **281**	$C_{33}H_{42}O_5$		
16.	*G. schomburgkiana*	Fruits	Schomburgkianone A **397**	$C_{43}H_{58}O_7$	Dong Thap, Vietnam	(Le et al., 2016)
			Schomburgkianone B **398**	$C_{43}H_{58}O_7$		
			Schomburgkianone C **399**	$C_{43}H_{58}O_7$		
			Schomburgkianone D **403**	$C_{38}H_{50}O_7$		

Table 2.6, continued.

No.	Plant species	Parts	Chemical constituents	Molecular formula	Site collection	References
			Schomburgkianone E **404**	$C_{43}H_{58}O_7$		
			Schomburgkianone F **400**	$C_{38}H_{50}O_7$		
			Schomburgkianone G **401**	$C_{38}H_{50}O_7$		
			(+)-Guttiferone K **289**	$C_{38}H_{50}O_6$		
			(+)-Oblongifolin C **291**	$C_{38}H_{50}O_5$		
			(−)-Garciyunnanin A* **402**	$C_{38}H_{50}O_5$		
			(+)-Garcicowin B **287**	$C_{43}H_{58}O_5$		
		Branches	Garschomcinol A **446**	$C_{43}H_{60}O_7$	Sisaket province, Thailand	(Kaennakam et al., 2022)
			Garschomcinol B **447**	$C_{44}H_{62}O_7$		
			Garschomcinol C **448**	$C_{45}H_{64}O_7$		
			Garschomcinol D **449**	$C_{36}H_{54}O_3$		
			Garschomcinol E **450**	$C_{31}H_{46}O_5$		
			Oblongifolin C **291**	$C_{43}H_{58}O_6$		
			Guttiferone K **289**	$C_{38}H_{50}O_6$		
			Garciyunnanin B **451**	$C_{43}H_{56}O_6$		
			Oxy-guttiferone K **306**	$C_{38}H_{48}O_6$		
			Oblongifolin G **452**	$C_{38}H_{48}O_6$		
17.	*G. subelliptica*	Fruits	(+)-Cycloxanthochymol* **252**	$C_{38}H_{50}O_6$	Taiwan	(Zhang et al., 2010)
			(-)-Cycloxanthochymol* **453**	$C_{38}H_{50}O_6$		
			(±)-Garcinialiptone A* **315**	$C_{38}H_{48}O_6$		
			Garcinialiptone B **454**	$C_{38}H_{48}O_6$		
			Garcinialiptone C **405**	$C_{38}H_{50}O_7$		
			Garcinialiptone D **406**	$C_{38}H_{50}O_6$		
			Xanthochymol a.k.a garcinielliptone FC **270**	$C_{38}H_{50}O_6$		
			Isoxanthochymol* **248**	$C_{38}H_{50}O_6$		

Table 2.6, continued.

No.	Plant species	Parts	Chemical constituents	Molecular formula	Site collection	References
		Seed	Garcinielliptone P **410**	$C_{30}H_{44}O_6$	Taiwan	(Lin et al., 2011)
		Seed	Garsubelone A **412**	$C_{60}H_{84}O_8$	Guangdong, P. R. of China	(Y.-L. Wang et al., 2019)
			Garsubelone B **411**	$C_{30}H_{42}O_4$		
		Branches & leaves	Subellinone aka garcinielliptin oxide **413**	$C_{30}H_{44}O_5$	Guangdong, P. R. of China	(Grossman & Yang, 2020)
			Garcinielliptone T **414**	$C_{31}H_{46}O_5$		
			Garcinielliptone E **415**	$C_{30}H_{46}O_6$		
		Heartwood	(-)-Garcinielliptone HG* **416**	$C_{25}H_{36}O_6$	Pingtung, Taiwan	(Liaw et al., 2019)
			(+)-Garcinielliptone HH* **455**	$C_{25}H_{36}O_6$		
		Seed	Garcinielliptone R **417**	$C_{30}H_{46}O_7$	Kaohsiung, Taiwan	(Lin et al., 2012)
			Xanthochymol a.k.a garcinielliptone FC **270**	$C_{38}H_{50}O_6$		
			Garcinielliptone A **407**	$C_{30}H_{46}O_5$		
			Garcinielliptone F **408**	$C_{30}H_{44}O_5$		
			Garsubelline A **419**	$C_{30}H_{44}O_5$		
18.	*G. verrucosa*	Stem bark	Garcicosin **409**	$C_{31}H_{46}O_4$	Andasibe-Mantadia	(Rajaonarivelo et al., 2016)
19.	*G. xanthochymus*	Fruits	Garcixanthochymone A **318**	$C_{38}H_{50}O_7$	Yunnan, P. R. of China	(Chen et al., 2017)
			Garcixanthochymone B **319**	$C_{38}H_{48}O_7$		
			Garcixanthochymone C **420**	$C_{38}H_{51}O_8$		
			Garcixanthochymone D **275**	$C_{33}H_{40}O_6$		
			Garcixanthochymone E **276**	$C_{33}H_{40}O_6$		
		Fruits	Garcixanthochymone F **456**	$C_{38}H_{48}O_7$	Yunnan Province, China	(Jin et al., 2021)
			Garcixanthochymone G **457**	$C_{38}H_{50}O_7$		
			Garcixanthochymone H **458**	$C_{38}H_{56}O_{10}$		
			Garcixanthochymone I **459**	$C_{38}H_{56}O_{10}$		

Table 2.6, continued.

No.	Plant species	Parts	Chemical constituents	Molecular formula	Site collection	References
			Garcixanthochymone J **460**	$C_{38}H_{48}O_6$		
			Garcixanthochymone K **461**	$C_{38}H_{48}O_6$		
			7-epi-isoxanthochymol **462**	$C_{38}H_{50}O_6$		
			7-epi-cycloxanthochymol **463**	$C_{38}H_{50}O_6$		
			Garcimultiflorone E **260**	$C_{38}H_{50}O_7$		
			Nujiangefolin C **372**	$C_{38}H_{50}O_7$		
			Coccinone D **464**	$C_{38}H_{52}O_8$		
			Coccinone E **465**	$C_{38}H_{52}O_8$		
			Nujiangefolin B **247**	$C_{38}H_{48}O_6$		
			Garcimultiflorone I **298**	$C_{33}H_{40}O_6$		
			Symphonone I **350**	$C_{38}H_{48}O_6$		
		Fruits	Xanthochymusone A **466**	$C_{38}H_{50}O_5$	Miami, FL, USA	(Xu et al., 2022)
			Xanthochymusone B **467**	$C_{38}H_{50}O_6$		
			Xanthochymusone C **468**	$C_{38}H_{50}O_5$		
			Xanthochymusone D **469**	$C_{38}H_{52}O_7$		
			Xanthochymusone E **470**	$C_{38}H_{52}O_7$		
			Xanthochymusone F **471**	$C_{38}H_{50}O_6$		
			Xanthochymusone G **472**	$C_{38}H_{50}O_6$		
			Xanthochymusone H **473**	$C_{38}H_{48}O_5$		
			Xanthochymusone I **474**	$C_{38}H_{48}O_6$		
			Xanthochymol a.k.a garcinielliptone FC **270**	$C_{38}H_{50}O_6$		
			Guttiferone E aka (+)-camboginol* **253**	$C_{38}H_{50}O_6$		
			Cycloxanthochymol* **252**	$C_{38}H_{50}O_6$		
			Isoxanthochymol* **248**	$C_{38}H_{50}O_6$		

Table 2.6, continued.

No.	Plant species	Parts	Chemical constituents	Molecular formula	Site collection	References
			14-deoxygarcinol **475**	$C_{38}H_{50}O_5$		
			14-deoxyisogarcinol **250**	$C_{38}H_{50}O_5$		
			7-*epi*-isogarcinol **312**	$C_{38}H_{50}O_6$		
			Coccinone C **476**	$C_{38}H_{52}O_7$		
			Nujiangefolin A **299**	$C_{38}H_{48}O_6$		
			Garcim-2 **477**	$C_{38}H_{48}O_6$		
			Nujiangefolin B **247**	$C_{38}H_{48}O_6$		
20.	*G. yunnanensis* Hu	Twigs, leaves, & fruits	Garciyunnanimine A **421**	$C_{38}H_{51}NO_5$	Yunnan, P. R. of China	Zheng 2017
			Garciyunnanimine B **423**	$C_{38}H_{51}NO_5$		
			Garciyunnanimine C **422**	$C_{43}H_{60}NO_5$		
			Garcinol aka (−)-camboginol aka guttiferone F* **254**	$C_{38}H_{50}O_6$		
			Guttiferone K **289**	$C_{38}H_{50}O_6$		
			Oblongifolin A **255**	$C_{38}H_{50}O_6$		
			Oblongifolin B **290**	$C_{38}H_{50}O_6$		
			Oblongifolin C **291**	$C_{43}H_{58}O_6$		
		Twigs, leaves, & fruits	Garciyunnanin C **478**	$C_{33}H_{42}O_6$	Yunnan, P. R. of China	(Zheng, Chen, et al., 2021)
			Garciyunnanin D **479**	$C_{33}H_{42}O_6$		
			Garciyunnanin E **480**	$C_{30}H_{34}O_7$		
			Garcoblone A aka Garciyunnanin F **439**	$C_{33}H_{42}O_7$		
			Garciyunnanin G **481**	$C_{27}H_{32}O_4$		
			Garciyunnanin J **482**	$C_{38}H_{48}O_7$		
			Garciyunnanin K **483**	$C_{43}H_{56}O_6$		
			Garciyunnanin L **484**	$C_{38}H_{48}O_6$		

* Refer to metabolites with enantiomer.

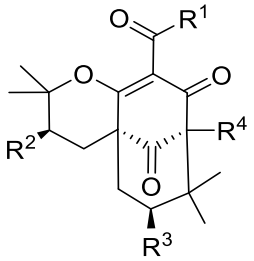

No.	R^1	R^2	R^3	R^4
248	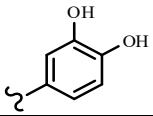	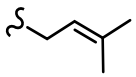	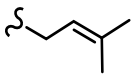	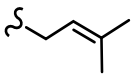
252	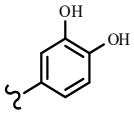	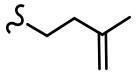	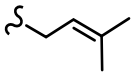	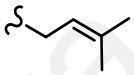
456	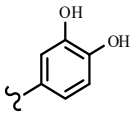	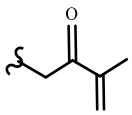	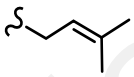	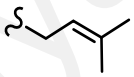
458	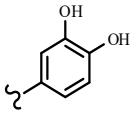	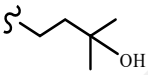	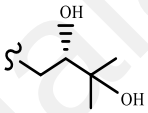	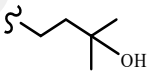
459	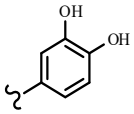	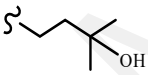	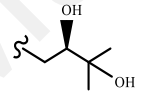	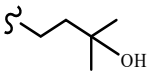
462	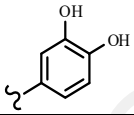	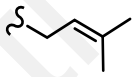	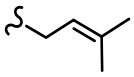	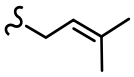
463	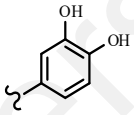	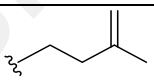	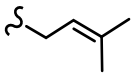	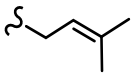
468	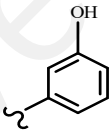	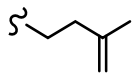	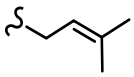	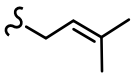
469	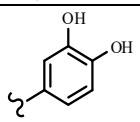	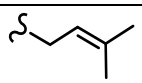	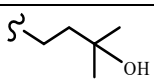	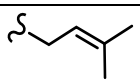
470	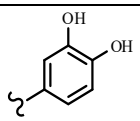	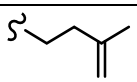	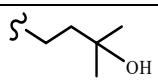	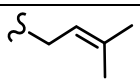

Figure 2.6: Structures of PPAPs isolated from *Garcinia* genus.

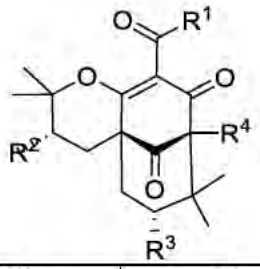

No.	R^1	R^2	R^3	R^4
250	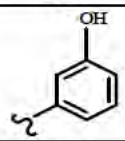	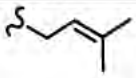	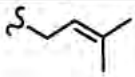	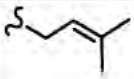
251	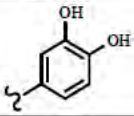	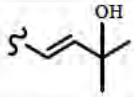	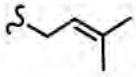	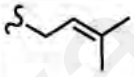
310	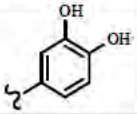	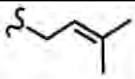	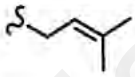	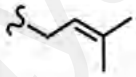
433	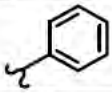	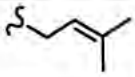	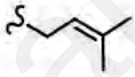	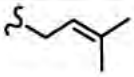
453	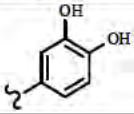		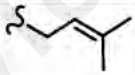	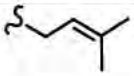
464	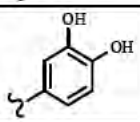	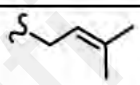	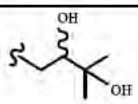	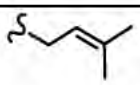
465	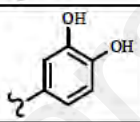	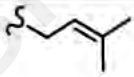	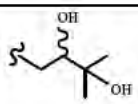	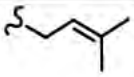
476	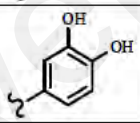	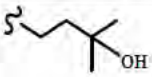	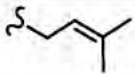	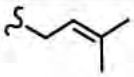

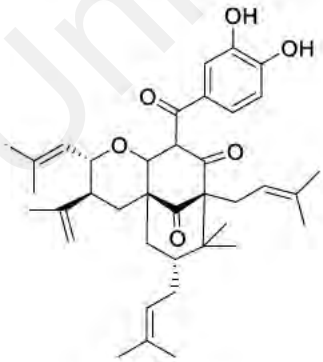

249

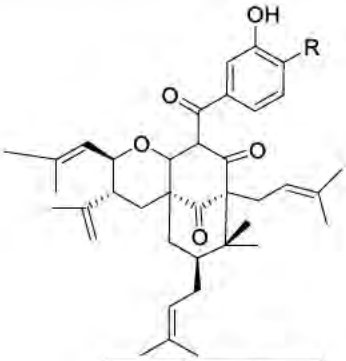

No.	R
473	H
474	OH

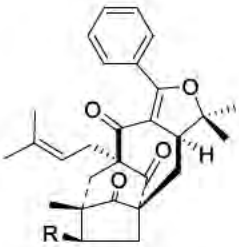

No.	R
271	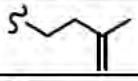
272	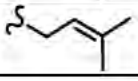

Figure 2.6, continued.

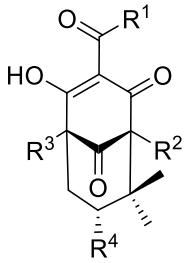

No.	R^1	R^2	R^3	R^4
253	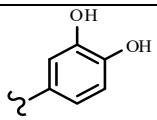	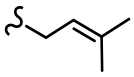	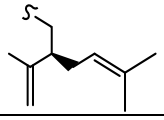	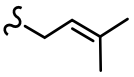
255	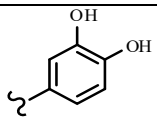	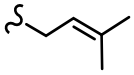	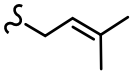	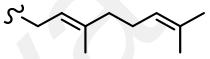
256	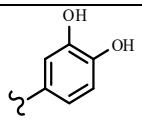	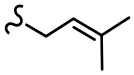	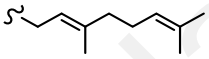	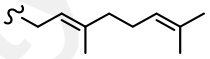
265	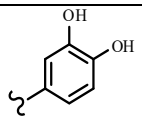	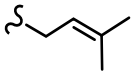	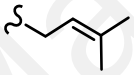	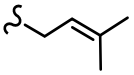
268	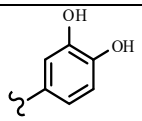	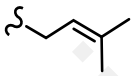	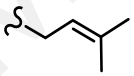	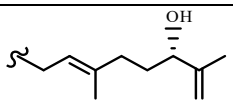
270	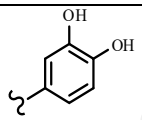	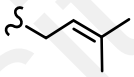	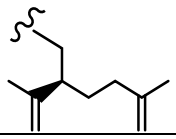	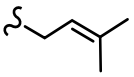
466	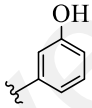	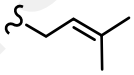	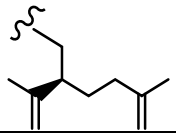	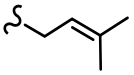

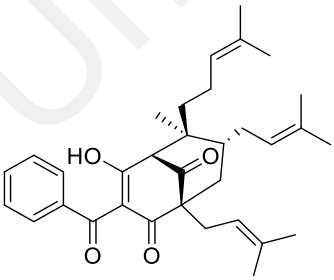

283

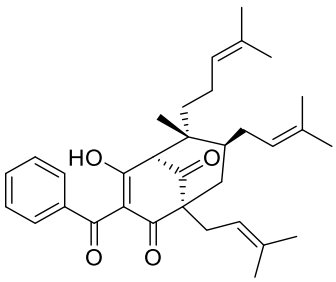

286

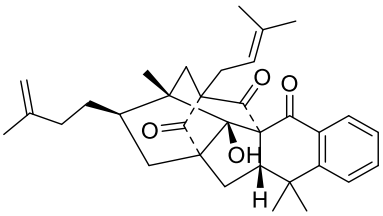

278

Figure 2.6, continued.

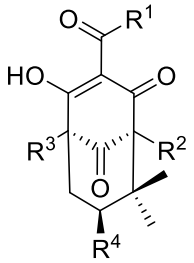

No.	R^1	R^2	R^3	R^4
254	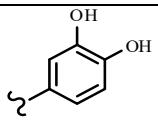	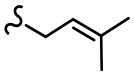	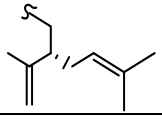	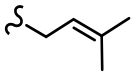
257	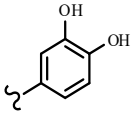	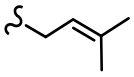	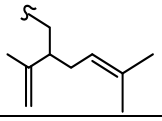	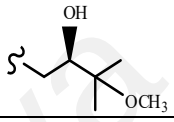
258	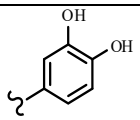	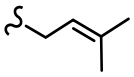	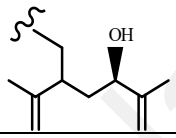	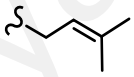
259	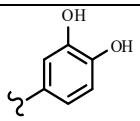	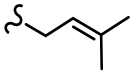	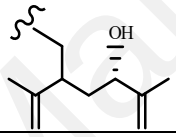	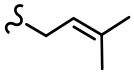
260	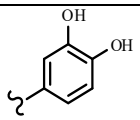	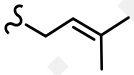	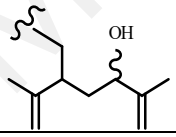	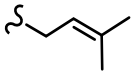
261	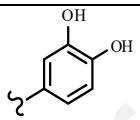	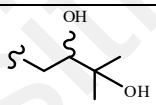	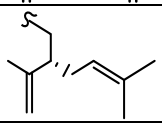	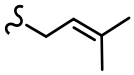
262	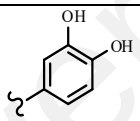	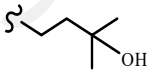	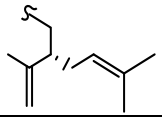	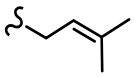
263	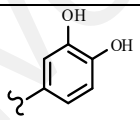	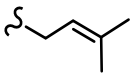	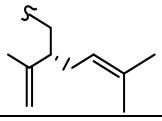	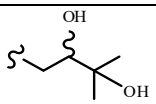
264	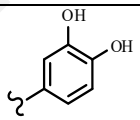	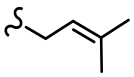	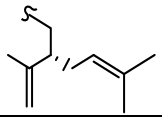	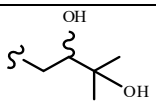
266	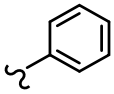	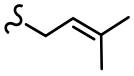	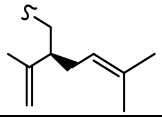	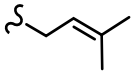
267	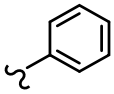	H	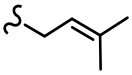	CH_3
269	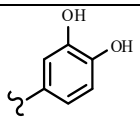	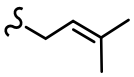	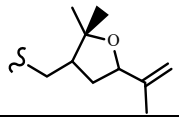	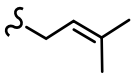
295	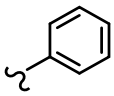	H	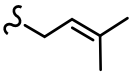	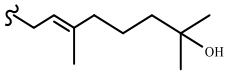

Figure 2.6, continued.

387	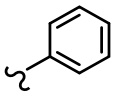	H	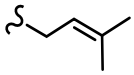	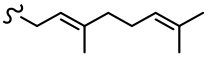
418	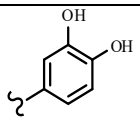	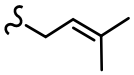	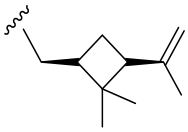	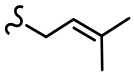
475	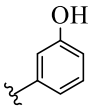	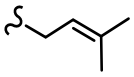	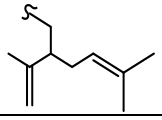	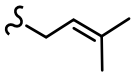
494	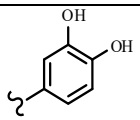	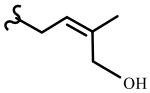	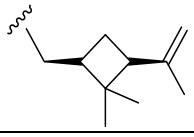	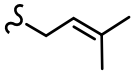
495	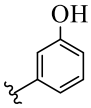	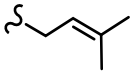	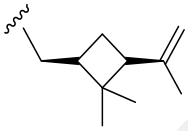	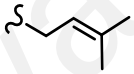
496	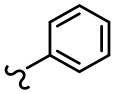	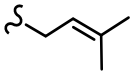	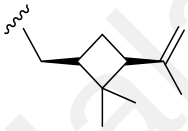	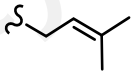
497	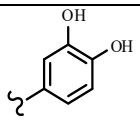	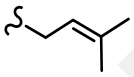	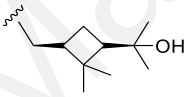	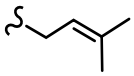
498	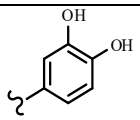	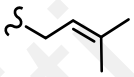	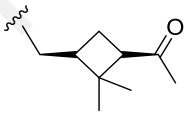	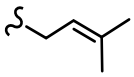

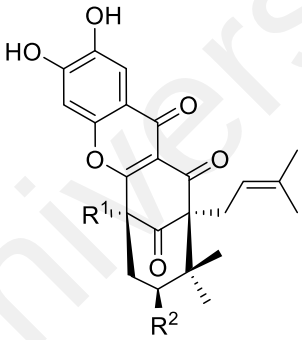

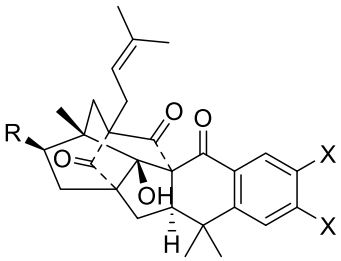

No.	R^1	R^2
246	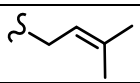	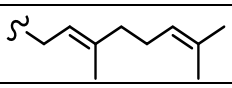
247	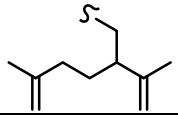	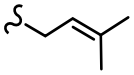
477	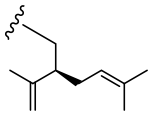	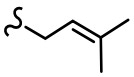

No.	R	X
273	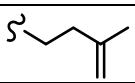	H
274	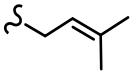	H
275	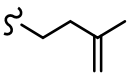	OH
276	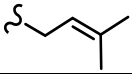	OH

Figure 2.6, continued.

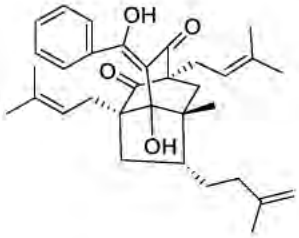

277

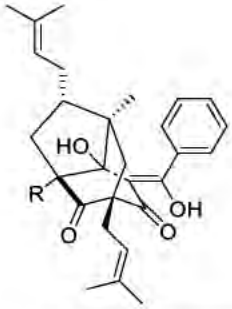

No.	R
371	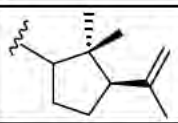
438	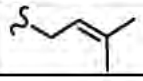

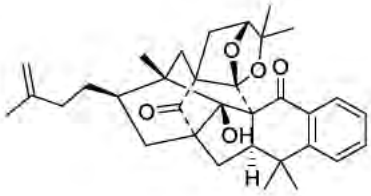

279

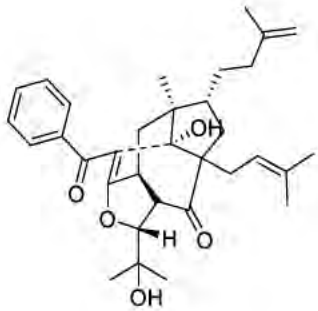

280

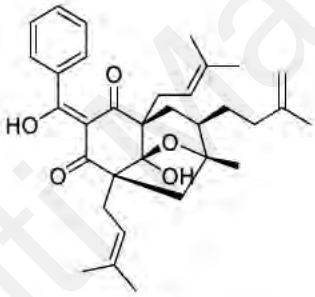

281

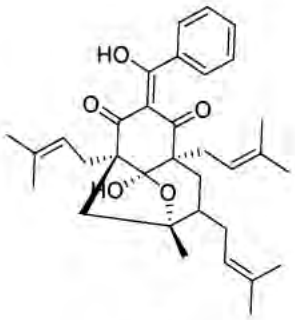

437

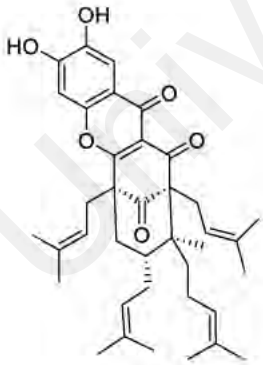

305

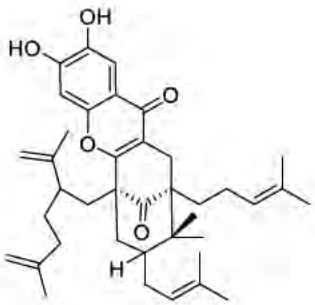

460

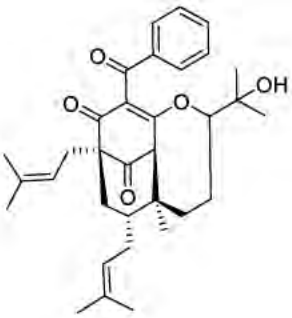

308

Figure 2.6, continued.

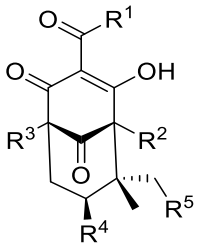

No.	R^1	R^2	R^3	R^4	R^5
282	OH, OH				H
284					
285	OH, OH				
287	OH				
288	OH, OH				H
289	OH, OH				
292	OH, OH				H
293	OH				H
294			H	O	H
377		H			H
378		H		O	H
379		H		O	H
380		H		OH	H
482	OH, OH				O

Figure 2.6, continued.

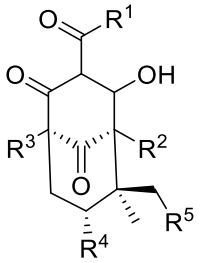

No.	R^1	R^2	R^3	R^4	R^5
290	OH, OH				H
291	OH, OH				
397	OH, OH			OH	
398	OH, OH			OH	
399	OH, OH			OH	
400	OH, OH			OH	
401	OH, OH			OH	
402	OH				
446	OH, OH			OH	
447	OH, OH			O	
448	OH, OH			O	
467	OH, OH				H

Figure 2.6, continued.

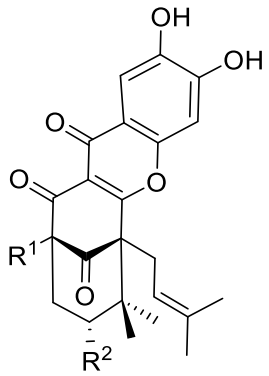

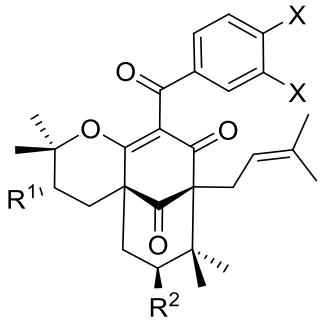

No.	R^1	R^2
296		
297	OH	
298		
336		

No.	R^1	R^2	X
311			OH
312			OH
436			H

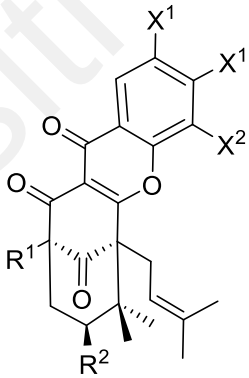

No.	R^1	R^2	X^1	X^2
299			OH	H
300		OH	OH	H
301			H	OH
493			OH	H

Figure 2.6, continued.

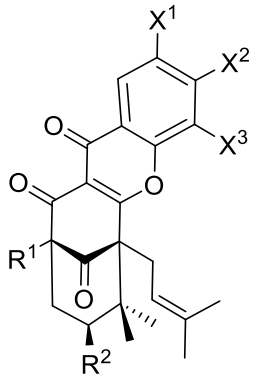

No.	R^1	R^2	X^1	X^2	X^3
302	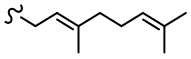	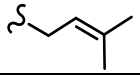	OH	OH	H
303	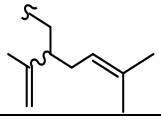	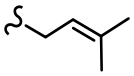	OH	OH	H
304	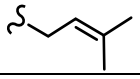	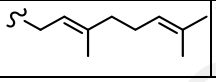	H	H	OH

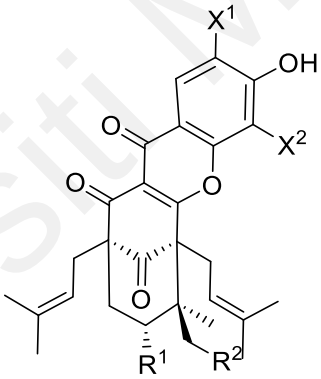

No.	R^1	R^2	X^1	X^2
306	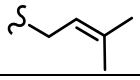	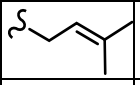	OH	H
451	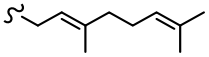	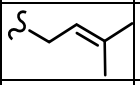	OH	H
452	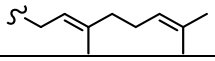	H	OH	H
483	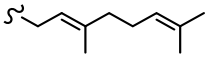	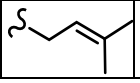	H	OH

Figure 2.6, continued.

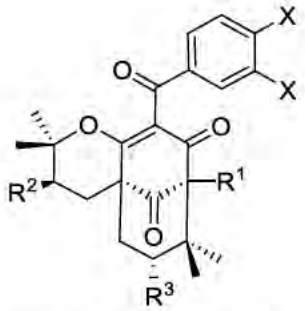

No.	R^1	R^2	R^3	X
384	H	H		H
471				OH

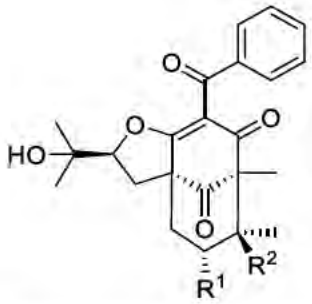

No.	R^1	R^2
307		
382		H

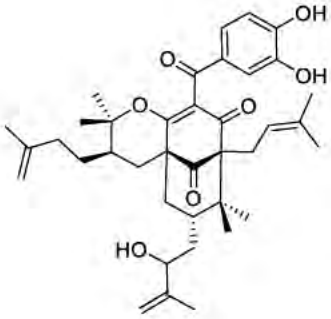

309

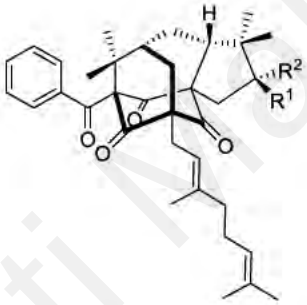

No.	R^1	R^2
313		H
314	H	OH

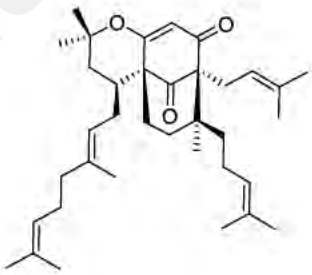

320

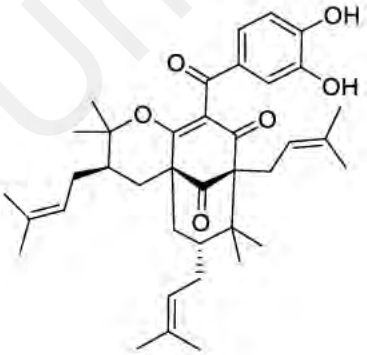

321

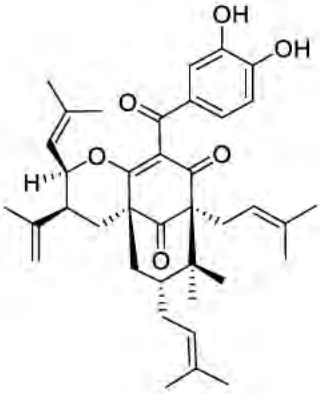

322

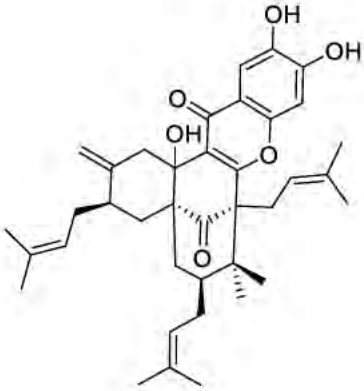

323

Figure 2.6, continued.

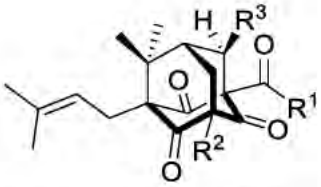

No.	R^1	R^2	R^3
315	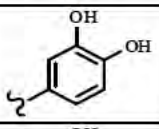	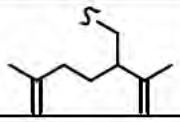	
316	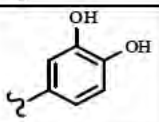	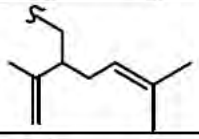	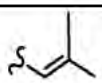
317	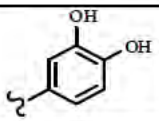	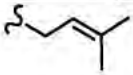	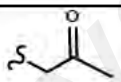
318	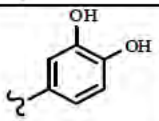	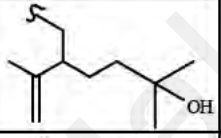	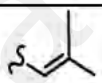
319	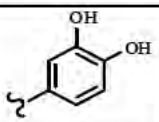	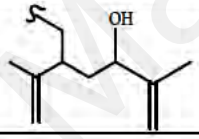	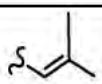

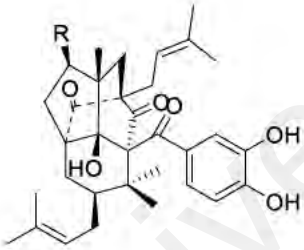

No.	R
324	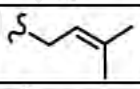
325	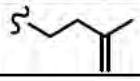

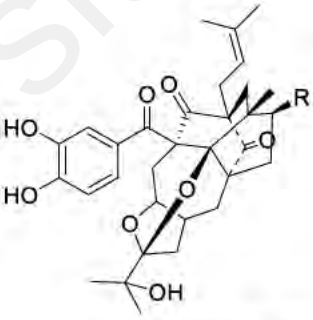

No.	R
326	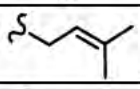
327	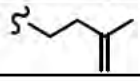

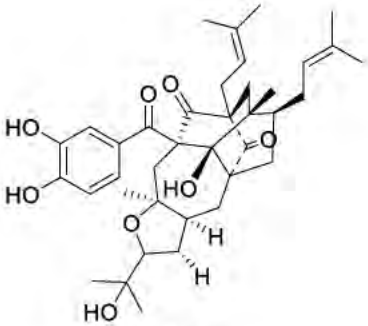

328

Figure 2.6, continued.

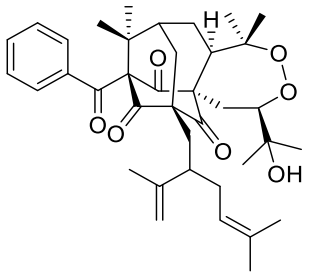

329

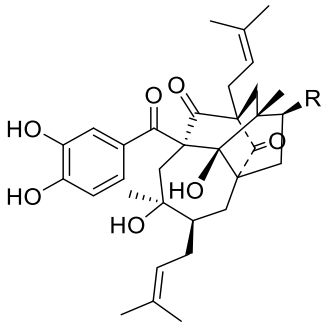

No.	R
330	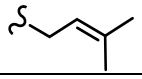
331	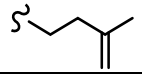

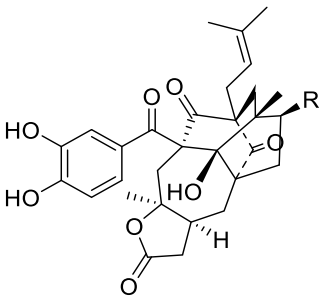

No.	R
332	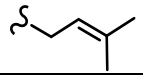
333	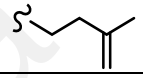

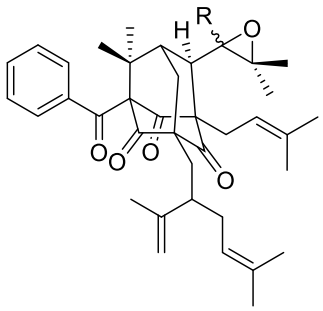

No.	R
334	
335	

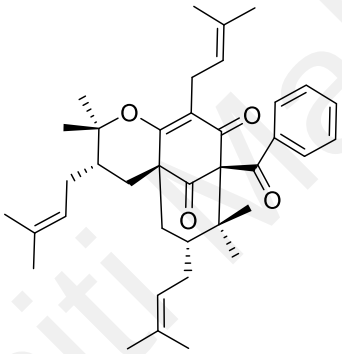

337

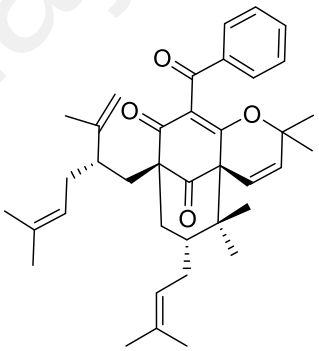

338

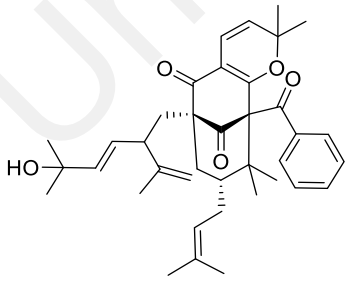

339

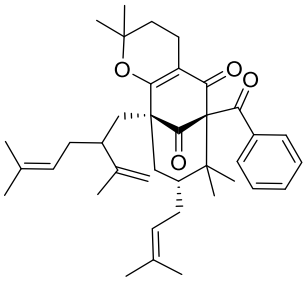

340

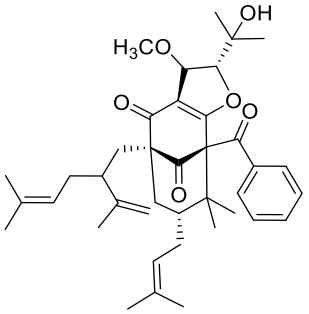

341

Figure 2.6, continued.

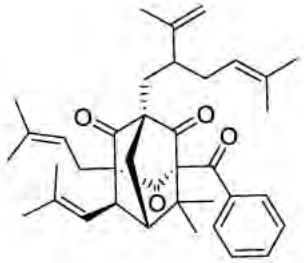

342

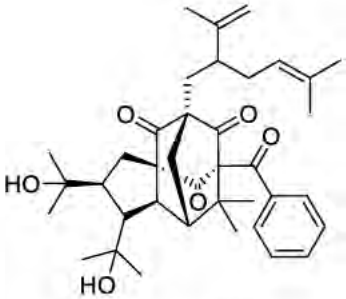

343

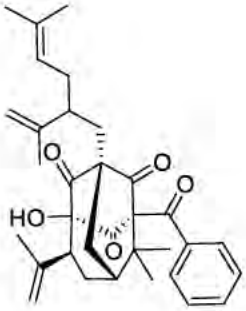

344

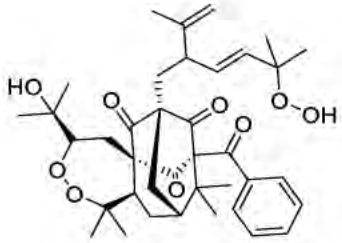

345

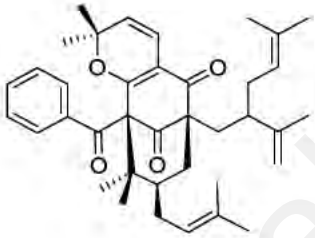

346

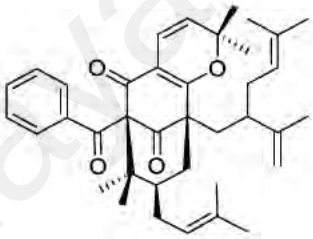

347

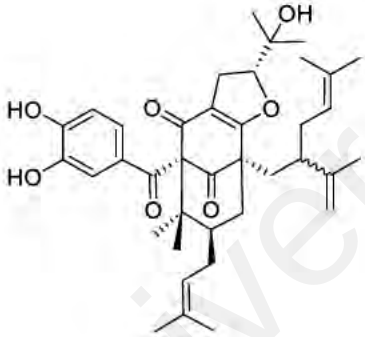

348

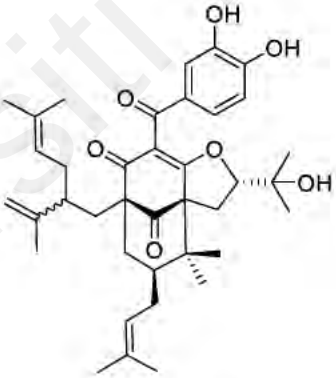

349

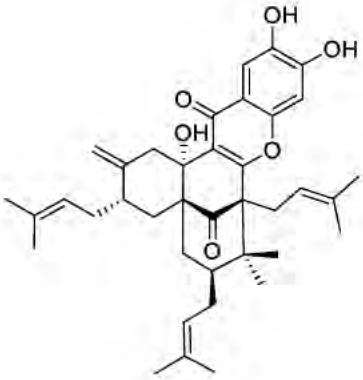

350

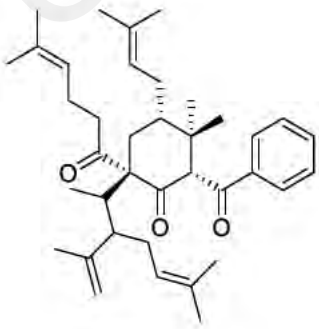

351

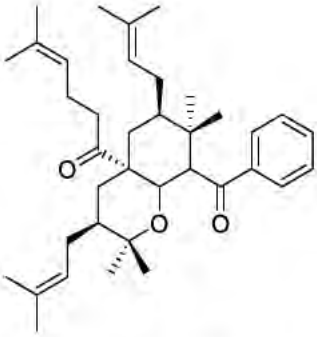

352

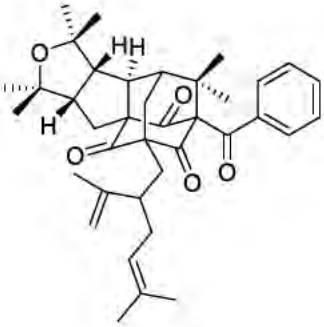

353

Figure 2.6, continued.

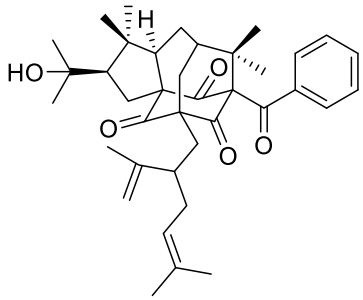

354

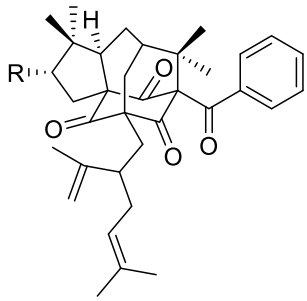

No.	R
355	OH
356	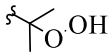

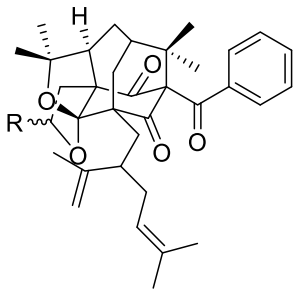

No.	R
357	
358	

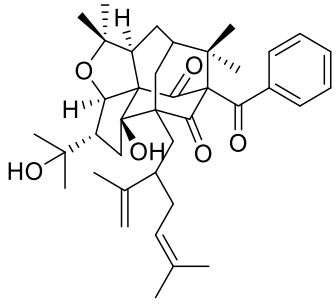

359

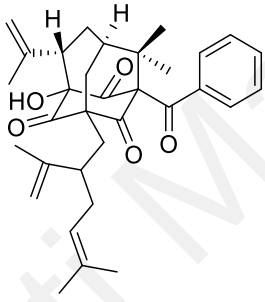

360

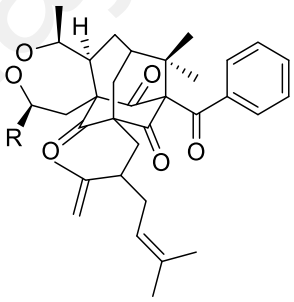

No.	R
361	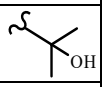
362	OH

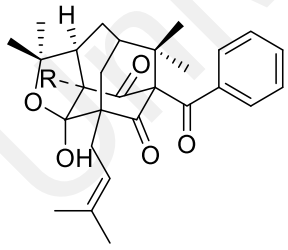

No.	R
363	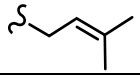
364	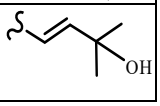

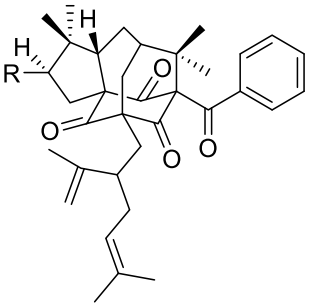

No.	R
365	
366	H

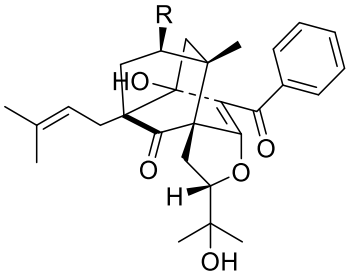

No.	R
367	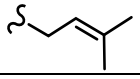
368	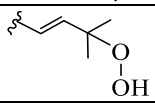

Figure 2.6, continued.

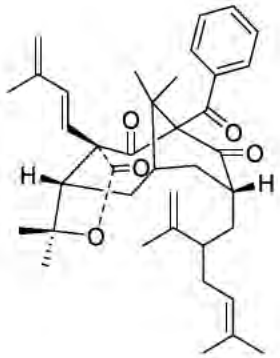

369

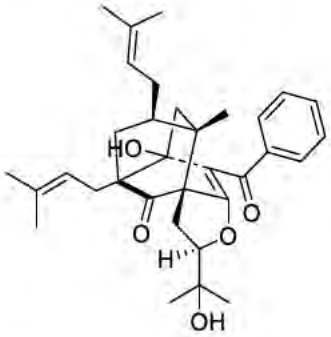

370

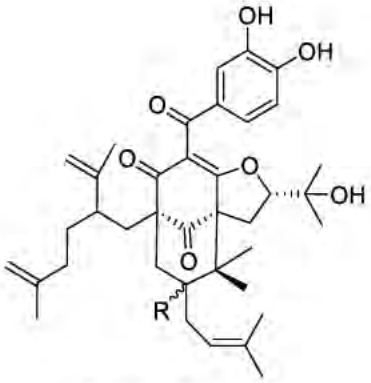

No.	R
372	α-H
457	β-H

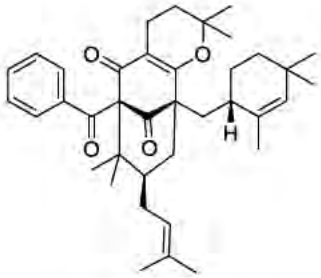

373

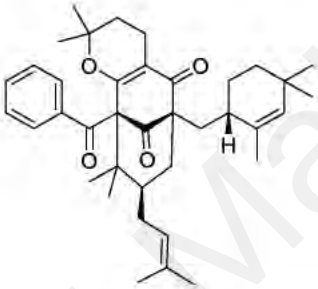

374

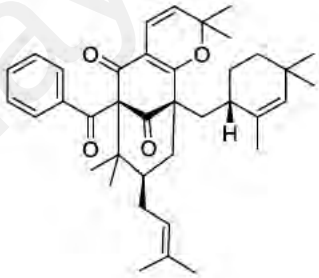

375

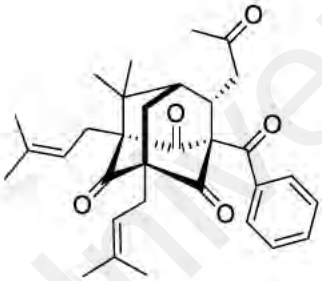

376

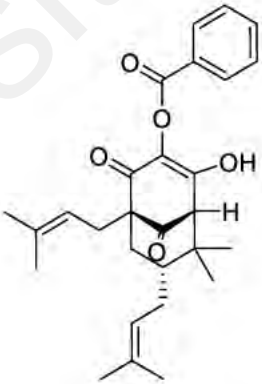

381

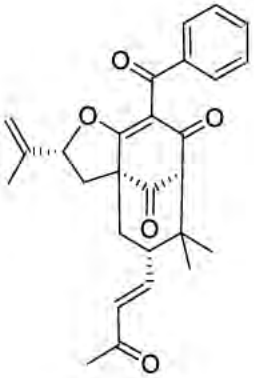

385

Figure 2.6, continued.

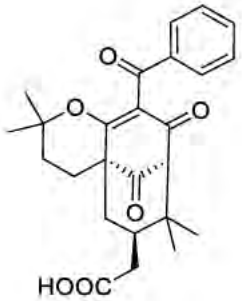

386

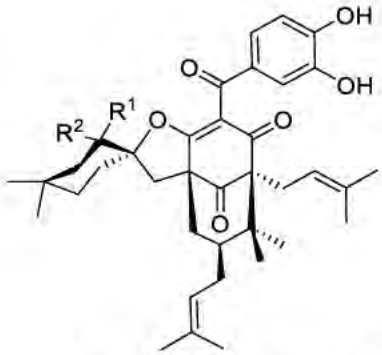

No.	R^1	R^2
388	CH_3	OH
389	OH	CH_3

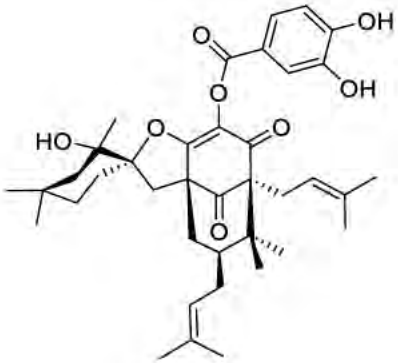

390

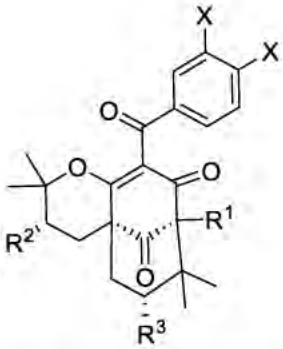

No.	R^1	R^2	R^3	X
383	H	OH	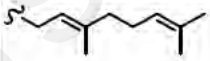	H
472	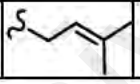	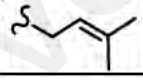	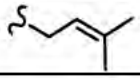	OH

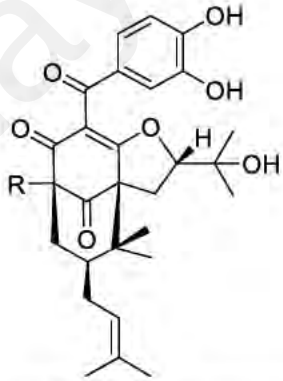

No.	R
392	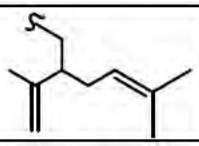
393	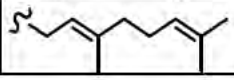

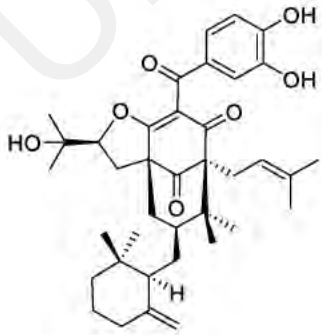

391

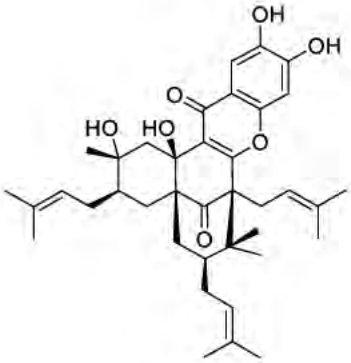

394

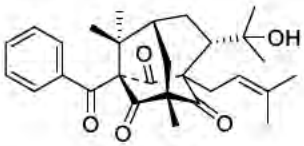

395

Figure 2.6, continued.

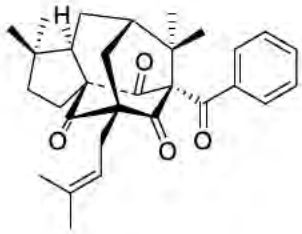

396

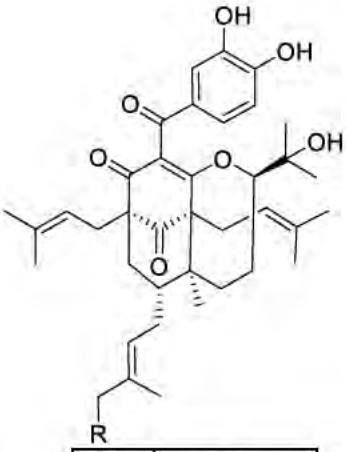

No.	R
403	H
404	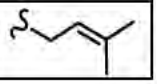

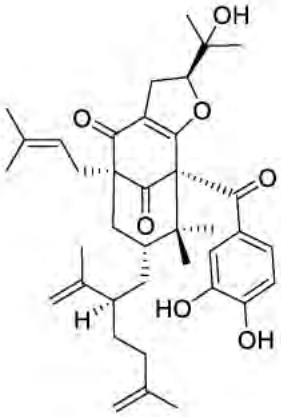

405

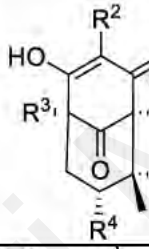

No.	R^1	R^2	R^3	R^4
406	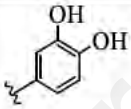		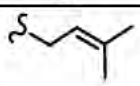	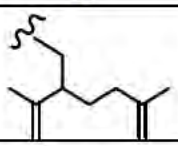
407		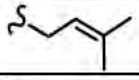	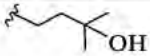	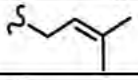
408		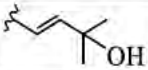	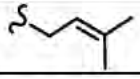	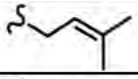
409	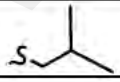	H	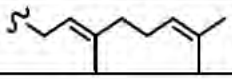	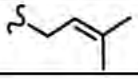

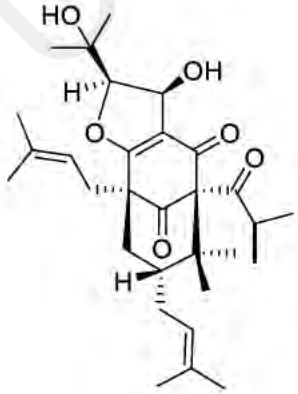

410

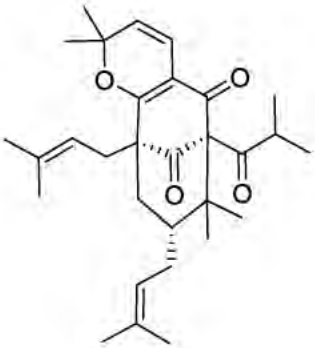

411

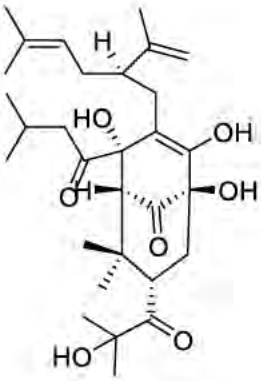

417

Figure 2.6, continued.

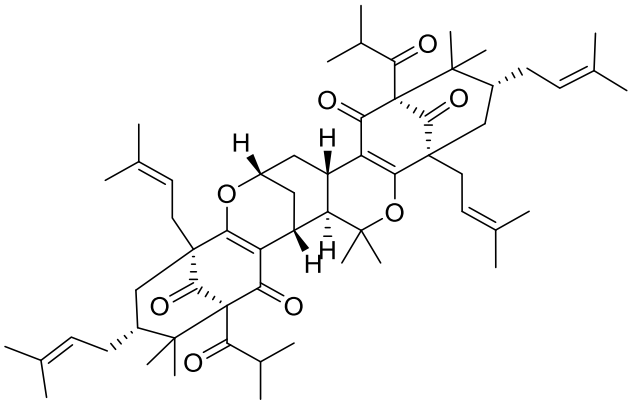

412

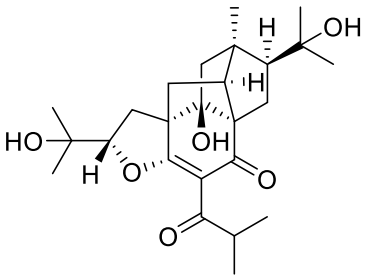

416

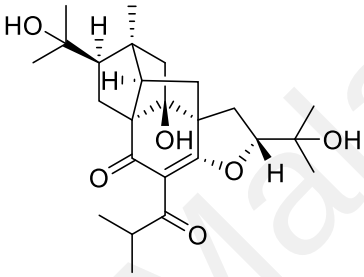

455

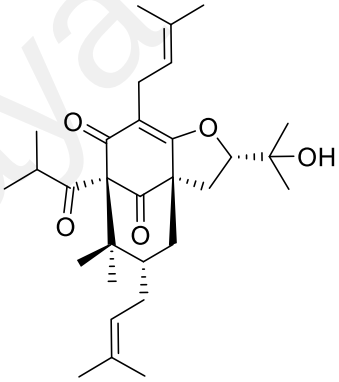

419

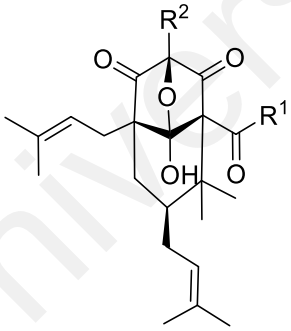

No.	R^1	R^2
413		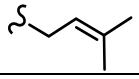
414	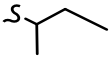	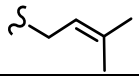
415		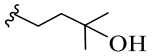

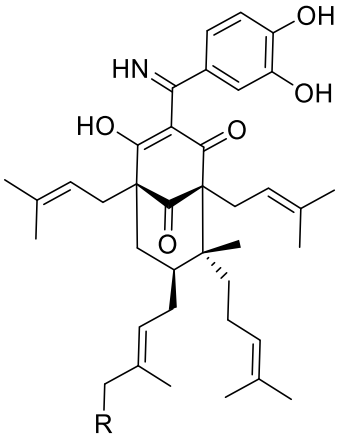

No.	R
421	H
422	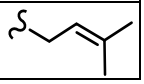

Figure 2.6, continued.

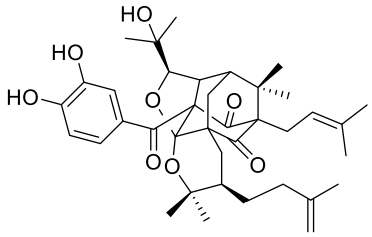

420

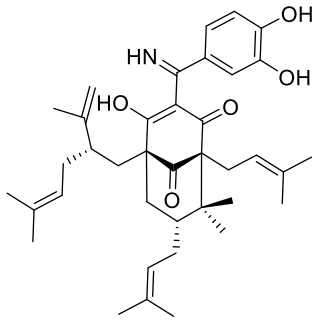

423

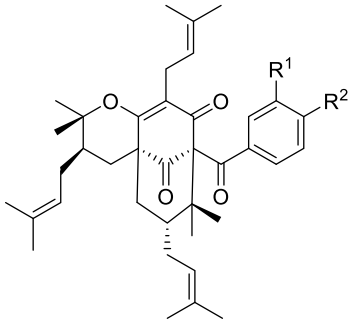

No.	R^1	R^2
424	H	H
425	OH	OH

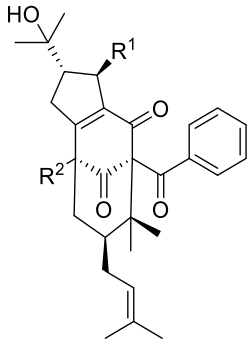

No.	R^1	R^2
426	H	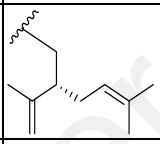
427	OCH_3	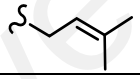

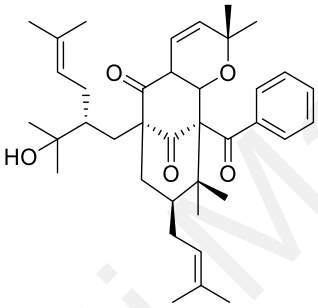

428

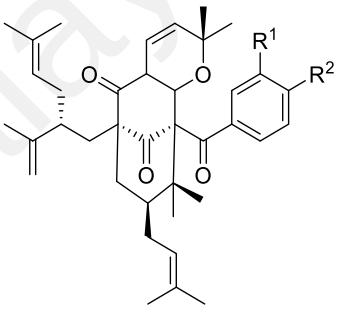

No.	R^1	R^2
429	H	H
430	OH	OH

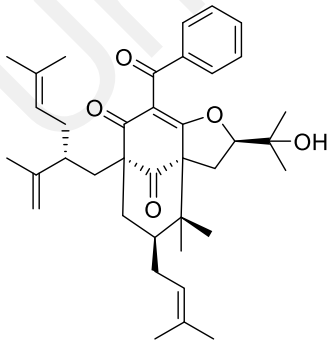

432

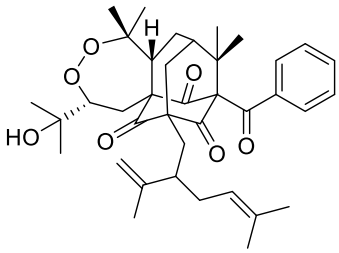

434

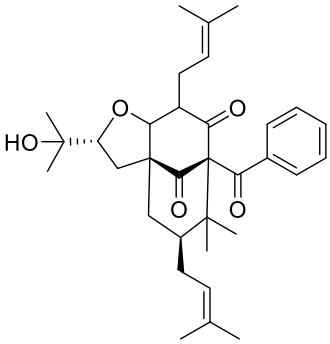

435

Figure 2.6, continued.

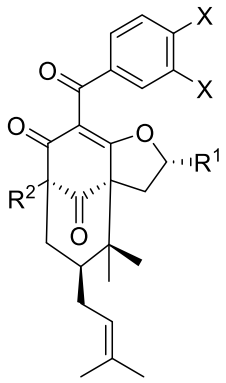

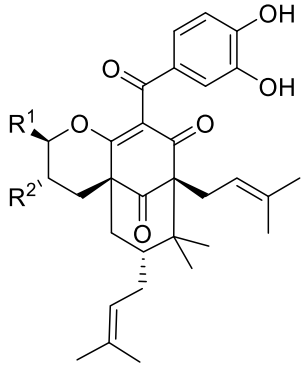

No.	R^1	R^2	X
431		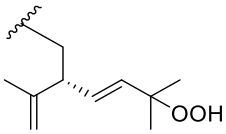	H
499	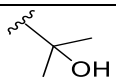	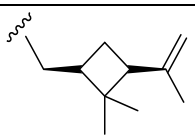	OH
500	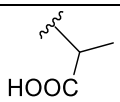	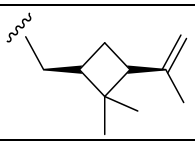	OH

No.	R^1	R^2
443	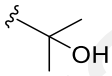	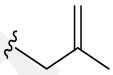
454	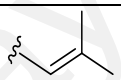	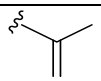

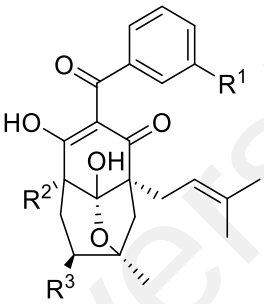

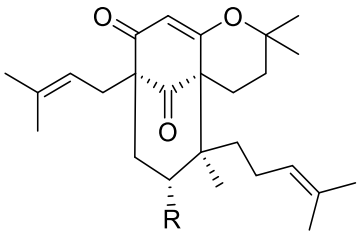

No.	R^1	R^2	R^3
439	H	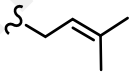	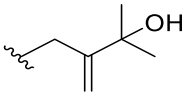
440	H	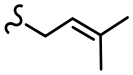	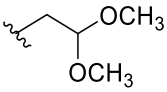
441	OH	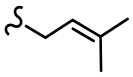	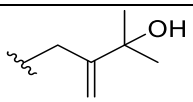
442	H	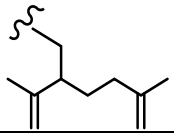	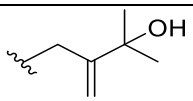
480	H	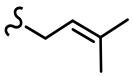	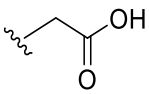

No.	R
449	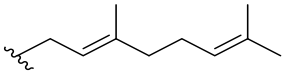
450	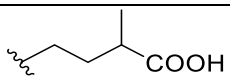

Figure 2.6, continued.

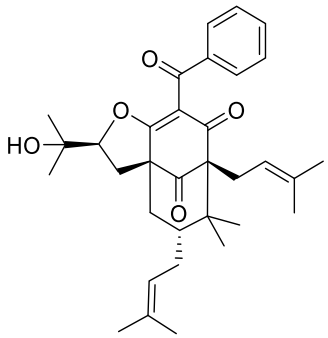

444

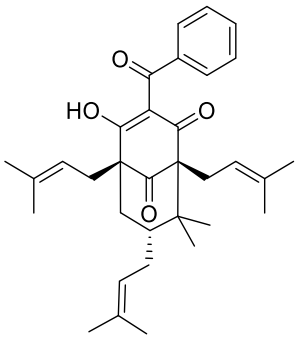

445

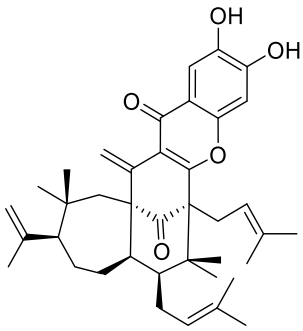

461

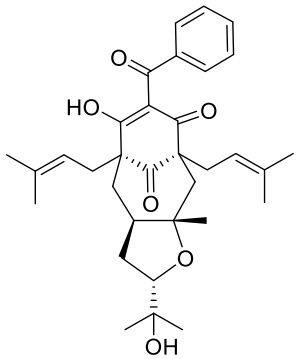

478

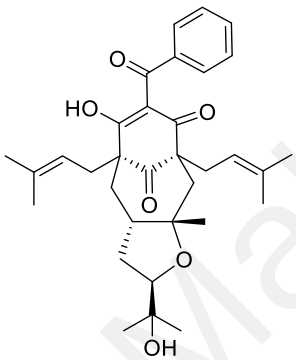

479

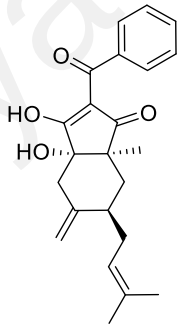

481

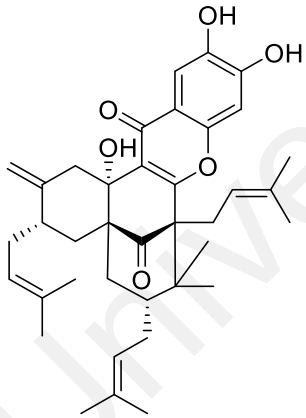

484

Figure 2.6, continued.

(b) ***Biosynthesis pathway of PPAPs***

The biosynthesis pathway of PPAPs involves a "mixed" mevalonate/methylerythritol phosphate and polyketide biosynthetic pathway (Ciochina & Grossman, 2006; Yang et al., 2018). Their acylphloroglucinol cores are produced by a characteristic polyketide-

type biosynthesis involving the condensation of one acyl-CoA and three malonyl-CoA units (Ciochina & Grossman, 2006; Yang et al., 2018). Prenylation of this core moiety affords monocyclic polyprenylated acylphloroglucinols (MPAPs), which may be further cyclized to PPAP-type metabolites with diverse carbon skeletons (Ciochina & Grossman, 2006; Yang et al., 2018). The type of acyl groups, the number and position of isoprenyl substituents, the degree of oxidation of isoprenyl side chains and corresponding locations of ether rings, and different types of secondary cyclization (such as aldol, Diels-Alder, *etc*.) create PPAPs' structural diversity and complexity (Ciochina & Grossman, 2006; Yang et al., 2018).

As suggested by Yang *et al.* 2018, all the PPAP profiles are generated from three major biosynthetic pathways and may be divided into three groups (I-III) according to their different scaffolds (Ciochina & Grossman, 2006; Yang et al., 2018). Only the type B PPAPs biosynthesis pathway was discussed as most of the PPAPs isolated from *Garcinia* belong to type B (Scheme 2.4). The bicyclic polyprenylated acylphloroglucinols (BPAPs) with major bicyclo [3.3.1] nonane-2,4,9-trione core are classified as group I (Ciochina & Grossman, 2006; Yang et al., 2018). The caged PPAPs with adamantane (tricyclo [3.3.1.1] decane) skeletons, derived *via* the enolic C-3 cyclizing onto C-27 and C-28 of normal *endo*-BPAPs, respectively, are included in group II (Ciochina & Grossman, 2006; Yang et al., 2018).

Other biosynthetically related metabolites, derived from direct cyclizations, of MPAPs rather than *via* formation of the BPAPs, are also brought into the PPAPs family and assigned to group III. This group contains complicated PPAPs derived from intramolecular [2+4] cycloadditions of MPAPs (Ciochina & Grossman, 2006; Yang et al., 2018).

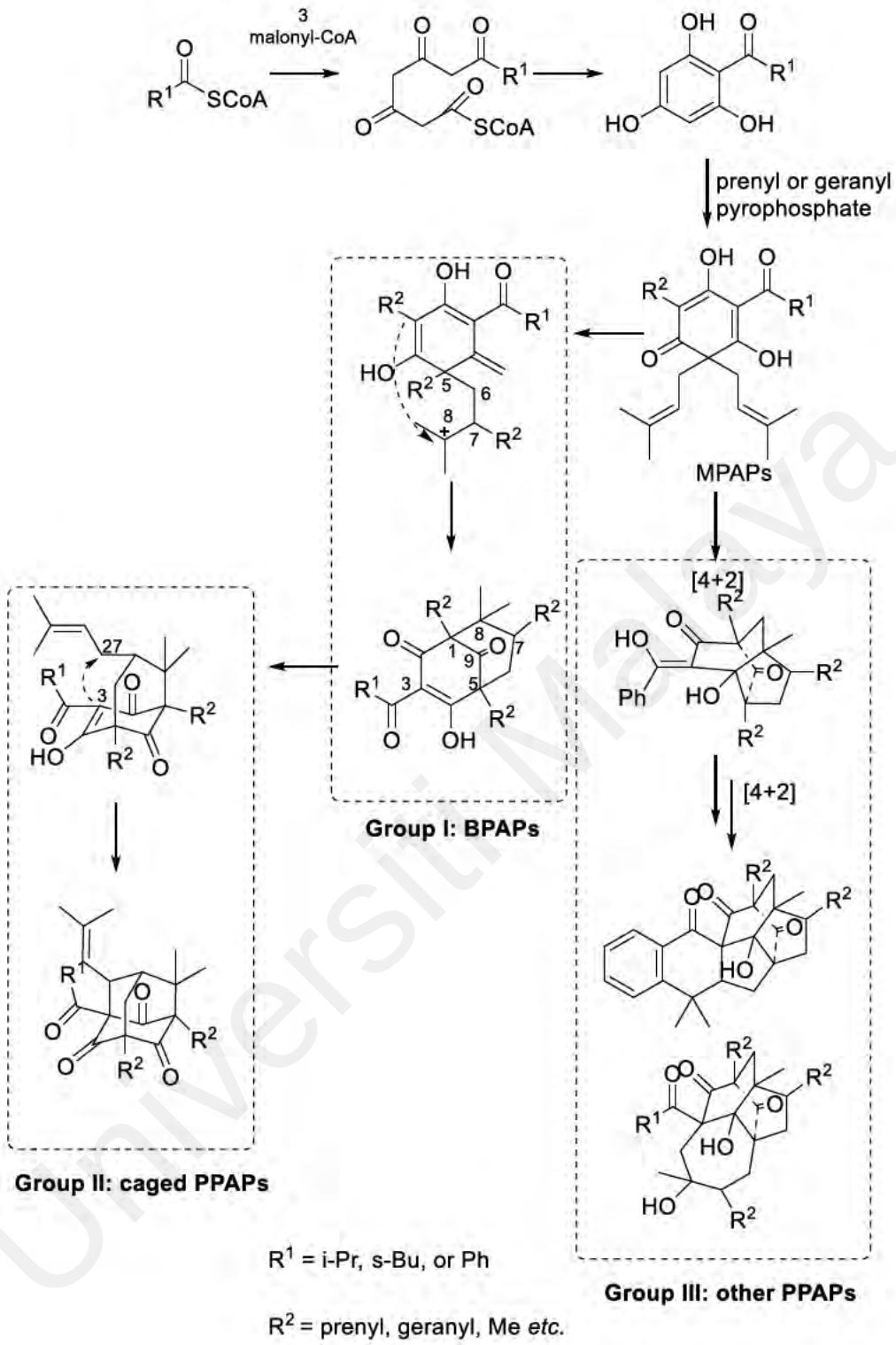

Scheme 2.4: Biosynthesis pathway of the type B PPAPs (Ciochina & Grossman, 2006; Yang et al., 2018).

2.2 ^{13}C-NMR dereplication

NPs research was once the focal point in pharmaceutical industry. Although, the ubiquity and variety of these plant - and microbe - derived compounds provide a great

measures of opportunities for potential drug development, they also present significant obstacles (Gao et al., 2020).

The iterative process of conventional approach in NPs research is tedious, time consuming, and lowest input. This often lead to the loss of interest from investors and grants in funding such work and thus become the bottleneck of the natural product research (Bakiri et al., 2017). Consequently, there is a need to seek for a strategy to efficiently and effectively access and valorize this natural chemical diversity (David et al., 2015). Rapidly identifying known compounds in complex plant extracts becomes significant for the dereplication of NPs, quality evaluation of traditional medicinal herbs, and plant metabolomics. Thus, automated approaches to elucidate the composition in extracts are indispensable and generally of great interest (Huang et al., 2020).

LC-MS and NMR are the two preferable tools that are frequently used for metabolite identification. As dereplication tools, both techniques demonstrate advantages and drawbacks while also being complimentary to one another (Bakiri et al., 2017). MS provides a higher sensitivity but with the risk of missing poor ionization compounds (Harvey et al., 2015) as well as problem of similar fragmentation of isomers. In contrary, NMR may have lower sensitivity, but the spectrum reveals all compounds and differentiation of stereoisomers can be detected. Anyhow, ^{1}H chemical shifts (δ_H) are solvent dependent and overlapping of signals may hinder the identification of metabolites unambiguously (Bruguière et al., 2018). Therefore, ^{13}C-NMR spectra which have low gyromagnetic ratio, low natural abundance of ^{13}C nuclei and less influence of the chemical shift deviation due to pH, temperature, and referencing variations (Huang et al., 2020) was suggested as the dereplication tool.

Algorithms, which are unfamiliar to most of us, are in our daily transaction, work, online shopping, and even virtual social life. Deep learning is used by large companies

such as Baidu, Google, and Facebook for facial recognition algorithms alone. Self-driving cars and robot helpers are no longer a pipe dream; they are becoming a reality in life. We currently live in an era surrounded by artificial intelligence software that employs machine learning to forecast our needs in various ways before we noticed what they are (Ekins, 2016; Rost et al., 2016). Hence, the application of algorithms was thought to benefit in NPs research, especially the process in identifying known chemotypes.

Indeed, the development of algorithms that allow systematic screening and dereplication of the structurally diverse NPs would be extremely valuable (Gao et al., 2020). The application of different computational approaches and machine learning algorithms to problems tends to follow the growth of datasets (Ekins, 2016). Hence, a complete set of databases (DBs) with the needed info of metabolites structures is crucial.

However, tandem MSMS data is not often employed for the structural elucidation of purified metabolites for phytochemical research. Though there is not much comprehensive and publicly available NMR DB of purified NPs, most of the published NPs have detailed and assigned NMR data which allowing you to develop your own DB. Thus, an algorithm on the based of NMR data that extracted from publications having extensive chemical and structural information, together with some software tools, is regarded as a viable approach to the rapid identification of known NPs (Huang et al., 2020).

In this study, a ^{13}C-NMR dereplication tool which is named MixONat (Mixture of Natural Products), a freely distributed algorithm tool, created by SONAS researchers was used to identify the various chemical constituents in *M. lepidota* and *G. griffithii*. MixONat is an algorithm based on Python 3.5, written by Bruguière *et al.* in 2020 (Bruguière et al., 2020), and can be downloaded from https://sourceforge.net/projects/mixonat/. MixONat proposed the presence of compounds

in a mixture based on the type of carbon through DEPT-135 and/or DEPT-90 experiments and classified compounds from a given DB according to decreasing scores.

Initially, ^{13}C, DEPT-135 and/or DEPT-90 NMR spectra of mixture have to be analysed and processed to align the chemical shifts of the spectra. Following that, a DB consisting of predicted (calculated by ACD NMR Predictors (C, H)) or experimental (literature values) chemical shifts of metabolites of interest must be constructed or retrieved from an online source, *e.g.*, Mendeley. Depending on the study's objective, the DB might be a chemotaxonomic based or a type of compound-based DB. The spectra data and DB are then imported to MixONat, which will analyse the chemical shifts, matches the carbons of each structure, and proposes the best-matching compounds based on the scores. Previous studies revealed that MixONat gave coherent results that guided the users towards the accurate structural types of compounds. Furthermore, MixONat findings enabled users to distinguish between structurally identical NPs, including stereoisomers.

Bruguière and his colleagues used MixONat to effectively identified alkaloids in *Papaver somniferum* extracts, diterpenes and triterpenes in *Rosmarinus officinalis* leaf extract, as well as xanthones in the pericarps extract of the *Garcinia mangostana* fruit (Bruguière et al., 2020).

Subsequently, several studies also utilised MixONat in the research. Xanthones has been identified from the extract of *G. parvifolia* bark and *Calophyllum brasiliense* (Meunier et al., 2023; Silva-Castro et al., 2021). More recently, the complex chemistry of various African propolis has been described using such strategy (Azonwade et al., 2023) as well as polyphenols from *Aloe vera* leaves (Yin et al., 2023). These studies demonstrated that the usage of MixONat in NPs research produced promising outcomes. Hence, this dereplication tool was chosen to be used in this study.

A two-step protocol was proposed in this study on *M. lepidota* and *G. griffithii* to dereplicate the extracts more efficiently and reliably. The first step of the dereplication strategy involved the HPLC chromatogram and MS spectral profile to identify known constituents in crude extracts (Knestrick et al., 2019). Followed by dereplication with MixONat using ^{13}C-NMR and DEPT-NMR spectra to identify constituents from the extracts.

2.3 Biological activities

AD is a neurodegenerative disorder that accounts for age-related dementia in more than 80% cases worldwide (Anand et al., 2014; Shal et al., 2018). It is a progressive disease leading to disturbances of memory and cognitive function (Shal et al., 2018). Alzheimer's Disease Foundation Malaysia (ADFM) predicted that there are more than 204,000 (8.5%) of Malaysians in the end-stage of dementia in year 2020 (*Dementia cases set to rise 312 per cent by 2050: Is Malaysia prepared?*). Besides, Malaysia is expected to become an ageing nation with the elderly population of 15% of the total population by the year 2030 (Abdul Rashid et al., 2016). The statistic showed that the AD and the ageing issue is not only a worldwide issue, but also a threat to Malaysians.

There are two hypotheses that explained the pathogenesis mechanism and disease symptoms of AD: the "amyloid hypothesis" and the "cholinergic hypothesis". The "amyloid hypothesis" is evaluated by intracellular deposits of tau proteins that affect intracellular transport and lead to cell death; whereby the extracellular deposits of β-amyloid peptides that is accompanied by oxidative stress and inflammation and leads to neuron degeneration (de Souza et al., 2016; Jiang et al., 2014). The "cholinergic hypothesis" is hypothesized by the main biochemical alteration presented in the patient's brain. The reduction of acetylcholine (ACh) lead to the severe loss of cholinergic neurons

in the hippocampus and cerebral cortex (de Souza et al., 2016; Stepankova & Komers, 2008). This study focused on the study of the "cholinergic hypothesis".

Cholinesterase is a family of enzymes that catalyzes the hydrolysis of the neurotransmitter ACh into choline and acetic acid (Colovic et al., 2013). This is an essential reaction that allow a cholinergic neuron to return to its resting state after activation (Colovic et al., 2013). Moreover, it has been found that amyloid protein plaques can be caused by both acetylcholinesterase (AChE EC 3.1.1.7) and butyrylcholinesterase (BuChE EC 3.1.1.8), and the inhibitors is useful in decreasing those plaques (Li et al., 2017; Yu et al., 2010). In fact, abnormalities in cholinergic system may also lead to other neurodegenerative disorders, such as Parkinson's Disease, dementia with Lewy bodies and vascular dementia (Grantham & Geerts, 2002; Li et al., 2017; Perry et al., 1999).

Previous research proved that the "cholinergic hypothesis" directly contributed to the cognitive decline. Hence, the treatment of AD nowadays is predominantly based on the "cholinergic hypothesis" (Zueva et al., 2019). Clinically treatment of AD focused on the enhancement of cholinergic function by prolonging the availability of ACh released into the neuronal synaptic cleft through the use of cholinesterase inhibitors to inhibit the enzyme responsible for breaking down ACh (Wan Othman et al., 2016). This laid the interest for the use of inhibitors of enzymes in cleaving the neurotransmitter ACh, AChE and BChE as therapies against AD (Zueva et al., 2019).

Currently, there are only a few clinical drugs approved by Food and Drug Administration (FDA) for treatment of AD, including the latest approved medicine, Aduhelm (aducanumab) (Tanzi, 2021). Some of them are AChE inhibitors, *i.e.*, tacrine, donepezil, rivastigmine and galantamine (Atri, 2019). However, these drugs has been much disputed due to the side effects, such as nausea, diarrhea, insomnia and a slower heart rate, even though certain therapeutic effects were shown (Fang et al., 2020).

Therefore, finding new cholinesterase inhibitors, which may be found in natural resources, with less adverse effects is prompted (Bui & Nguyen, 2017).

Mesua and *Garcinia* were two genera that exhibit various biological activities, *i.e.*, anti-cholinesterase, anti-inflammatory, and anticancer. Previous research showed that *Mesua* and *Garcinia* genera possess high potential anticholinergic compounds. Study conducted by Awang *et al.* demonstrated that mesuagenin A **79**, B **80**, and D **75**, isolated from *M. elegans*, exhibited significant AChE inhibitory activity (with IC_{50} range of 0.7-8.73 μM) (Awang et al., 2010). α-mangostin **107** and a synthetic derivative compound, congestiflorone acetate **485** isolated from *Mesua* are potential lead compounds of anticholinesterase agents too (Teh et al., 2016).

Moreover, *G. hombroniana*, *G. mangostana*, and *G. fusca* were reported *Garcinia* species that contained active cholinesterase inhibitors. Garciflavonol A **486** isolated from *G. atroviridis* was dual inhibitor with IC_{50} values of 18.00 μM and 18.58 μM against AChE and BChE, respectively (Tan et al., 2014). Besides, garcinone C **487** and γ-mangostin **488** isolated from *G. mangostana* exhibited potent inhibitory activities against AChE and BChE too (Khaw et al., 2014). From *G. fusca*, cowagarcinone E **489** were the isolated compound which exhibited remarkable BChE inhibitory activity (Saenkham et al., 2020).

In this study, Ellman's assay with some modification was used as the method of the tests of anticholinesterase inhibitory activities (Ahmed & Gilani, 2009). Spectrophotometry according to Ellman's method was the most used photometric method for cholinesterase activity study (Ellman et al., 1961; Holas et al., 2012). Through this method, thiocholine liberated during the enzymatic reaction and reacts with 5,5'-dithio-bis-(2-nitrobenzoic) acid (DTNB) to formed 3-carboxy-4-nitrothiolate anion (TNB anion) which has a strong absorption at 412 nm. The acetylthiocholine (ATCh) for AChE and

butyrylthiocholine (BTCh) for BChE were the substrates with the best specificity/stability ratio (Dietz et al., 1973; Holas et al., 2012; Yamada et al., 2001). In addition, AChE from *Electrophorus electricus* and BChE from equine serum were used as hydrolases for this research, owing to the complete homology of their active sites compared to the human isoform were similar, albeit with some notable differences (Kitagawa et al., 2019; Yücel et al., 2008).

CHAPTER 3: EXPERIMENTAL

This chapter will discuss the experimental procedure of each plant, *M. lepidota* and *G. griffithii.* The discussion is divided into seven main subtopics: plant material, instrumentation, chemicals and enzymes, ^{13}C-NMR dereplication with MixONat, phytochemical studies of both plants, physical data of isolated compounds, as well as cholinesterase inhibitory activity which including enzyme kinetics study, molecular docking, and molecular dynamics simulations of the most potent compound.

3.1 Plant Material

Mesua lepidota (Family Calophyllaceae) and *G. griffithii* (Family Clusiaceae) were selected for the study. Both plants were identified by the botanist, Mr. Teo Leong Eng and were deposited in the Herbarium of Department of Chemistry, Faculty of Science, Universiti Malaya, Kuala Lumpur, Malaysia. The info of the collections of both species were stated in Table 3.1.

Table 3.1: Plant species and the collection info.

Voucher specimen	Plant species	Collection site	Collection date
KL 5436	*M. lepidota*	Hutan Simpan Madek, Lenggor, Kluang, Johor	22nd June 2007
KL 5303	*G. griffithii*	Hutan Simpan Sungai Badak, Jitra, Kedah.	18th September 2006

3.2 Instrumentation

- 1D and 2D NMR spectra were obtained using Bruker AVN400 FT NMR and Bruker AVN600 FT NMR (Bruker, Massachusetts, USA).

- Mass spectrometry was performed on the Agilent (Santa Clara, USA) LC-MS system composed of an Agilent 1260 Infinity HPLC coupled with an Agilent 6530 ESI-QTOF-MS as well as AB Sciex Triple TOF 5600 system with Turbo V source and ESI probe.
- UV spectra were recorded on a Shimadzu (Tokyo, Japan) UV-Visible Recording Spectrophotometer using AR grade ethanol as solvent with mirror UV cell.
- The infrared (IR) spectra were obtained through Perkin Elmer FT-IR Spectrometer Spectrum 400.
- A Jasco P-1020 polarimeter was used to record the optical rotation $[\alpha]_D^{25}$. The optical rotation values are expressed in degree.[dm.g/cm^3]$^{-1}$ for a concentration of compound g/cm^3.
- Tecan Infinite 200 Pro Microplate spectrometer was used to measure the absorbance of plates in the biological activity test.

3.3 Chemicals and enzymes

The chemicals and enzymes used for this study were discussed in the following sections.

3.3.1 Chromatography

Several chromatography methods were used, including column chromatography, thin layer chromatography, and HPLC.

3.3.1.1 Thin layer chromatography (TLC)

Aluminium supported silica gel 60 F254 plates were used to visualize the spots of the isolated compounds. UV Light Model UVGL-58 Mineral light Lamp 230 V~50/60 Hz was used to examine spots or bands on the TLC after spraying with the specified reagents.

3.3.1.2 Preparative thin layer chromatography (PTLC)

PTLC silica gel 60 F254 glass plate (20 x 20 cm) were used for isolation of compounds besides conventional column chromatography. Bands on the PTLC were visualized using a UV Lamp Model UVGL-58.

3.3.1.3 Column chromatography (CC)

Distilled industrial grade solvents were used for column chromatography. Silica gel 60, 230-400 mesh ASTM (Merck 9385) was used as the stationary phase for column chromatography. A slurry of silica gel 60 (approximately 30:1 silica gel to sample ratio) in non-polar solvent system was poured into a glass column of appropriate size with gentle tapping to remove trapped air bubbles. Then, the crude extract was dissolved in minimum amount of solvent and loaded on top of the packed column. The extract was eluted with an appropriate solvent system at a certain flow rate. Fractions were collected in conical flasks/test tube and concentrated. TLC was used to visualize the spot of compounds in each fraction. Fractions with similar compounds were combined.

3.3.1.4 High performance liquid chromatography (HPLC)

Waters HPLC System was used for HPLC separation, equipped with a Waters 486 Tunable Absorbance UV detector. Chromatographic analysis and separations were performed on ZORBAX Eclipse Plus C18 (4.6 mm i.d. x 150 mm x 5 µm), ZORBAX Eclipse Plus C18 (9.4 mm i.d. x 250 mm x 3.5 µm), X bridge semi preparative column (10 mm × 250 mm × 5 µm) and Lichrospher 100 RP-18 (4.6 mm i.d. x 150 mm x 5 µm) HPLC columns. Methanol (MeOH) (HPLC grade), Acetonitrile (ACN) (HPLC grade), and deionized water with formic acid were used as mobile phase solvents. All solvents and samples were filtered with 0.45 µm nylon membrane filter prior to HPLC analysis.

3.3.2 Reagent

The reagent used for detection of secondary metabolites contents was vanillin-sulfuric acid. Besides, the reagents, enzymes and chemicals used for anticholinesterase activities were discussed in the following sections.

3.3.2.1 Vanillin- sulfuric acid

1.0 g vanillin in 10 mL of concentrated H_2SO_4 was added upon cooling to 90 mL of ethanol before spraying onto the TLC plate. The TLC plate was then heated at ~50 ºC until full development of colors had occurred. The occurrence of blue, purple, dark green, grey, or brown spots indicated the presence of phenolic compounds, *i.e.*, coumarins and PPAPs.

3.3.2.2 Chemical, reagents, and enzyme for biological activities

AChE from electric eel, 5,5′-dithiobis (2-nitrobenzoic acid) (DTNB), acetylthiocholine iodide (ATCI), BChE esterase from equine serum, *S*-butyrylthiocholine chloride, donepezil and galantamine hydrobromide were purchased from Sigma (St. Louis, MO). Sodium dihydrogen phosphate anhydrous was purchased from R&M Chemicals (Essex, UK) while disodium hydrogen phosphate anhydrous was purchased from Merck (Darmstadt, Germany). All the other reagents and chemicals used were analytical grade.

3.4 ^{13}C-NMR dereplication with MixONat

MixONat is a ^{13}C-NMR dereplication tool used in this research to identify metabolites from extracts or fractions. Initially, ^{13}C and DEPT-135 and/or DEPT-90 NMR spectra of mixture were obtained and processed. Then, the building of DBs through different sources, *i.e.*, LOTUS DB, SciFinder and Dictionary of Natural Products (DNP) was executed. The spectra data and DB were then imported to MixONat. Finally, MixONat

analyzed and proposed the compounds with decreasing scores. The details of the process were presented in Scheme 3.1. and discussed in sections 3.4.1 to 3.4.3.

3.4.1 NMR analyses and data processing

Experiments (^{1}H-NMR, ^{13}C-NMR, DEPT-135, DEPT-90 and 2D NMR) were performed on a Bruker AVN400 FT spectrometer (Bruker, Massachusetts, USA) equipped with a 5 mm BBO probe (ATM). Chemical shifts (δ_H and δ_C) were expressed in ppm and ^{1}H coupling constants (*J*) in Hz. The hexane extract (30 mg) of *M. lepidota* (HML) and the DCM extract (30 mg) of *G. griffithii* (DGG) were dissolved in 600 µL of $CDCl_3$. Then, the fraction of *G. griffithii* (30 mg) was dissolved in 600 µL of deuterated methanol (CD_3OD) + 0.1% trifluoroacetic acid (TFA).

For ^{13}C-NMR (100 MHz) spectra, a WALTZ-16 decoupling sequence was used with an acquisition time of 1.29 s (32768 complex data points) and a relaxation delay of 2 s. The number of acquisitions was ten thousand scans. A 1 Hz exponential line-broadening filter was applied to each FID prior Fourier transformation. Raw data were processed by the MestReNova 12.0.2 (Mestrelab Research, Santiago de Compostela, Spain) and calibrated to solvent peaks at δ_C 77.16 ($CDCl_3$) or δ_C 49.00 (CD_3OD). Manual phasing and baseline correction were applied. Alignments of DEPT experiments were done with ^{13}C spectra using a given δ_C.

3.4.2 Databases (DBs)

Different DBs were created and used in the study based on the objectives. In this study, two chemotaxonomic DBs prepared from different sources were used on the dereplication of *M. lepidota* while a chemotaxonomic DB and a compound type (PPAPs) DB were used on the dereplication of *G. griffithii*. The details of the DBs were presented in the following sections.

NMR analyses and data processing

- Run ^{13}C, DEPT-135 and/or DEPT-90 NMR for about 30 mg of mixture
- Process raw data by manual phasing and baseline correction
- Alignment of DEPT-NMR spectra with ^{13}C-NMR spectrum
- Save the data of chemical shifts and intensities in .csv file for each spectrum

Databases- general information

- Gather the structure of compounds of interest from different sources, *i.e.*, LOTUS, SciFInder, DNP, then save as structure data file (.sdf).
- Predict the δ_C of each compound by using a NMR prediction software (*i.e.*, ACD/Labs Spectrus processor and C/H NMR Predictor).
- Sort the chemical shifts by carbon types and save as new SDF file.
- Label the DB as c_type DB

Imported to

MixONat Inputs and parameters

- Default setting and parameters were used.
- MW filter was filled if the LC-MS-MS profile was determined.
- Tolerance that reflects the accuray of rhe DB was set at 1.3 ppm.
- DEPT-alignment parameter was set at 0.02 ppm.
- Equivalent carbon factor is OFF.
- Run the tool.
- Result save as a text and image file.

Scheme 3.1: The process of ^{13}C-NMR dereplication with MixONat to identify compounds.

3.4.2.1 *M. lepidota*

A c-type_Mesua DB1 was created. In 2018, a search on SciFinder (*CAS. SciFinder*) using *Mesua* as a keyword. A file consisting of 440 metabolites cited in the related publications was saved in structure data file (.sdf). The predicted $\delta_{C\text{-}SDF}$ of the structures was generated using ACD NMR Predictors (C,H) (version 0.03)(ACD/Labs, 2011) . The resulting SDF was exported and submitted to the C-typeGen program in MixONat software to obtain the predicted $\delta_{C\text{-}SDF}$ organized as methyl, methylene, methine or quaternary carbons, that are compatible for MixONat.

A second DB, namely c-type_LOTUS_Mesua DB2 was created in 2021. A search of NPs using the keyword *Mesua* in the LOTUS DB containing 276 518 NPs (Adriano Rutz et al., 2022) allowed to obtain a DB of 145 NPs as a SDF. $\delta_{C\text{-}SDF}$ were predicted using the ACD NMR predictors (C,H) software as well as the methodology previously described by Nuzillard (Nuzillard, 2021) to obtain directly the c-type SDF ready for use by MixONat.

3.4.2.2 *G. griffithii*

Two DBs were prepared and used for the ^{13}C-NMR dereplication of *G. griffithii*.

A *Garcinia* DB named c_type_garcinia_DNP was prepared in year 2016. The structures of compounds in literature review of *Garcinia* (gathered 718 metabolites) were compiled by downloading from DNP website (ChemNetBase, 2015) in year 2015. The files were saved in SDF, and the predicted δ_C of the structures was generated through ACD/Labs Spectrus processor and C/H NMR Predictor. The SDFiles were then imported in the C-typeGen program in MixONat to organize the chemical shifts according to carbon type.

A PPAPs DB was built in 2018 by downloading the structures of the PPAPs previously described from the "Table of Naturally Occurring PPAPs" made freely available by Grossman (Grossman 2018, http://www.uky.edu/~rbgros1/PPAPs/allPPAPs.html) (Yang et al., 2018; Yang; et al.). Briefly, to obtain the SDF, the procedure was as follows:

1. Use Chrome to open http://www.uky.edu/~rbgros1/PPAPs/allPPAPs.html.

2. Choose View / Developer / JavaScript console.

3. In the top bar, press Sources.

4. On the left, right-click on molStrucs.js, and save it to the desktop.

5. Open molStrucs.js with a text editor such as Notepad++.

6. Globally replace **\n** with a **return character**.

7. Globally delete **': '** [single-quote colon space single-quote].

8. Globally replace **',** [single-quote comma] with $$$$.

9.Globally delete →**'** [tab single-quote].

10. Delete the first line, including the return character, and the last four lines (the last $$$$ and after) of the file. There should be no blank lines at the beginning of the file nor after each $$$$ line.

11. Save the changes to a new file with the extension sdf to obtain a structure data file containing 762 PPAPs.

Using ACD C/H NMR predictor, absolute configurations of asymmetric carbons were manually checked and corrected. Their predicted δ_C were generated through ACD/Labs Spectrus processor and C/H NMR Predictor. The SDFiles were then imported in the c-typeGen program in MixONat to organize the chemical shifts according to carbon type.

3.4.3 MixONat- A ^{13}C-NMR dereplication software

MixONat (Figure 3.1) (Bruguière et al., 2020) is a freely distributed algorithm developed by SONAS lab, Université Angers. It allows dereplication of mixtures of NPs

by comparing the δ_C of NPs as mixtures with those - experimental or predicted - of compounds gathered in a given DB, taking into account multiplicities. The use of DEPT-135 and DEPT-90 NMR data in MixONat will enhance the accuracy of dereplication result.

MixONat implemented the algorithm in the Python 3.5 programming language. The open-source cheminformatics package RDKit was used to draw the molecular structures and read SDFiles. This software can be downloaded from http://sourceforge.net/projects/mixonat (Bruguière et al., 2020; *MixONat*).

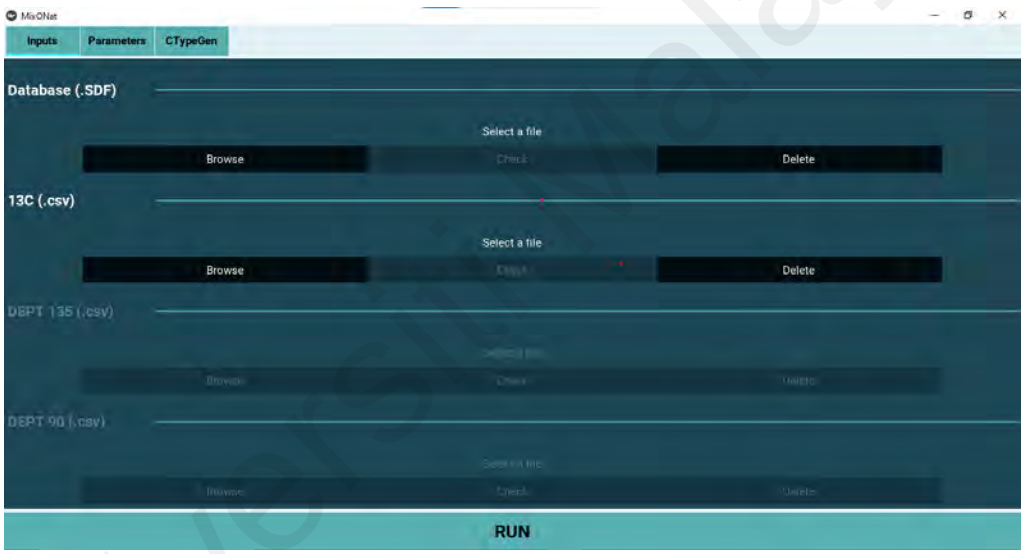

Figure 3.1: MixONat Software.

3.4.3.1 Inputs in MixONat

The ready used c_type_genus DB, ^{13}C, DEPT-135 and DEPT-90 NMR (.csv file) were imported in MixONat software. Default setting and parameters were used. The molecular weight filter was filled if the LC-MS-MS profile of the extract or fraction was determined. In this study, molecular weight filter was used in the ^{13}C-NMR dereplication of *M. lepidota* to reduce the hit of fatty acids in the result. The range of molecular weight of metabolites in the fraction or extract can be obtained through the profile. MixONat analyzed and proposed the compounds with decreasing scores.

3.5 Phytochemical studies of *M. lepidota* and *G. griffithii*

Two different objectives were set for the research on *M. lepidota* and *G. griffithii*. Hence, the experimental of phytochemical studies in the research were discussed according to the plant species.

3.5.1 *M. lepidota*

The experimental details of extraction, isolation, and purification of secondary metabolites from the stem barks of *M. lepidota* were discussed from sections 3.5.1.1 to 3.5.1.3.

3.5.1.1 Extraction of bark of *M. lepidota*

1.5 kg of dried, grounded bark was macerated in hexane at room temperature for three days. Then, the hexane extract was filtered and dried with rotary evaporator. The procedure was repeated three times to produce yellow gummy hexane crude (9.1 g). This hexane extract of *M. lepidota* bark was labelled as HML bark.

3.5.1.2 Dereplication with HPLC-PDA and LC-MS^n analysis of HML bark

The HML bark was analyzed using HPLC-PDA and LC-MS^n to determine possible chromophores in the extract (Figure 3.2).

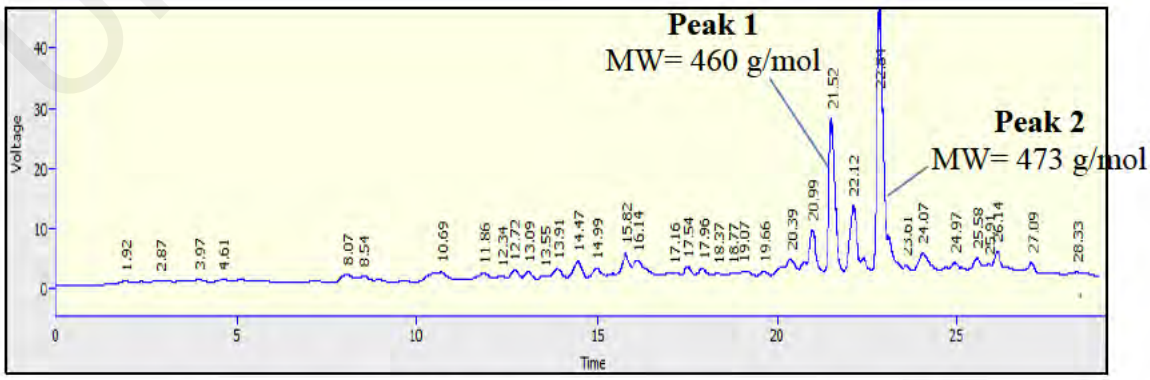

Figure 3.2: HPLC-PDA chromatogram of the HML bark.

The HPLC-PDA chromatogram revealed that there are at least two coumarins in the HML bark (Table 3.2). By comparison of UV spectra, mass spectra and fragmentations with literature review, the two compounds were suggested as lepidotol A **70** and lepidotol B **71** and will be further confirmed by isolation.

Table 3.2: Retention time (t_R) and ESI-MS^2 data for the major compounds in the HML bark.

Peak	t_R (min)	UV λ_{max} (nm)	(+)-ESI-MS *m/z*	(+)-ESI-MS^2 m/z	(-)-ESI-MS *m/z*	(-)-ESI-MS^2 m/z	Suggested molecular weight (Da)	Hypothetical structure
1	21.52	298, 363	461	391(-70), 337(-124)	459	390 (-69), 347(-112)	460	Lepidotol A **70**
2	22.81	302, 363	497, 475	429(-84), 391(-84), 351(-124)	473	404 (-69), 361(-112)	473	Lepidotol B **71**

3.5.1.3 Isolation and purification of HML bark

2.1 g of the HML bark was fractionated by HPLC on Zorbax C-18 column with MeOH and water + 0.01% formic acid as gradient eluent (70 → 100% MeOH 0-20 minutes) (Figure 3.3). Ten fractions were collected and screened for biological activity. The anticholinesterase activity screening showed that fractions 1, 2 and 4 were active (details of the result were recorded in Table 4.19). Hence, isolation of compounds was proceeded on these three (3) fractions (Scheme 3.2).

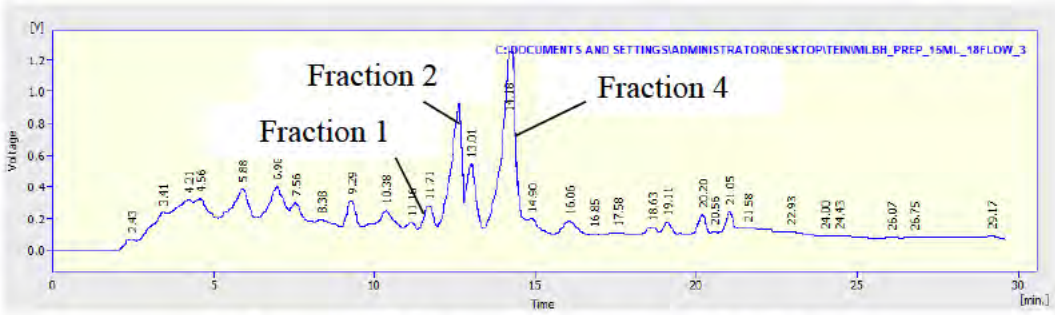

Figure 3.3: Chromatogram of *HML* bark.

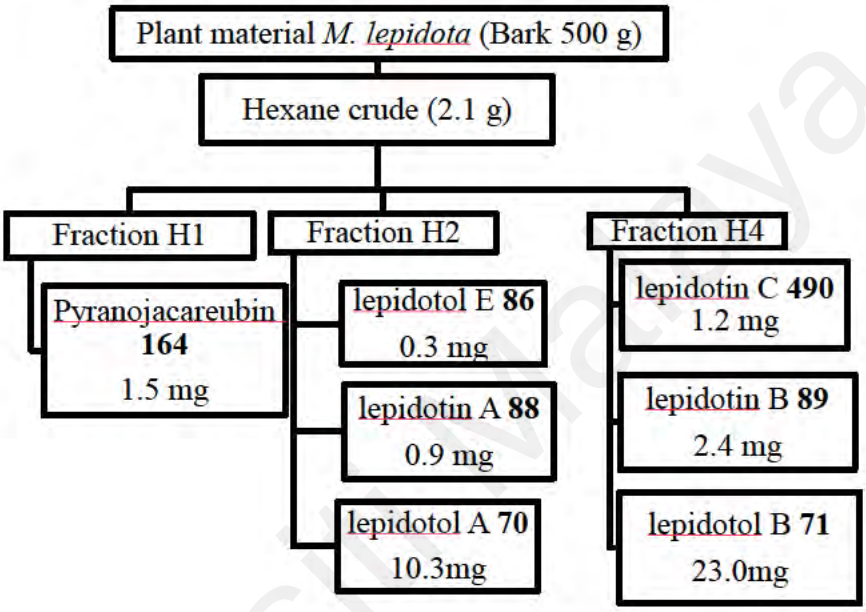

Scheme 3.2: Purification of compounds 70, 71, 86, 88, 89, 164 and 490 from the active fraction of HML bark.

Fraction 1 (155 mg) was subjected into RP-HPLC through Zorbax C18 column to afford pyranojacareubin **164** (1.5 mg, t_R 54.0 min). The isocratic solvent system, MeOH-H_2O + 0.1% formic acid 75:25 was used as mobile phase (Figure 3.4).

Preparative HPLC was used to fractionate fraction 2 (47 mg) through a Zorbax C18 column with an isocratic mobile phase of MeOH-H_2O + 0.1% formic acid, 78: 22 at flow rate 15 mL/min to obtain lepidotol A **70** (10.3 mg, t_R 90.1 min), lepidotin A **88** (0.9 mg, t_R 81.0 min) and lepidotol E **86** (0.3 mg, t_R 25.0 min) (Figure 3.5).

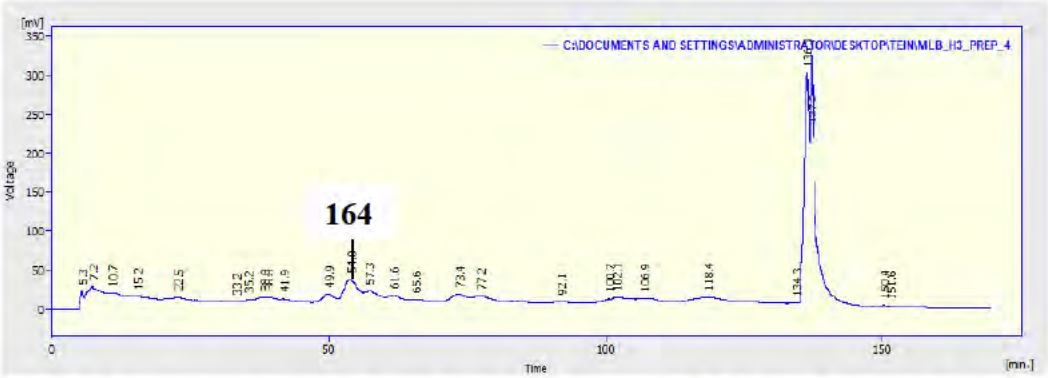

Figure 3.4: Chromatogram of the isolation of compound 164 from fraction 1 of HML bark.

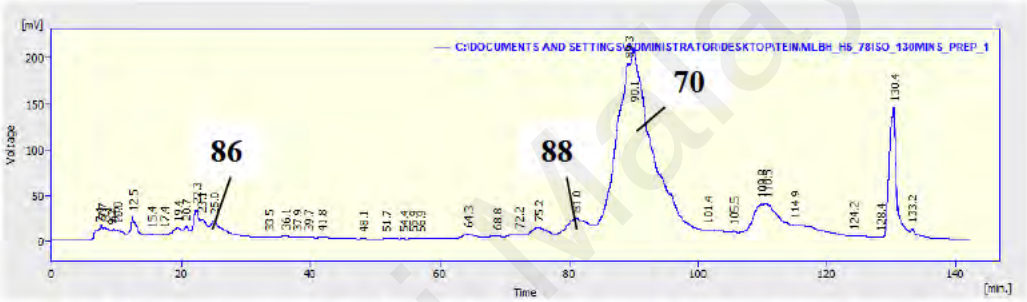

Figure 3.5: Chromatogram of the isolation of compounds 70, 86, and 88 from fraction 2 of HML bark.

Fraction 4 (102 mg) was separated through the same column for RP-HPLC with an isocratic mobile phase of MeOH-H_2O + 0.1% formic acid, 82: 18 and flow rate 15 mL/min. As a result, lepidotol B **71** (23 mg, t_R66.7 min), lepidotin B **89** (2.4 mg., t_R 58.0 min) and lepidotin C **490** (1.2 mg, t_R 51.0 min) were purified (Figure 3.6).

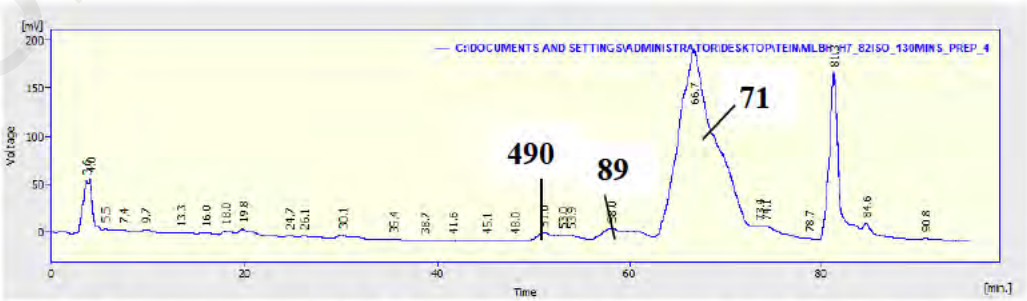

Figure 3.6: Chromatogram of the isolation of compounds 71, 89 and 490 from fraction 4 of HML bark.

To investigate the presence of other types of compounds in the extract, another fractionation was done on 7.0 g of HML through column chromatography (CC) with silica gel (230-400 mesh) as the stationary phase. Ten fractions were collected based on the gradient elution method. The fractions were spotted on thin layer chromatography (TLC) to check on the purity. Further purification was done with different chromatography methods until pure substances were isolated. The details of the isolated constituents were shown in Scheme 3.3.

Preparative thin layer chromatography (PTLC) was used to isolate glutinol **491** from fraction 2 ($C_6H_{14}/CH_3COOC_2H_5$ 9:1, 0.74 g). The solvent system used was 95:5 of hexane and ethyl acetate. Then, friedelin **186** and friedelinol **189** were purified from fraction 4 ($C_6H_{14}/CH_3COOC_2H_5$ 7:3, 0.23 g) through PTLC with solvent system of 80:20 of hexane and chloroform. Fraction 6 ($C_6H_{14}/CH_3COOC_2H_5$ 5:5, 0.76 g) was subjected to CC with C18 as stationary phase and using MeOH and H_2O+0.01% as gradient eluent (50 → 100% MeOH). The products obtained were betulinic acid **177,** lepidotol A **70** and lepidotol B **71**. Fraction A6 from this fraction was further purified with HPLC on Phenomenex C18 column using MeOH and H_2O+0.01% formic acid as eluent (50 → 100% MeOH, 0-40 min) at 5mL/ min flow rate to yield ochrocarpin E **76** (1.0 mg, t_R 34.5 min). Besides, fraction A11 was also subjected to HPLC on the same column and same flow rate with solvent system of ACN: H_2O +0.1%FA (v/v 65:35, 0-100 min) to obtain mammea A/BB cyclo F **77** (1.6 mg, t_R 65.5 min).

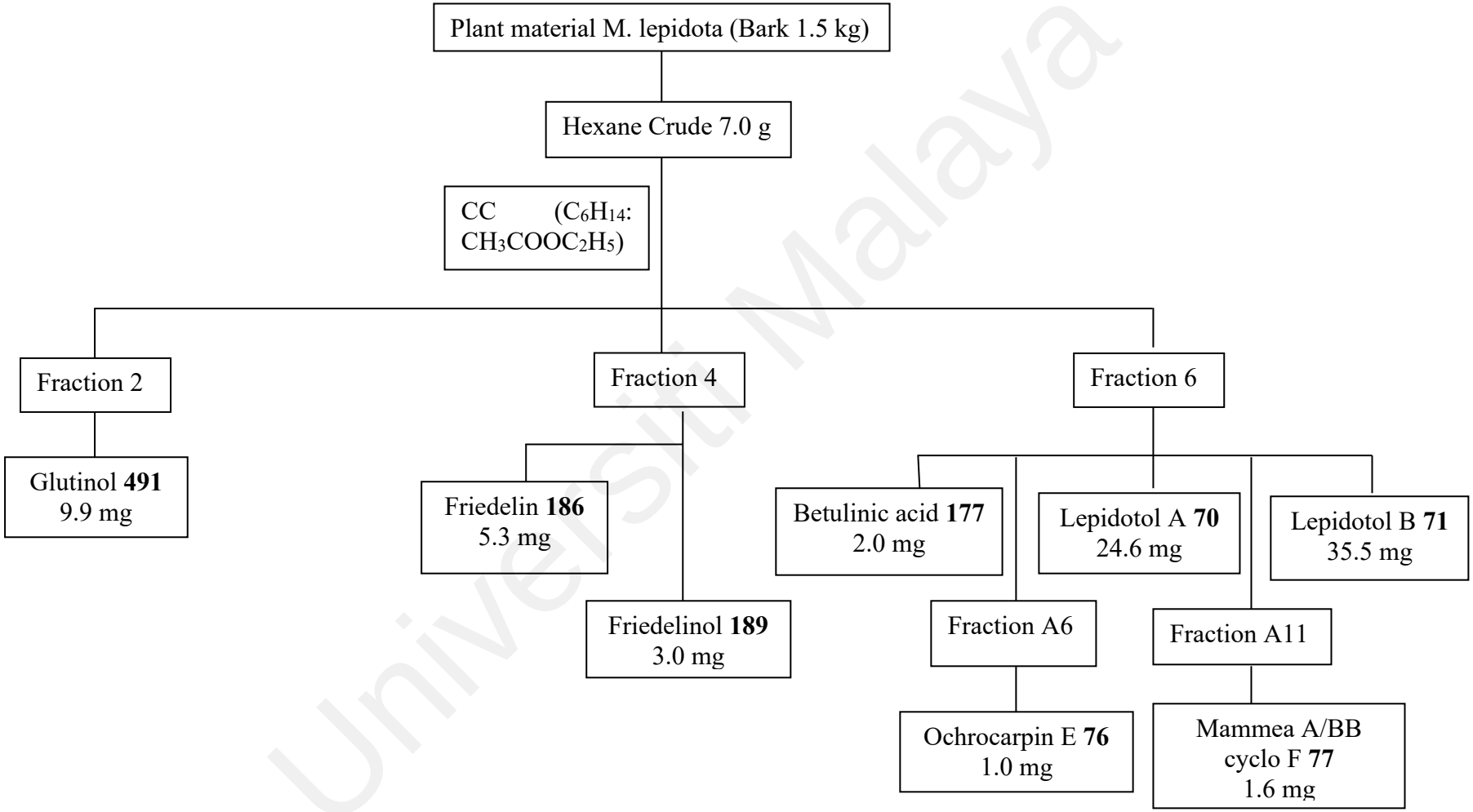

Scheme 3.3: Purification of compounds 70, 71, 76, 77, 177, 186, 189 and 491 from the fraction 2, 4, and 6 of HML bark.

3.5.2 *G. griffithii*

The following sections, section 3.5.2.1, 3.5.2.2, and 3.5.2.3 discussed the experimental details of extraction, isolation, and purification of secondary metabolites from the leaves of *G. griffithii*.

3.5.2.1 Extraction of leaves of *G. griffithii*

1.5 kg of dried, grounded leaves were macerated in dichloromethane (DCM) at room temperature for three days. Then, the extract was filtered and dried in a rotary evaporator. The procedure was repeated three times. This DCM extract of *G. griffithii* leaves was labelled as DGG leaves.

3.5.2.2 Dereplication with HPLC-PDA and LC-MS^n analysis of DGG leaves

The DGG leaves were analyzed using HPLC-PDA and LC-MS^n to determine possible chromophores in the extract (Figure 3.7). Several possible structures were hypothesized and written in Table 3.3. The confirmation of structures was done through an isolation process.

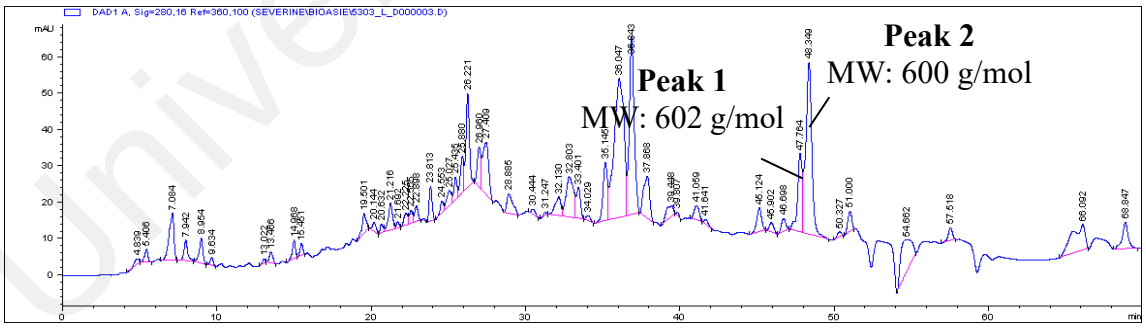

Figure 3.7: HPLC-PDA chromatogram of the DGG leaves.

Table 3.3: Retention time (t_R) and ESI-MS^2 data for the major compounds in the DGG leaves.

Peak	t_R (min)	UV λ_{max} (nm)	(+)-ESI-MS *m/z*	(+)-ESI-MS^2 m/z	(-)-ESI-MS *m/z*	(-)-ESI-MS^2 m/z	Suggested molecular weight (Da)	Hypothetical structure
1.	47.76	234, 280, 314	603	585 (-18), 547 (-56), 411 (-192)	633, 599	615 (-18), 479 (-172)	602	Isoxanthochymol **248**
2.	48.35	234, 280, 316	601	617, 499 (-102), 411 (-190)	633	601 (-32), 463 (-170)	600	Oxy-guttiferone M **302**, K **306** & K2 **305**, oblongifolin G **452**, guttiferone O **246**, garcinialiptone A **315** & B **454**, garciniagifolone A **316**

3.5.2.3 Isolation and purification of DGG leaves

As PPAPs were compound of interest and the molecular weight of most of the PPAPs were bigger than 500 g/mol, CC with Sephadex LH-20 as stationary phase and 70: 30 DCM: MeOH as mobile phase, was used to fractionate 5.2 g of DGG leaves. Seven (7) fractions were collected (Scheme 3.4).

Fraction D5 were injected into X bridge semi preparative column (250 × 10 mm, 5 µm) using a H_2O (0.1% HCOOH) − MeOH gradient system (80→100 % MeOH 0-30 min, 100% MeOH 30-45 min) with a flow rate of 3 mL/ min. isoxanthochymol **248** (4.8 mg, t_R 37.1 min) was purified (Figure 3.8).

Fraction H6 from fraction D5 was further purified through RP-HPLC on a Lichrospher 100 with an isocratic mobile phase consisting of MeOH−H_2O + 0.1% formic acid, 83:17 to afford xanthochymol **270** (2.2 mg, t_R 56.6 min) and (+)-camboginol **253** (0.8 mg, t_R 50.3 min) (Figure 3.9).

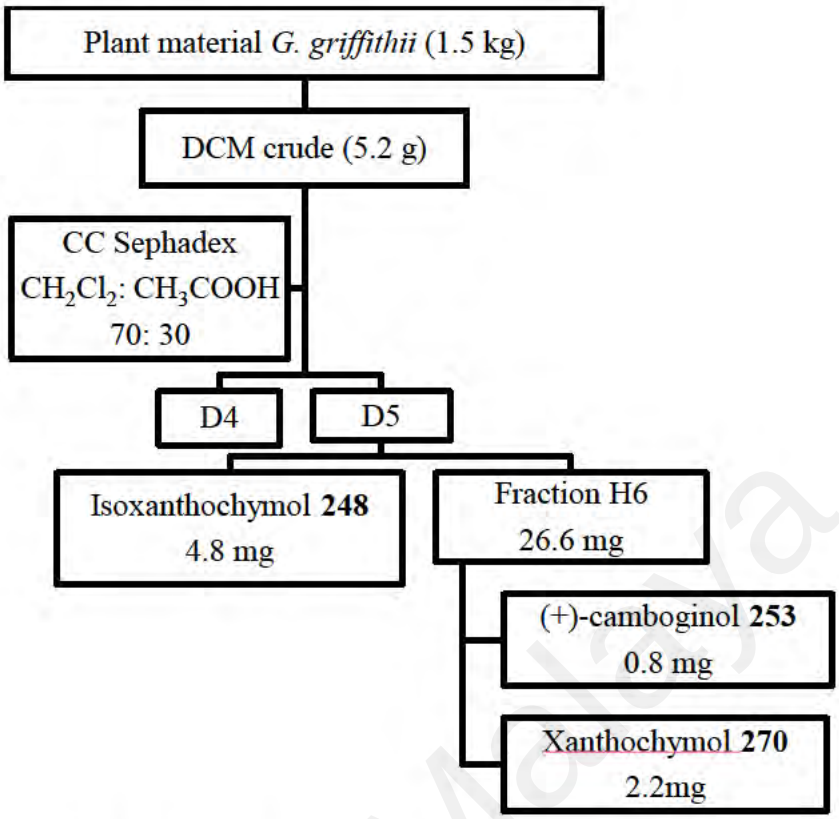

Scheme 3.4: Isolation of compound 248, 253, and 270 from DGG leaves.

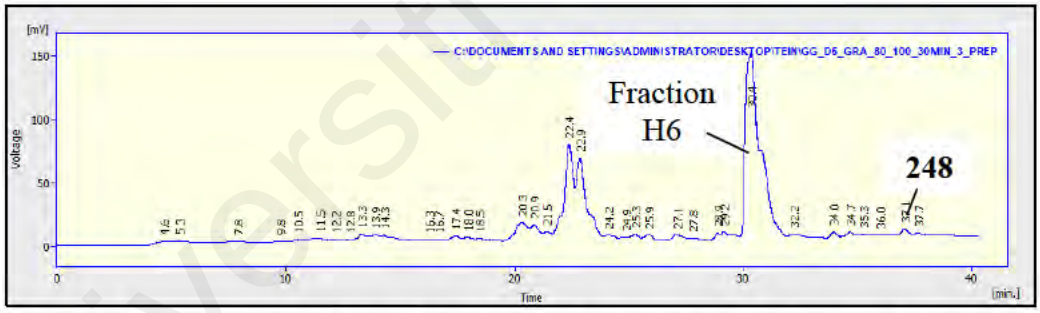

Figure 3.8: Chromatogram of the isolation of compound 248 from fraction D5 of DGG leaves.

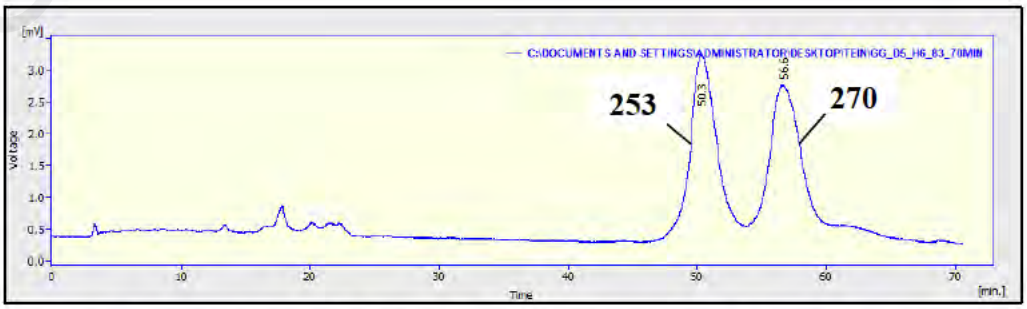

Figure 3.9: Chromatogram of the isolation of compounds 253 and 270 from fraction H6 of fraction D5 of DGG leaves.

3.6 Physical data of the isolated compounds

3.6.1 *M. lepidota*

Lepidotol A 70

Physical appearance : Yellow amorphous

Molecular formula : $C_{29}H_{32}O_5$

Mass spectrum *m/z* : 461.2325 $[M+H]^+$ (calcd for $C_{29}H_{33}O_5$, 461.2323)

UV (nm, MeOH) λ_{max} (log ε) : 224 (4.00), 296 (3.94)

IR V_{max} cm^{-1} : 3435 (OH), 1751 (δ-lactone), 1594 (chelated acyl group), 1378 (geminal dimethyl), 757 (trisubstituted alkene)

^{1}H-NMR ($CDCl_3$) δ ppm : See Table 4.5

^{13}C-NMR ($CDCl_3$) δ ppm : See Table 4.5

Lepidotol B 71

Physical appearance : Yellow amorphous

Molecular formula : $C_{30}H_{34}O_5$

Mass spectrum *m/z* : 473.2319 $[M-H]^-$ (calcd for $C_{30}H_{33}O_5$, 473.2333)

$[\alpha]_D^{25}$: +4.3° (c 0.1, $CHCl_3$)

UV (nm, MeOH) λ_{max} (log ε) : 229 (4.05), 298 (4.05)

IR V_{max} cm^{-1} : 3477 (OH), 1754 (δ-lactone), 1595 (chelated acyl group), 1379 (geminal dimethyl), 766 (trisubstituted alkene)

^{1}H-NMR ($CDCl_3$) δ ppm : See Table 4.6

^{13}C-NMR ($CDCl_3$) δ ppm : See Table 4.6

Lepidotol E 86

Physical appearance : Yellow amorphous

Molecular formula : $C_{29}H_{32}O_6$

Mass spectrum *m/z* : 475.2125 $[M–H]^-$ (calcd for $C_{29}H_{31}O_6$, 475.2126)

^{1}H-NMR ($CDCl_3$) δ ppm : See Table 4.7

^{13}C-NMR ($CDCl_3$) δ ppm : See Table 4.7

Lepidotin A 88

Physical appearance : Yellow amorphous

Molecular formula : $C_{24}H_{24}O_5$

Mass spectrum *m/z* : 393.1692 $[M+H]^+$ (calcd for $C_{24}H_{25}O_5$, 393.1697)

$[\alpha]_D^{25}$: +3.8° (c 0.026, $CHCl_3$)

UV (nm, MeOH) λ_{max} (log ε) : 204 (3.99), 225 (3.91), 293 (3.74)

IR V_{max} cm^{-1} : 3459 (OH), 1741 (δ-lactone), 1598 (chelated acyl group), 1382 (geminal dimethyl)

^{1}H-NMR ($CDCl_3$) δ ppm : See Table 4.8

^{13}C-NMR ($CDCl_3$) δ ppm : See Table 4.8

Lepidotin B 89

Physical appearance : Yellow amorphous

Molecular formula : $C_{25}H_{26}O_5$

Mass spectrum *m/z* : 407.1848 $[M+H]^+$ (calcd for $C_{25}H_{27}O_5$, 407.1853)

$[\alpha]_D^{25}$: +2.4° (c 0.008, $CHCl_3$)

UV (nm, MeOH) λ_{max} (log ε) : 204 (4.25), 225 (4.05), 295 (4.05)

IR V_{max} cm^{-1} : 3452 (OH), 1741 (δ-lactone), 1599 (chelated acyl group), 1384 (geminal dimethyl)

^{1}H-NMR ($CDCl_3$) δ ppm : See Table 4.9

^{13}C-NMR ($CDCl_3$) δ ppm : See Table 4.9

Lepidotin C 490

Physical appearance : Yellow amorphous

Molecular formula : $C_{25}H_{26}O_5$

Mass spectrum *m/z* : 407.1848 $[M+H]^+$ (calcd for $C_{25}H_{27}O_5$, 407.1853)

$[\alpha]_D^{25}$: -4 ° (c 0.0015, $CHCl_3$)

UV (nm, MeOH) λ_{max} (log ε) : 204 (4.28), 226 (4.28), 297 (4.22)

IR V_{max} cm^{-1} : 3460 (OH), 1741 (δ-lactone), 1598 (chelated acyl group), 1385 (geminal dimethyl)

^{1}H-NMR ($CDCl_3$) δ ppm : See Table 4.10

^{13}C-NMR ($CDCl_3$) δ ppm : See Table 4.10

Ochrocarpin E 76

Physical appearance : White amorphous

Molecular formula : $C_{24}H_{24}O_6$

Mass spectrum *m/z* : 409.2822 $[M+H]^+$ (calcd. for $C_{24}H_{25}O_6$, 409.1651)

$[\alpha]_D^{25}$: -2.85° (c 0.0035, $CHCl_3$)

UV (nm, MeOH) λ_{max} (log ε) : 204 (4.03), 224 (3.95), 297 (3.84)

IR V_{max} cm^{-1} : 3455 (OH), 1721 (δ-lactone), 1603 (chelated acyl group), 1382 (geminal dimethyl)

^{1}H-NMR ($CDCl_3$) δ ppm : See Table 4.11

^{13}C-NMR ($CDCl_3$) δ ppm : See Table 4.11

Mammea A/BB cyclo F 77

Physical appearance : White amorphous

Molecular formula : $C_{25}H_{26}O_6$

Mass spectrum *m/z* : 423.3013 $[M+H]^+$ (calcd for $C_{25}H_{27}O_6$, 423.4792)

$[\alpha]_D^{25}$: -3.3 ° (c 0.004, $CHCl_3$)

UV (nm, MeOH) λ_{max} (log ε) : 203 (4.15), 226 (4.08), 298 (4.01)

IR V_{max} cm^{-1} : 3458 (OH), 1744 (δ-lactone), 1603 (chelated acyl group), 1386 (geminal dimethyl)

^{1}H-NMR ($CDCl_3$) δ ppm : See Table 4.12

^{13}C-NMR ($CDCl_3$) δ ppm : See Table 4.12

Friedelin 186

Physical appearance : White crystal

Molecular formula : $C_{30}H_{50}O$

Mass spectrum *m/z* : 427.3931 $[M+H]^+$ (calcd. for $C_{30}H_{51}O$, 427.3934)

$[\alpha]_D^{25}$: −20.8° (c 0.053, $CHCl_3$)

IR V_{max} cm^{-1} : 2926, 2869, 1715 (C=O), 1452, 1388

^{1}H-NMR ($CDCl_3$) δ ppm : See Table 4.13

^{13}C-NMR ($CDCl_3$) δ ppm : See Table 4.13

3*β*-friedelinol 189

Physical appearance : White crystal

Molecular formula : $C_{30}H_{52}O$

Mass spectrum *m/z* : 427.4995 $[M-H]^-$ (calcd. for $C_{30}H_{51}O$, 427.3985)

$[\alpha]_D^{25}$: +5.5° (c 0.09, $CHCl_3$)

IR V_{max} cm^{-1} : 3474 (OH), 1385 (geminal methyl), 1171, 1001, 981

^{1}H-NMR ($CDCl_3$) δ ppm : See Table 4.14

^{13}C-NMR ($CDCl_3$) δ ppm : See Table 4.14

Betulinic acid 177

Physical appearance : White crystal

Molecular formula : $C_{30}H_{48}O_3$

Mass spectrum *m/z* : 421.1667 $[M+Cl]^-$ (Calcd. for $C_{30}H_{48}O_3$-Cl, 421.3603)

$[\alpha]_D^{25}$: +6.7° (c 0.09, $CHCl_3$)

IR V_{max} cm^{-1} : 2926 (OH), 2869 (OH), 1715(carboxyl), 1641, 1448, 1377 (geminal dimethyl), 1223, 1194, 1108, 1033, 984, 881

^{1}H-NMR ($CDCl_3$) δ ppm : See Table 4.15

^{13}C-NMR ($CDCl_3$) δ ppm : See Table 4.15

Glutinol 491

Physical appearance : White amorphous

Molecular formula : $C_{30}H_{50}O$

Mass spectrum *m/z* : 425.1621 $[M-H]^-$ (calcd. for $C_{30}H_{49}O$, 425.7106)

$[\alpha]_D^{25}$: +30.1° (c 0.1, $CHCl_3$)

UV (nm, MeOH) λ_{max} (log ε) : 212 (4.04)

IR V_{max} cm^{-1} : 3446 (OH), 2927 (C=C), 2865, 1457, 1386 (geminal dimethyl), 1035

^{1}H-NMR ($CDCl_3$) δ ppm : See Table 4.16

^{13}C-NMR ($CDCl_3$) δ ppm : See Table 4.16

Pyranojacareubin 164

Physical appearance : Yellow amorphous

Molecular formula : $C_{23}H_{20}O_6$

Mass spectrum *m/z* : 393.4036 $[M+H]^+$ (calcd. for $C_{23}H_{21}O_6$, 393.4101)

UV (nm, MeOH) λ_{max} (log ε) : 228 (4.20), 297 (4.17)

IR V_{max} cm^{-1} : 3472 (OH), 2964, 2931, 2876, 1737 (C=O), 1623, 1601, 1455, 1150, 855

^{1}H-NMR ($CDCl_3$) δ ppm : See Table 4.17

^{13}C-NMR ($CDCl_3$) δ ppm : See Table 4.17

3.6.2 *G. griffithii*

(+)-camboginol 253

Physical appearance : Yellow amorphous

Molecular formula : $C_{38}H_{50}O_6$

Mass spectrum *m/z* : 603.3527 $[M+H]^+$ (calcd for $C_{38}H_{51}O_6$, 603.3607)

$[\alpha]_D^{25}$: +50° (c 0.018, $CHCl_3$)

UV (nm, MeOH) λ_{max} (log ε) : 230 (4.00), 277 (3.85)

IR V_{max} cm^{-1} : 3401 (OH), 2927, 1724 (six-membered cyclic C=O), 1598 (conjugated C=O), 1376, 1292, 1116, 1058

^{1}H-NMR (CD_3OD+0.1 % TFA) δ ppm : See Table 4.28

^{13}C-NMR (CD_3OD+0.1 % TFA) δ ppm : See Table 4.28

Xanthochymol 270

Physical appearance : Yellow amorphous

Molecular formula : C_{38} H_{50} O_6

Mass spectrum *m/z* : 603.3672 $[M+H]^+$ (calcd for $C_{38}H_{51}O_6$, 603.3607)

$[\alpha]_D^{25}$: +162.5° (c 0.048, $CHCl_3$)

UV (nm, MeOH) λ_{max} (log ε) : 233 (3.97), 274 (3.90)

IR V_{max} cm^{-1} : 3397 (OH), 2971, 2930, 1725 (six-membered cyclic C=O), 1647 (conjugated C=O), 1444, 1376, 1145

^{1}H-NMR (CD_3OD+0.1 % TFA) δ ppm : See Table 4.29

^{13}C-NMR (CD_3OD+0.1 % TFA) δ ppm : See Table 4.29

Isoxanthochymol 248

Physical appearance : Yellow amorphous

Molecular formula : $C_{38}H_{50}O_6$

Mass spectrum *m/z* : 603.3682 $[M+H]^+$ (calcd for $C_{38}H_{51}O_6$, 603.3607)

$[\alpha]_D^{25}$: +183.3° (c 0.09, $CHCl_3$)

UV (nm, MeOH) λ_{max} (log ε) : 234 (3.70), 273 (3.74)

IR V_{max} cm^{-1} : 3359 (OH), 1718 (six-membered cyclic C=O), 1678, 1592 (conjugated C=O), 1382, 1296, 1120

^{1}H-NMR (CD_3OD+0.1 % TFA) δ ppm : See Table 4:27

^{13}C-NMR (CD_3OD+0.1 % TFA) δ ppm : See Table 4:27

3.7 Cholinesterase inhibitory activity as well as enzyme kinetic study, molecular docking, and molecular dynamics simulations of the most potent compound.

The experimental cholinesterase inhibitory activity as well as enzyme kinetic study, molecular docking and molecular dynamics simulations of the most potent compound were discussed in the following sections.

3.7.1 Cholinesterase inhibitory assay (Jamila et al., 2015)

Cholinesterase inhibitory potential of the extracts and constituents was determined by Ellman's assay with some modifications. Briefly, 140 µL of 0.1 M sodium phosphate buffer (pH 8.0) was added to 96-well microplate followed by 20 µL of test samples and

20 µL of 0.09 U/mL AChE enzyme. After 15 min of pre-incubation at room temperature, 10 µL of 10 mM DTNB was added into each well followed by 10 µL of 14 mM of ATCI. Absorbance of the colored end product was measured using Tecan Infinite 200 Pro Microplate spectrometer at 412 nm at 30 min after initiation of the enzymatic reaction. Absorbance of the test samples was corrected by subtracting the absorbance of their respective blank. BChE inhibitory assay adopted the same procedure using the BChE and *S*-butyrylthiocholine chloride as substrate. Donepezil and galatamine were used as reference standard. The test samples and standards were prepared in DMSO at the initial concentration of 1 mg/mL. The concentration of DMSO in final reaction mixture was 1%. Initial cholinesterase inhibitory activity of the compounds was evaluated at 50 µg/mL. Compounds having more than 50% inhibition were further evaluated for determination of their 50% inhibitory concentration (IC_{50}). A set of five concentrations (50.0, 25.0, 12.5, 6.25 and 3.125 µM) was used for determination of the IC_{50} values.

3.7.2 BChE kinetic study (Wan Othman et al., 2016)

The kinetic of BChE inhibition was determined through the constructing of Lineweaver- Burk (LB) plots; reciprocal plots of velocity (1/V) versus reciprocal of substrate concentration (1/[S]). The cholinesterase inhibitory assay was executed by using four different concentrations of substrate *S*-butyrylthiocholine chloride (1.75, 3.5, 7 and 14.0 mM) in the presence of three different concentrations of inhibitors. The inhibition constant (K_i) value was derived from the secondary plot of Lineweaver-Burk plot.

3.7.3 Molecular docking and molecular dynamics simulations (MDs)

Molecular docking was conducted following the method as described by Abdul Wahab *et al.* (Abdul Wahab et al., 2016). Briefly, molecular docking of the compound was performed using Autodock 3.0.5 along with AutoDockTools (ADT) (Morris et al., 1998). The two-dimensional structure of the compound was built using Hyperchem 8 and energy

minimization was carried out with a convergence criterion of 0.05 kcal/(molA). The three-dimensional crystal structures of BChE from *Homo sapiens* (PDB ID: 2WIJ) (Carletti et al., 2009) was retrieved from the Protein Data Bank. The protein was edited using ADT to remove all the water molecules and hydrogen atoms were added. Non-polar hydrogens and lone pairs were then merged, and each atom was assigned with Gasteiger partial charges. A grid box of 60×60×60 points with spacing of 0.375 Ǻ was generated at the center of the active site gorge. One hundred independent dockings were performed for each docking experiment with a population size of 150 and 2,500,000 energy evaluations. The best conformation with the lowest docked energy in the most populated cluster was selected for molecular dynamics simulations using AMBER20 software package (D.A. Case et al., 2023). The molecular properties of the proteins and ligands were described by Amber ff19SB and GAFF force fields. The protein-ligand complexes were solvated in a cubical box using TIP3P water and counterions were added to neutralize the charge of the complex. MD simulations were performed using a time step of 2 fs. The long-range interactions were computed under periodic boundary conditions based on the Particle Mesh Ewald (PME) method. The SHAKE algorithm and Langevin dynamics were used to constrain bonds involving hydrogen and to control the temperature, respectively. The simulated systems were heated up to 300 K over a period of 60 ps of NVT dynamics. Binding free energy were calculated under Molecular Mechanics Generalized Born Surface Area (MM-GBSA) protocol using MMPBSA.py module (Miller et al., 2012) using 500 snapshots sampled from the final 20 ns of a production run. Analysis and visualization of protein complex was conducted using BIOVIA discovery studio visualizer v20.1.0.19295.

CHAPTER 4: RESULTS AND DISCUSSIONS

Two plants were studied: *M. lepidota* and *G. griffithii* using different strategies. The strategy on the first plant, *M. lepidota*, was focused on bioassay guided fractionation. Ten fractions were collected using HPLC and UV detector, and their cholinesterase inhibitory activities were screened. The fractions with potent AChE and/or BChE inhibition were further fractionated to isolate the compounds potentially responsible for the cholinesterase inhibitory activity. Due to the limitations of HPLC-UV detector, compounds without chromophore can be missed out. Therefore, another fractionation was done on the same extract using conventional method, *i.e.,* CC, to investigate the possible presence of other types of compounds. In addition, a MixONat analysis was also performed on the crude to identify other compounds that exist in the plant.

For the second plant, *G. griffithii*, the objective was to identify the presence of PPAPs in *G. griffithii*. PPAPs are of interest because it has a unique bicyclo[3.3.1]nonane-2,4,9-trione core structure. MixONat was used to analyze the DGG leaves, revealing the presence of this type of natural product. The extract was then fractionated into seven (7) fractions. The fractions containing PPAPs (fraction D4 and D5) were subjected to ^{13}C-NMR dereplication analyses to identify the specific compounds present. Subsequently, the fractions with PPAPs were further fractionated to isolate as many compounds as possible. The isolated PPAPs were then tested for their ability to inhibit cholinesterase enzymes, which break down ACh, a neurotransmitter important for learning and memory.

Therefore, this chapter will discuss the results obtained from each plant on three different parts. The three parts were:

(i) ^{13}C-NMR dereplication with the aid of MixONat;

(ii) Phytochemical studies;

(iii) Cholinesterase inhibitory activities as well as enzyme kinetic study, molecular docking, and molecular dynamics simulations of the most potent compound.

4.1 *M. lepidota*

The results of ^{13}C-NMR dereplication, phytochemical studies, anti-cholinesterase activities (including enzyme kinetics study, molecular docking, and molecular dynamics simulations of the most potent compound) of *M. lepidota* were discussed in the following subchapters.

4.1.1 ^{13}C-NMR dereplication with the aid of MixONat

MixONat analyses the ^{13}C-NMR chemical shifts according to carbon types, with the information given by DEPT-135 and DEPT-90 NMR experiments. The software will then compare the experiment chemical shifts with data of the structures in the designated DB. The number of matching carbon chemical shifts (with the signals difference of less than 1.3 ppm) were calculated and presented as a score. The higher the score indicated the higher the matching. Furthermore, the used parameters in MixONat for each analysis will be presented in the results. The structure of most matching compounds, together with the ID, rank, score (percentage of matching carbon) and deviation of each structure were shown too. To confirm the presence of the structures proposed by MixONat, the experimental spectroscopic data of the mixtures must compare with the literature chemical shifts (in the same deuterated solvent) of the proposed metabolite; a difference of no greater than 0.4 ppm confirm the identification of structure (Bruguière et al., 2020; Silva-Castro et al., 2021).

4.1.1.1 ^{13}C-NMR dereplication of *M. lepidota*

$CDCl_3$ was used to dissolve the crude of *M. lepidota* for NMR experiment. As to reduce the hit of fatty acids in the result, molecular weight filter (MW > 300 Da) was

used in the analysis. Then the result obtained was compared to the literature and predicted ^{13}C-NMR chemical shifts.

Before the further analysis of the result, from the ^{1}H and ^{13}C-NMR (within 10-50 ppm) spectra, a cluster of methyls and methines peaks which is one of the signatures of triterpenes and sterols was determined. These types of constituents did not exhibited peaks on the chromatogram of HPLC-PDA (refer to Figure 3.1). However, MixONat proposed the presence of sterols and triterpenes in the extract. As the bark of *M. lepidota* exudate oleo-gum resin, the suggested result demonstrated by the MixONat and NMR were corresponded.

The ^{13}C-NMR spectrum of the HML bark in $CDCl_3$ (Figure 4.1-4.3) suggested a very complex mixture of major NPs, exemplified by more than 350 chemical shifts.

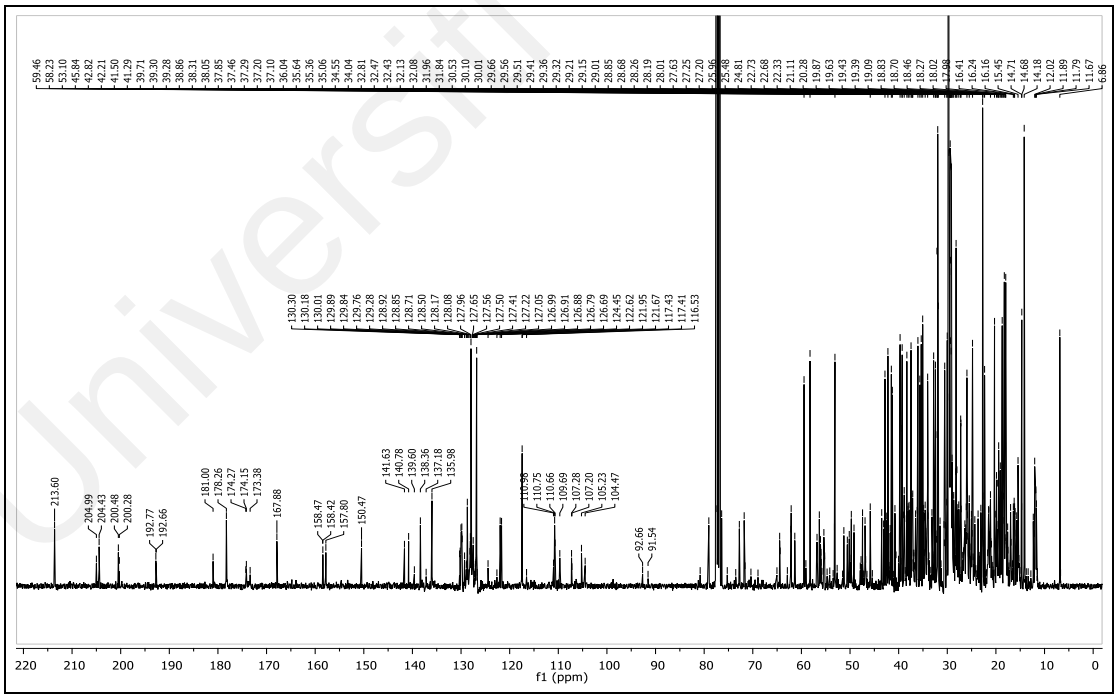

Figure 4.1: ^{13}C-NMR spectrum (10000 scans) of the HML bark (30 mg) recorded in $CDCl_3$ at 100 M*Hz*.

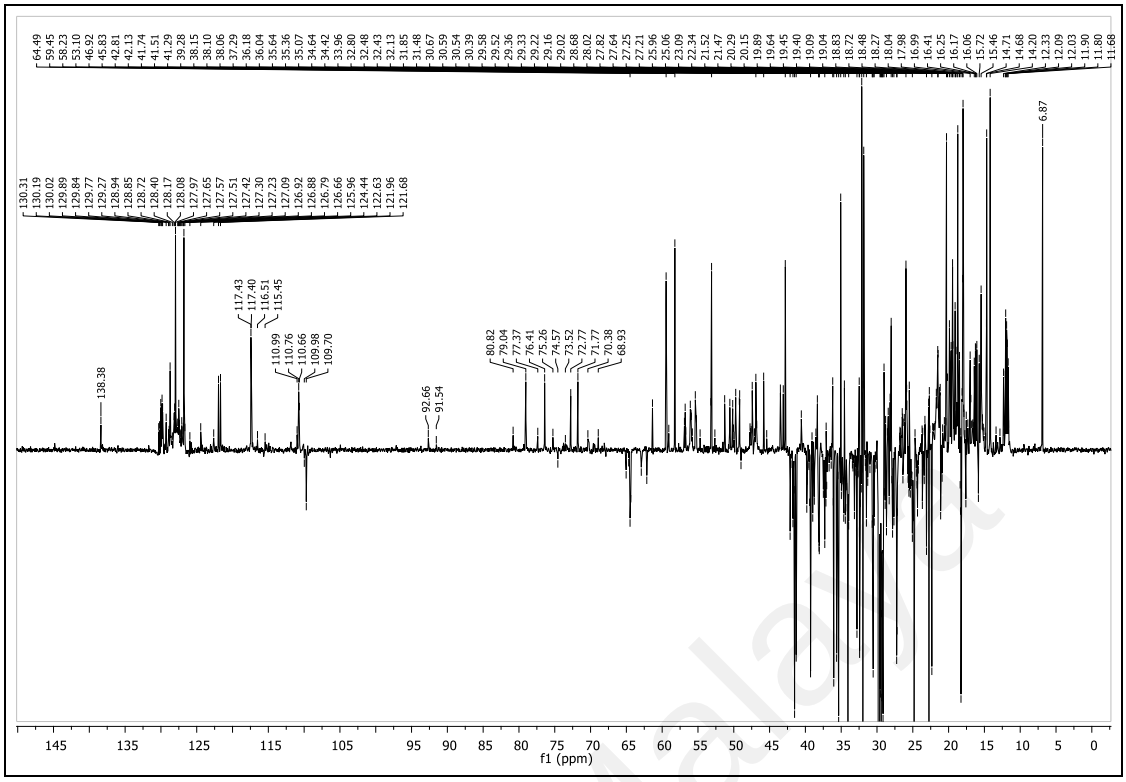

Figure 4.2: DEPT-135 NMR spectrum (5000 scans) of the HML bark (30 mg) recorded in $CDCl_3$.

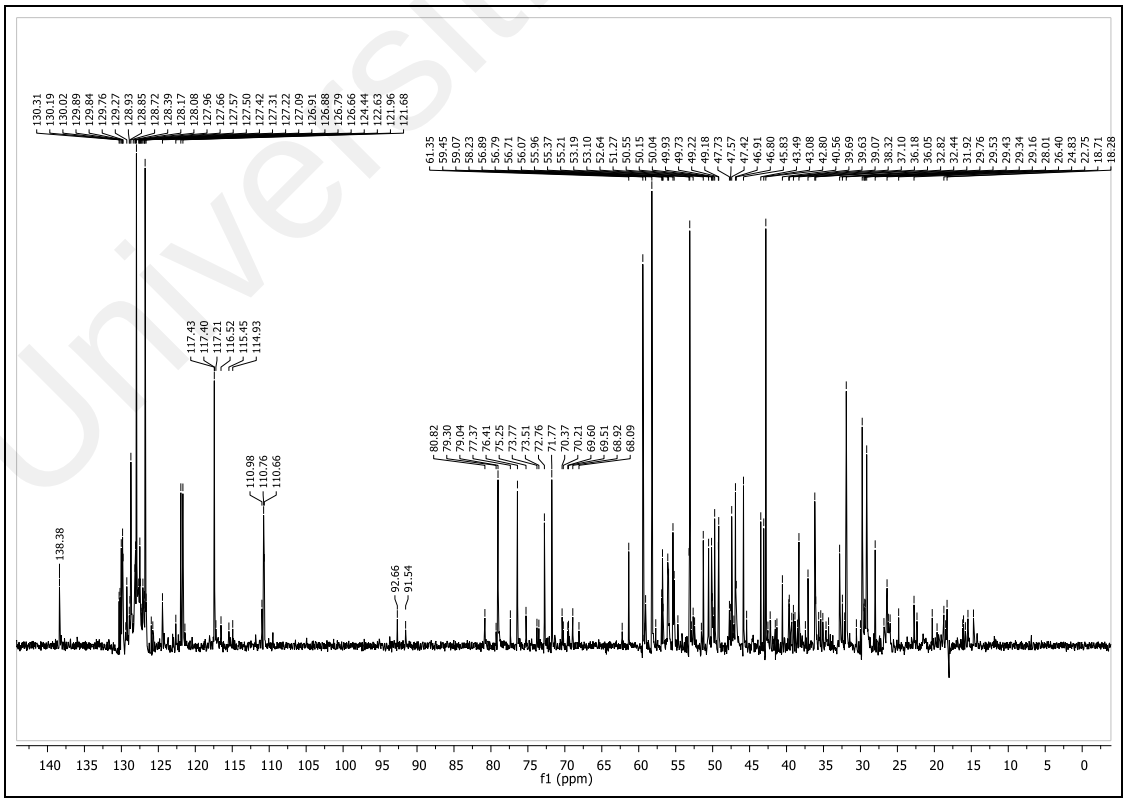

Figure 4.3: DEPT-90 NMR spectrum (3000 scans) of the HML bark (30 mg) recorded in $CDCl_3$.

A first dereplication was undertaken by using the c-type_Mesua DB1. Using a molecular weight filter (MW > 300 Da) to remove putative fatty acids in such an apolar extract, MixONat displayed a total of seventy (70) compounds with good matching score (score ranging from 1.0 to 0.73) including thirty (30) sterols and triterpenes, thirty-six (36) coumarins and four (4) other types of compounds (Appendix A & B). Triterpenes, sterols and coumarins were the major suggested metabolites by using c-type_LOTUS_Mesua DB2 too (Appendix C).

Sitosterol **174** and stigmasterol **173** are very common sterols in plants and their nonpolar extracts. MixONat predicted the presence of both NPs in the extract [rank 1, score: 1.0 (29/29 C), DB1 and DB2; rank 19, score: 0.93 (27/29 C), DB1 and rank 9, score: 0.93 (27/29 C), DB2 respectively] (Table 4.1). The presence of both sterols was confirmed with a high level of confidence.

Besides, four (4) triterpenes, one ursane and three (3) lupane types of triterpenes were suggested by MixONat software. The presence of α-amyrin **194** [rank 3, score: 1.0 (30/30 C), DB1], the ursane type triterpene, was further confirmed by comparison with reported data (Table 4.2). For lupane type of triterpenes, myrtifolic acid **188** [rank 6, score: 0.97 (29/30 C), DB1] , lupenone **181** [rank 7, score: 0.97 (29/30 C), DB1], friedelin **186** [rank 8, score: 0.97 (29/30 C), DB1; rank 4, score: 0.97 (29/30 C), DB2], 3β-friedelinol **189** [rank 9, score: 0.97 (29/30 C), DB1], lupeol **178** [rank 10, score: 0.97 (29/30 C), DB1] as well as betulinic acid **177** [rank 12, score: 0.97 (29/30 C), DB1; rank 3, score: 0.97 (29/30 C), DB2] were proposed by MixONat. By comparison with the previously published data, friedelin **186**, 3β-friedelinol **189** and betulinic acid **177** (Table 4.2) were confirmed in the extract.

Further careful examination of metabolites hypothesized by MixONat also suggested lepidotol A **70** and lepidotol B **71** as major NPs in the extract. The presence of lepidotol

A **70** [rank 41, score: 0.79 (23/29 C), DB1] and lepidotol B **71** [rank 48, score: 0.77 (23/30 C), DB1] (Table 4.3) was further confirmed (Rouger et al., 2015). These two coumarins were not found on the LOTUS website hence they were not recorded in DB2.The results emphasize the importance of using several DBs in such dereplication processes.

Lepidotin A **88** [rank 44, score: 0.79 (19/24 C), MESUA_DB1] and lepidotin B **89** [rank 53, score: 0.76 (19/25 C), MESUA_DB1] were proposed by MixONat and reported in literature review (Rouger et al., 2015) of the same species too. However, there were some missing or hidden quaternary δ_C of both compounds from the experimental spectrum of extract, even though the difference of both experimental and literature data is trivial (Table 4.3). For instance, carbon 2, 4, 4a, 5, 6, 7, 8a and 1''' of lepidotin A **88** is absent from the experimental spectrum of the crude extract. The missing quaternary carbons signals were probably had lower intensity and being exempted during peak picking. Hence, the presence of lepidotin A **88** and lepidotin B **89** in the extract were confirmed after isolation process.

Finally, eight (8) NPs with different types of structures, *i.e.*, coumarins, sterols and triterpenes were unambiguously identified in the mixture by using MixONat. Only the coumarins have been previously reported from the fruits of *M. lepidota* (Rouger et al., 2015).

Table 4.1: Experimental and reported spectroscopic data (δc) in $CDCl_3$ for sterols and triterpene predicted in the HML bark.

Carbon numbering	**Sitosterol 174** (Rouger, 2015)		**Stigmasterol 173** (Rouger, 2015)		**α-amyrin 194** (Seo et al., 1975)	
	Literature	δc (ppm) matched in extract	Literature	δc (ppm) matched in extract	Literature	δc (ppm) matched in extract
1	37.4	37.3	37.4	37.5	38.7	38.4
2	29.8	29.8	29.8	29.8	27.2	27.2
3	72.0	71.8	72.0	71.8	78.8	79.0
4	42.5	42.4	42.5	42.5	38.7	38.9
5	140.9	140.8	140.9	140.8	55.2	55.2
6	121.9	121.7	121.9	122.0	18.3	18.3
7	32.1	32.0	32.1	32.1	32.9	33.0
8	32.1	32.1	32.1	32.1	40.0	40.0
9	50.3	50.2	50.3	50.2	47.7	47.7
10	36.7	36.6	36.7	36.7	36.9	37.0
11	21.2	21.1	21.2	21.2	17.4	17.5
12	39.8	39.8	39.8	39.8	124.3	124.5
13	42.4	42.1	42.4	42.4	139.3	139.6
14	56.9	56.8	56.9	56.9	42.0	42.1
15	24.5	24.4	24.5	24.5	28.7	29.0
16	28.4	28.3	28.4	28.4	26.6	26.4
17	56.1	56.1	56.1	56.1	33.7	33.8
18	12.0	11.9	12.0	12.0	58.9	59.1
19	19.6	19.4	19.6	19.6	39.6	39.6
20	36.3	36.2	40.6	40.5	39.6	39.7
21	18.9	18.8	21.2	21.2	31.2	31.3
22	34.1	34.0	138.5	138.4	41.5	41.6

Table 4:1, continued.

Carbon numbering	**Sitosterol 174** (Rouger, 2015)		**Stigmasterol 173** (Rouger, 2015)		**α-amyrin 194** (Seo et al., 1975)	
	Literature	δc (ppm) matched in extract	Literature	δc (ppm) matched in extract	Literature	δc (ppm) matched in extract
23	26.2	26.4	129.4	129.8	28.1	27.9
24	46.0	45.8	51.4	51.5	15.6	15.5
25	29.0	29.2	31.8	31.8	15.6	15.7
26	19.6	19.7	21.4	21.5	16.8	16.9
27	19.2	19.0	18.9	18.8	23.3	23.3
28	23.2	23.1	25.6	25.7	28.1	28.4
29	12.2	12.3	12.4	12.3	23.3	23.4
30	-	-	-	-	21.3	21.5

Table 4.2: Experimental and reported spectroscopic data (δ_C) in $CDCl_3$ for triterpenes predicted in the HML bark.

Carbon numbering	**Friedelin 186** (Oladoye et al., 2015)		**Friedelinol 189** (Oladoye et al., 2015)		**Betulinic acid 177** (Sharma et al., 2010)	
	Literature	δc (ppm) matched in extract	Literature	δc (ppm) matched in extract	Literature	δc (ppm) matched in extract
1	22.3	22.3	15.8	15.8	38.7	38.8
2	41.5	41.6	36.1	36.0	27.4	27.3
3	213.3	213.6	72.8	72.8	78.9	79.0
4	58.2	58.2	49.2	49.2	38.8	38.7
5	42.2	42.1	39.3	39.3	55.3	55.4
6	41.3	41.3	41.8	41.7	18.3	18.3
7	18.3	18.3	17.6	17.6	34.3	34.0

Table 4:2, continued.

Carbon numbering	**Friedelin 186** (Oladoye et al., 2015)		**Friedelinol 189** (Oladoye et al., 2015)		**Betulinic acid 177** (Sharma et al., 2010)	
	Literature	δc (ppm) matched in extract	Literature	δc (ppm) matched in extract	Literature	δc (ppm) matched in extract
8	53.1	53.1	53.2	53.2	40.7	40.7
9	37.5	37.2	37.1	37.2	50.5	50.6
10	59.5	59.5	61.4	61.4	37.2	37.0
11	35.6	35.6	35.4	35.4	20.8	20.9
12	30.5	30.5	30.6	30.6	25.5	25.7
13	38.3	38.7	37.9	37.9	38.4	38.3
14	39.7	39.7	38.4	38.4	42.4	42.4
15	32.4	32.4	32.4	32.3	30.5	30.5
16	36.0	36.0	35.6	35.6	32.1	32.1
17	30.1	30.2	30.0	30.2	56.3	56.3
18	42.8	42.8	42.9	42.8	46.8	46.8
19	35.4	35.4	35.2	35.6	49.2	49.2
20	28.2	28.3	28.2	28.3	150.3	150.5
21	32.8	32.8	32.8	32.8	29.7	29.7
22	39.3	39.3	39.7	39.7	37.0	37.3
23	6.8	6.9	11.6	11.9	27.9	28.0
24	14.7	14.7	16.4	16.4	15.3	15.1
25	18.0	18.0	18.2	18.1	16.0	15.7
26	20.3	20.3	20.1	20.1	16.1	16.2
27	18.7	18.8	18.6	18.8	14.7	14.7
28	32.1	32.1	32.1	32.1	180.5	181.0
29	35.0	35.1	35.0	35.1	109.6	109.7
30	31.8	31.8	31.8	31.8	19.4	19.4

Table 4.3: Experimental and reported spectroscopic data (δ_C) in $CDCl_3$ for coumarins predicted in the HML bark.

Carbon numbering	**Lepidotol A 70** (Rouger, 2015)		**Lepidotol B 71** (Rouger, 2015)		**Lepidotin A 88** (Rouger, 2015)		**Lepidotin B 89** (Rouger, 2015)	
	Literature	δc (ppm) matched in extract	Literature	δc (ppm) matched in extract	Literature	δc (ppm) matched in extract	Literature	δc (ppm) matched in extract
2	158.6	158.5	158.4	158.4	159.4	158.5	159.4	-
3	110.8	110.8	110.7	110.7	110.9	111.0	111.0	111.0
4	157.9	157.9	157.7	157.8	155.6	-	155.5	-
4a	107.3	107.3	107.2	107.2	98.5	-	98.5	-
5	200.4	200.5	200.4	200.3	161.2	-	161.2	-
6	62.3	62.2	62.1	62.1	118.2	-	118.2	-
7	192.8	192.8	192.7	192.7	164.8	-	164.8	-
8	104.6	104.5	105.2	105.2	104.1	104.5	104.6	104.5
8a	168	167.9	167.8	167.9	157.2	-	157.2	-
1'	138.5	138.4	138.3	138.4	137.6	137.2	137.7	-
2'	126.9	126.9	126.7	126.7	127.5	127.2	127.5	127.2
3'	128.1	128.1	127.9	127.7	127.8	128.0	127.8	128.0
4'	128.8	128.9	128.7	128.5	128.8	128.9	128.8	128.9
5'	128.1	128.1	127.9	127.7	127.8	127.7	127.8	127.7
6'	126.9	126.9	126.7	126.7	127.5	127.4	127.5	127.4
1"a	38.2	38.1	38.1	38.1	-	-	-	-
1"b	38.2	38.1	38.1	38.1	-	-	-	-
2"a	117.5	117.4	117.4	117.4	91.5	91.5	91.5	91.5
2"b	117.5	117.4	117.4	117.4	-	-	-	-
3"a	136.2	136	136.0	136.0	43.4	43.0	43.4	43.0
3"b	136.2	136	136.0	136.0	-	-	-	-
4"a	18.1	18.1	18.0	18.0	14	14.2	14.1	14.2

Table 4:3, continued.

Carbon numbering	**Lepidotol A 70** (Rouger, 2015)		**Lepidotol B 71** (Rouger, 2015)		**Lepidotin A 88** (Rouger, 2015)		**Lepidotin B 89** (Rouger, 2015)	
	Literature	δc (ppm) matched in extract	Literature	δc (ppm) matched in extract	Literature	δc (ppm) matched in extract	Literature	δc (ppm) matched in extract
4"b	18.1	18.1	18.0	18.0	-	-	-	-
5"a	26.1	26.1	25.9	25.9	20.2	20.1	20.3	20.4
5"b	26.1	26.1	25.9	25.9	-	-	-	-
6"	-	-	-	-	25.4	25.5	25.4	25.5
1'''	205.2	205	204.4	204.4	210.8	-	210.7	-
2'''	37.2	37.2	43.5	43.5	40.2	40.6	46.8	47.1
3'''	19.6	19.6	27.6	27.6	19.3	19.4	27.3	27.2
4'''	19.6	19.6	11.7	11.7	19.4	19.4	11.8	11.8
5'''	-	-	17.0	17.0	-	-	16.7	16.6

4.1.2 Phytochemical studies *M. lepidota*

In total, there are thirteen (13) chemical constituents that were isolated from the HML bark. Out of the thirteen (13) chemical constituents, eight (8) were 4-phenyl coumarins, including a new coumarin (lepidotin C **490**), four (4) were triterpenes and a xanthone (Table 4.4). The details of the chemical constituents were discussed.

Table 4.4: Compounds isolated from *M. lepidota.*

No.	Type of constituent	Compound	Yield (mg)	% of yield
1.	Coumarin	Lepidotol A **70**	34.9	0.3835
2.	Coumarin	Lepidotol B **71**	58.5	0.6429
3.	Coumarin	Lepidotol E **86**	0.3	0.0033
4.	Coumarin	Lepidotin A **88**	0.9	0.0099
5.	Coumarin	Lepidotin B **89**	2.4	0.0264
6.	Coumarin	Lepidotin C **490**	1.2	0.0132
7.	Coumarin	Mammea A/BB cyclo F **77**	1.6	0.0176
8.	Coumarin	Ochrocarpin E **76**	1.0	0.0110
9.	Triterpene	Friedelin **186**	5.3	0.0582
10.	Triterpene	3β-friedelinol **189**	3.0	0.0330
11.	Triterpene	Betulinic acid **177**	2.0	0.0220
12.	Triterpene	Glutinol **491**	9.9	0.1088
13.	Xanthone	Pyranojacareubin **164**	1.5	0.0165

4.1.2.1 Lepidotol A 70

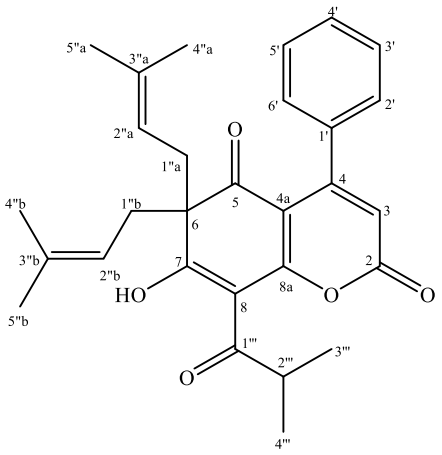

Lepidotol A **70**, a major compound in this study, was successfully isolated and characterized through various analytical techniques. Based on the ^{13}C-NMR data and high-resolution electron ionization mass spectrometry (HRESIMS) $[M+H]^+$ ion at *m/z* 461.2325, the compound was determined to have the molecular formula $C_{29}H_{32}O_5$. The UV spectrum exhibited absorbances at λ_{max} 224 and 296 nm. Meanwhile, the IR spectrum showed absorption bands at 3435, 1751, 1594, 1378 and 757 cm^{-1} which were attributed to O-H, δ-lactone, chelated acyl group, geminal dimethyl, and trisubstituted alkene functional groups.

A 4-phenyl coumarin moiety was present, as shown by the singlet signal at δ_H 5.94 and a highly hydrogen-bonded hydroxy group at δ_H 18.87 in the ^{1}H-NMR spectrum. Additionally, five aromatic protons were detected at δ_H 7.15 (2H, *dd*, *J* = 8.0, 1.8 Hz, H-2' and H-6') and δ_H 7.39 (3H, *m*, H-3' to H-5'). Two prenyl groups were also detected at δ_H 4.82 (2H, *t*, *J* = 7.6 Hz, H-2"a and H-2"b), 2.65 (4H, *m*, H-1"a and H-1"b), 1.60 (6H, *s*, Me-5"a and Me-5"b), and 1.54 (6H, *s*, Me-4"a and Me-4"b) in the ^{1}H-NMR spectrum (Figure 4.4).

29 carbon signals were visible in the ^{13}C-NMR spectrum and DEPT-135, including six methyls, two methylenes, nine methines, three carbonyls, and nine quartenary carbons

(Figure 4.5). The monosubstituted phenyl ring was characterized by signals at δ_C 138.5 (C-1'), 128.8 (C-4'), 128.1 (C-3' and C-5'), and 126.9 (C-2' and C-6'). Meanwhile, the α-pyrone carbonyl carbon was detected at δ_C 158.6 (C-2), and the two methylene carbons were observed at C-3 (δ_C 110.8) and C-4 (δ_C 158.0).

Through the HMBC correlation, it was found that the geminal prenyl group was attached to C-6 (δ_C 62.3), and an isobutyryl group was linked to C-8 (δ_C 104.6) based on the presence of two methyls at δ_H 1.30 (6H, *d*, *J* = 6.7 Hz, Me-3‴ and Me-4‴), a methine proton at δ_H 3.99 (1H, *sept*, *J* = 6.7 Hz, H-2‴), and a carbonyl carbon at δ_C 205.2 (C-1‴). Thus, it was suggested that the compound had a structure similar to that of a 6-*gem*-diprenyl-8-acyl-4-phenyl coumarin.

The consistency of the ^{1}H and ^{13}C-NMR spectra with literature data confirmed the structure of lepidotol A **70** and the data was recorded in Table 4.5.

Table 4.5: ^{1}H and ^{13}C-NMR spectral data of lepidotol A 70 in $CDCl_3$.

Position	Experimental ($CDCl_3$)		Reference ($CDCl_3$) (Rouger et al., 2015)	
	δ_H, *J* (Hz)	δ_C	δ_H, *J* (Hz)	δ_C
2	-	158.6	-	158.6
3	5.94, *s*	110.8	5.94, *s*	110.8
4	-	158.0	-	157.9
4a	-	107.3	-	107.3
5	-	200.4	-	200.4
6	-	62.3	-	62.3
7	-	192.8	-	192.8
8	-	104.6	-	104.6
8a	-	168.0	-	168.0
1′	-	138.5	-	138.5
2′	7.15, *dd* (8.0, 1.8)	126.9	7.15, *dd* (7.9, 1.4)	126.9
3′	7.39, *m*	128.1	7.39, *m*	128.1
4′	7.39, *m*	128.8	7.39, *m*	128.8
5′	7.39, *m*	128.1	7.39, *m*	128.1
6′	7.15, *dd* (8.0, 1.8)	126.9	7.15, *dd* (7.9, 1.4)	126.9
1″a, 1″b	2.65, *m*	38.2	2.64, *m*	38.2
2″a, 2″b	4.82, *t* (7.6)	117.5	4.83, *t* (7.5)	117.5
3″a, 3″b	-	136.2	-	136.2
4″a, 4″b	1.54, *s*	18.1	1.55, *s*	18.1
5″a, 5″b	1.60, *s*	26.0	1.61, *s*	26.1
1‴	-	205.2	-	205.2
2‴	3.99, *sept* (6.7)	37.2	3.99, *sept* (6.7)	37.2
3‴	1.30, *d* (6.7)	19.6	1.31, *d* (6.7)	19.6
4‴	1.30, *d* (6.7)	19.6	1.31, *d* (6.7)	19.6
7-OH	18.87, *s*	-	18.87, *s*	-

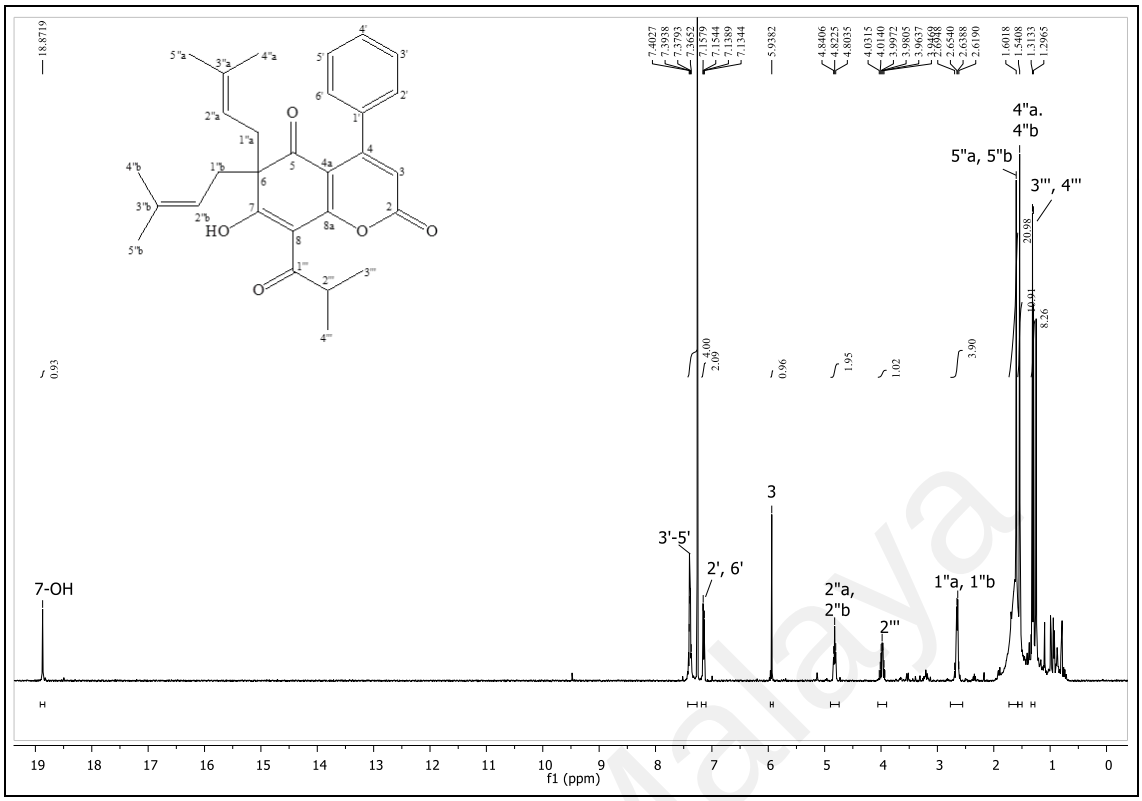

Figure 4.4: ^{1}H-NMR of lepidotol A 70.

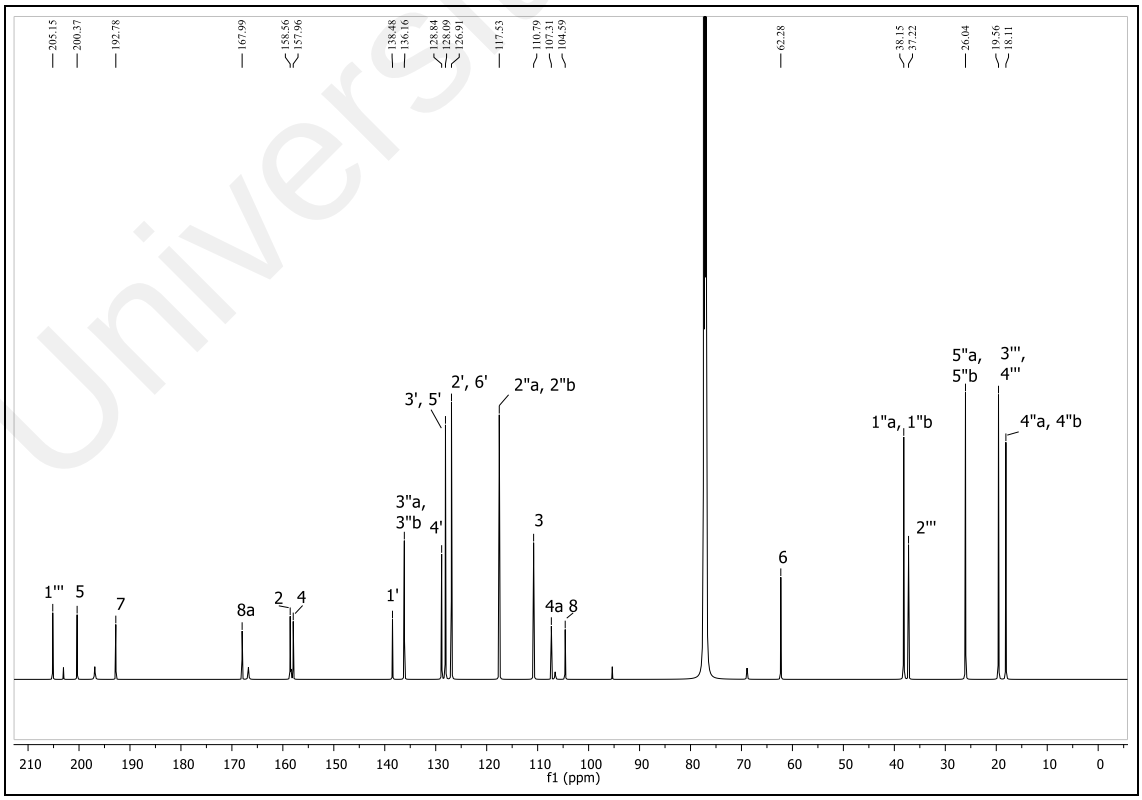

Figure 4.5: ^{13}C-NMR of lepidotol A 70.

4.1.2.2 Lepidotol B 71

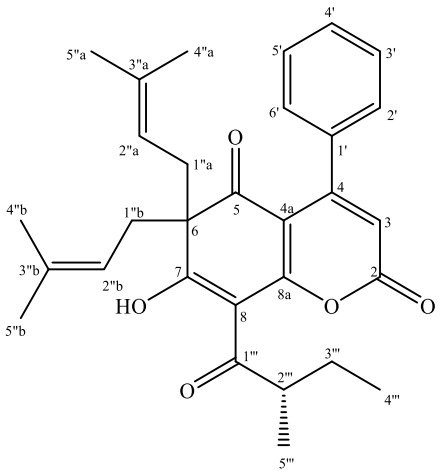

Lepidotol B **71**, the major constituent, was obtained as a yellow amorphous powder with a negative optical rotation of$[\alpha]_D^{25}$ = +4.3° (c 0.1, $CHCl_3$). The HRESIMS data of lepidotol B **71** revealed an $[M–H]^-$ ion at *m/z* 473.2319, indicating a molecular formula of $C_{30}H_{34}O_5$, which was also supported by the ^{13}C-NMR data. The main difference between lepidotol B **71** and lepidotol A **70** was the presence of an additional methylene group in the acyl chain of lepidotol B **71**. The UV and IR spectra of lepidotol B **71** were similar to those of lepidotol A **70**, with absorbance bands at 229 and 298 nm in the UV spectrum, indicating the same coumarin skeleton. The IR spectrum showed the presence of O-H, δ-lactone, chelated acyl group, geminal dimethyl, and trisubstituted alkene at 3477, 1754, 1595, 1379, and 766 cm^{-1}, respectively.

In the ^{1}H-NMR spectrum (Figure 4.6), a singlet at δ_H 5.94 for the H-3 of a 4-phenylcoumarin moiety and a chelated hydroxyl at δ_H 18.89 were observed. Additionally, the multiplet at δ_H 7.40 and doublet at δ_H 7.15 of the ^{1}H-NMR were identified as mono-substituted phenyl. These observations confirmed the presence of a 4-phenyl coumarin skeleton.

A total of 30 carbon signals were detected on the ^{13}C and DEPT-135 NMR spectra, including six methyls, three methylenes, nine methines, three carbonyls, and nine

quaternary carbons (Figure 4.7). The additional methylene group [δ_H 1.88 (1H, *sext*, *J*= 7.2 Hz) and 1.55 (1H, *s*); δ_C 27.7 (C-3‴)] and a deshielded methine [δ_H 3.82, *sext*, *J* = 6.8 Hz; 43.6 (C-2‴)] confirmed the presence of a 2-methylbutyryl group in the acyl side chain attached to C-8 (δ_C 105.3).

The examined substance was identified as lepidotol B **71** after a thorough analysis of the 1D and 2D-NMR spectrum data (Table 4.6) as well as comparison with values from the literature.

Table 4.6: ^{1}H and ^{13}C-NMR spectral data of lepidotol B 71 in $CDCl_3$.

Position	**Experimental ($CDCl_3$)**		**Reference ($CDCl_3$)** (Rouger et al., 2015)	
	δ_H, *J* (Hz)	**δ_C**	**δ_H, *J* (Hz)**	**δ_C**
2	-	158.5	-	158.4
3	5.94, *s*	110.9	5.94, *s*	110.7
4	-	157.9	-	157.7
4a	-	107.4	-	107.2
5	-	200.6	-	200.4
6	-	62.2	-	62.1
7	-	192.9	-	192.7
8	-	105.3	-	105.2
8a	-	168.0	-	167.8
1′	-	138.5	-	138.3
2′	7.15, *d* (6.6)	126.9	7.15, *dd* (8.0, 1.6)	126.7
3′	7.40, *m*	128.1	7.39, *m*	127.9
4′	7.40, *m*	128.8	7.39, *m*	128.7
5′	7.40, *m*	128.1	7.39, *m*	127.9
6′	7.15, *d* (6.6)	126.9	7.15, *dd* (8.0, 1.6)	126.7
1″a, 1″b	2.64, *m*	38.3	2.65, *m*	38.1
2″a, 2″b	4.83, *m*	117.5	4.82, *m*	117.4
3″a, 3″b	-	136.1	-	136.0
4″a, 4″b	1.55, *s*	18.2	1.55, *s*	18.0
	1.54, *s*		1.54, *s*	
5″a, 5″b	1.61, *s*	26.1	1.61, *s*	25.9
	1.59, *s*		1.58, *s*	
1‴	-	204.6	-	204.4
2‴	3.82, *sext* (6.8)	43.6	3.81 *sext* (7.0)	43.5
3‴	1.88, *sext* (7.2)	27.7	1.87, *sext* (7.0)	27.6
	1.55, *m*		1.55, *m*	
4‴	1.00, *t* (7.2)	11.9	1.00, *t* (7.0)	11.7
5‴	1.29, *d* (6.8)	17.1	1.30, *d* (7.0)	17.0
7-OH	18.89, *s*	-	18.91, *s*	-

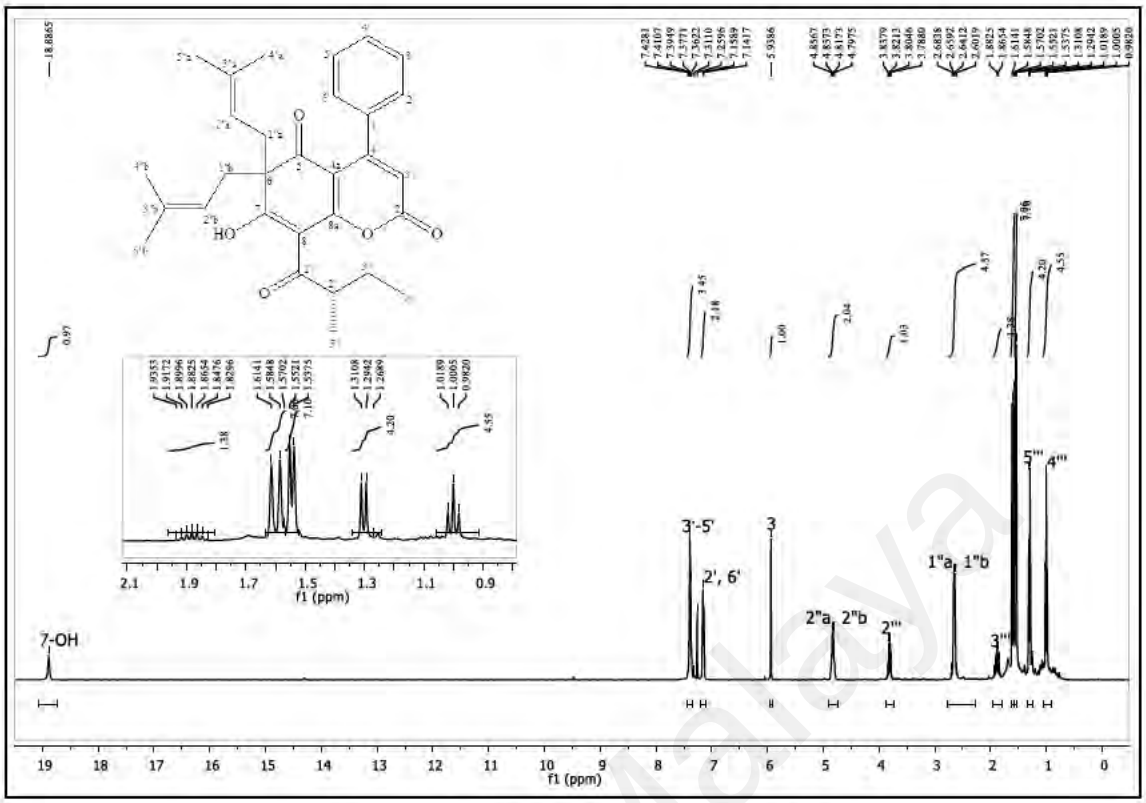

Figure 4.6: ^{1}H-NMR of lepidotol B 71.

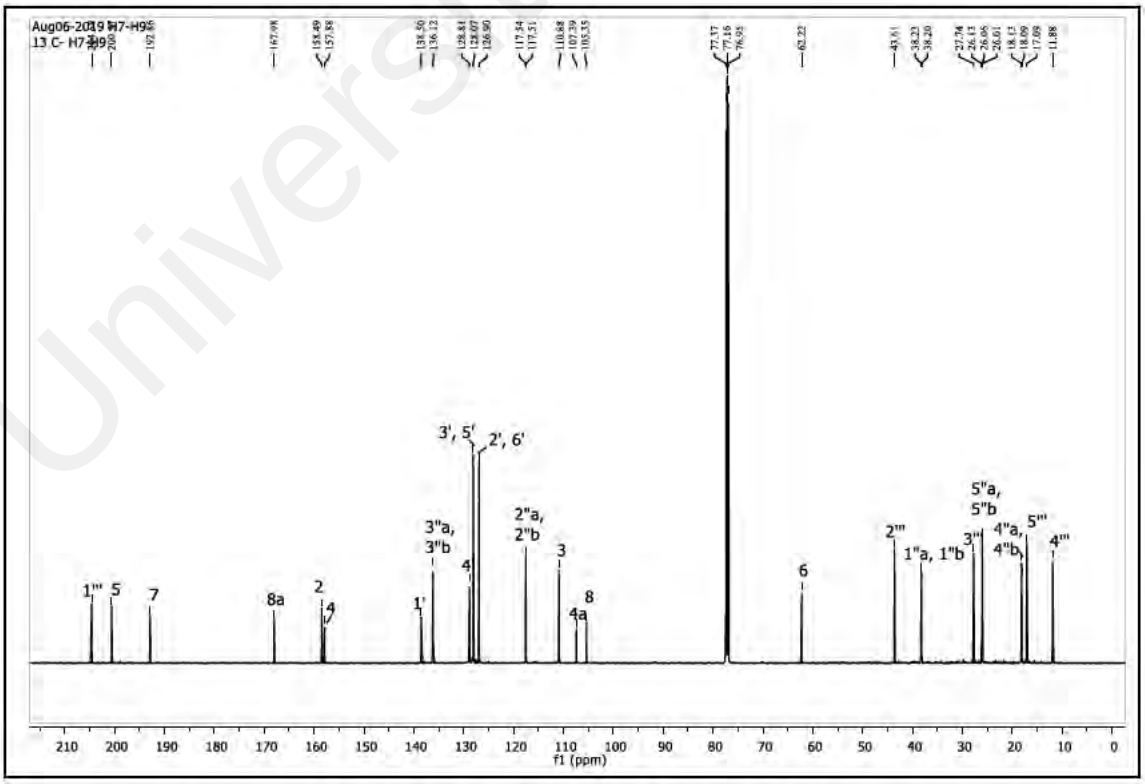

Figure 4.7: ^{13}C-NMR of lepidotol B 71.

4.1.2.3 Lepidotol E 86

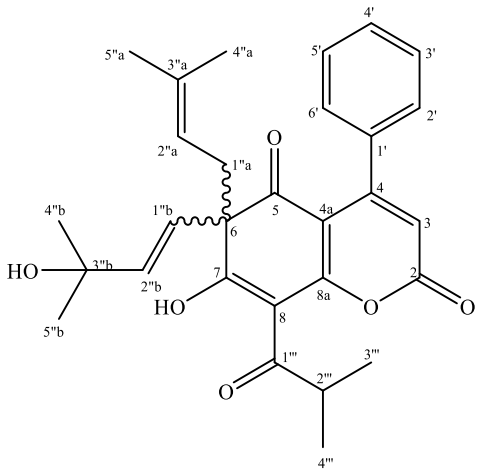

Lepidotol E **86** [$C_{29}H_{32}O_6$ with $[M–H]^–$ at *m/z* 475.2125; was isolated as yellow amorphous powder. The mass pointed to the addition of an oxygen atom in lepidotol E **86** compared to lepidotol A **70**.

The characteristic singlet of H-3 of 4-phenyl coumarin was noticed at δ_H 5.97 and the chelated hydroxyl peak was determined at δ_H 18.83. Furthermore, the mono-substituted phenyl group was determined at δ_H 7.40 (*m*) and δ_H 7.17 (*m*) from the ^{1}H-NMR (Figure 4.8). Hence, the skeletal of the structure was confirmed as a 4-phenyl coumarin. The ^{1}H-NMR spectrum (Figure 4.8) revealed two *E*-ethylenic protons that appeared as an AB doublet at δ_H 5.70 (1H, *d*, *J* = 15.9 Hz, H-1″ b) and δ_H 5.78 (1H, *d*, *J* = 15.9 Hz, H-2″ b), respectively, as well as the typical signs for one prenyl chain.

A total of 29 carbon signals were detected on the ^{13}C and DEPT-135 NMR spectra: six methyls, a methylenes, ten methines, three carbonyls and nine quaternary carbons (Figure 4.9). A deshielded sp3 carbon was visible in the ^{13}C-NMR spectra at δ_C 70.0, which corresponded to both H-1"b and H-2"b in the HMBC-NMR spectrum, confirming the presence of a 3-hydroxy-3-methylbutenyl chain at C-6.

The structure was confirmed as lepidotol E **86**. The details of the ^{1}H and ^{13}C-NMR spectra was recorded in the Table 4.7.

Table 4.7: ^{1}H and ^{13}C-NMR spectral data of lepidotol E 86 in $CDCl_3$.

Position	Experimental ($CDCl_3$)		Reference ($CDCl_3$) (Rouger et al., 2015)	
	δ_H, *J* (Hz)	δ_C	δ_H, *J* (Hz)	δ_C
2	-	158.3	-	158.3
3	5.97, *s*	110.7	5.97, *s*	110.7
4	-	156.9	-	157.9
4a	-	107.8	-	107.0
5	-	199.0	-	199.3
6	-	63.5	-	63.4
7	-	190.2	-	190.0
8	-	103.1	-	103.7
8a	-	168.3	-	168.5
1′	-	137.3	-	138.0
2′	7.17, *m*	126.6	7.17, *m*	126.6
3′	7.40, *m*	128.1	7.39, *m*	128.1
4′	7.40, *m*	128.8	7.39, *m*	128.9
5′	7.40, *m*	128.1	7.39, *m*	128.1
6′	7.17, *m*	126.6	7.17, *m*	126.6
1″a	2.81, *d* (7.1)	35.0	2.81, *d* (7.1)	34.9
2″a	4.75, *t* (7.1)	117.9	4.74, *t* (7.1)	117.9
3″a	-	135.1	-	135.9
4″a	1.57, *m*	18.1	1.57, *m*	18.1
5″a	1.67, *m*	25.8	1.67, *m*	25.8
1″b	5.70, *d* (15.9)	124.9	5.70, *d* (15.9)	124.9
2″b	5.78, *d* (15.9)	141.7	5.78, *d* (15.9)	141.6
3″b	-	70.3	-	70.0
4″b	1.30, *m*	29.8	1.31, *m*	29.8[a]
5″b	1.30, *m*	29.9	1.31, *m*	29.9[a]
1‴	-	204.8	-	204.8
2‴	3.98, *hept* (6.7)	36.8	3.98, *hept* (6.6)	36.8
3‴	1.36, *d* (6.7)	19.5	1.32, *d* (6.6)	19.5
4‴	1.36, *d* (6.7)	19.5	1.32, *d* (6.6)	19.5
7-OH	18.83, *s*	-	18.85, *s*	-

[a] Interchangeable.

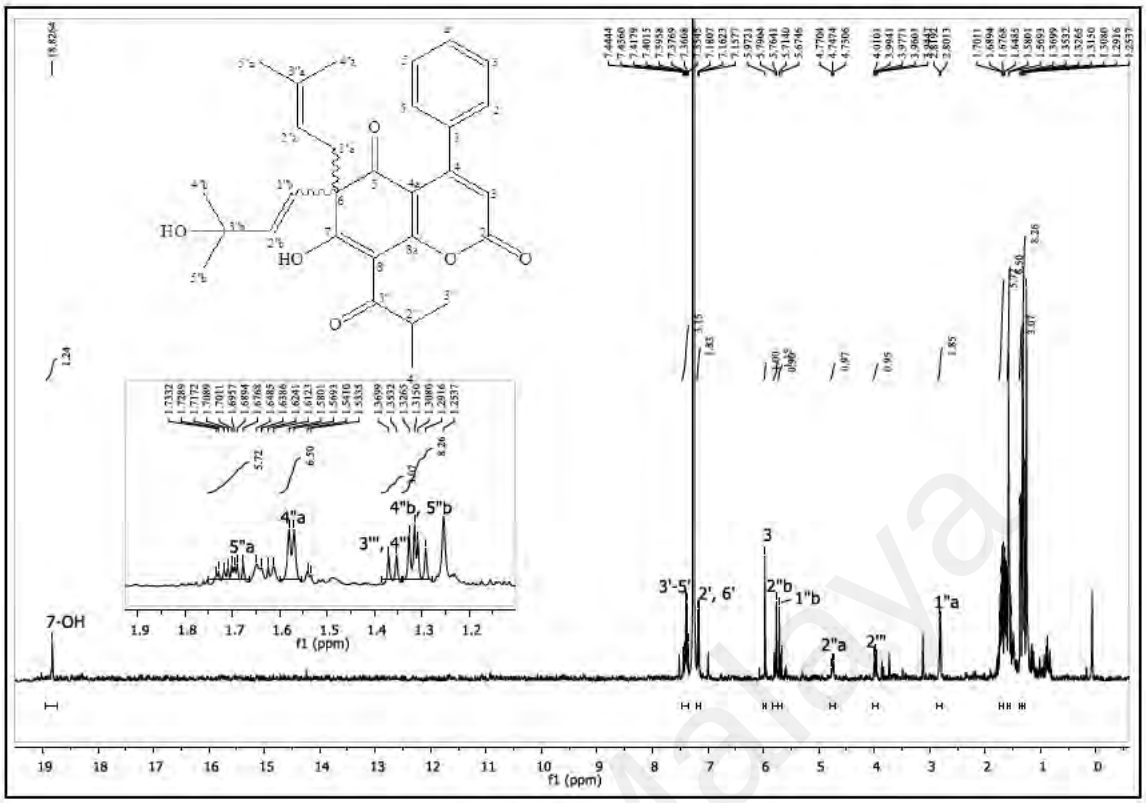

Figure 4.8: ^{1}H-NMR of lepidotol E 86.

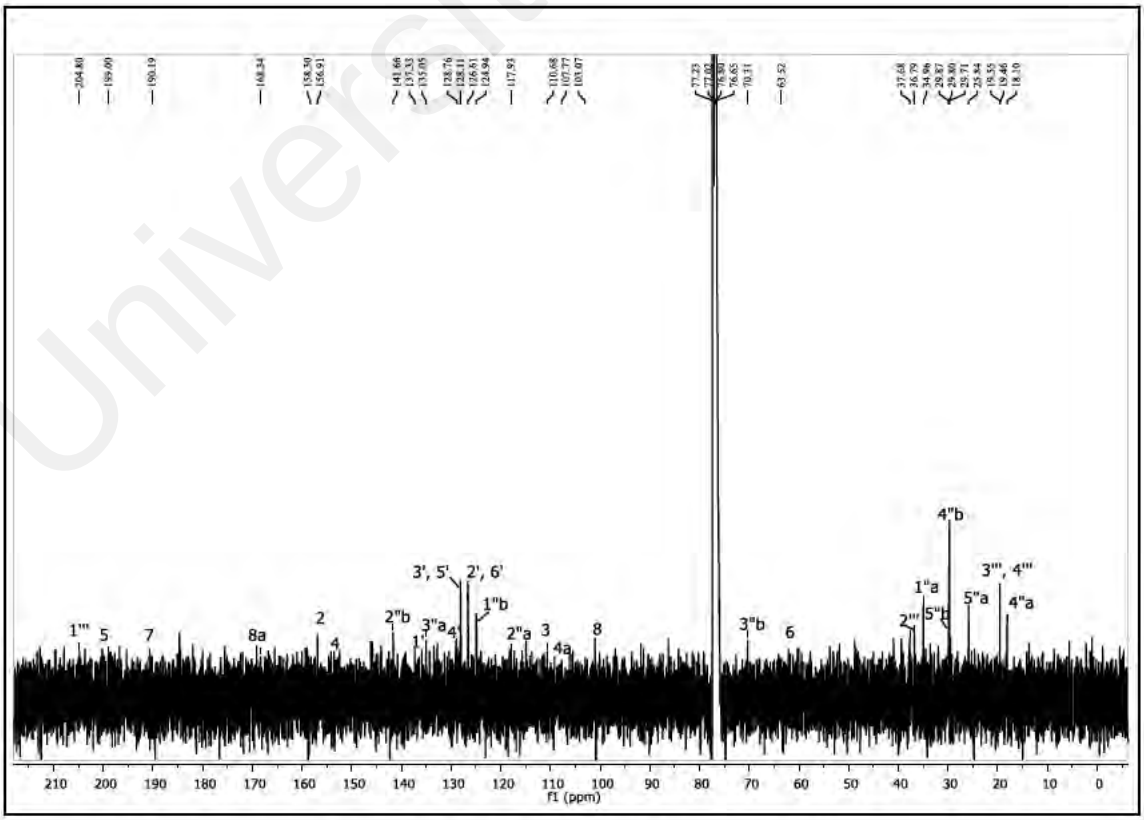

Figure 4.9: ^{13}C-NMR of lepidotol E 86.

4.1.2.4 Lepidotin A 88

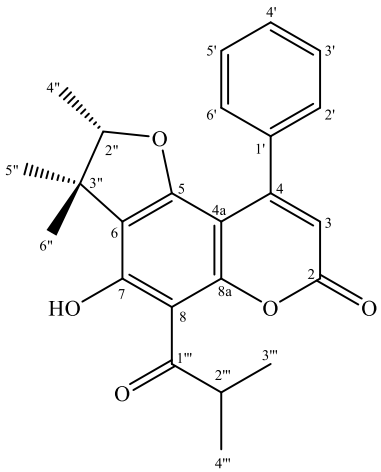

Lepidotin A **88** was obtained as yellow amorphous powder, with the $[\alpha]_D^{25}$= +3.8° (c 0.026, $CHCl_3$). The molecular formula, $C_{24}H_{24}O_5$, was confirmed by ^{13}C-NMR data and an $[M+H]^+$ ion at *m/z* 393.1692. Maximum absorption was seen in the UV spectrum at λ_{max} 204, 225, and 293 nm, resemblance to the absorption bands of coumarin structure. The IR spectrum showed strong absorption at υ_{max} at 3459 (OH), 1741 (δ-lactone), 1598 (chelated acyl group), 1382 (geminal dimethyl) cm^{-1}.

The ^{1}H-NMR spectrum (Figure 4.10) illustrated the characteristic chemical shifts observed in 4-phenylcoumarin derivatives. The designated feature at H-3 singlet was observed at δ_H 6.05 and the chelated hydroxyl was revealed at δ_H 14.25 as a singlet. The mono-substituted phenyl group at C-4' exhibited distinct multiplet patterns in the ^{1}H-NMR spectrum, with two sets of signals observed at δ_H 7.29 (H-2' and H-6') and δ_H 7.38 (H3'-H5'), representing two and three aromatic protons, respectively.

The ^{13}C-NMR spectrum (Figure 4.11) displayed a total of 24 carbon signals: five methyls, eight methines, two carbonyls and nine quaternary carbons. Besides an oxygen substituent was attached to the deshielded C-2" and H-2" [δ_C 91.5; δ_H 4.24 (1H, *q*, *J* = 6.4 Hz)], a methyl (C-4") was also substituted at C-2" according to the HMBC corrrelation. Dimethyl group (C-5" and C-6") was noticed at C-3" (δ_C 43.4 ppm) which is more

deshielded through HMBC corelation. Hence, the structure was confirmed to be a 4,4-dimethyl-5-methyldihydrofuran moiety. Moreover, an isobutyryl chain [δ_H 1.27 (3H, *d*, *J* = 6.4 Hz, Me-3‴), 1.30 (3H, *d, J* = 6.4 Hz, Me-4‴), 4.06 (1H, *sept*, *J* = 6.4 Hz, H-2‴), and δ_C 210.8 (C-1‴)] was attached to C-8 like lepidotol A **70**.

The structure of lepidotin A **88** was confirmed after comparing it with literature data. The details of the ^{1}H and ^{13}C-NMR data were shown in the Table 4.8.

Table 4.8: ^{1}H and ^{13}C-NMR spectral data of lepidotin A 88 in $CDCl_3$.

Position	**Experimental ($CDCl_3$)**		**Reference ($CDCl_3$)** (Rouger et al., 2015)	
	δ_H	**δ_C**	**δ_H**	**δ_C**
2	-	159.4	-	159.4
3	6.05, *s*	110.9	6.05, *s*	110.9
4	-	155.6	-	155.6
4a	-	98.5	-	98.5
5	-	161.2	-	161.2
6	-	118.3	-	118.2
7	-	164.8	-	164.8
8	-	104.1	-	104.1
8a	-	157.2	-	157.2
1’	-	137.6	-	137.6
2′	7.29, *m*	127.5	7.30, *m*	127.5
3′	7.38, *m*	127.8	7.40, *m*	127.8
4′	7.38, *m*	128.8	7.40, *m*	128.8
5′	7.38, *m*	127.8	7.40, *m*	127.8
6′	7.29, *m*	127.5	7.30, *m*	127.5
2″	4.24, *q* (6.4)	91.5	4.26, *q* (6.6)	91.5
3″	-	43.4	-	43.4
4″	1.07, *d* (6.4)	14.0	1.07, *d* (6.6)	14.0
5″	1.19, *s*	20.2	1.19, *s*	20.2
6″	1.39, *s*	25.4	1.39, *s*	25.4
1‴	-	210.8	-	210.8
2‴	4.06, s*ept* (6.4)	40.2	4.10, s*ept* (6.7)	40.2
3‴	1.27, *d* (6.4)	19.2	1.29, *d* (6.7)	19.3
4‴	1.30, *d* (6.4)	19.4	1.30, *d* (6.7)	19.4
7-OH	14.25, *s*	-	14.25, *s*	-

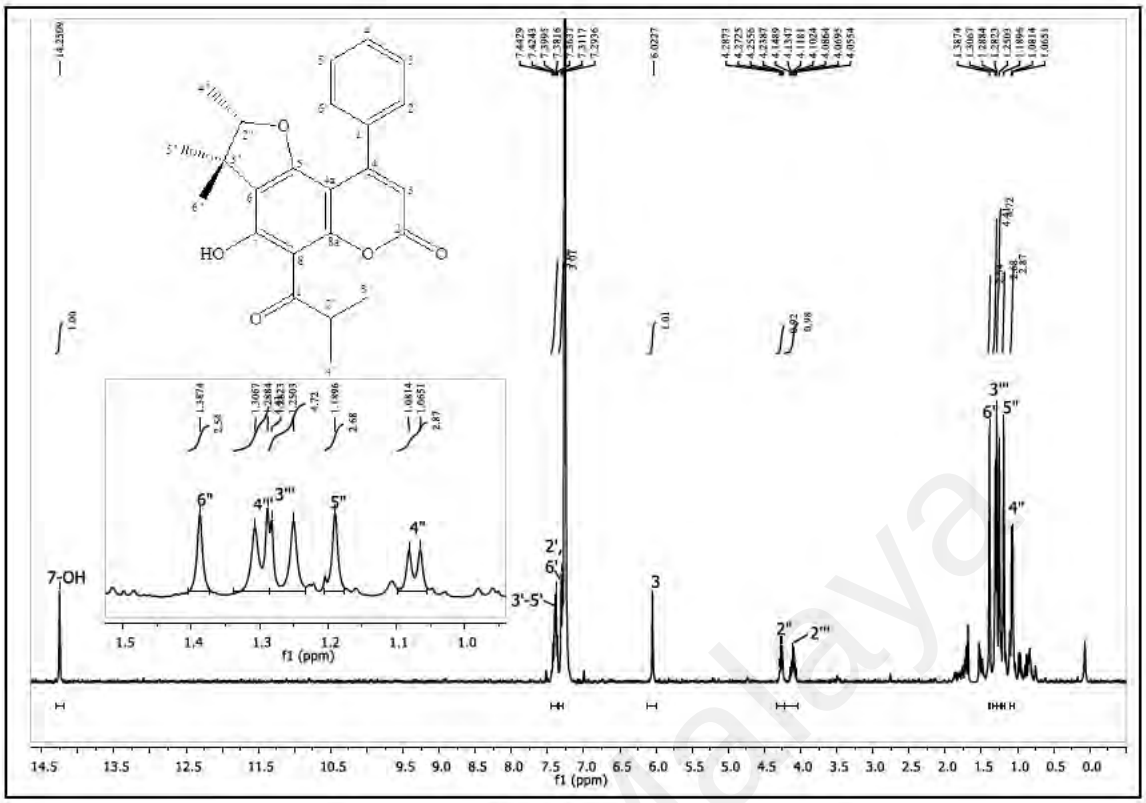

Figure 4.10: ^{1}H-NMR of lepidotin A 88.

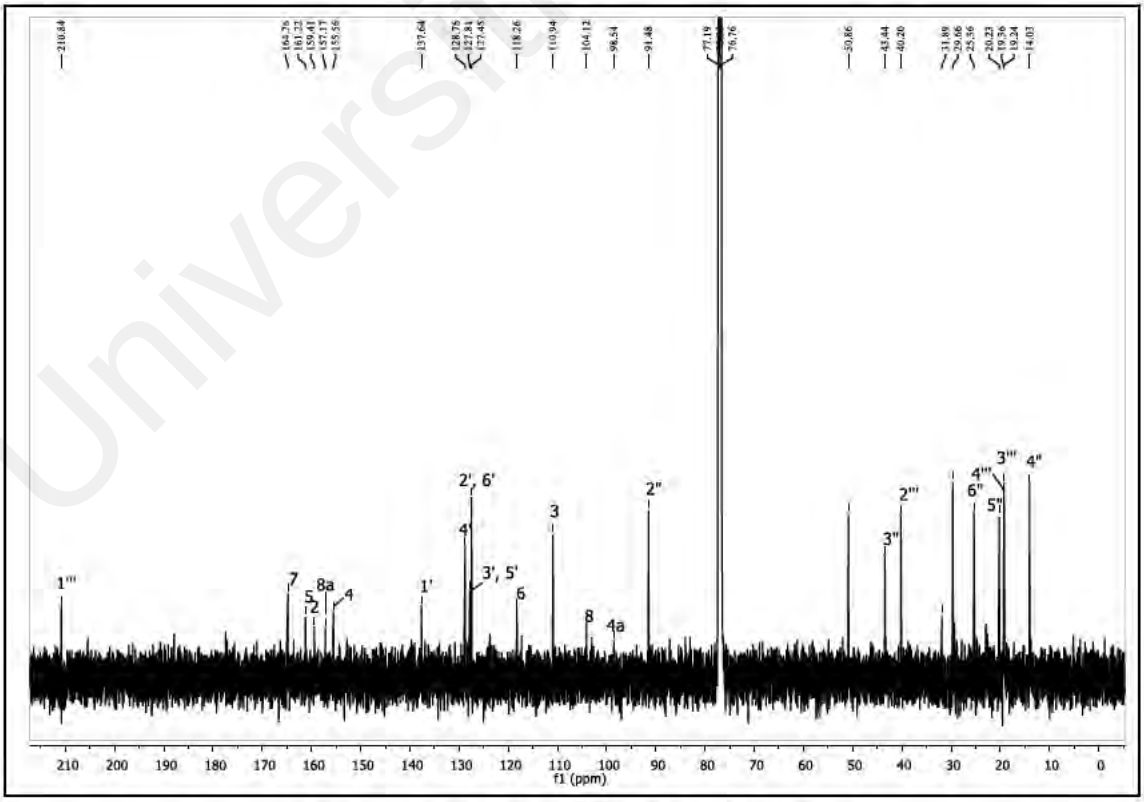

Figure 4.11: ^{13}C-NMR of lepidotin A 88.

4.1.2.5 Lepidotin B 89

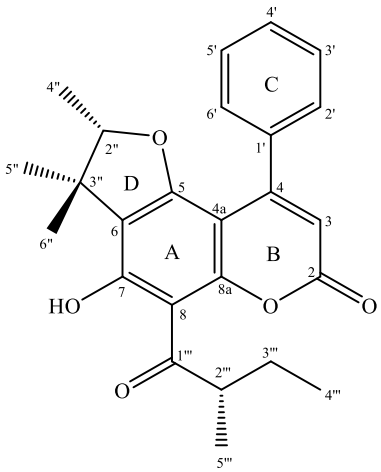

Lepidotin B **89** was isolated as yellow amorphous powder with the $[\alpha]_D^{25}$ +2.4° (c 0.008, $CHCl_3$). The molecular formula of lepidotin B **89** was denoted as $C_{25}H_{26}O_5$ based on ^{13}C-NMR data and an $[M+H]^+$ ion at *m/z* 407.1848 (calcd 407.1853). As for lepidotols A **70** and B **71**, The 14 Da discrepancy between lepidotin A **88** and B **89** was attributable to an additional methylene group (δ_H 1.94, *m* and 1.49, *m*: δ_C 27.2) in the acyl side chain. Both UV and IR spectra were also identical to lepidotin A **88**; absorption at λ_{max} 204, 225, and 295 nm were shown in the UV spectrum and the IR spectrum revealed the absorption bands at 3452 (O-H), 1741 (δ-lactone), 1599 (chelated acyl group), 1384 (geminal dimethyl) cm^{-1}.

In the ^{1}H-NMR (Figure 4.12), δ_H 6.05 that assigned to H-3 singlet and δ_H 14.30 which referred to the chelated hydroxyl group were the characteristic features of 4-phenylcoumarin. Two sets of multiplets were detected at aromatic region [δ_H 7.30 (H-2' and H-6') and δ_H 7.39 (H3'-H5')] were assigned to the benzene ring that attached to C-4.

25 carbon signals were found on the ^{13}C-NMR spectra (Figure 4.13): five methyls, a methylene, eight methines, two carbonyls and nine quaternary carbons. As for lepidotin A **88**, a 4,4-dimethyl-5-methyldihydrofuran was attached to C-5/C-6. Moreover, from the

^{1}H and ^{13}C-NMR spectra, a 2-methylbutyryl moiety that is identical to lepidotol B **71** was found attached to C-8 acyl chain.

The NMR spectral data of lepidotin B **89**, along with corresponding literature data, were compiled in Table 4.9.

Table 4.9: ^{1}H and ^{13}C-NMR spectral data of lepidotin B 89 in $CDCl_3$.

Position	Experimental ($CDCl_3$)		Reference ($CDCl_3$) (Rouger et al., 2015)	
	δ_H	δ_C	δ_H	δ_C
2	-	159.5	-	159.4
3	6.05, *s*	111.2	6.05, *s*	111.0
4	-	155.7	-	155.5
4a	-	98.7	-	98.5
5	-	161.4[a]	-	161.2[a]
6	-	118.4[a]	-	118.2[a]
7	-	164.9 & 164.9[a]	-	164.8 & 164.7[a]
8	-	104.8 & 104.7[a]	-	104.6 & 104.5[a]
8a	-	157.4[a]	-	157.2[a]
1′	-	137.9	-	137.7
2′	7.30, *m*	127.6	7.30, *m*	127.5
3′	7.39, *m*	128.0	7.39, *m*	127.8
4′	7.39, *m*	128.9	7.39, *m*	128.8
5′	7.39, *m*	128.0	7.39, *m*	127.8
6′	7.30, *m*	127.6	7.30, *m*	127.5
2″	4.26, *q* (6.6)	91.7 & 91.6[a]	4.26, *q* (6.6)	91.5 & 91.4[a]
3″	-	43.6	-	43.4
4″	1.08, *d* (6.6) & 1.07, *d* (6.6) [a]	14.3 & 14.2[a]	1.08, *d* (6.6) & 1.07, *d* (6.6) [a]	14.1 & 14.0[a]
5″	1.20, *s* & 1.18, *s*[a]	20.44 & 20.41[a]	1.20, *s* & 1.18, *s*[a]	20.3 & 20.2[a]
6″	1.39, *s* & 1.38, *s*[a]	25.6 & 25.5[a]	1.39, *s* & 1.38, *s*[a]	25.4 & 25.3[a]
1‴	-	210.9 & 210.8[a]	-	210.7 & 210.6[a]
2‴	3.95, *sext* (6.6)	47.0[a]	3.95, *sext* (6.6)	46.8[a]
3‴	1.94, *m* & 1.49, *m*[a]	27.4 & 27.3[a]	1.94, *m* & 1.49, *m*[a]	27.3 & 27.2[a]
4‴	1.03, *t* (7.3) & 1.01, *t* (7.3)[a]	12.0[a]	1.03, *t* (7.5) & 1.01, *t* (7.5)[a]	11.8[a]
5‴	1.29, *d* (6.6) & 1.28, *d* (6.6)[a]	16.9 & 16.8[a]	1.29, *d* (6.6) & 1.28, *d* (6.6)[a]	16.7 & 16.6[a]
7-OH	14.30, *s* & 14.28, *s*[a]	-	14.32, *s* & 14.30, *s*[a]	-

[a]The signals of the two tautomeric forms are observable.

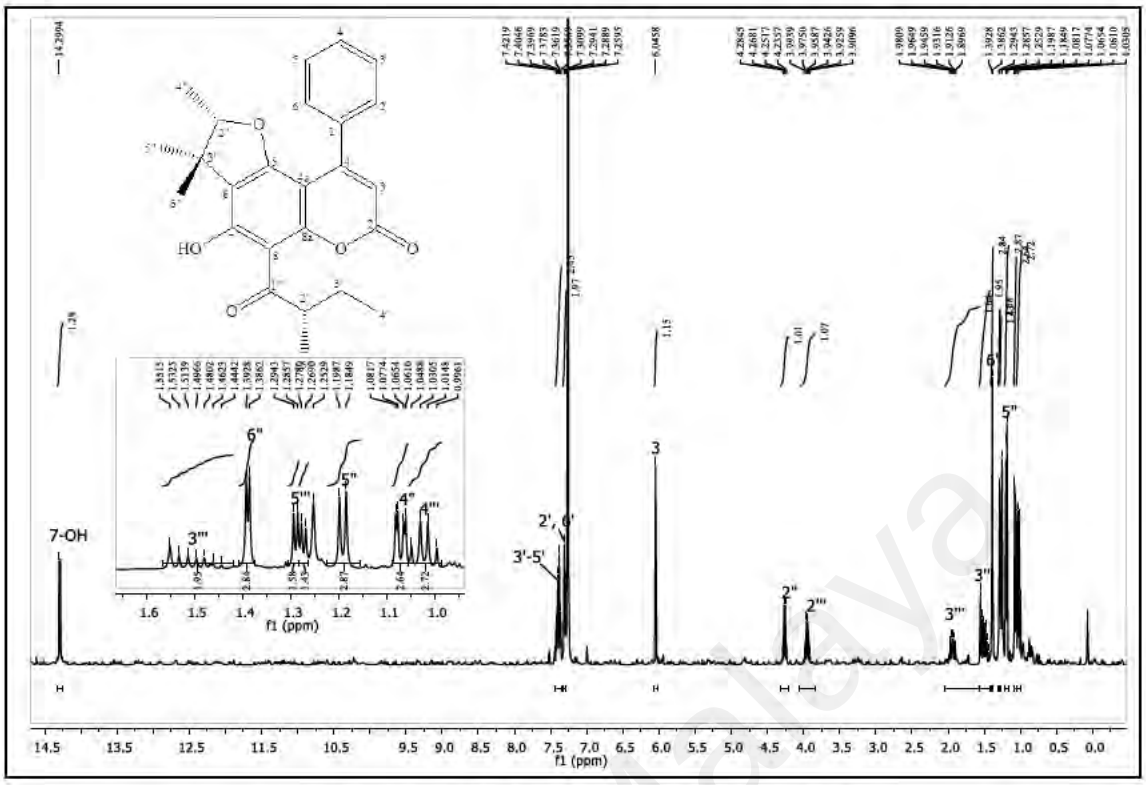

Figure 4.12: ^{1}H-NMR of lepidotin B 89.

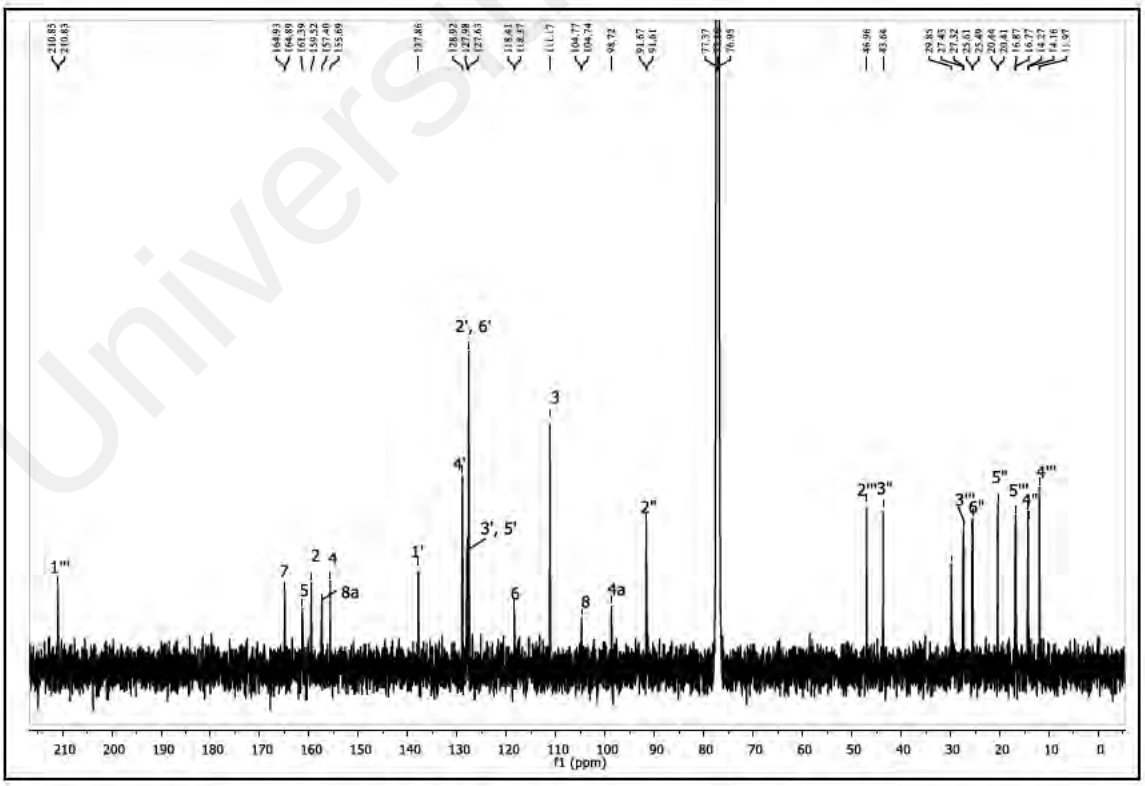

Figure 4.13: ^{13}C-NMR of lepidotin B 89.

Figure 4.14: Predicted ^{1}H and ^{13}C-NMR chemical shifts of lepidotin B 89 analyzed by ACD/ Spectrus Processor software.

4.1.2.6 Lepidotin C 490

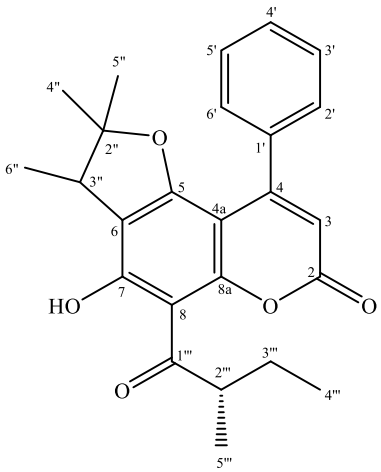

Lepidotin C **490** was isolated as yellow amorphous powder with the $[\alpha]_D^{25}$ -4° (c 0.0015, $CHCl_3$). The molecular formula of lepidotin C **490** was established as $C_{25}H_{26}O_5$ based on ^{13}C NMR data and an $[M+H]^+$ ion at *m/z* 407.1848 (calcd 407.1850), which was identical to lepidotin B **89**. Besides, the UV and IR spectra were also identical to lepidotin B **89**; absorption at λ_{max} 204, 226, and 297 nm were shown in the UV spectrum demonstrated a 4-phenyl coumarin skeleton. The IR spectrum showed the absorption bands at 3460 (O-H), 1741 (δ-lactone), 1598 (chelated acyl group), and 1385 (geminal dimethyl) cm^{-1}.

In the ^1H-NMR spectrum (Figure 4.16), the typical H-3 singlet of a 4-phenyl coumarin moiety was noticed at δ_H 6.04. and a chelated hydroxyl group (7-OH) was observed at δ_H 14.33. Besides, two sets of multiplets at aromatic region [δ_H 7.29 (H-2' and H-6') and 7.39 (H3'-H5')], were corresponding to the aromatic ring that attached to C-4. The above observations suggested the presence of an 8-acyl-5,7-dioxy-4-phenyl coumarin as the skeleton of the structure.

From the ^{13}C- (Figure 4.17) and DEPT-NMR (Figure 4.18) spectra, there were a total of 25 carbon signals examined. Out of the 25 signals, five were methyls, one was methylene, eight were methines, two were carbonyls and nine were quaternary carbons.

From the ^{1}H and ^{13}C-NMR spectra, a 2-methylbutyryl moiety that is identical to lepidotol B **71** and lepidotin B **89** was found attached to C-8 acyl chain.

The ^{1}H and ^{13}C-NMR spectra of lepidotin C **490** were similar to those of lepidotin B **89**. The only differences observed were on the ^{1}H chemical shifts (δ_H) of the furan moiety attached to C-5/C-6. In lepidotin B **89**, δ_H value of H-2" in the furan ring is δ_H 4.26. However, in the furan moiety of lepidotin C **490**, this δ_H value appeared at a more upfield region, at δ_H 3.13. This suggested that this proton is attached to C-3" instead of C-2" in lepidotin C **490**. H-3" is more shielded (compared to H-2" in lepidotin B **89**) since it is not directly vicinal to the electronegative oxygen atom. It was hypothesized that C-2" of lepidotin C **490** bearing the *gem*-dimethyl group is vicinal to the oxygen in the furan ring, whereas C-3" bearing the single methyl group is adjacent to C-6. This hypothesis was substantiated by the HMBC correlation of H-6"/C-6 and H-3"/C-6 (Figure 4.15). Moreover, Chamberlain *et al.* proposed a biosynthesis pathway for 1,1- to 1,2-dimethylallyl derivatives, which matched the formation of lepidotin B **89** and C **490** through Claisen rearrangement mechanisms(Chamberlain et al., 1969) (refer scheme 4.1).

The ACD/Spectrus Processor software further strengthens the hypothesis on the structure of lepidotin C **490**. The predicted spectra for lepidotin B **89** (Figure 4.14) and lepidotin C **490** (Figure 4.22) showed good agreement with the experimental spectra. Thus, it was further confirmed that lepidotin C **490** bears a 5,5-dimethyl-4-methyldihydrofuran while lepidotin B **89** has a 4,4-dimethyl-5-methyldihydrofuran. Furthermore, the assignments of all the proton and carbon signals of lepidotin C **490** were confirmed by HSQC, COSY and HMBC experiments too (Table 4.10 and Figure 4.16-4.21). Hence, lepidotin C **490** was deduced as a new compound isolated from *M. lepidota.*

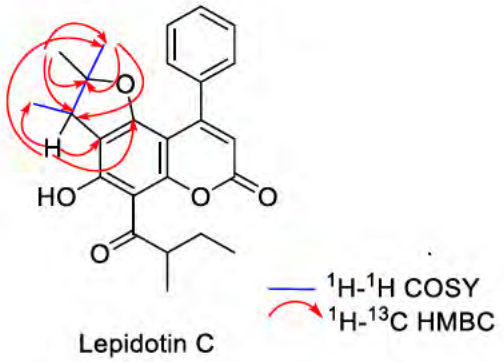

Figure 4.15: Selected COSY and HMBC correlations of lepidotin C 490.

Table 4.10: ^{1}H, ^{13}C, COSY and HMBC-NMR spectral data of lepidotin C 490 in $CDCl_3$.

Position	Experimental ($CDCl_3$)			
	δ_H	δ_C	COSY	HMBC
2	-	159.59		
3	6.04, *s*	110.89		2, 4a, 1'
4	-	155.81		
4a	-	98.95		
5	-	160.92		
6	-	115.11		
7	-	164.90		
8	-	104.51		
8a	-	157.56		
1′	-	137.81		
2′	7.29, *m*	127.54		4, 4'
3′	7.39, *m*	128.05		1', 2', 6'
4′	7.39, *m*	128.85		2', 6'
5′	7.39, *m*	128.05		1', 2', 6'
6′	7.29, *m*	127.54		4, 4'
2″	-	93.39		
3″	3.13, *q* (7.0)	42.91	6"	5, 6, 5", 6"
4″	1.10, *br s*	21.98		2", 3", 5"
5″	1.18, *s* & 1.19, *s*[a,b]	28.41	3"	2", 3"
6″	1.20, *d*[b]	14.29		2", 3", 4"
1‴	-	210.69		
2‴	3.96, *sext* (6.6)	46.89	3‴, 5‴	1‴, 3‴, 5‴
3‴	1.94, *dt* (13.5, 6.0), 1.49, *m*[a]	27.38	2‴, 4‴	1‴, 2‴, 4‴, 5‴
4‴	1.03, *t* (7.3) & 1.01, *t* (7.3)[a]	11.98	3‴	2‴, 3‴
5‴	1.29, *d* (6.6) & 1.28, *d* (6.7)[a]	16.81	2‴	1‴, 2‴, 3‴
7-OH	14.33, *s*	-		

[a]The signals of the two tautomeric forms are observable.
[b]The signals were overlapping.

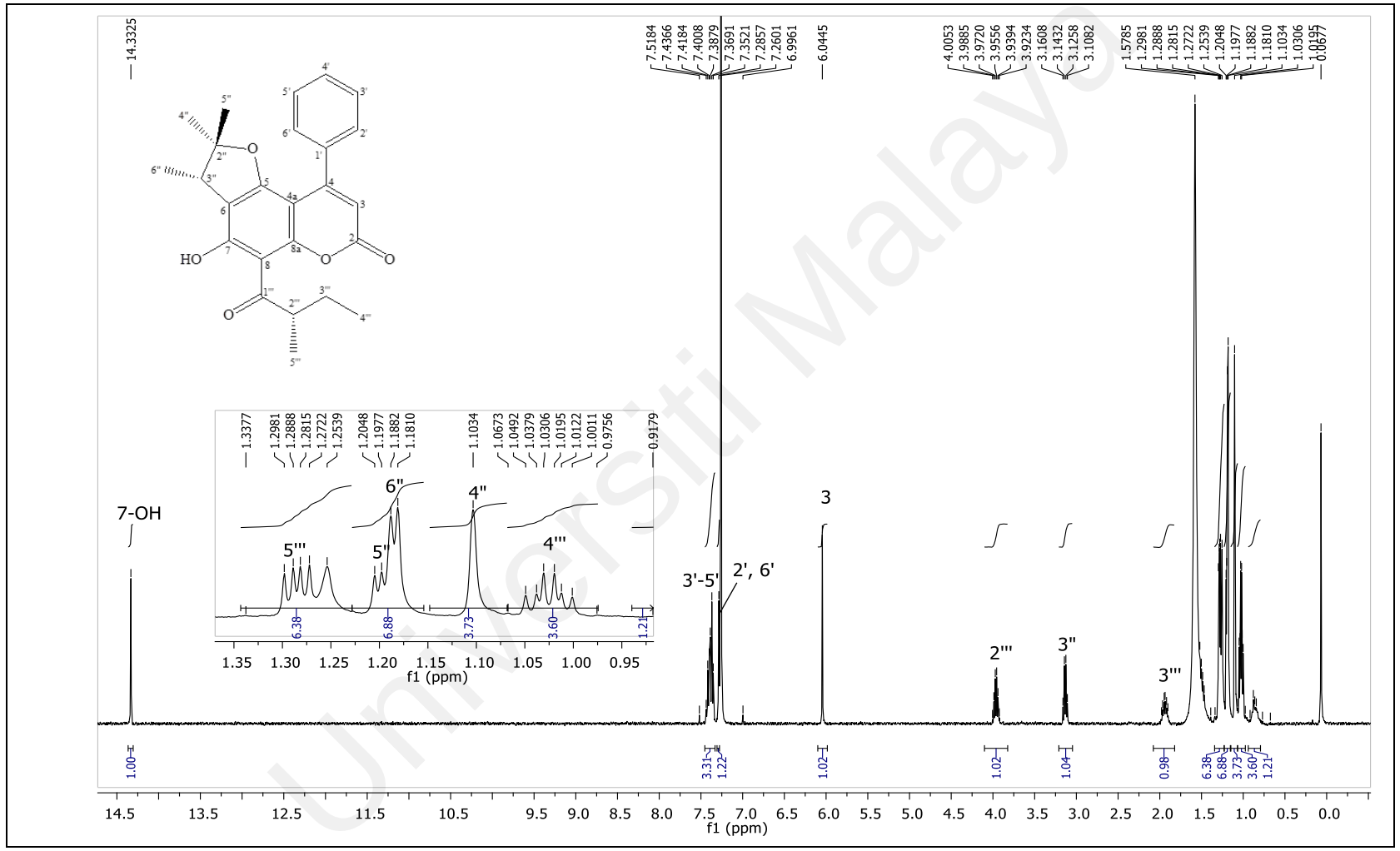

Figure 4.16: ^{1}H-NMR of lepidotin C 490.

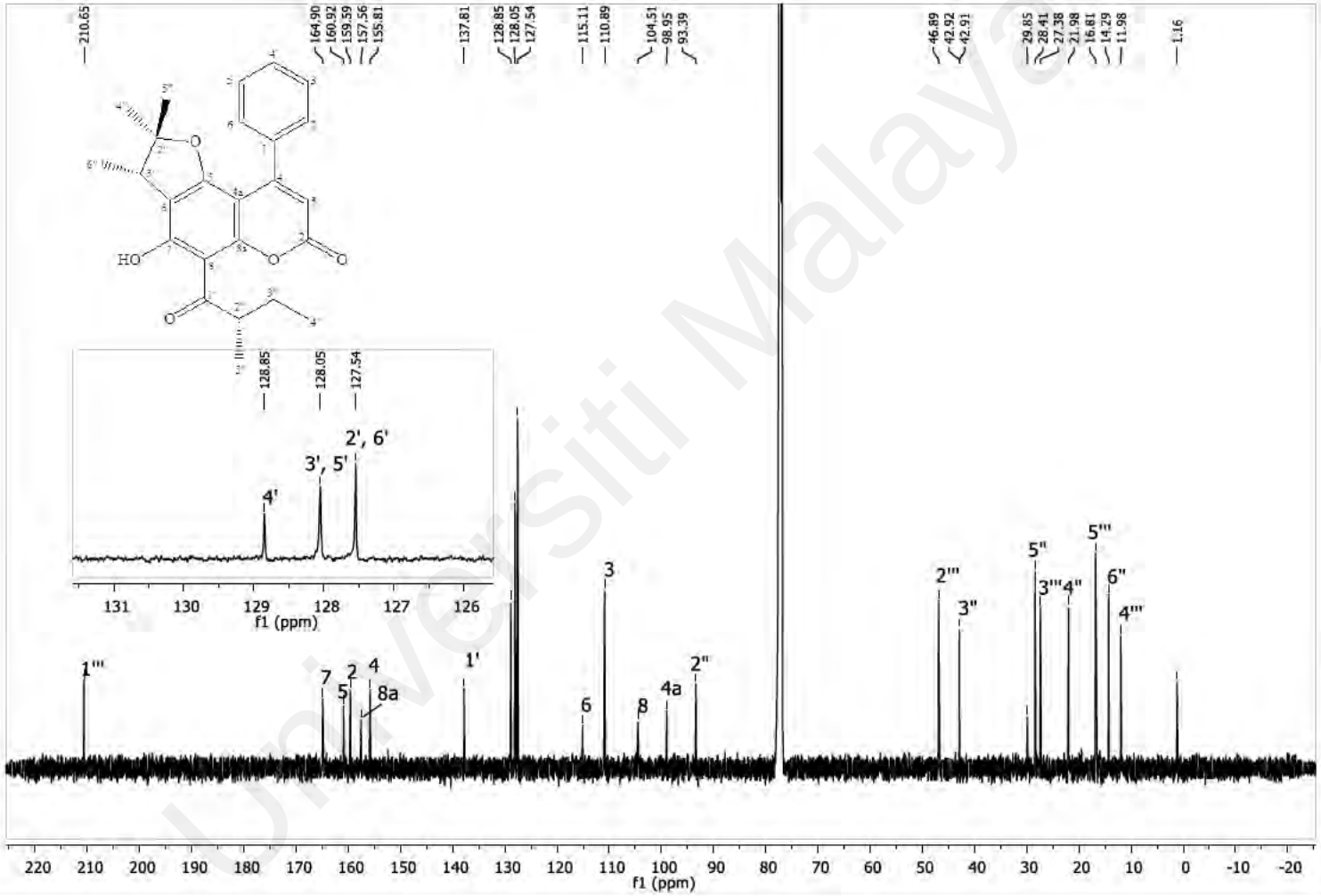

Figure 4.17: ^{13}C-NMR of lepidotin C 490.

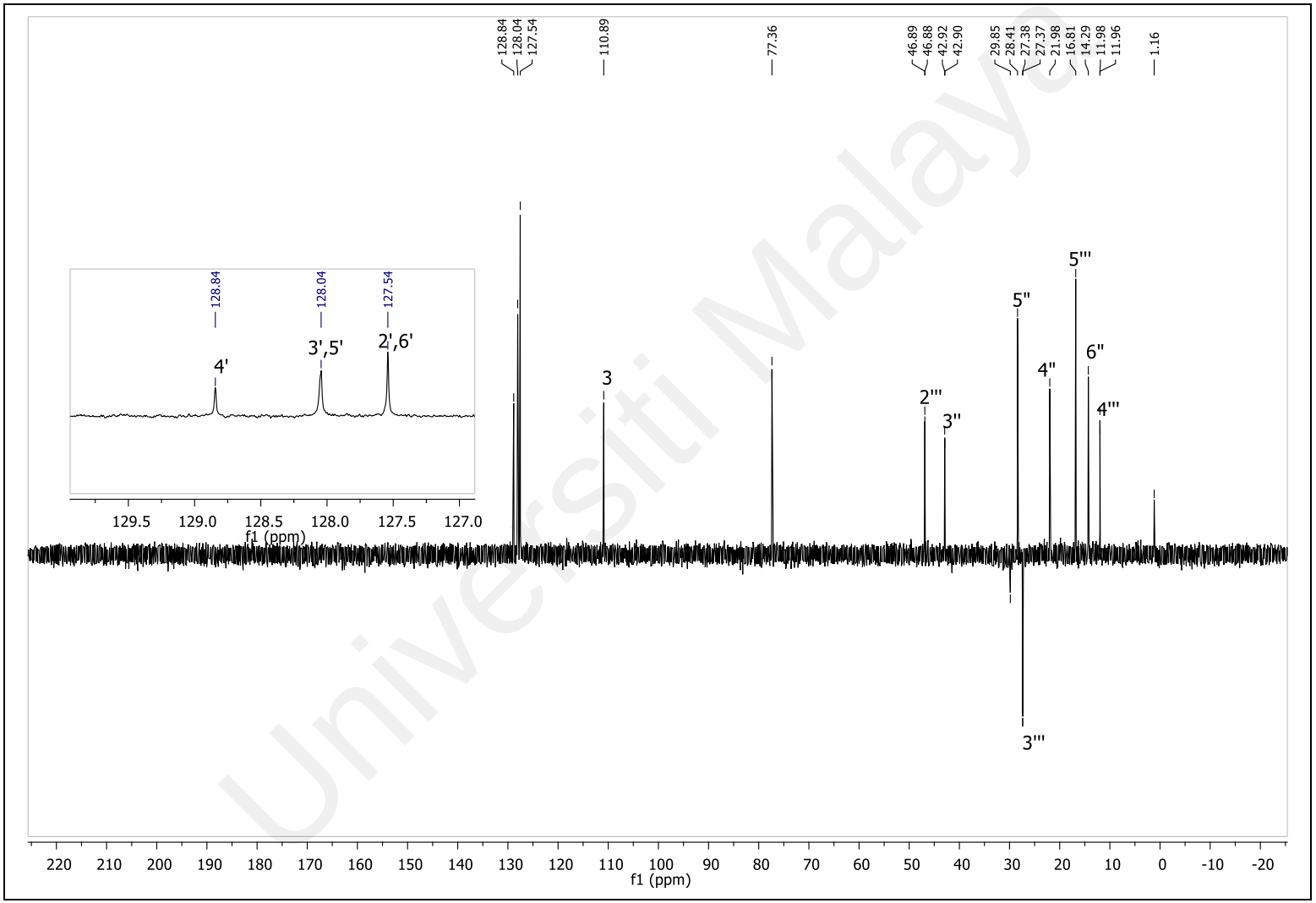

Figure 4.18: DEPT-135 NMR of lepidotin C 490.

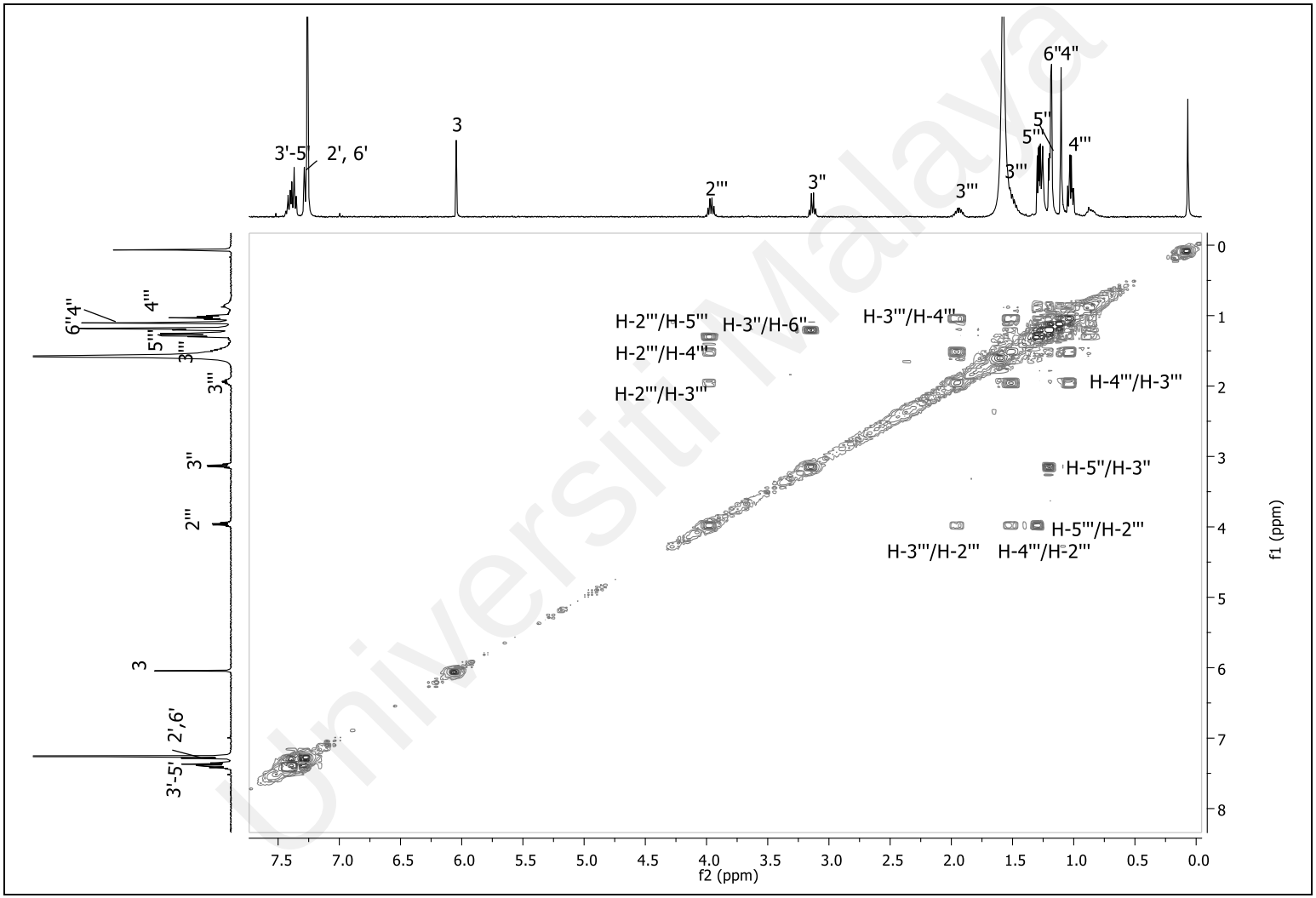

Figure 4.19: COSY-NMR of lepidotin C 490.

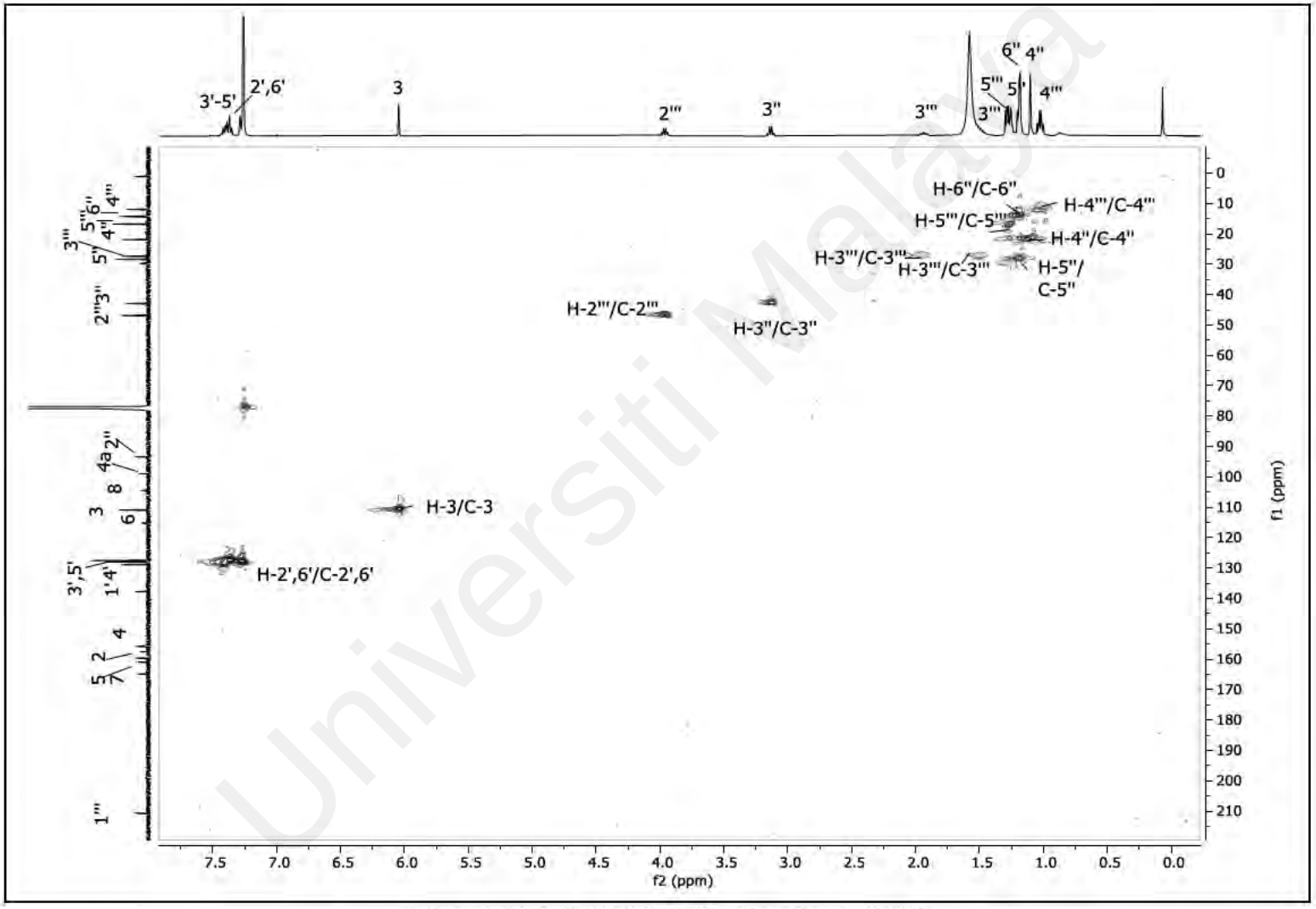

Figure 4.20: HSQC-NMR of lepidotin C 490.

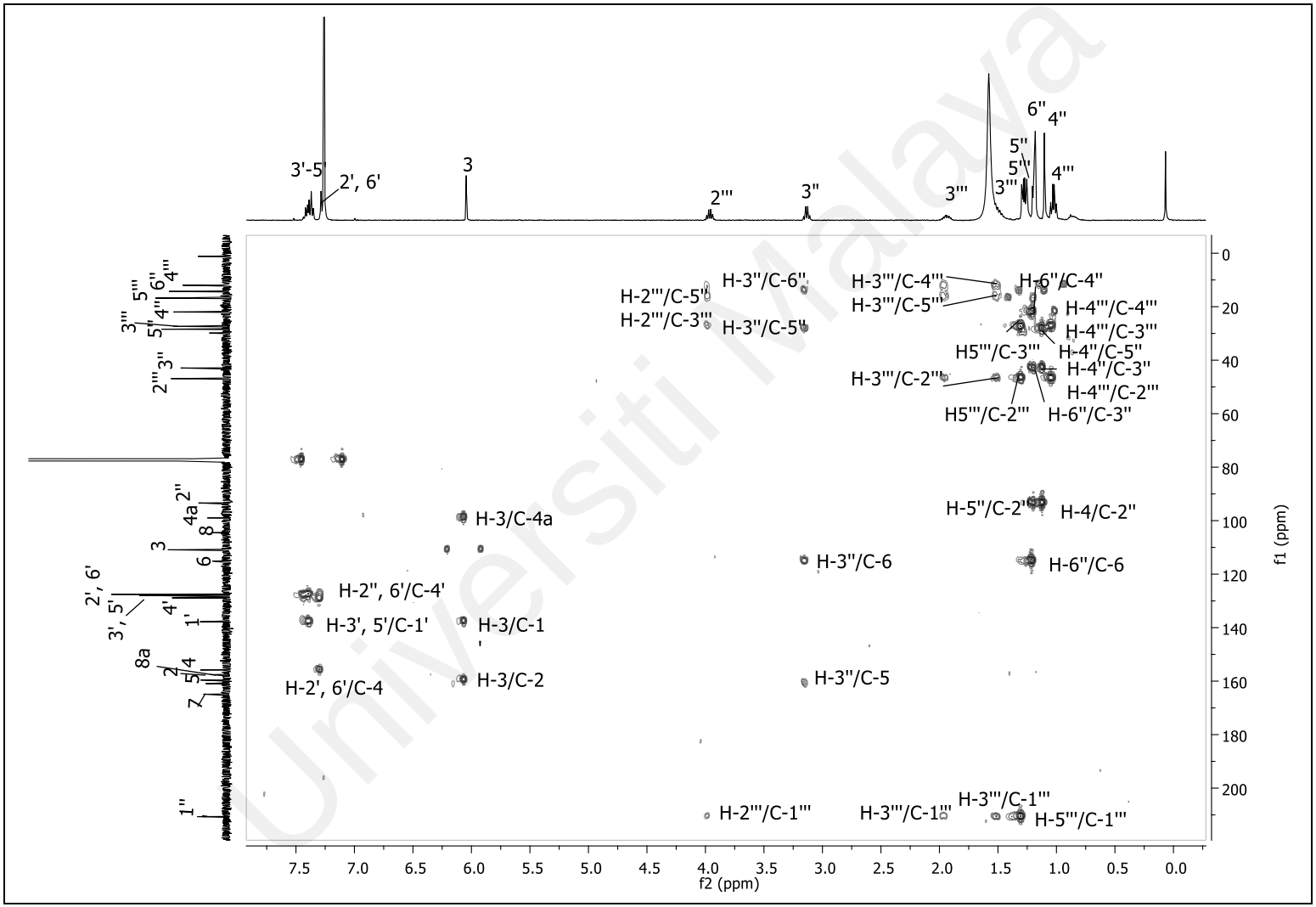

Figure 4.21: HMBC-NMR of lepidotin C 490.

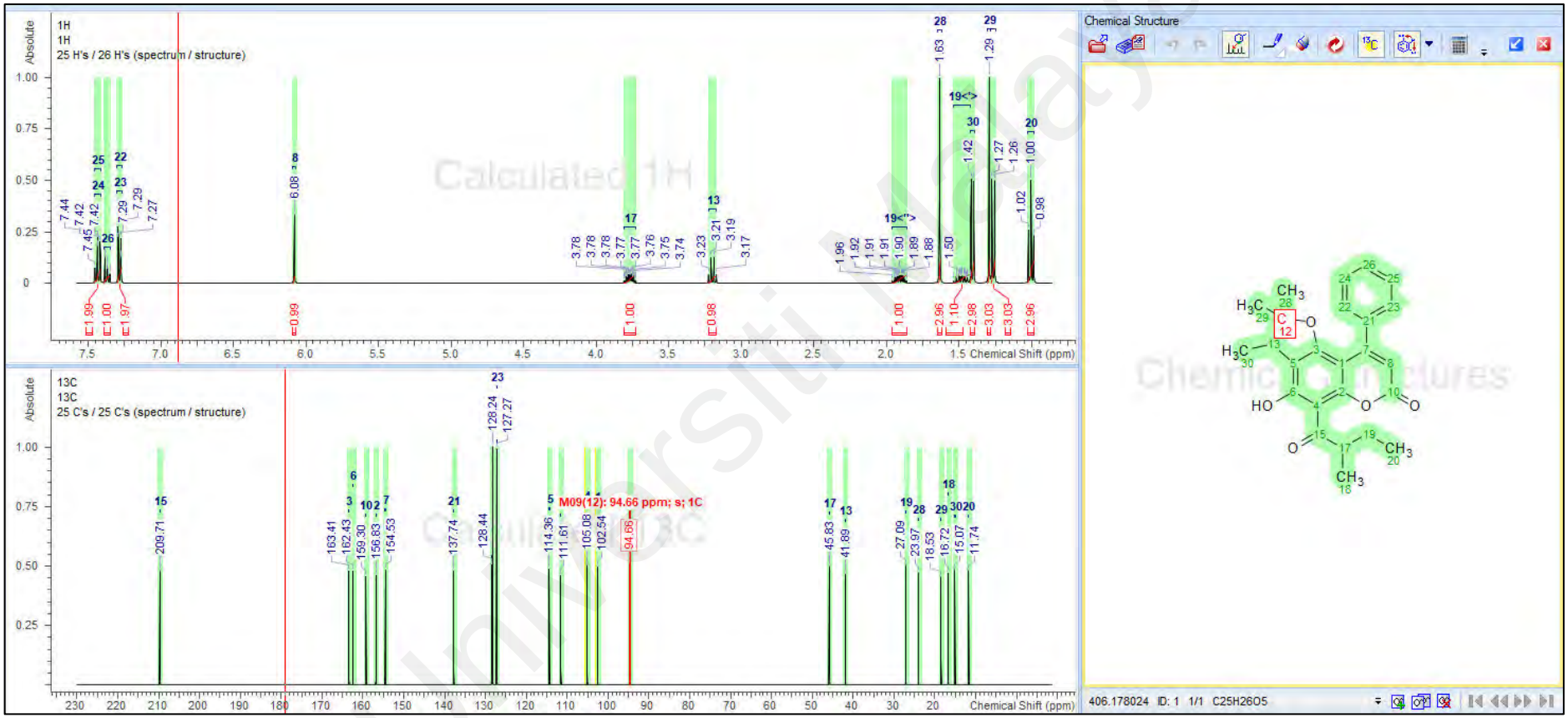

Figure 4.22: Predicted ^{1}H and ^{13}C-NMR chemical shifts of lepidotin C 490 analyzed by ACD/ Spectrus Processor software.

4.1.2.7 Ochrocarpin E 76

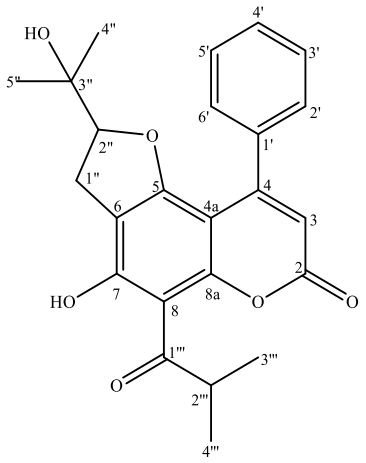

Ochrocarpin E **76** was yielded as white amorphous powder with the $[\alpha]_D^{25}$ -2.85° (c 0.0035, $CHCl_3$). The HRESIMS measurement demonstrated a $[M+H]^+$ ion at *m/z* 409.2822 (calcd. for $C_{24}H_{25}O_6$, 409.1651), which matched the molecular formula of $C_{24}H_{24}O_6$. The 8-acyl-5,7-dioxycoumarin type was corroborated by the UV spectrum absorption bands at 204, 224, and 297 nm. The IR spectrum displayed absorptions at υ_{max} 3455 (OH), 1721 (δ-lactone), 1603 (chelated acyl group) and 1382 (geminal dimethyl) cm^{-1}.

The characteristic singlet of a 4-substituted coumarin at H-3 was found at δ_H 6.07 in the proton spectrum, and a mono-substituted phenyl group at C-4 was validated by the presence of two multiplets at aromatic region [δ_H 7.32 (H-2' and H-6') and δ_H 7.44 (H-3' - H-5')] in proton NMR spectrum (Figure 4.23). Moreover, the presence of a chelated hydroxyl was confirmed by a singlet revealed at δ_H 14.24 (7-OH) from ^{1}H-NMR spectrum, together with the broad OH absorption depicted from the IR at υ_{max} 3455 (OH) cm^{-1}. Based on these findings, it can be inferred that the compound possesses an 8-acyl-5,7-dioxy-4-phenyl coumarin type skeleton. (Morel, Guilet, et al., 1999).

There were 24 signals revealed on the ^{13}C-NMR spectrum (Figure 4.24) of ochrocarpin E **76**: four methyls, one methylene, eight methines, nine quaternary carbons as well as

two carbonyls. A dihydrofuran moiety that attached to C-5/C-6 was revealed by the presence of two doublets of doublets at δ_H 3.07 (1H, J = 8.4, 14.8 Hz, H-1" α) and δ_H 2.93 (1H, J = 9.6, 15.0 Hz, H-1"β) respectively, as well as a triplet at δ_H 4.51 (1H, J = 8.9 Hz, H-2"). Furthermore, two methyls at δ_H 1.01 (Me-4") and δ_H 0.93 (Me-5") were correlated to δ_C 92.9 (C-2") and δ_C 71.8 (C-3") in the HMBC-NMR spectrum. An isobutyryl moiety with the signals at δ_H 4.12 (1H, *m*, H-2'") and δ_H 1.30 (6H, *d*, J = 6.6 Hz, H-3'" and H-4'") was attached to the C-8.

The detailed of the ^{1}H and ^{13}C-NMR spectral data were documented in the Table 4.11 together with the literature data.

Table 4.11: ^{1}H and ^{13}C-NMR spectral data of ochrocarpin E 76 in $CDCl_3$.

Position	**Experimental ($CDCl_3$)**		**Reference ($CDCl_3$)** (Chaturvedula et al., 2002)	
	δ_H	**δ_C**	**δ_H**	**δ_C**
2	-	159.3	-	159.4
3	6.07, *s*	111.1	6.07, *s*	114.2
4	-	155.2	-	155.0
4a	-	98.9	-	99.2
5	-	162.0	-	161.9
6	-	110.3	-	110.0
7-OH	14.24, *s*	164.1	14.24, *s*	164.2
8	-	162.0	-	161.9
8a	-	157.4	-	157.9
1'	-	138.3	-	138.2
2'	7.32, *m*	127.6	7.34, *m*	127.4
3'	7.44, *m*	129.0	7.42, *m*	127.8
4'	7.44, *m*	128.1	7.42, *m*	129.0
5'	7.44, *m*	129.0	7.42, *m*	127.8
6'	7.32, *m*	127.6	7.34, *m*	127.4
1"α	3.07, *dd*, (8.4, 14.8)	27.1	3.06, *dd*, (10.0, 15.2)	27.0
1"β	2.93, *dd*, (9.6, 15.0)		2.93, *dd* (8.4, 15.5)	
2"	4.51, *t* (8.9)	92.9	4.50, *t* (9.1)	92.7
3"-OH	-	71.8	-	71.7
4"	1.01, *s*	23.4	1.01, *s*	23.3
5"	0.93, *s*	23.4	0.93, *s*	23.3
1'"	-	210.8	-	204.5
2'"	4.12, *m*	40.4	4.12, *m*	40.4
3'"	1.30, *d* (6.6)	19.4	1.29, *d* (6.5)	19.4
4'"	1.30, *d* (6.6)	19.4	1.29, *d* (6.5)	19.4

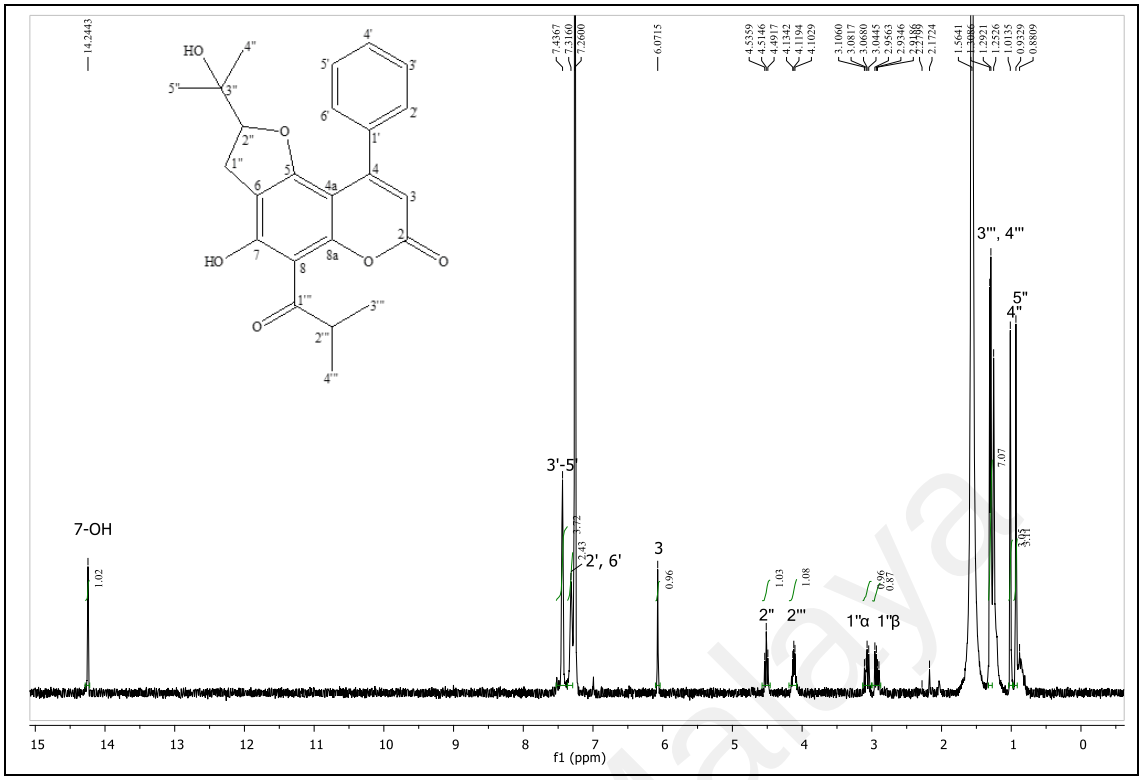

Figure 4.23: ^{1}H-NMR of ochrocarpin E 76.

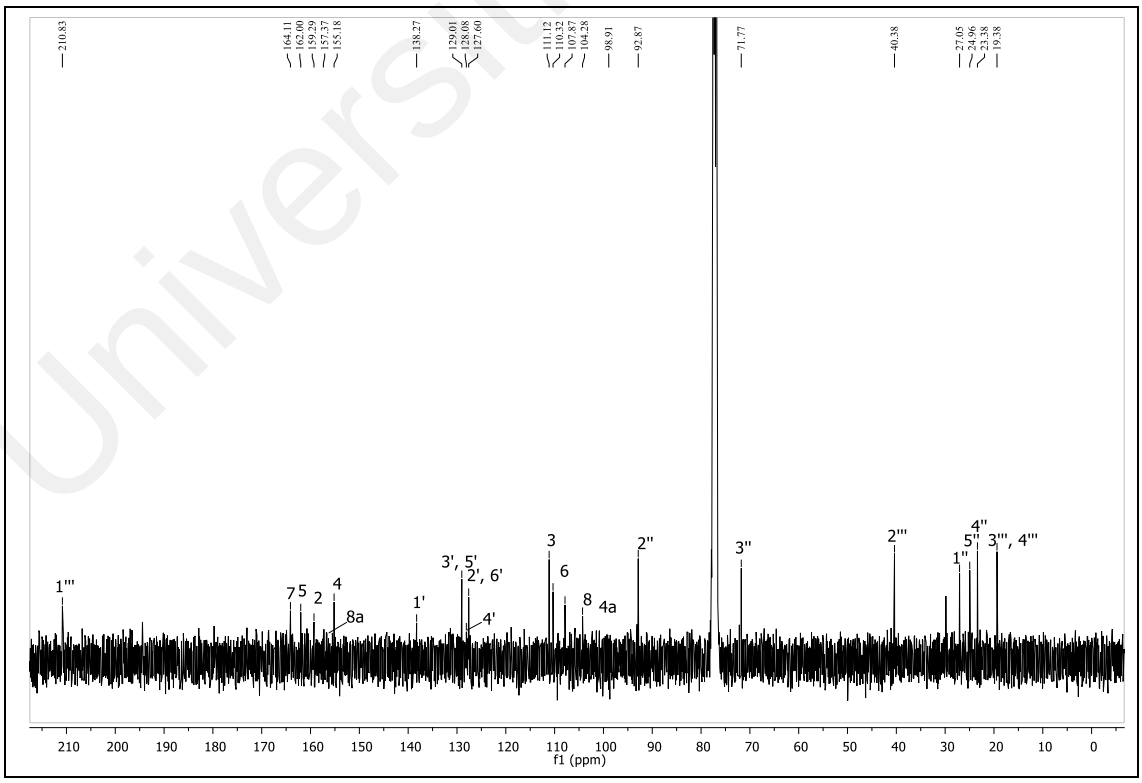

Figure 4.24: ^{13}C-NMR of ochrocarpin E 76.

4.1.2.8 Mammea A/BB cyclo F 77

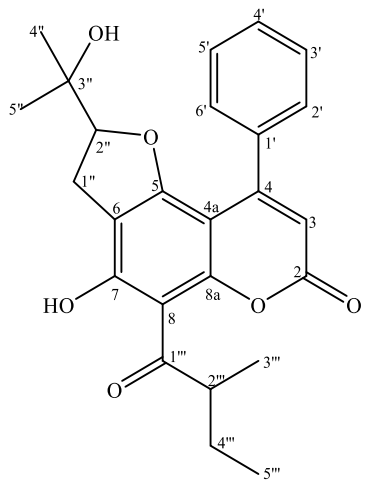

Mammea A/BB cyclo F **77** was obtained as colourless amourphous with $[\alpha]_D^{25}$ −3.3 ° (c 0.004, $CHCl_3$). The HRESIMS spectrum showed a pseudomolecular ion peak $[M+H]^+$ at *m/z* 423.3013 (calculated 423.4792), which proposed a molecular formula of $C_{25}H_{26}O_6$. The difference of 14 Da between mammea A/BB cyclo F **77** and ochrocarpin E **76** was attributed to an extra methylene group (δ_H 1.94 *m* and δ_H 1.49 *m*: δ_C 27.2) in the acyl side chain. The similar physical data supported an 8-acyl-5,7-dioxycoumarin type too with the UV absorptions at λ_{max} 203, 226, and 298 nm. The IR spectrum showed absorptions at υ_{max} 3458 (OH), 1744 (δ-lactone), 1603 (chelated acyl group), 1386 (geminal dimethyl) cm^{-1}.

On the ^{1}H-NMR spectrum (Figure 4.25), the singlet exhibited at δ_H 6.07 and the chelated hydroxyl at C-7 (δ_H 14.29) illustrated the characteristic of 4-phenyl coumarin. The mono-substituted phenyl moiety was revealed on the upfield of the ^{1}H-NMR at δ_H 7.44 (H-3' - H-5') and δ_H 7.32 (H-2' and H-6'). Hence, the same 8-acyl-5,7-dioxy-4-phenylcoumarin skeleton (Morel, Guilet, et al., 1999) exemplified by mammea A/BB cyclo F **77**.

In the ^{13}C-NMR spectrum (Figure 4.26), a total of 25 carbon signals were detected. These signals included four methyl groups, two methylene groups, eight methine groups, two carbonyl groups, and nine quaternary carbons. A dihydrofuran moiety attached to C-5/C-6 and identity of ochrocarpin E **76** was revealed with the presence of a triplet at δ_H 4.51 (1H, J = 9.2 Hz, H-2") and two doublets of doublets at δ_H 3.07 (1H, J = 15.5, 9.8 Hz, H-1" α) and δ_H 2.93 (1H, J = 15.5, 8.7 Hz, H-1" β) respectively.

The HMBC resonances revealed correlations between the methylene protons, specifically δ_H 1.50 (1H, *m*, H-4'α) and δ_H 1.93 (1H, *m*, H-4'β), and neighboring carbon atoms. These correlations were observed with the carbonyl carbon (C-1''', δ_C 210.7), a methine carbon (C-2''', δ_C 47.0), and two methyl carbons (C-3''', δ_C 16.7 and C-5''', δ_C 11.9). Furthermore, the ^{1}H-NMR spectrum demonstrated that the two methyl groups (H-3''', H-5''') appeared as a doublet at δ_H 1.29 (J = 6.7 Hz) and a triplet at δ_H 1.02 (J = 6.7 Hz), respectively. Hence, the attachment of a 2-methylbutanoyl moiety to the C-8 of mammea A/BB cyclo F **77** was verified and recorded in Table 4.12.

Table 4.12: ^{1}H and ^{13}C-NMR spectral data of mammea A/BB cyclo F 77 in $CDCl_3$.

Position	Experimental ($CDCl_3$)		Reference ($CDCl_3$) (Guilet et al., 2001)	
	δ_H	δ_C	δ_H	δ_C
2	-	159.2	-	159.1
3	6.07, *s*	111.2	6.07, *s*	111.0
4	-	155.1	-	154.9
4a	-	98.9	-	98.7
5	-	162.0	-	161.8
6	-	110.3	-	110.1
7-OH	14.29, *s*	164.1	14.32, *s*	163.9
8	-	104.8	-	104.5
8a	-	157.3	-	157.1
1'	-	138.3	-	138.1
2'	7.32, *m*	127.6	7.32, *m*	127.4
3'	7.44, *m*	128.0	7.44, *m*	127.9
4'	7.44, *m*	129.0	7.44, *m*	128.8
5'	7.44, *m*	128.0	7.44, *m*	127.9
6'	7.32, *m*	127.6	7.32, *m*	127.4
1"α	3.07, *dd* (15.5, 9.8)	27.1	3.07, *dd* (10.0, 15.0)	26.6
1"β	2.93, *dd* (15.5, 8.7)		2.93, *dd* (8.0, 15.0)	
2"	4.51, *t (9.2*)	92.9	4.52, *t* (9.0)	92.6
3"-OH	-	71.8	-	71.6
4"	0.93, *s*	25.0	0.94, *s*	24.8
5"	1.02, *s*	23.4	1.02, *s*	23.2
1'''	-	210.7	-	210.4
2'''	3.97, *m*	47.0	3.96, *m*	46.7
3'''	1.29, *d* (6.7)	16.7	1.28, *d*, (7.0)	16.5
4'''α	1.50, *m*	27.4	1.50, *m*	27.1
4'''β	1.93, *m*		1.94, *m*	
5'''	1.02, *t* (6.7)	11.9	1.01, *t*, (7.0)	11.8

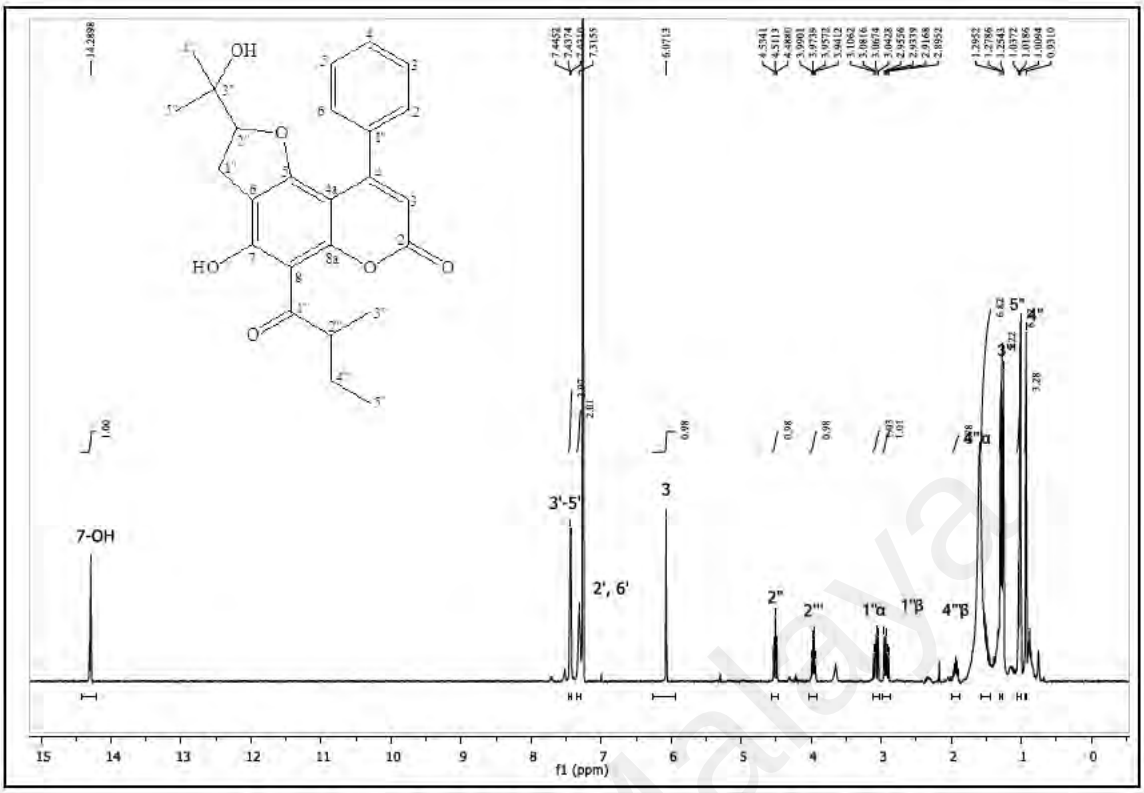

Figure 4.25: ^{1}H-NMR of mammea A/BB cyclo F 77.

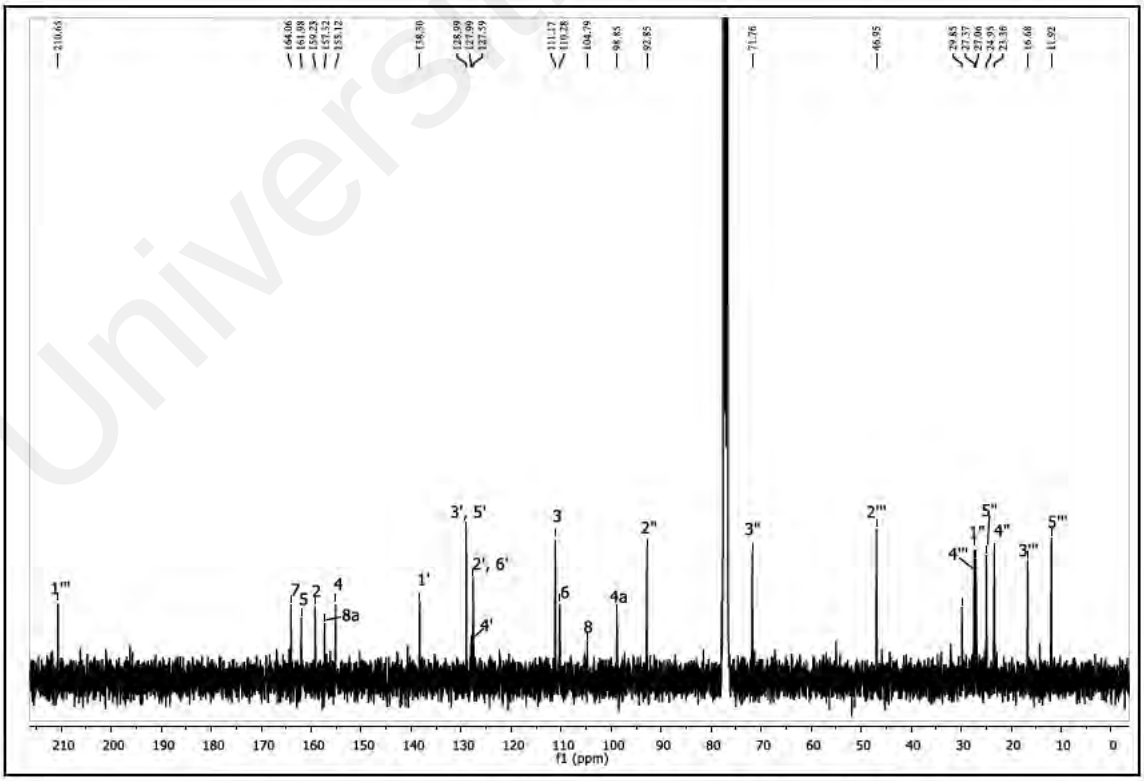

Figure 4.26: ^{13}C-NMR of mammea A/BB cyclo F 77.

4.1.2.9 Friedelin 186

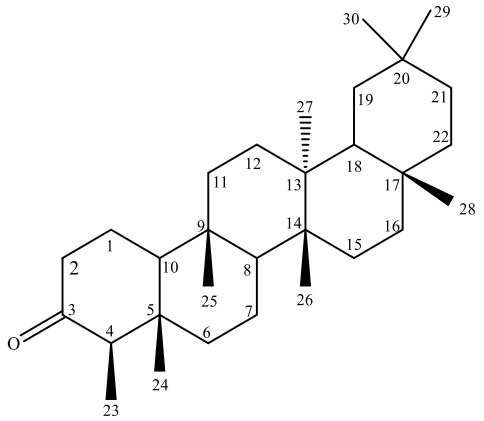

Friedelin **186** was isolated as colorless needles, with the $[\alpha]_D^{25}$−20.8° (c 0.053, $CHCl_3$). The HREIMS mass spectrum revealed the molecular ion peak at *m/z* 427.3931 $[M+H]^+$ (calcd. 427.3934), which suggested the molecular formula $C_{30}H_{50}O$. The IR spectrum showed an intense band at 1715 cm^{-1} consistent with a six membered ring ketone; while the other absorption at υ_{max} 2926, 2869, 1452, 1388 cm^{-1} revealed the C-H stretching.

A total of 30 carbon signals were found on the ^{13}C-NMR spectrum (Figure 4.28): a carbonyl, eight sp^3 methyls, eleven sp^3 methylenes, four sp^3 methines and six quaternary sp^3 carbons. The six degrees of unsaturation of the molecular formula concluded the structure as a pentacylic triterpene with the presence of a ketone.

The presence of eight methyls: a secondary [δ_H 0.88 (*d*, H-23)] and seven quaternary methyls [δ_H 0.72 (*s*, H- 24), 0.871 (*s*, H-25), 1.00 (*s,* H-26), 1.050 (*s*, H-27), 1.18 (*s*, H-28), 0.95 (*s*, H-29) and 1.00 (*s*, H-30)] were observed in the ^{1}H-NMR spectrum (Figure 4.27). The ^{1}H-NMR resonances suggested the structure as friedelane skeleton.

From the complete spectroscopic data analysis and comparison with literature data (Table 4.13), the structure is assigned as friedelin **186**.

Table 4.13: ^{1}H and ^{13}C-NMR spectral data of friedelin 186 in $CDCl_3$.

Position	Experimental ($CDCl_3$)		Reference ($CDCl_3$) (Escobedo-Martínez et al., 2012)	
	δ_H	δ_C	δ_H	δ_C
1	1.96, *m* & 1.68, *m*	22.4	1.96, *m* & 1.68, *m*	22.30
2	2.39, *m* & 2.31, *m*	41.7	2.39, *m* & 2.30, *m*	41.54
3	-	213.4	-	213.33
4	2.25, *q* (6.5)	58.4	2.25, *q* (6.5)	58.24
5	-	42.3	-	42.16
6	1.75, *m* & 1.28, *m*	41.4	1.74, *m* & 1.27, *m*	41.31
7	1.48, *m* & 1.37, *m*	18.4	1.48, *m* & 1.38, *m*	18.25
8	1.39, *m*	53.3	1.39, *m*	53.12
9	-	37.6	-	37.46
10	1.53, *m*	59.6	1.53, *m*	59.50
11	1.46, *m* & 1.26, *m*	35.8	1.46, *m* & 1.26, *m*	35.64
12	1.34, *m*	30.7	1.34, *m*	30.52
13	-	38.5	-	38.31
14	-	39.9	-	39.72
15	1.54, *m* & 1.31, *m*	32.6	1.53, *m* & 1.31, *m*	32.44
16	1.57, *m* & 1.36, *m*	36.2	1.57, *m* & 1.36, *m*	36.03
17	-	30.1	-	30.10
18	1.56, *m*	42.9	1.56, *m*	42.81
19	1.38, *m* & 1.21, *m*	35.5	1.38, *m* & 1.21, *m*	35.36
20	-	28.3	-	28.18
21	1.47, *m* & 1.27, *m*	32.9	1.47, *m* & 1.27, *m*	32.79
22	1.50, *m* & 0.95, *m*	39.4	1.50, *m* & 0.95, *m*	39.27
23	0.88, *d* (6.5)	7.0	0.88, *d* (6.5)	6.83
24	0.72, *s*	14.8	0.725, *s*	14.67
25	0.871, *s*	18.1	0.871, *s*	17.96
26	1.00, *s*	20.4	1.008, *s*	20.27
27	1.050, *s*	18.8	1.050, *s*	18.67
28	1.18, *s*	32.2	1.181, *s*	32.10
29	0.95, *s*	35.2	0.954, *s*	35.04
30	1.00, *s*	31.9	1.001, *s*	31.79

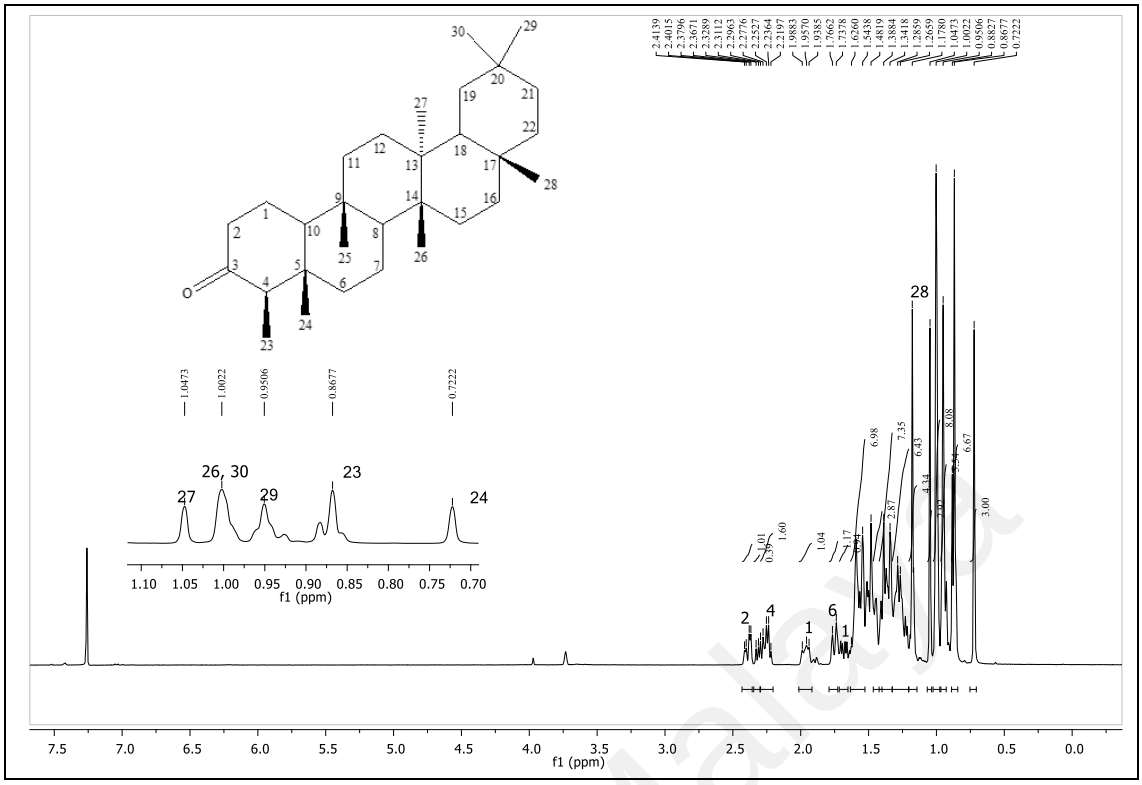

Figure 4.27: ^{1}H-NMR of friedelin 186.

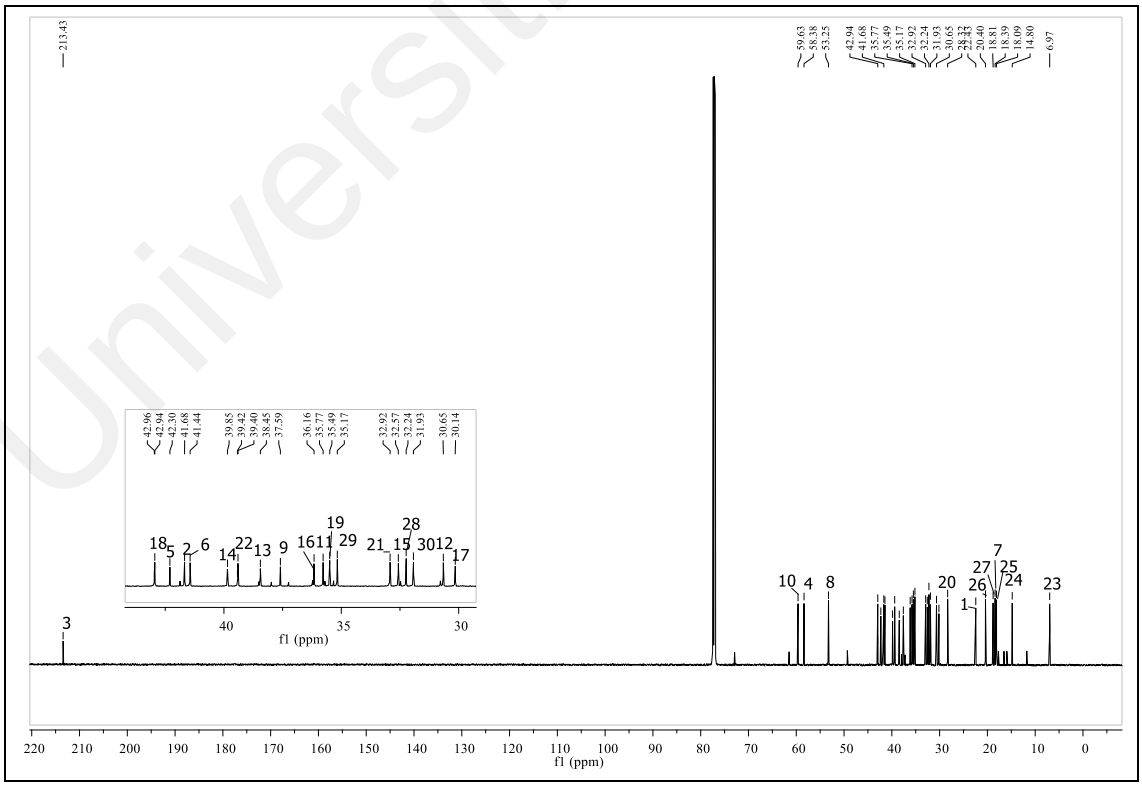

Figure 4.28: ^{13}C-NMR of friedelin 186.

4.1.2.10 3β-friedelinol 189

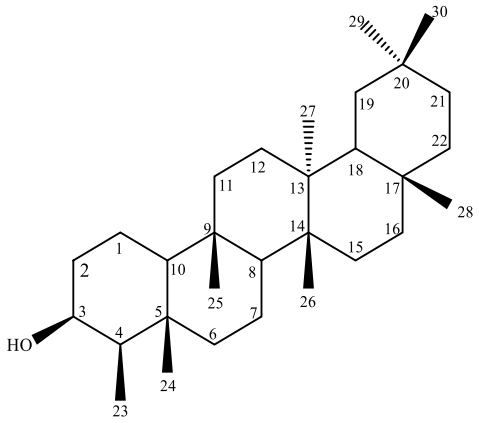

3β-friedelinol **189** was obtained as colourless needles, with the $[\alpha]_D^{25}$ +5.5° (c 0.09, $CHCl_3$). The HREIMS mass spectrum with the molecular ion peak at *m/z* 427.4995 $[M-H]^-$ (calcd. 427.3985) indicated the molecular formula $C_{30}H_{52}O$, with two more hydrogen compared to friedelin **186**. A strong and broad peak appeared at υ_{max} 3474 cm^{-1} in the IR spectrum implied the O-H stretching. The absorptions at 1385 and 1171 cm^{-1} were attributed to the asymmetric and symmetric C–O stretches, respectively.

The ^{13}C-NMR (Figure 4.30) and DEPT-135 spectra indicated the presence of 30 carbon signals: eight methyls, eleven methylenes, five methines and six quaternary carbons. With the degree of unsaturation of five, the molecular formula showed the pattern of pentacyclic skeleton. A carbinolic carbon signal was revealed on the ^{1}H (Figure 4.29) and ^{13}C-NMR spectra at δ_H 3.73, *m* and δ_C 72.9. Moreover, a secondary methyl and seven quaternary methyls were observed on the ^{1}H-NMR spectrum. The secondary methyl signal at δ_H 0.93 (*d*, *J*= 1.8 Hz) assigned to H-23 and the quaternary methyls assigned to H-24 (δ_H 0.96, *s*), H-25 (δ_H 0.86, *s*), H-26 (δ_H 0.99, *s*), H-27 (δ_H 1.00, *s*), H-28 (δ_H 1.17, *s*), H-29 (δ_H 0.94, *s*), H-30 (δ_H 0.99, *s*).

The recorded ^{1}H and ^{13}C-NMR spectra of 3β-friedelinol **189** were consistent with the literature data. These spectra have been included in the Table 4.14 as reference.

Table 4.14: ^{1}H and ^{13}C-NMR spectral data of 3β-friedelinol 189 in $CDCl_3$.

Position	Experimental ($CDCl_3$)		Reference ($CDCl_3$) (Yan et al., 2004)	
	δ_H	δ_C	δ_H	δ_C
1	-	15.9	-	15.8
2	-	36.2	-	36.1
3	3.73, *m*	72.9	3.72, *m*	72.8
4	-	49.3	-	49.2
5	-	38.0	-	39.3
6	-	41.9	-	41.8
7	-	17.7	-	17.6
8	-	53.4	-	53.2
9	-	37.3	-	37.1
10	-	61.5	-	61.4
11	-	35.5	-	35.4
12	-	30.8	-	30.6
13	-	38.5	-	37.9
14	-	39.8	-	38.4
15	-	32.5	-	32.4
16	-	35.7	-	35.6
17	-	30.2	-	30.0
18	-	43.0	-	42.9
19	-	35.3	-	35.2
20	-	28.3	-	28.2
21	-	33.0	-	32.8
22	-	39.4	-	39.7
23	0.93, *d* (1.8)	11.8	0.93, *d* (6.8)	11.6
24	0.96, *s*	16.5	0.95, *s*	16.4
25	0.86, *s*	18.4	0.85, *s*	18.2
26	0.99, *s*	20.3	0.97, *s*	20.1
27	1.00, *s*	18.8	1.00, *s*	18.6
28	1.17, *s*	32.2	1.16, *s*	32.1
29	0.94, *s*	35.2	0.94, *s*	35.0
30	0.99, *s*	31.9	0.98, *s*	31.8

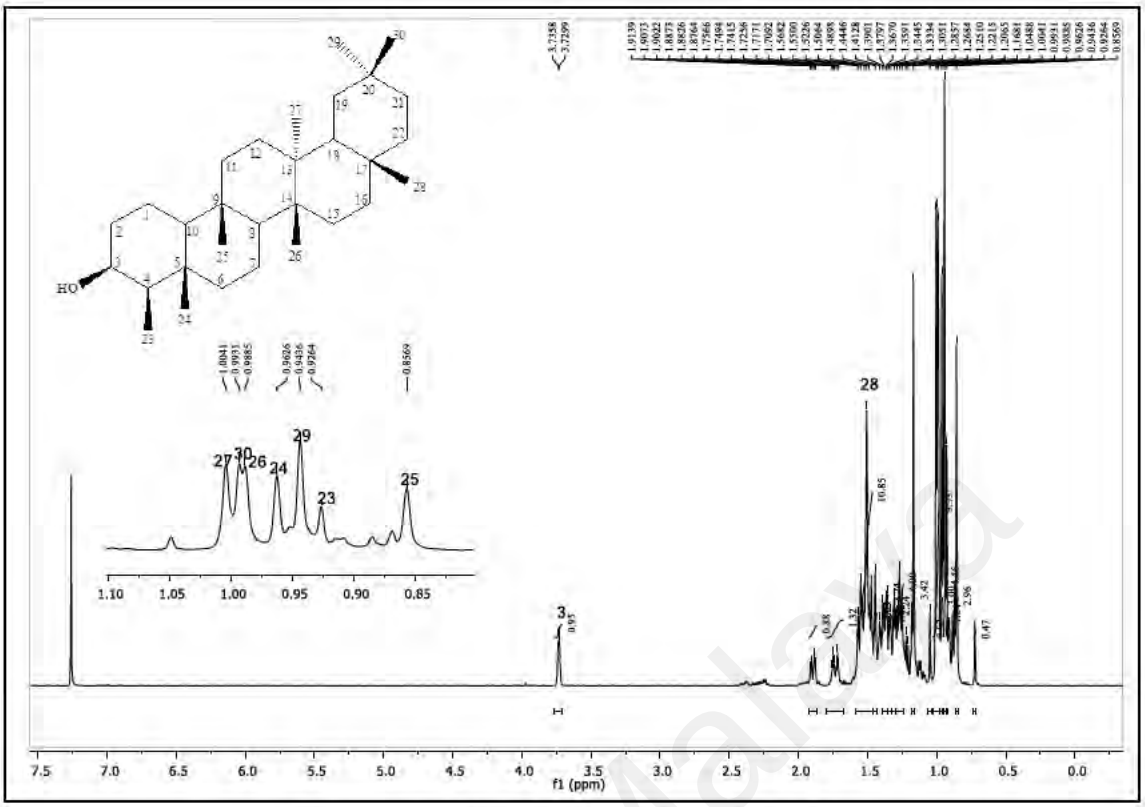

Figure 4.29: ^{1}H-NMR of 3β-friedelinol 189.

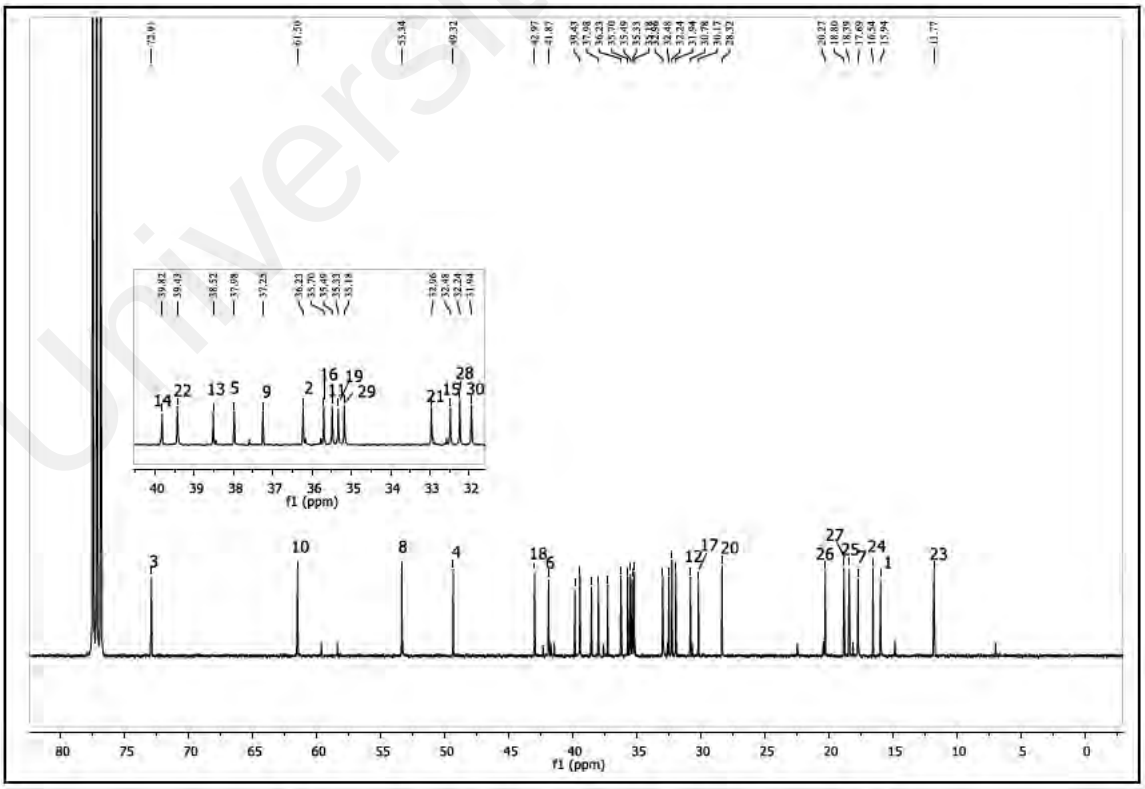

Figure 4.30: ^{13}C-NMR of 3β-friedelinol 189.

4.1.2.11 Betulinic acid 177

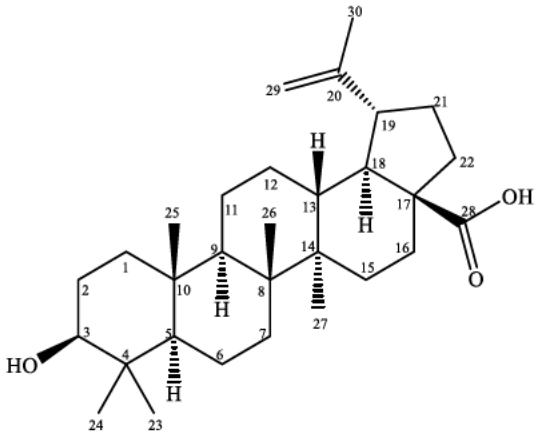

Betulinic acid **177** was yielded as colorless crystals, with $[\alpha]_D^{25}$ +6.7° (c 0.09, $CHCl_3$). The mass spectrum exhibited a prominent molecular ion peak at *m/z* 421.1667 $[M+Cl]^-$ (calcd. 421.3603) indicated the molecular formula corresponding to its molecular formula $C_{30}H_{48}O_3$. The IR spectrum revealed the presence of broad absorptions bands at 2926, 2869 and 1715 cm^{-1} for hydroxyl and carboxyl functions respectively.

The ^{13}C-NMR (Figure 4.32) and DEPT-135 spectra displayed 30 carbon signals: six methyls, eleven methylenes, six methines and seven quaternary carbons. From the ^{1}H-NMR spectrum, five tertiary methyls were revealed as singlet at δ_H 0.75, 0.82, 0.93, 0.96 and 0.97, which corresponded to H-23, H-24, H-25, H-26, and H-27. Besides, the methyl group at C-30 was observed as sharp singlet at δ_H 1.69 from the ^{1}H-NMR spectrum (Figure 4.31). The two broad singlets at δ_H 4.60 and δ_H 4.74 were assigned to the vinyl protons at H-29.

The ^{1}H and ^{13}C-NMR spectral data were in close agreement with the literature value of betulinic acid **177** and reported in Table 4.15.

Table 4.15: ^{1}H and ^{13}C-NMR spectral data of betulinic acid 177 in $CDCl_3$.

Position	Experimental ($CDCl_3$)		Reference ($CDCl_3$) (Sharma et al., 2010)	
	δ_H	δ_C	δ_H	δ_C
1	-	38.8	-	38.7
2	-	28.1	-	27.4
3	3.19, *dd* (5.02, 11.18)	79.2	3.27, *dd*	78.9
4	-	39.0	-	38.8
5	-	55.5	-	55.3
6	-	18.4	-	18.3
7	-	34.4	-	34.3
8	-	40.8	-	40.7
9	-	50.6	-	50.5
10	-	37.3	-	37.2
11	-	21.0	-	20.8
12	-	25.6	-	25.5
13	-	38.5	-	38.4
14	-	42.6	-	42.4
15	-	30.7	-	30.5
16	-	32.3	-	32.1
17	-	56.4	-	56.3
18	-	47.0	-	46.8
19	2.35, *m*	49.4	2.30, *m*	49.2
20	-	150.6	-	150.3
21	-	29.8	-	29.7
22	-	37.2	-	37.0
23	0.75, *s*	27.5	0.76, *s*	27.9
24	0.82, *s*	15.5	0.78, *s*	15.3
25	0.93, *s*	16.2	0.82, *s*	16.0
26	0.96, *s*	16.3	0.96, *s*	16.1
27	0.97, *s*	14.8	1.03, *s*	14.7
28	-	179.9	-	180.5
29	4.60, *s* & 4.74, *s*	109.9	4.56, *s* & 4.68, *s*	109.6
30	1.69, *s*	19.5	1.68, *s*	19.4

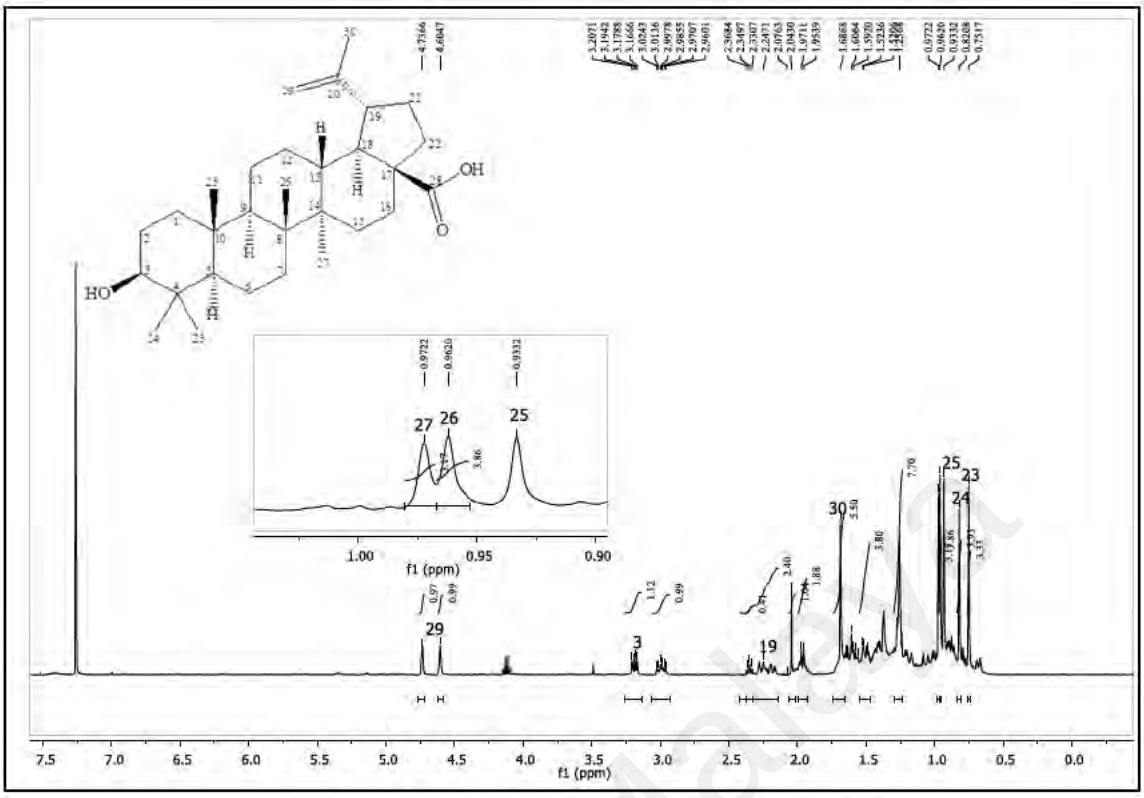

Figure 4.31: ^{1}H-NMR of betulinic acid 177.

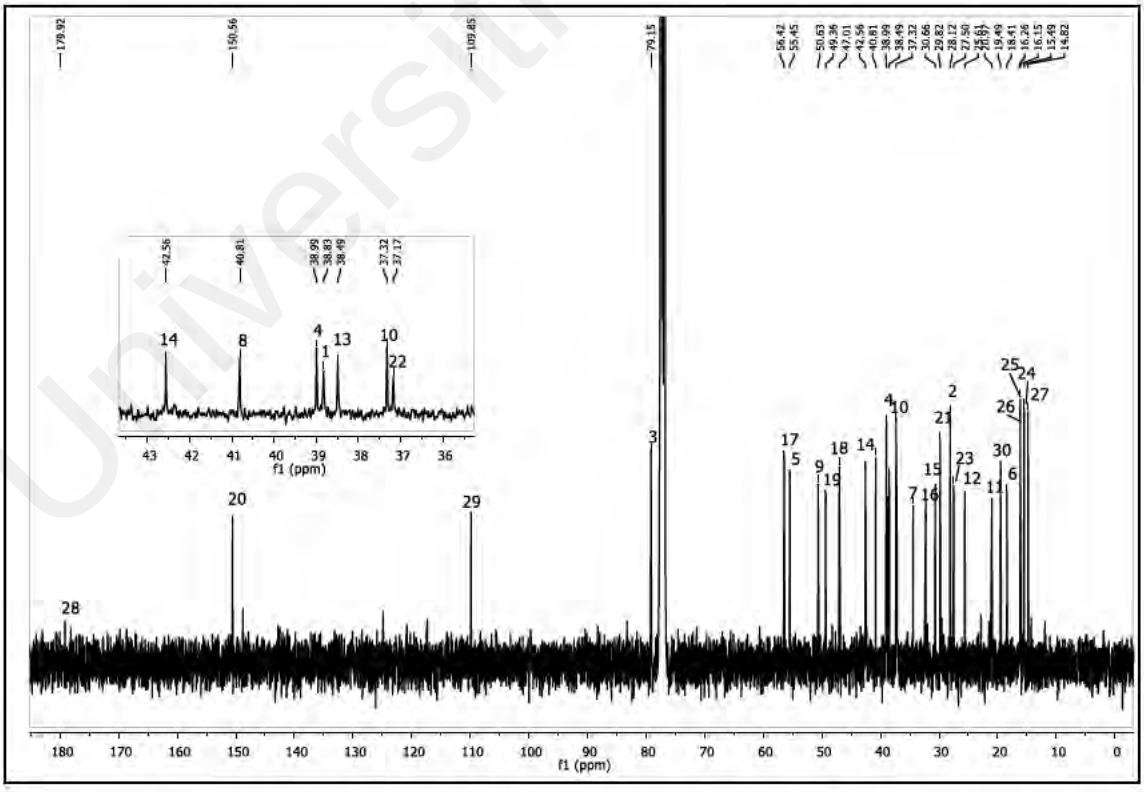

Figure 4.32: ^{13}C-NMR of betulinic acid 177.

4.1.2.12 Glutinol 491

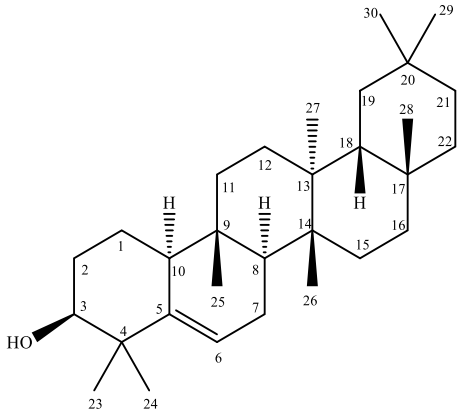

Glutinol **491** was purified as a white amorphous material with the $[\alpha]_D^{25}$= +30.1° (c 0.1, $CHCl_3$). The HREIMS display the *m/z* at 425.1621 $[M-H]^-$ (calcd. 425.7106,), corresponding to the formula $C_{30}H_{50}O$. In the UV spectrum, the absorption peak at λ_{max} 240 nm was observed. The IR absorption was shown at υ_{max} 3446, 2927, and 1386 cm^{-1} which indicates the presence of O-H stretching, –C=C–H and geminal methyl respectively.

30 carbon signals were observed on the ^{13}C-NMR spectrum (Figure 4.34). With the degree of unsaturation of five, the structure was suggested to be a pentacyclic skeleton. eight tertiary methyls together with ten methylenes, five methines, and seven quaternary carbons were demonstrated on the ^{13}C and DEPT-135 NMR spectra. The signals of the methyls were shown on δ_H 1.14, 1.04, 0.85, 1.09, 1.00, 1.16, 0.95, and 0.99 as sharp singlets, and they corresponded to H-23, H-24, H-25, H-26, H-27, H-28, H-29, and H-30. The C-3 signal was observed at δ_C 76.5 in ^{13}C-NMR spectrum and H-3 was noticed at δ_H 3.46 (1H, *t*, *J*= 3.78 Hz) on ^{1}H-NMR (Figure 4.33).

The structure was confirmed as glutinol **491** after the analysis of the spectral data as well as the comparison with the literature data (Table 4.16).

Table 4.16: ^{1}H and ^{13}C-NMR spectral data of glutinol 491 in $CDCl_3$.

Position	Experimental ($CDCl_3$)		Reference ($CDCl_3$) (Rushdey El-Seedi †, 2005)	
	δ_H	δ_C	δ_H	δ_C
1	-	23.8	-	23.56
2	-	18.4	-	18.13
3	3.46, *t* (3.78)	76.5	3.45, *t* (3.0)	76.17
4	-	39.5	-	39.25
5	-	141.8	-	141.58
6	5.62, *d* (9.18)	122.2	5.6, *d* (5.6)	121.94
7	-	28.0	-	27.74
8	-	43.2	-	42.96
9	-	35.0	-	34.79
10	-	49.9	-	49.65
11	-	34.8	-	34.56
12	-	30.5	-	30.33
13	-	38.0	-	37.77
14	-	41.0	-	40.75
15	-	32.2	-	32.04
16	-	36.2	-	35.94
17	-	30.3	-	30.04
18	-	47.6	-	47.40
19	-	35.2	-	35.06
20	-	28.4	-	28.23
21	-	33.3	-	33.03
22	-	39.1	-	38.92
23	1.14, *s*	29.1	1.10, *s*	28.91
24	1.04, *s*	26.0	1.05, *s*	25.44
25	0.85, *s*	16.4	0.85, *s*	16.17
26	1.09, *s*	18.6	1.08, *s*	18.42
27	1.00, *s*	19.8	0.99, *s*	19.64
28	1.16, *s*	32.5	1.16, *s*	32.36
29	0.95, *s*	34.7	0.94, *s*	34.56
30	0.99, *s*	32.2	0.98, *s*	32.04

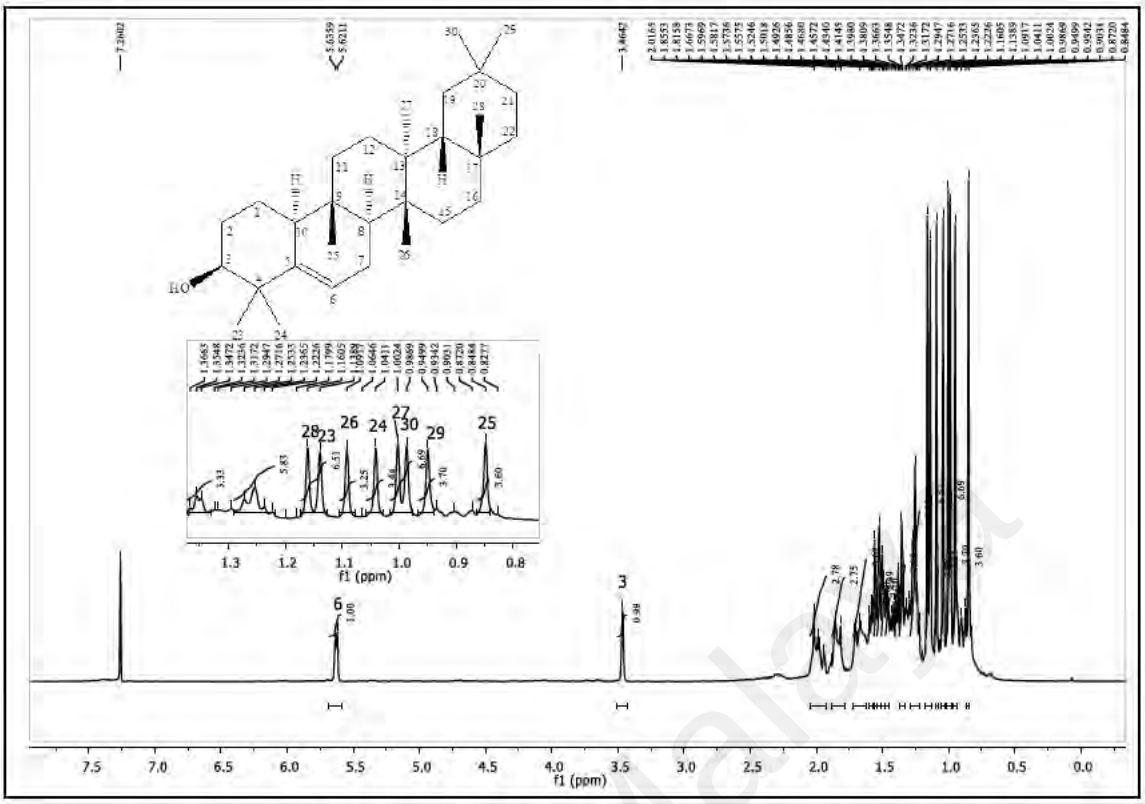

Figure 4.33: ^{1}H-NMR of glutinol 491.

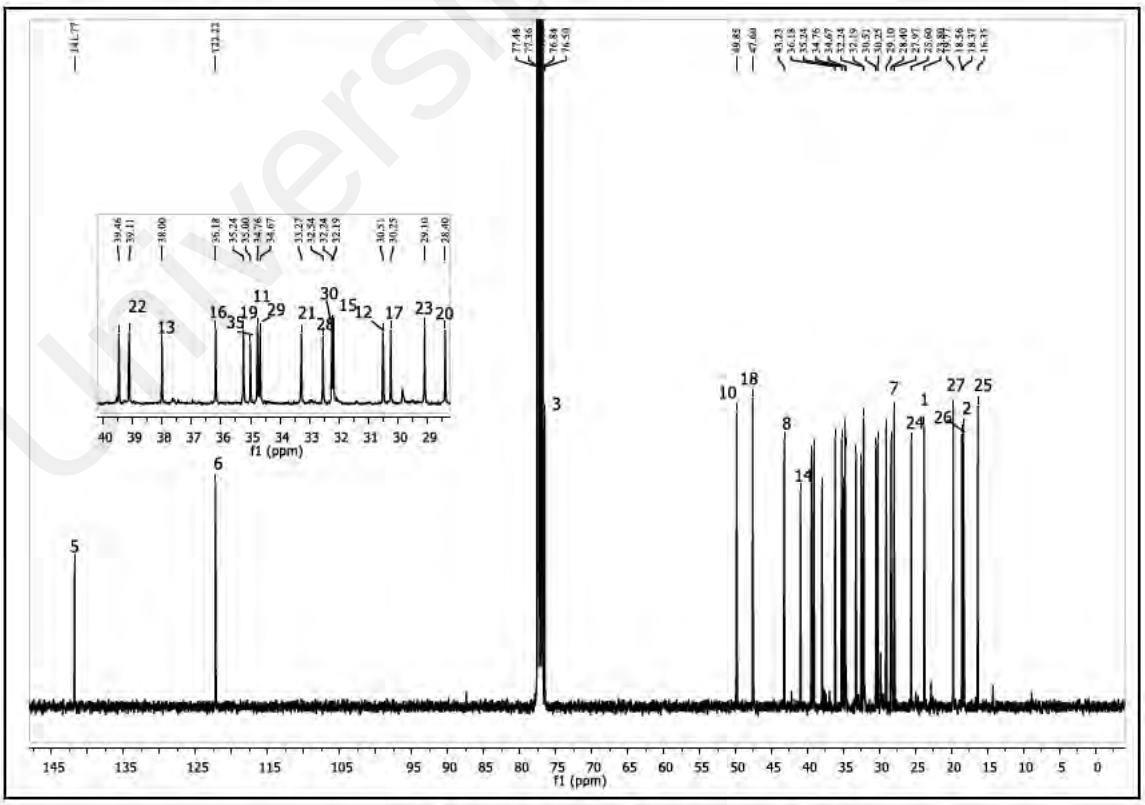

Figure 4.34: ^{13}C-NMR of glutinol 491.

4.1.2.13 Pyranojacareubin 164

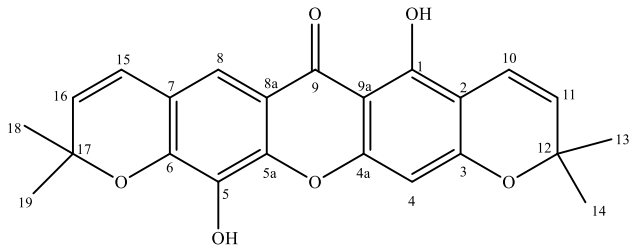

Pyranojacareubin **164** was obtained as yellow amorphous with a pseudomolecular $[M+H]^+$ ion at *m/z* 393.4036 (calcd. 393.4101) was detected in the HREIMS spectrum, which associated with the molecular formula $C_{23}H_{20}O_6$. The UV absorption was determined at λ_{max} 297 and 228 nm. The IR spectrum revealed the absorption at υ_{max} 3472 and 1737 cm^{-1} revealed the hydroxyl and carbonyl group.

The ^{1}H-NMR (Figure 4.35) displayed a broad signal for hydroxyl at δ_H 5.59 (5-OH) and a chelated hydroxyl at δ_H 13.30 (1-OH). Signals for two aromatic protons were resonating at δ_H 6.43 (H-4) and 7.47 (H-8) as two singlets. The remaining protons resonances typical of two 2,2-dimethyl pyrano systems with two singlets (6H each) at δ_H 1.47 (H-13 and H-14) and 1.54 (H-18 and H-19) together with two olefinic resonances (*J*=10 Hz) at δ_H 6.72 (*d*, H-10) and 5.59 (*d*, H-11) as well as δ_H 6.45 (*d*, H-15) and 5.73 (*d*, H-16) as the signals of pyran ring.

There are 23 carbon signals observed on the ^{13}C (Figure 4.36) and DEPT-135 NMR spectra: four methyls, six methines, twelve quaternary and a carbonyl carbon. The chelated hydroxyl was linked to C-1 of the xanthone skeleton as evidenced by the HMBC correlation between the hydroxyl proton signal at δ_H 13.30 and carbon signal at δ_C 157.9 (C-1) and δ_C 104.9 (C-2).

Spectral data indicated the structure as 1,3,5,6-tetraoxygenated xanthone with two 2,2-dimethyl-*2H*-pyran rings. Hence the structure was identified as pyranoacareubin **164** after

the analysis of complete spectra data and comparison with the literature review (Table 4.17).

Table 4.17: ^{1}H and ^{13}C-NMR spectral data of pyranojacareubin 164 in $CDCl_3$.

Position	Experimental ($CDCl_3$)		Reference ($CDCl_3$) (Cheng et al., 2004)	
	δ_H	δ_C	δ_H	δ_C
1	13.30, *s*, -OH	157.9	13.29, *s*, -OH	157.8
2	-	104.9	-	104.8
3	-	159.2	-	159.4
4	6.43, *s*	95.5	6.43, *s*	95.4
4a	-	157.0	-	156.9
5	5.59, *br s*, -OH	132.2	5.5, *br s*, -OH	132.1
5a	-	145.3	-	145.0
6	-	144.9	-	144.8
7	-	117.9	-	117.9
8	7.47, *s*	113.7	7.47, *s*	113.6
8a	-	114.8	-	114.7
9	-	179.3	-	178.8
9a	-	103.4	-	103.8
10	6.72, *d* (10.0)	115.6	6.73, *d* (10.0)	115.5
11	5.59, *d* (10.0)	127.7	5.73, *d* (10.0)	127.6
12	-	78.3	-	78.2
13	1.47, *s*	28.5	1.48, *s*	28.4
14	1.47, *s*	28.5	1.48, *s*	28.4
15	6.45, *d* (10.0)	121.5	6.44, *d* (10.0)	121.5
16	5.73, *d* (10.0)	131.2	5.59, *d* (10.1)	131.1
17	-	79.1	-	79.0
18	1.54, *s*	28.6	1.54, *s*	28.5
19	1.54, *s*	28.6	1.54, *s*	28.5

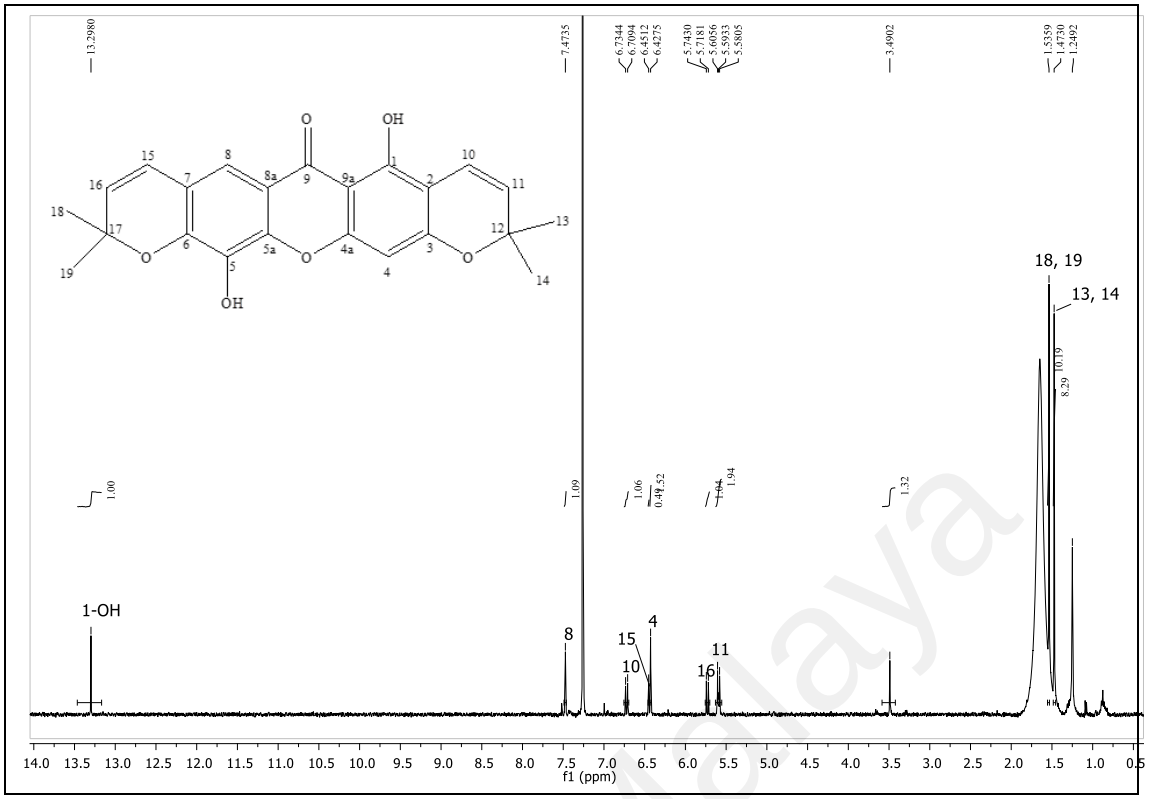

Figure 4.35: ^{1}H-NMR of pyranojacareubin 164.

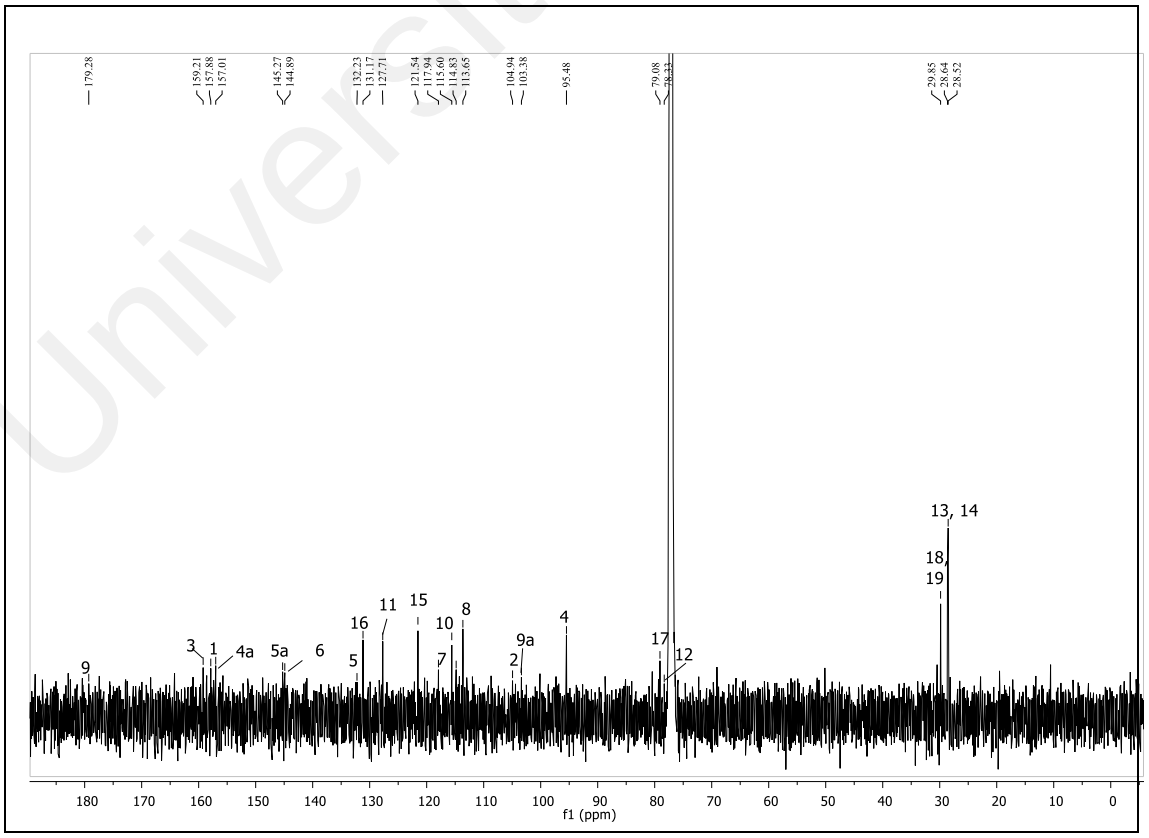

Figure 4.36: ^{13}C-NMR of pyranojacareubin 164.

4.1.2.14 Hypothetical biogenesis pathway of 4-phenyl coumarins isolated from *M. lepidota.*

The biogenesis pathway of the isolated 4-phenyl coumarins was proposed based on the hypothesis from Rouger *et al*. (Rouger et al., 2015). The two main precursors; 5,7-dihydroxy-8-(2-methyl-1-oxopropyl)-4-phenyl-2H-1-benzopyran-2-one (a) and mammea A/OB **62** were acylated 4-phenyl coumarins. The biogenesis reactions are mainly through *C*- prenylation at position C-6 or *O*-prenylation of the hydroxyl group that is attached to C-5. The hypothetical biogenesis pathway was demonstrated in Scheme 4.1.

Two times of *C*-prenylation on 5,7-dihydroxy-8-(2-methyl-1-oxopropyl)-4-phenyl-2H-1-benzopyran-2-one (a) gave lepidotol A **70**. As for lepidotin A **88**, it is proposed that *O*-prenylation occurred on compound (a), followed by Claisen rearrangement and cyclization. Lepidotol A **70** was proposed to undergo epoxidation, followed by hydrolysis and dehydration to form lepidotol E **86**. Furthermore, *C*-prenylation of compound (a), then hydroxylation, followed by dehydration and cyclization to give ochrocarpin E **76**.

A similar pathway was proposed for the formation of lepidotol B **71** and lepidotin B **89** from mammea A/OB **62**. Mammea A/OB **62** went through *C*-prenylation twice to give lepidotol B **71**. *O*-prenylation on mammea A/OB **62**, followed by Claisen rearrangement (Chamberlain et al., 1969) on structure (h) led to the formation of the two compounds, lepidotin B **89** and lepidotin C **490**. The biosynthesis pathway that involved the rearrangement of 1,1-dimethylally derivative (i) to 1,2-dimethylallyl derivative (j) contributed to the formation of lepidotin C **490**. Moreover, *C*-prenylation of mammea A/OB **62** followed by hydroxylation and cyclization resulting in the formation of mammea A/BB cyclo F **77**.

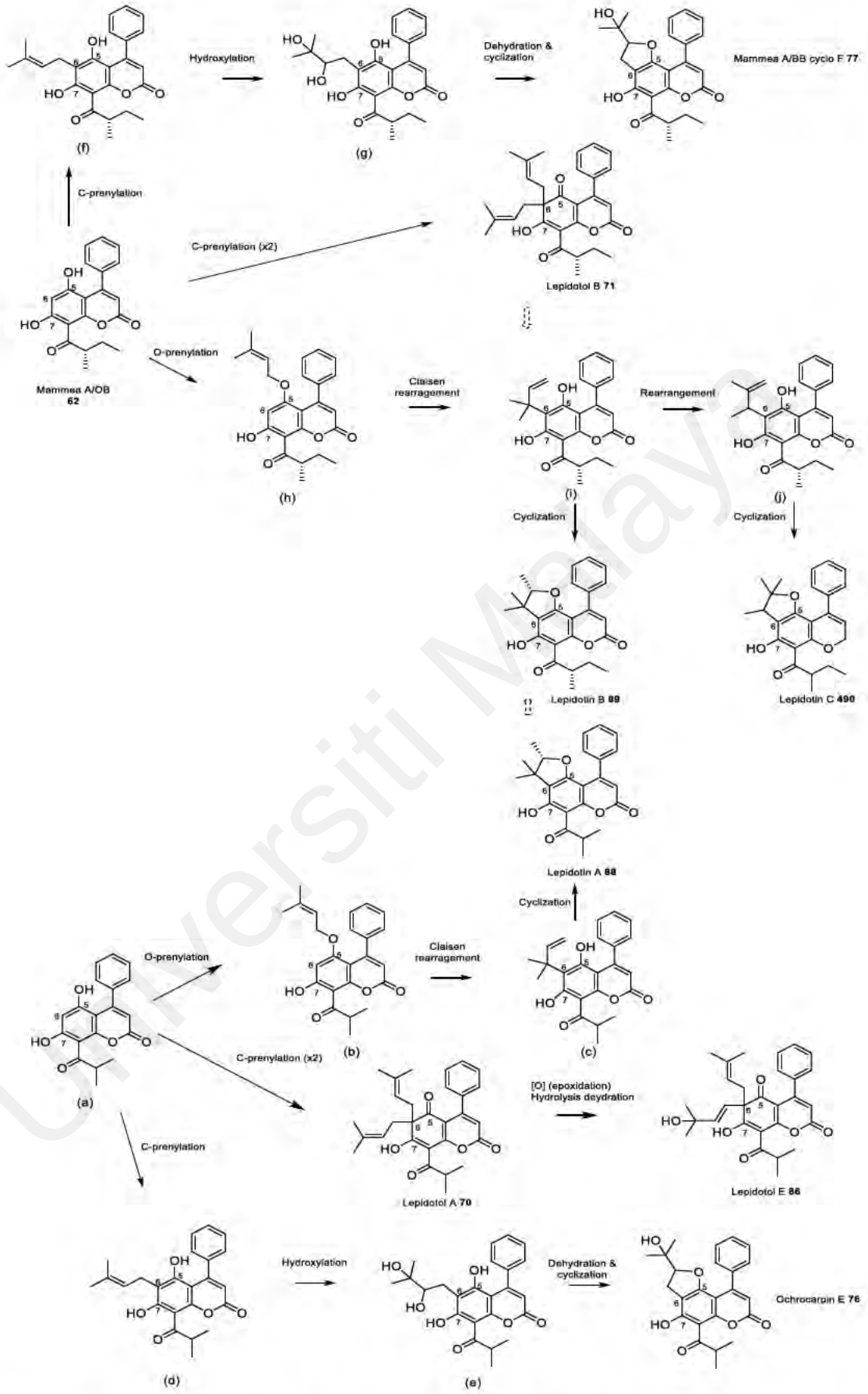

Scheme 4.1: Hypothetical biogenesis pathway of 4-phenyl coumarins isolated from *M. lepidota.*

4.1.3 Cholinesterase inhibitory activity as well as enzyme kinetic study, molecular docking, and molecular dynamics simulations of the most potent compound.

The following sections discussed the results obtained from cholinesterase inhibitory activity of HML bark, fractions, and isolated compounds from *M. lepidota*. Besides, enzyme kinetic study, molecular docking, and molecular dynamics simulations result of the most potent compound, lepidotin B **89** were discussed too.

4.1.3.1 Cholinesterase inhibitory activities of *M. lepidota*

AChE plays a predominantly role in cognitive function, especially in memory processes (Li et al., 2021; S. Zhou & Huang, 2022). However, both enzymes complement each other for their role in cholinergic neurotransmission. The ability of BChE to compensate for the insufficient hydrolysis of ACh by AChE in order to maintain normal cholinergic pathways as well as the correlation of BChE with β-amyloid deposition suggested that BChE may be a target to slow AD (Ha et al., 2020; Li et al., 2021; S. Zhou & Huang, 2022). Hence, BChE inhibitors or dual target (AChE and BChE) inhibitors have become a new pivot (S. Zhou & Huang, 2022) as the therapy for neurodegenerative diseases.

The cholinesterase inhibitory activities of the research were evaluated with the modified colorimetric Ellman's method. As tabulated in Table 4.18, the HML bark inhibited BChE (with the IC_{50} values of 2.24 ± 0.84 µg/mL) in the same range as galantamine which was used as a reference.

The crude extract was fractionated, and fractions were screened for their anticholinesterase activity. Fractions 1, 2 and 4 exhibited potent BChE inhibition (Table 4.18). Fraction 1 showed 79% of BChE inhibition at 200 µg/mL, while the most active fraction, fraction 2 demonstrated 93.4% of BChE inhibition at 200 µg/mL. Then the fraction 4 also showed 85.2% of BChE inhibition at 200 µg/mL.

Initial cholinesterase inhibitory activities of the isolated compounds (except lepidotol E **86** as having minute mass) were assayed at 100 µg/mL. IC_{50} determination only carried out for those compounds having at least 50% inhibition at 100 µg/ml. The result of the cholinesterase inhibitory activities of compounds isolated from *M. lepidota* was recorded in Table 4.19.

Table 4.18: Cholinesterase inhibitory activities of HML bark and fractions.

	AChE		**BChE**	
	% inhibition at 200 µg/mL	IC_{50} (µg/mL)	% inhibition at 200 µg/mL	IC_{50} (µg/mL)
HML bark	35.09	218.26±22.24	91.25	2.24 ± 0.84
Fraction 1	54.78	-	78.94	-
Fraction 2	3.34	-	93.40	-
Fraction 3	12.94	-	68.53	-
Fraction 4	26.44	-	85.17	-
Fraction 5	7.99	-	51.74	-
Fraction 6	16.32	-	61.90	-
Fraction 7	11.55	-	41.23	-
Fraction 8	5.24	-	26.91	-
Fraction 9	22.90	-	39.16	-
Fraction 10	34.29	-	39.37	-
Galantamine (standard)	-	2.92±0.23	-	6.98±0.06

All the twelve compounds showed mild AChE inhibition, except lepidotin B **89** and betulinic acid **177** demonstrated moderate AChE inhibition with the IC_{50} of 110.57±22.36 µM and 58.39±4.03 µM, respectively. Nevertheless, all the isolated 4-phenyl coumarins displayed moderate to strong BChE inhibition with the IC_{50} range of 1.60-16.84 µM except lepidotol A **70**. Besides, the isolated triterpenes and pyranojacareubin **164** exhibited strong to moderate BChE inhibition too, with the IC_{50} range of 6.02-74.15 µM excluded friedelin **186** had mild BChE inhibition. Lepidotin B **89**, lepidotin C **490** and mammea A/BB cyclo F **77** showed higher BChE inhibition potency compared to galantamine, with the IC_{50} of 6.98±0.06 µM.

Table 4.19: Cholinesterase inhibitory activities of compounds isolated from *M. lepidota* and standards.

	AChE		BChE	
	% inhibition at 100 µg/mL	IC_{50} (µM)	% inhibition at 100 µg/mL	IC_{50} (µM)
Lepidotol A 70	37.96	-	46.04	-
Lepidotol B 71	21.01	-	81.60	16.84±2.77
Lepidotin A 88	28.79	-	80.50	14.14±1.26
Lepidotin B 89	62.43	110.57±22.36	99.85	1.60±0.26
Lepidotin C 490	2.55	-	91.50	1.79±0.07
Mammea A/BB cyclo F 77	4.35	-	89.40	2.24±0.12
Ochrocarpin E 76	37.17	-	87.10	5.66±0.77
Friedelin 186	23.17	-	49.19	-
Friedelinol 189	22.05	-	52.57	74.15±13.32
Betulinic Acid 177	58.04	58.39±4.03	69.57	19.54±1.04
Glutinol 491	29.47	-	77.79	6.02±1.41
Pyranojacareubin 164	29.83	-	73.46	26.04±3.17
Donepezil (standard)	-	0.05±0.004	-	0.73±0.11
Galantamine (standard)	-	2.92±0.23	-	6.98±0.06

As most of the inhibitors of BChE in this study belong to the *Mammea* coumarin type, one may suggest that the 7-hydroxy-4-phenylchromen-2-one moiety correlates to the activity and the substructures further enhance or reduce the activity. This hypothesis was supported by the docking and molecular dynamics simulations result (refer to Table 4.22) which showed the binding at the five common regions of the enzyme with lepidotin B **89**.

Upon observing all isolated coumarins, two factors were evident in influencing the BChE activity. The first is the substitution pattern at C-5/C-6 in which the coumarins with hydrofuran ring at C-5/C-6 (*i.e.,* lepidotin A-C **(88-89, 490)** were more active than the ones with open chain (*i.e.*, lepidotol A **70** & B **71**). For example, lepidotin B **89**, which has hydrofuran ring fused at C-5/C-6 exhibited more potent inhibitory effect with an IC_{50} value 1.60±0.26 µM as compared to its open chained counterpart, lepidotol B **71** (IC_{50} value of 16.84±2.77 µM).

The second factor is the type and size of the acyl substituent at C-8. The inference is due to the result obtained for lepidotin B **89** and C **490** which have *sec*-butyl group attached to C=O of acyl exhibited better BChE inhibition compared to lepidotin A **88** that has an isopropyl group attached to C=O. Hence, the authors suggested that the hydrofuran ring and the size and type of the acyl moiety attached to C-8 may influence the BChE inhibitory activity of *Mammea* coumarins isolated from *M. lepidota*.

4.1.3.2 BChE Kinetic study

The mode of inhibition of the most potent compound, lepidotin B **89** on BChE was further determined through the Lineweaver-Burk plots (Table 4.20). The graphical analysis of the L-B plots (Figure 4.37) suggested that lepidotin B **89** was mix-mode inhibitors of BChE, indicated by the intersection of their data lines in the first quadrants (Khaw et al., 2014). This type of inhibitors can bind to both the enzyme's active site and/or allosteric site. In addition, the K_i value of 1.03 µM was obtained from the L-B secondary plots (Table 4.21 & Figure 4.38) for lepidotin B **89**.

Table 4.20: Data for Lineweaver-Burk (L-B) plot.

Sample concentration (µM)	Substrate concentration, [S]	$\frac{1}{[S]}$	Velocity, V	$\frac{1}{V}$
2	3.5	0.2857	0.0069	144.2308
	7	0.1429	0.0121	82.8729
	14	0.0714	0.0172	58.1395
3	3.5	0.2857	0.0044	227.2727
	7	0.1429	0.0091	110.2941
	14	0.0714	0.0146	68.4932
4	3.5	0.2857	0.0029	340.9091
	7	0.1429	0.0065	153.0612
	14	0.0714	0.0115	86.7052

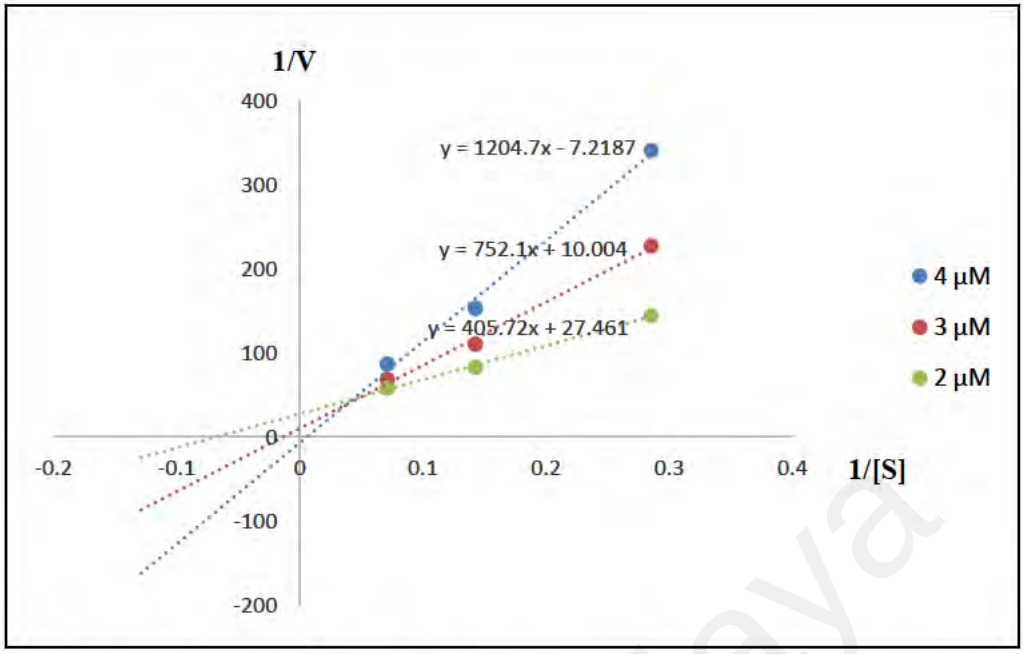

Figure 4.37: L-B plots of BChE activity over a range of substrate concentration (1.75 to 14.0 µM) for lepidotin B 89.

Table 4.21: Data for secondary plot of L-B plot.

Sample concentration (µM)	$\frac{Km}{Vm}$ (Slope)
2	405.72
3	752.1
4	1204.7

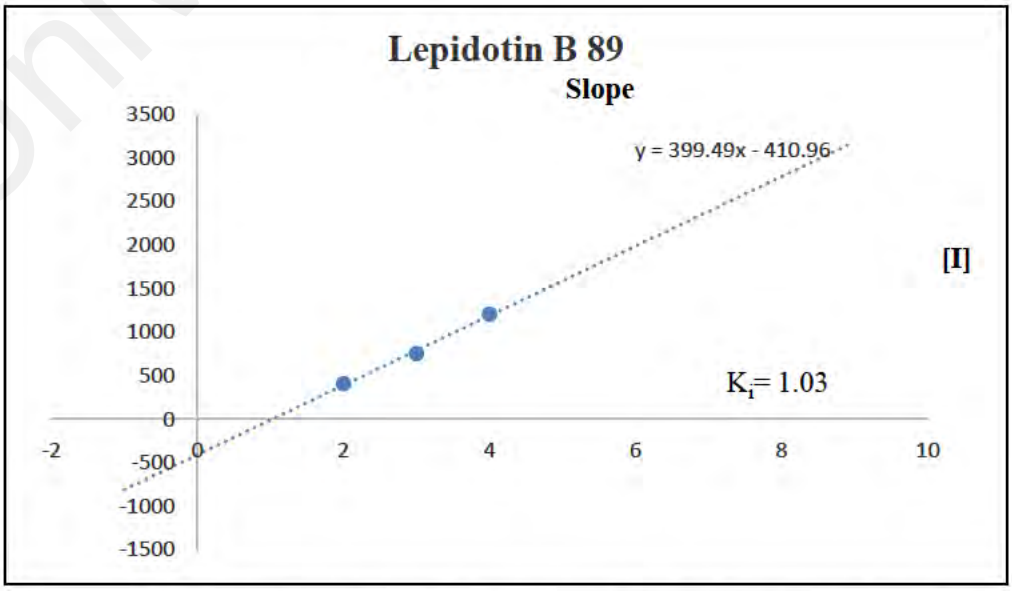

Figure 4.38: Secondary plots of Lineweaver-Burk plots of lepidotin B 89.

4.1.3.3 Molecular docking and molecular dynamics simulations of lepidotin B 89

Conducting a comprehensive investigation, a molecular docking study was executed to elucidate the binding interactions between lepidotin B **89** and BChE. To delve into the dynamics and stability of these complexes on an atomic scale over time, 100 ns molecular dynamics (MD) simulations were undertaken. Figure 4.39 portrays the ultimate structure resulting from the 100 ns molecular dynamics simulations (top), accompanied by a depiction of the 2D interactions (bottom) between lepidotin B **89** and the amino acid residues of BChE.

Upon analysing the last 20 ns of the production run, five common binding regions (Table 4.22) (Çokuğraş, 2003; Sukumaran et al., 2018) within the 20 Å deep and narrow gorge of BChE were identified as engaging with lepidotin B **89**. In the first region (1), the peripheral anionic site (PAS) residues Asp70 and Tyr332 exhibited interactions involving van der Waals forces and π-Alkyl interactions at ring D of lepidotin B **89**, as well as C-4", C-5", and C-6". Within region (2), the acyl hydrophobic pocket containing Leu286 interacted with ring C of lepidotin B **89**. In region (3), the catalytic triad residues Ser198 and His438 displayed interactions with ring B of lepidotin B **89**, forming a carbon-hydrogen bond with oxygen. Particularly, His438 is a vital amino acid residue within the enzyme's active site (catalytic triad) where ACh hydrolysis occurs (Wan Othman et al., 2016). Moving to the fourth region (4), interactions occurred with the oxyanion hole (OH) residues Gly116 and Gly117, forming π-alkyl interactions with both rings A and B (De Boer et al., 2021). Lastly, in region (5), the choline binding site residue Trp82 engaged in π -alkyl interactions with C-3''' and C-5'''. Furthermore, a significant binding interaction was observed with Thr120, involving hydrogen bonding, as well as multiple π-π stacking and π-π T-shaped interactions with Phe329.

The collective findings suggest that lepidotin B **89** engages both the active site and allosteric sites of BChE. This observation agrees with enzyme kinetic results that indicated a mixed type of inhibition. The energetic contribution, as depicted in Table 4.23, further validated the stability of this ligand within the binding pockets. Notably, the binding free energy, -37.65 ± 0.14 kcal/mol, indicated favourable binding. Of this, the van der Waal energy in the gas phase (-53.86 ± 0.12 kcal/mol) surpassed the electrostatic interaction energy (-20.35 ± 0.18 kcal/mol).

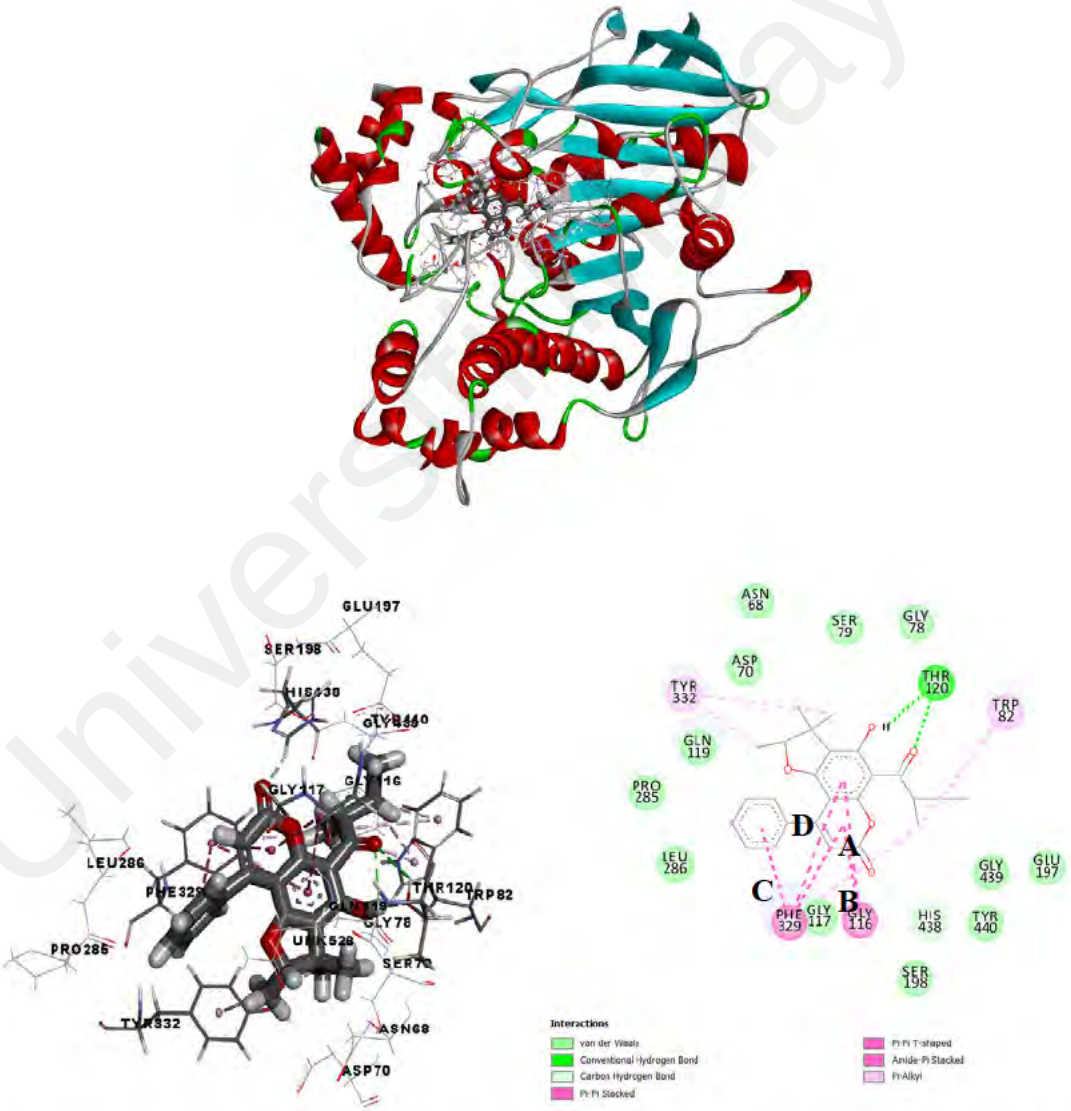

Figure 4.39: Binding complex (top) and 2D interactions (bottom) of lepidotin B 89 with amino acid residues of BChE from the final structure of 100 ns molecular dynamics simulations.

Table 4.22: Binding interaction data for lepidotin B 89 from *M. lepidota* in the active site gorge of BChE. The amino acids residues in the 3.5 Å region were in bold.

Ligand/ Compound	Binding Energy (kcal/mol)	Interacting site	Residue	Type of Interaction	Ligand Interacting
Lepidotin B **89**	-37.65 ±0.14	Peripheral anionic site (PAS) residues	**Asp70,** **Tyr332**	van der Waals π-Alkyl	Ring D C-4", C-5", C-6"
		The acyl pocket residues	**Leu286**, Val288	van der Waals N/A	Ring C
		The catalytic triad residues	**Ser198,** Glu325, **His438**	van der Waals N/A C-H bond	Ring B O
		The oxyanion hole (OH) residues	**Gly116,** **Gly117**, Ala199	Π-Alkyl π-Alkyl N/A	Ring B Ring A
		Choline binding site residues	**Trp82**	π-Alkyl	C-3''', C-5'''

Table 4.22, continued.

Ligand/ Compound	Binding Energy (kcal/mol)	Interacting site	Residue	Type of Interaction	Ligand Interacting
Lepidotin B **89**	-37.65 ±0.14	Others	**Thr120** **Phe329** **Asn68, Gly78, Ser79, Gln119, Glu197, Pro285, Leu286, Gly439, Tyr440.**	H bonding π-π stacked π-π T-shaped van der Waals	OH, O Ring A, B Ring C

Table 4.23: The energy contribution of binding free energy.

Energy Component	Average	Std. Err. of Mean
VDWAALS	-53.8637	± 0.1218
EEL	-20.3512	±0.1827
EGB	40.9520	± 0.1180
ESURF	-4.3839	±0.0059
DELTA G gas	-74.2149	±0.1954
DELTA G solv	36.5681	±0.1176
DELTA TOTAL	-37.6467	±0.1359

4.2 *G. griffithii*

The results and discussions on the research on *G. griffithii* were divided into three sections too: ^{13}C-NMR dereplication, phytochemical studies and biological activities.

4.2.1 ^{13}C- NMR dereplication with the aid of MixONat

Chloroform-D was used to dissolve the DGG leaves for NMR experiments. The DGG leaves ^{13}C-NMR spectra, which had more than 240 chemical shifts, revealed a complicated combination (Figure 4.40 & 4.41). There are several different types of structures indicated by MixONat, the majority of which are phloroglucinols and PPAPs, along with terpenoids, tocotrienols, and xanthones.

In this study, ^{13}C-NMR dereplication was used to identify PPAPs in the extract/ fractions of *G. griffithii*. However, three (3) factors made it challenging to analyze this outcome: first, different deuterated solvents were used in the literature for the NMR spectra of PPAPs, therefore it is now impossible to compare experimental chemical shifts and literature data for those compounds. In addition, as elucidating PPAPs is more challenging than elucidating other NPs, some structure revisions have been published. For example, garcinol **254** is also known as (−)-camboginol **254** and guttiferone F **254** (Zheng, Jiang, et al., 2021). The third factor is different stereoisomers, including diastereomers and enantiomers, were reported for PPAPs and the identification of enantiomer using the ^{13}C-NMR dereplication is impossible. This is because the enantiomer should be reported with the same/identical NMR spectra data. As enantiomer identification using ^{13}C-NMR dereplication is not achievable, both structures of enantiomer will be proposed in this study if enantiomer was the proposed results from MixONat. In this research, the revised structures and enantiomer will be discussed if they were suggested by MixONat. Anyhow, utilizing MixONat, three compounds from the extract were effectively identified or proposed; two of them were PPAPs and one was phloroglucinol.

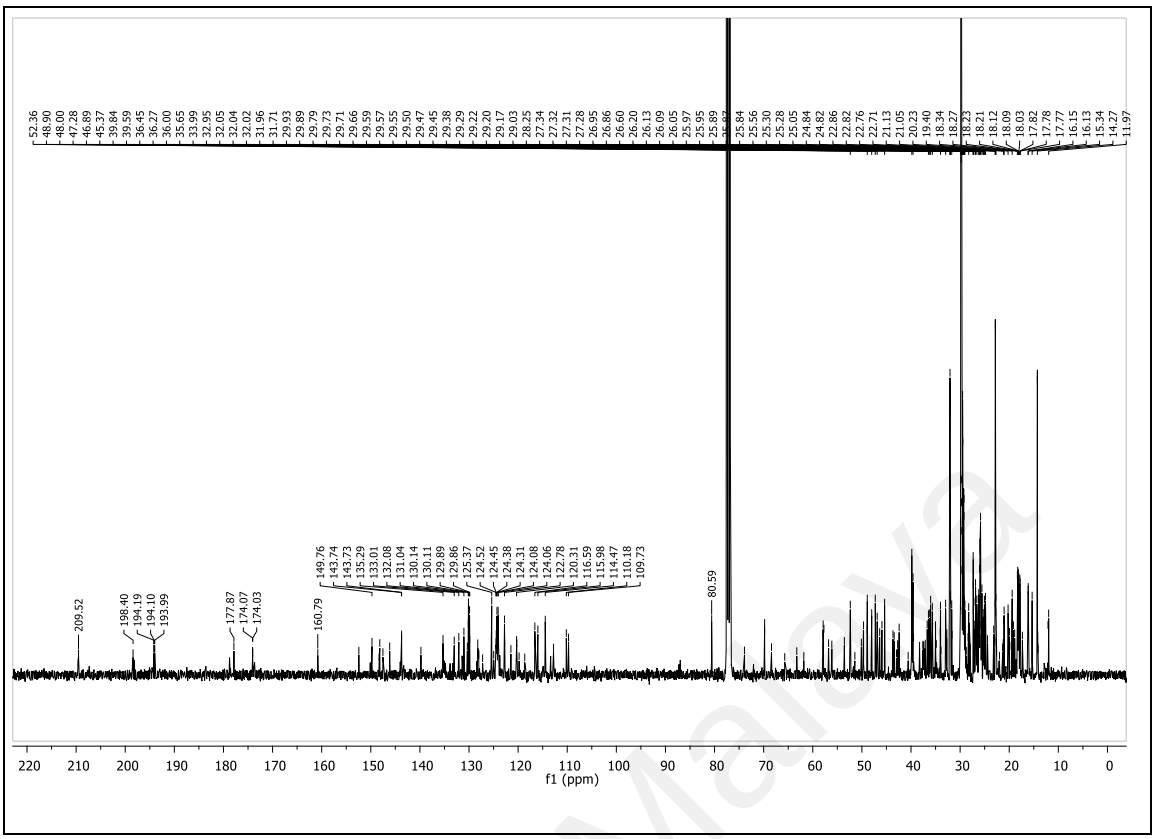

Figure 4.40: ^{13}C-NMR (10000 scans) of DGG leaves (30 mg) recorded in $CDCl_3$ at 100 M*Hz*.

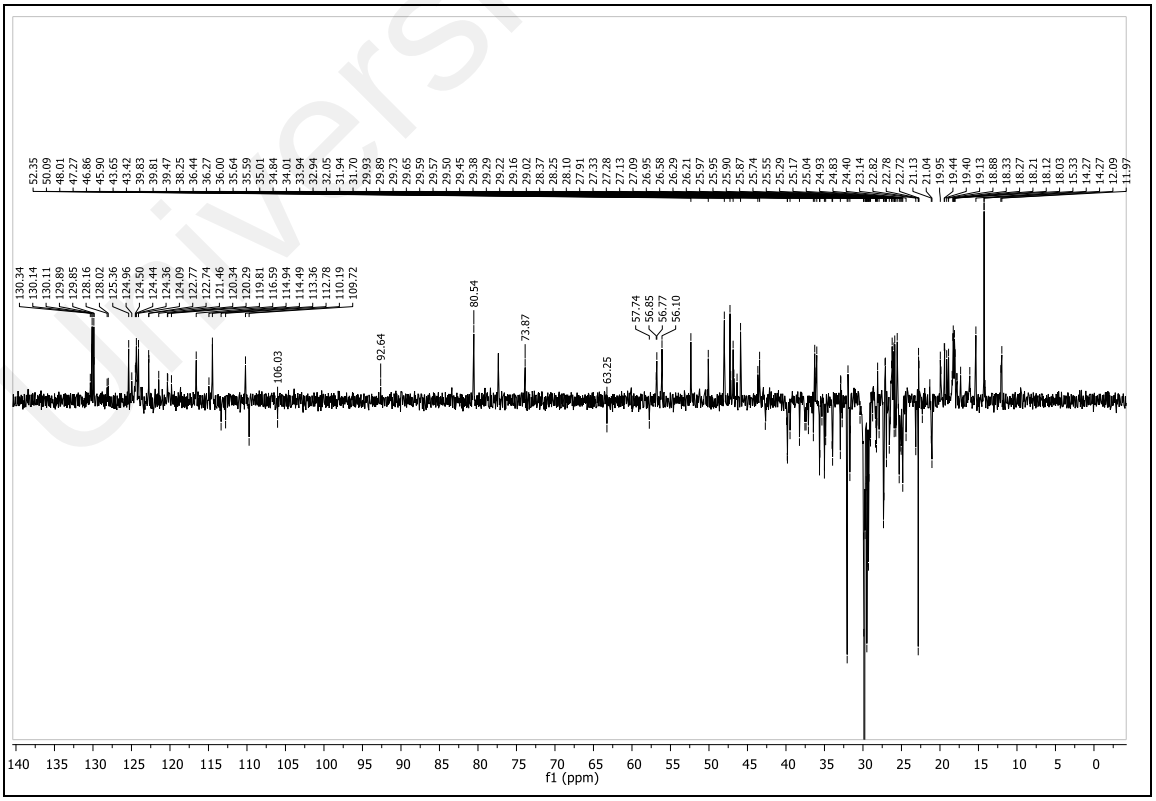

Figure 4.41: DEPT-135 NMR (5000 scans) of DGG leaves (30 mg) recorded in $CDCl_3$.

The first and second positions of the *Garcinia* DB (Appendix D) were predicted by MixONat with two PPAPs, guttiferone E **253** [rank 1, Garcinia DB, score 0.97 (37/38 C); rank 2, PPAPs DB, score 1.0 (38/38 C)] and guttiferone K **289** [rank 2, Garcinia DB, score 0.97 (37/38 C); rank 7, PPAPs DB, score 0.97 ((37/38 C)]. Additionally, the PPAPs DB (Appendix E) placed guttiferone F **254** [rank 3, score 1.0 (38/38 C)] and garcinol **254** [rank 1, score 1.0 (38/38 C)] in the first and third positions, respectively. Garcinol **254** and guttiferone F **254** were revised to have the same structure as (−)-camboginol **254**, and guttiferone E **253** was also known as (+)-camboginol **253**. The experimental spectra and data from the literature were compared (Table 4.24), and the structure was determined to be (±)-camboginol **253**/**254**. The experimental data cannot be compared to the literature chemical shifts for guttiferone K **289** because a different deuterated solvent was utilized there. The extract was used to identify the PPAPs structure, xanthochymol **270**, which had experimental chemical shifts that differed from published data (Table 4.25) by less than 0.4 ppm and was ranked 8 in the *Gacinia* DB with a score of 0.95 (36/38 C) and ranked 5 in the PPAPs DB with a score of 0.97 (37/38 C). Phloroglucinol with a high degree of confidence was identified from the extract as parvifoliol F **492** (Table 4.26) [rank 40, score 0.89 (24/27 C), *Garcinia* DB].

The crude was then separated based on the molecular weight of the metabolites in order to detect additional PPAPs from the DGG leaves. In fractions D4 and D5, PPAPs were gathered. Since CD_3OD + 0.05% TFA is the deuterated solvent most frequently used in the literature for PPAPs, it was used to perform the NMR of these two fractions (Figure 4.42-4.44).

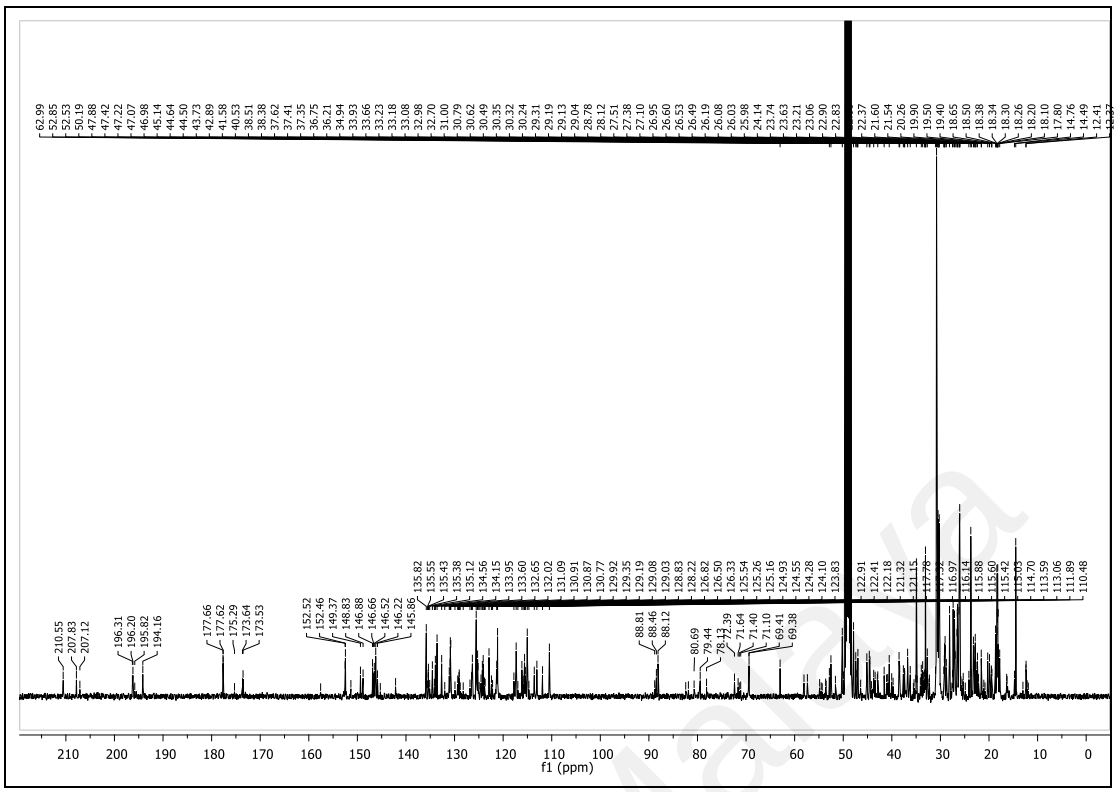

Figure 4.42: ^{13}C-NMR (10000 scans) of fraction D5 of *G. griffithii* recorded in CD_3OD+0.1 % TFA at 100 M*Hz*.

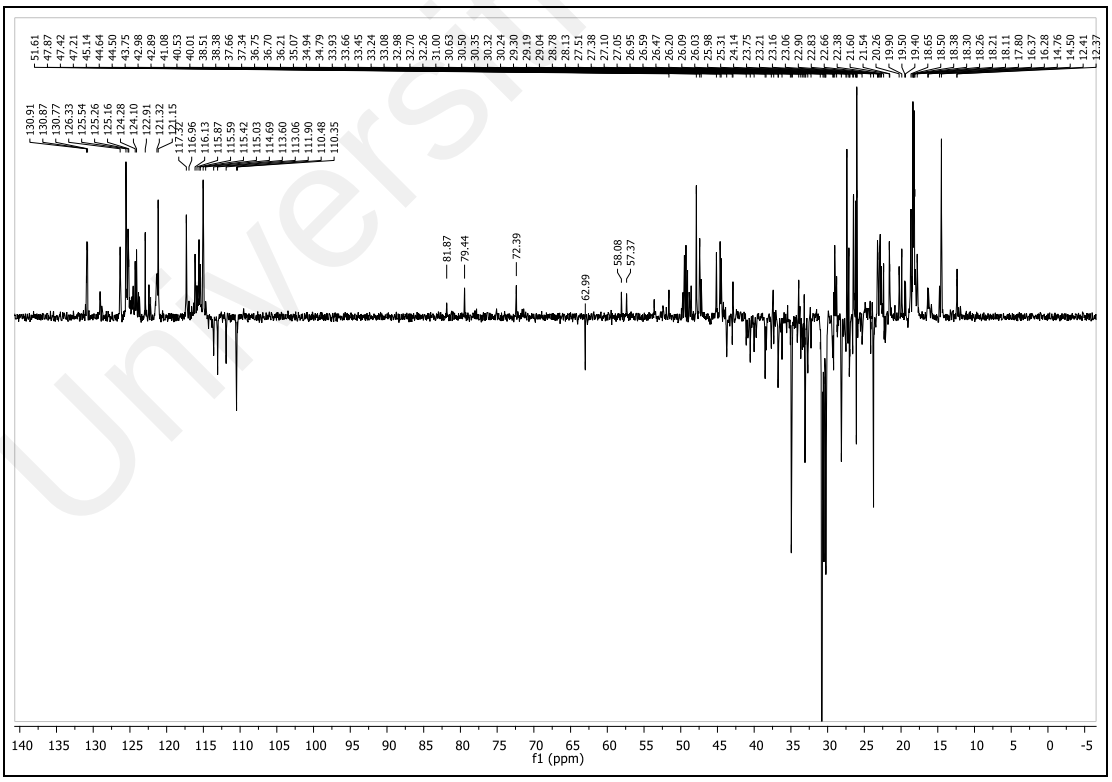

Figure 4.43: DEPT-135 NMR (5000 scans) of fraction D5 of *G. griffithii* recorded in CD_3OD+0.1 % TFA.

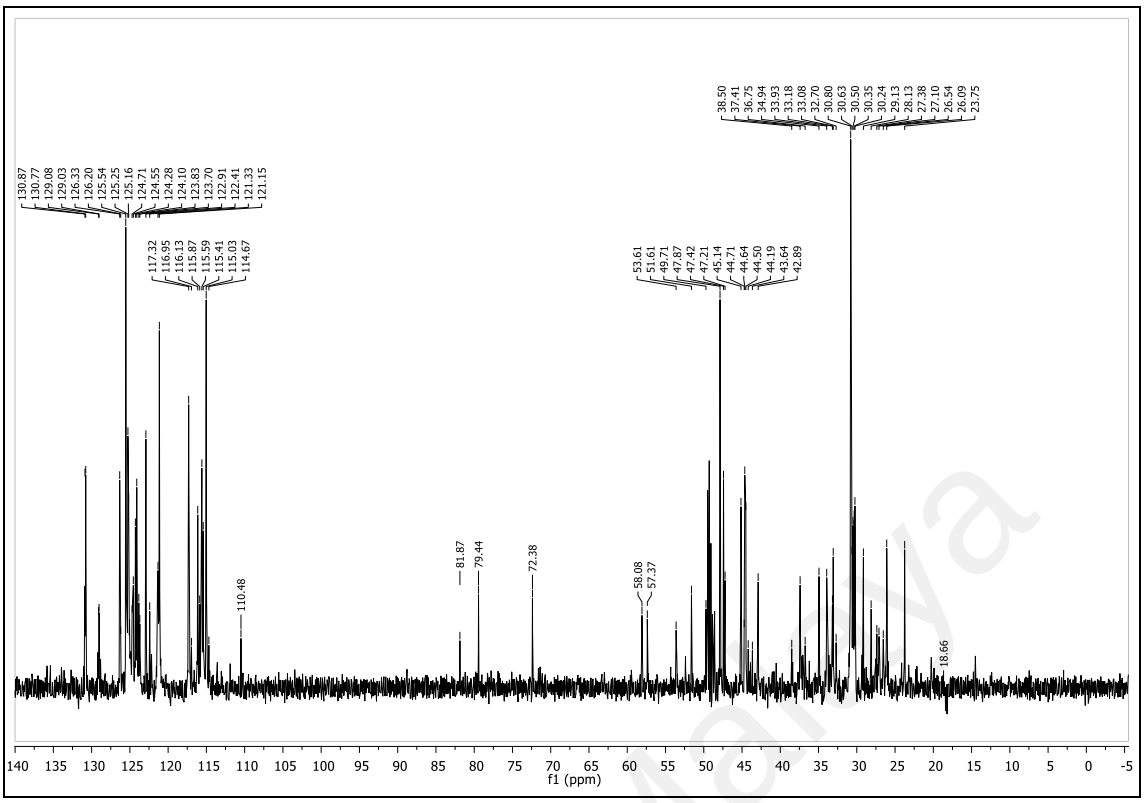

Figure 4.44: DEPT-90 NMR (3000 scans) of fraction D5 of *G. griffithii* recorded in CD_3OD+0.1 % TFA.

The best-matched structures were suggested by MixONat to be (+)-cycloxanthochymol **252** [rank1, *Garcinia* DB and PPAPs DB, score 0.97 (37/38 C)] and (-)-cycloxanthochymol **453** [rank2, PPAPs DB, score 0.97 (37/38 C)]. After contrasting it with literature-based information, this structure was validated with a high level of confidence (Table 4.27).

In addition, isoxanthochymol **248** [rank 8, *Garcinia* DB, score 0,92 (35/38 C); rank 5, PPAPs DB, score 0.95 (36/38 C)] and its enantiomer, isogarcinol **310** and 30-*epi*-cambogin **310** [ranks 4 and 6, respectively, PPAPs DB, score 0.95 (37/38 C)] were proposed by MixONat. Isogarcinol **310** and 30-*epi*-cambogin **310** share the identical structure, according to Zheng *et al.* (Zheng, Jiang, et al., 2021). However, following a study of the DBs, it was found that isogarcinol **310** and/or 30-*epi*-cambogin **310** were only included in the PPAPs DB (Appendix G) and not the *Garcinia* DB (Appendix F). The experimental

chemical shifts were carefully checked with the literature data of this enantiomer and the compound was identified (Table 4.27).

After comparing the experimental chemical shifts with data from the literature (Table 4.27), garcimultiflorone D **262** [rank 15, *Garcinia* DB, score 0.89 (34/38 C); rank 79, PPAPs DB, score 0.87 (33/38 C)] was also identified with a difference of less than 0.4ppm.

(±)-Camboginol **253/254** and xanthochymol **270** were confidently identified from the fraction as extracts. In addition, fraction D5 yielded the successful identification of four more PPAPs. In overall, (±)-cycloxanthochymol **252/453**, isoxanthochymol **248**, garcimultiflorone D **262**, and (±)-camboginol **253/254** were the compounds that were identified through ^{13}C-NMR dereplication.

Table 4.24: Experimental and reported spectroscopic data (δ_C) for garcinol 254 and guttiferone F 254 predicted in the DGG leaves.

Carbon numbering	**Garcinol 254 ($CDCl_3$)** (Zheng, Jiang, et al., 2021)		**Guttiferone F 254 (CD_3OD)** (Fuller et al., 1999)	
	Literature	δc (ppm) matched in extract	Literature	δc (ppm) matched in fraction
1	194.0	194.0	196.1	196.1
2	116.0	116.0	117.9	117.5
3	195.2	195.1	193.7	193.6
4	69.9	69.8	69.4	69.4
5	49.8	49.7	50.2	50.1
6	47.0	46.9	47.9	47.8
7	42.7	42.7	43.8	43.8
8	58.1	57.9	59.7	59.4
9	207.0	207.3	210.6	210.3
10	199.1	199.5	195.5	195.3
11	127.8	128.0	129.5	129.6
12	116.6	116.6	117.3	117.3
13	143.9	143.7	146.3	146.3
14	149.9	149.8	152.5	152.3
15	114.4	114.5	115.0	115.0
16	120.2	120.3	125.3	125.2
17	27.2	27.1	27.1	27.0
18	122.8	122.8	121.3	121.3
19	135.5	135.3	135.9	135.7
20	26.2	26.2	26.4	26.4
21	18.4	18.3	18.3	18.2
22	22.9	22.9	23.2	23.2
23	27.2	27.3	27.3	27.2
24	29.1	29.1	30.3	30.3
25	123.9	124.1	125.6	125.4
26	133.1	133.0	133.6	133.8
27	25.9	25.9	25.9	25.9
28	18.1	18.1	18.2	18.2
29	36.3	36.3	37.3	37.3
30	43.7	43.7	45.2	44.9
31	148.2	148.2	149.5	149.6
32	112.9	112.8	113.0	113.1
33	17.8	17.8	18.2	18.2
34	32.8	32.8	33.5	33.5
35	124.2	124.3	124.1	124.1
36	132.2	132.1	132.7	132.6
37	26.0	26.0	26.0	26.0
38	18.1	18.1	18.2	18.2

Table 4.25: Experimental and reported spectroscopic data (δ_C) for xanthochymol 270 in $CDCl_3$ and CD_3OD predicted in the DGG leaves.

Carbon numbering	Xanthochymol 270 ($CDCl_3$) (Blount & Williams, 1976)		Xanthochymol 270 (CD_3OD) (Roux et al., 2000)	
	Literature	δc (ppm) matched in extract	Literature	δc (ppm) matched in fraction
1	194.9	195.1	195.7	195.8
2	115.2	114.9	117.9	117.8
3	194.0	194.0	194.4	194.2
4	70.0	69.8	69.8	69.4
5	49.8	49.7	50.4	50.2
6	46.7	46.8	48.1	47.9
7	42.9	43.0	43.9	43.7
8	58.1	57.9	59.9	58.1
9	209.2	209.5	209.8	210.6
10	198.6	198.4	196.4	196.3
11	127.9	128.0	129.5	129.4
12	116.6	116.6	117.5	117.3
13	143.8	143.7	147.0	146.9
14	147.5	147.5	152.5	152.5
15	114.5	114.5	115.2	115.0
16	120.2	120.3	125.3	125.3
17	27.2	27.1	27.2	27.1
18	123.9	124.1	121.4	121.3
19	133.1	133.0	136.0	135.8
20	26.3	26.2	26.6	26.6
21	18.5	18.3	18.5	18.5
22	22.8	22.8	23.3	23.2
23	26.6	26.6	27.5	27.5
24	29.2	29.2	30.4	30.4
25	124.2	124.3	125.7	125.5
26	135.4	135.3	133.7	133.6
27	26.1	26.1	26.1	26.1
28	18.2	18.2	18.4	18.4
29	36.8	36.7	37.8	37.6
30	43.6	43.7	44.8	44.6
31	149.9	149.8	149.0	148.8
32	113.5	113.4	113.7	113.6
33	17.4	17.3	17.9	17.8
34	32.1	32.1	32.9	33.0
35	35.7	35.7	36.9	36.8
36	146.1	146.2	149.5	149.4
37	109.8	109.7	110.6	110.5
38	23.0	22.9	23.0	23.1

Table 4.26: Experimental and reported spectroscopic data (δ_C) for parvifoliol F 492 in $CDCl_3$ predicted in the DGG leaves.

Carbon numbering	**Parvifoliol F 492 ($CDCl_3$)** (Rukachaisirikul et al., 2006)	
	Literature	δc (ppm) matched in extract
2	75.3	75.4
3	31.4	31.7
4	22.5	22.6
4a	121.3	121.5
5	112.6	112.8
6	127.4	127.2
7	115.7	116.0
8	147.8	147.5
8a	146	146.2
9	39.7	39.8
10	22.2	22.0
11	124.3	124.4
12	135.1	135.3
13	39.7	39.6
14	26.6	26.6
15	124.4	124.4
16	135	135.3
17	39.7	39.5
18	26.8	26.9
19	124.3	124.3
20	131.3	131.0
21	17.7	17.8
22	25.7	25.7
23	15.9	15.3
24	16	16.2
25	24.3	24.4
26	16	16.1

Table 4.27: Experimental and reported spectroscopic data (δ_C) for PPAPs in CD_3OD predicted in the fraction D5 of DGG.

Carbon numbering	(±)-Cycloxanthochymol 252/453 (Bruguiére, 2019)		Isoxanthochymol 248 (Gustafson et al., 1992)		Garcimultiflorone D 262 (Liu et al., 2010)		30-*epi* Cambogin 310 (Fuller et al., 1999)	
	Literature	δc (ppm) matched in extract	Literature	δc (ppm) matched in extract	Literature	δc (ppm) matched in extract	Literature	δc (ppm) matched in extract
1	52.9	52.85	196	195.95	173.9	173.64	172.4	172.67
2	173.8	173.64	117.8	117.46	110.2	110.48	110.6	110.54
3	126.8	126.82	194	193.99	196.3	196.31	196.1	196.07
4	196.4	196.31	69.7	69.44	69.6	69.41	70.4	70.32
5	69.5	69.41	50.2	50.13	46.7	46.42	47.4	47.45
6	47.4	47.42	48	47.76	47.5	47.42	47.5	47.29
7	47.1	47.07	43.9	43.91	40	40.02	38.8	38.6
8	39.7	39.74	59.8	59.41	52.6	52.53	49.6	49.85
9	207.9	207.83	210.9	210.26	208	207.83	209.9	210.26
10	194.2	194.16	195.5	195.32	194.3	194.16	194.1	194.19
11	131.1	131.09	129.6	129.62	131.2	131.09	131.1	130.98
12	115.9	115.88	117.4	117.42	116.3	116.14	116.1	116
13	146.7	146.66	146.1	146.18	146.8	146.88	146.4	146.47
14	152.6	152.52	152.4	152.3	152.5	152.52	152.5	152.3
15	115.4	115.42	115.1	114.95	115.6	115.6	115.5	115.49
16	124.6	124.55	125.1	125.08	124.4	124.28	124.3	124.2
17	26.6	26.6	29.5	29.68	26.5	26.53	26.3	26.28
18	121.2	121.15	27.1	27.04	121.1	121.15	121.2	121.27
19	135.5	135.55	71.3	71.28	135.3	135.38	135.2	135.24
20	26.6	26.53	29.2	29.3	26.3	26.19	26.5	26.51
21	18.3	18.3	29.1	29.14	18.2	18.2	18.3	18.24

Table 4.27, continued.

Carbon numbering	**(±)-Cycloxanthochymol 252/453** (Bruguiére, 2019)		**Isoxanthochymol 248** (Gustafson et al., 1992)		**Garcimultiflorone D 262** (Liu et al., 2010)		**30-*epi* Cambogin 310** (Fuller et al., 1999)	
	Literature	δc (ppm) matched in extract	Literature	δc (ppm) matched in extract	Literature	δc (ppm) matched in extract	Literature	δc (ppm) matched in extract
22	22.9	22.9	27.4	27.45	22.8	22.83	22.7	22.7
23	27	26.95	23.2	23.22	27	26.95	27.1	27.04
24	30.5	30.49	30.3	30.29	30	30.24	30.5	30.57
25	126.3	126.33	125.6	125.43	126.2	126.33	126.4	126.39
26	134	133.95	133.6	133.77	133.5	133.6	133.8	133.77
27	26.1	26.08	25.9	25.93	26.1	26.08	26.2	26.22
28	18.6	18.65	18.2	18.2	18.5	18.5	18.1	18.01
29	28.7	28.78	37.9	37.68	29	29.04	30.2	30.19
30	42.9	42.89	45.5	45.97	44.7	44.64	41.1	40.96
31	88.6	88.46	149.3	149.13	88.1	88.12	87.2	87.89
32	21.5	21.54	113.4	113.65	29	29.04	22.2	22.23
33	28.8	28.78	17.8	17.89	21.3	21.06	28.4	28.6
34	29.3	29.31	42.8	42.79	30.5	30.49	31	30.76
35	36.2	36.21	121.4	121.27	122.8	122.91	122.7	122.78
36	146	145.86	135.7	135.65	134.6	134.56	135.1	135.12
37	11.9	11.91	26.4	26.36	26.1	26.08	26	25.99
38	22.3	22.3	18.3	18.24	17.8	17.8	18.7	18.65

4.2.2 PPAPs isolated from *G. griffithii*

There were three PPAPs isolated from the DGG leaves. The isolated PPAPs were (+)-camboginol **253**, xanthochymol **270**, and isoxanthochymol **248**.

4.2.2.1 (+)-camboginol 253

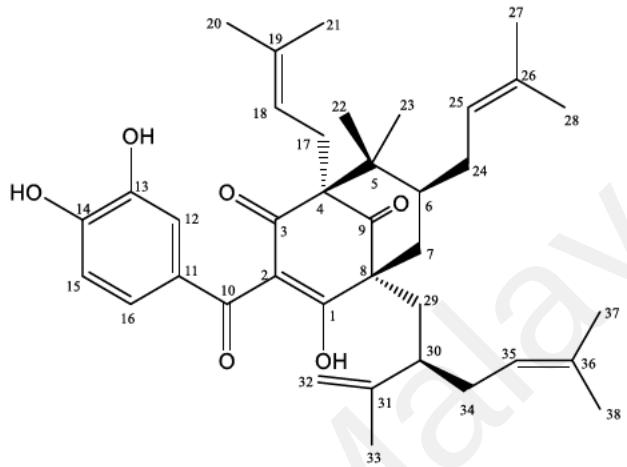

(+)-camboginol, **253** a yellow amorphous compound, with an optical rotation of +50° (c 0.0018, $CHCl_3$), has been isolated and identified by its spectroscopic data. The HRESIMS measurement showed the $[M+H]^+$ ion peak at m/z 603.3527 (calculated for $C_{38}H_{51}O_6$, 603.3607), and the IR spectrum showed characteristic peaks at υ_{max} 3401 (phenolic OH group), 2927, 1724 (six-membered cyclic C=O), 1598 (conjugated C=O), 1376, 1291, 1115, and 1058 cm^{-1}. The UV spectrum showed two absorption maxima at 277 and 230 nm, indicating a PPAPs type compound.

The ^{1}H-NMR spectrum (Figure 4.45) showed signals for the characteristic peaks of the three aromatic protons on the 3,4-dihydroxybenzoyl group at δ_H7.21 (1H, *d*, *J*= 2.1 Hz, H-12), 6.98 (1H, *dd*, *J*= 8.3 Hz, 2.1 Hz, H-16), and 6.71 (1H, *d*, *J*= 8.3 Hz, H-15). Additionally, two prenyl groups were observed at δ_H 5.08 (1H, *m*, H-18), 1.76 and 1.72 (3H, *s*, H-20, and H-21) as well as δ_H 4.91 (1H, *m*, H-25), 1.68 and 1.52 (3H, *s*, H-27, and H-28) each. The lavandulyl group was shown as a multiplet at δ_H 5.05 (H-35), a broad singlet of 2H at 4.48 (H-32), and 3 singlets of methyls at δ_H 1.61 (H-33), 1.68 (H-37), and

1.60 (H-38). Additionally, two methyl groups of saturated carbon were observed on the ^{1}H-NMR spectrum at two singlets of 3H at δ_H 1.02 (H-23) and δ_H 1.18 (H-22), respectively.

The ^{13}C (Figure 4.46) and DEPT-NMR spectra revealed 38 carbon signals, including nine methyls, six methylenes, eight methines, and fifteen quaternary carbons. Six aromatic carbons were identified at δ_C 129.6, 117.3, 146.3, 152.6, 115.1, and 125.3, and a bicyclo [3.3.1] nonane-2,4,9-trione moiety with three quaternary carbons (δ_C 69.2, 50.3, and 59.6), a methine (δ_C 48.0), a methylene (δ_C 43.9), a non-conjugated ketone (δ_C 210.7), and an enolized 1,3-diketone (δ_C 196.5, 118.9, and 193).

In conclusion, the structural identification of (+)-camboginol **253** was accomplished by comparing its spectroscopic data with previous literature (Table 4.28).

Table 4.28: ^{1}H and ^{13}C-NMR spectral data of (+)-camboginol 253 in CD_3OD+0.1 % TFA.

Position	Experimental (CD_3OD+0.1% TFA)		Reference (CD_3OD+0.1% TFA) (Fuller et al., 1999)	
	δ_H, *J* (Hz)	δ_C	δ_H, *J* (Hz)	δ_C
1	-	196.53	-	196.1
2	-	118.91	-	117.9
3	-	192.98	-	193.7
4	-	69.23	-	69.4
5	-	50.27	-	50.2
6	1.52, *m*	47.98	1.49, *m*	47.9
7	2.04, pro-*S*, *dd* (14.0, 5.8) 2.27 pro-*R*, *d* (14.0)	43.85	2.04 pro-*S*, *dd* (13.5, 7.4) 2.24 pro-*R*, *d* (13.5)	43.8
8	-	59.61	-	59.7
9	-	210.68	-	210.6
10	-	195.15	-	195.5
11	-	129.57	-	129.5
12	7.21, *d* (2.1)	117.34	7.19, *d* (2.0)	117.3
13	-	146.33	-	146.3
14	-	152.55	-	152.5
15	6.71, *d* (8.3)	115.12	6.68, *d* (8.0)	115.0
16	6.98, *dd* (8.3, 2.0)	125.31	6.96, *dd* (8.0, 2.0)	125.3
17	2.59 pro-*S*, *dd* (13.3, 9.0) 2.73, pro-*R*, *dd* (13.3, 9.2)	27.12	2.56 pro-*S*, *dd* (13.3) 2.71 pro-*R*, *dd* (13.9)	27.1
18	5.08, *m*	121.44	5.03, *m*	121.3
19	-	135.92	-	135.9
20	1.76, *s*	26.47	1.73, *s*	26.4
21	1.72, *s*	18.37	1.69, *s*	18.3
22	1.18, *s*	23.21	1.15, *s*	23.2
23	1.02, *s*	27.38	0.99, *s*	27.3
24	2.17, *m* 2.07, *m*	30.32	2.09, *m* 2.02, *m*	30.3
25	4.91, *m*	125.61	4.87, *m*	125.6
26	-	133.70	-	133.6
27	1.68, *s*	25.95	1.65, *s*	25.9
28	1.52, *s*	18.24	1.49, *s*	18.2
29	1.94 pro-*S*, *dd* (14.0, 5.4) 2.24 pro-*R*, *m*	37.35	1.92 pro-*S*, *dd* (13.5, 4.5) 1.98, pro-*R*, *m*	37.3
30	2.64, *m*	45.28	2.62, *m*	45.2
31	-	149.53	-	149.5
32	4.48, *s*	113.02	4.45, *s*	113.0
33	1.61, *s*	18.20	1.58, *s*	18.2
34	2.14, *m*	33.52	2.01, *m*	33.5
35	5.05, *m*	124.17	5.03, *m*	124.1
36	-	132.78	-	132.7
37	1.68, *s*	25.99	1.65, *s*	26.0
38	1.60, *s*	18.20	1.57, *s*	18.2

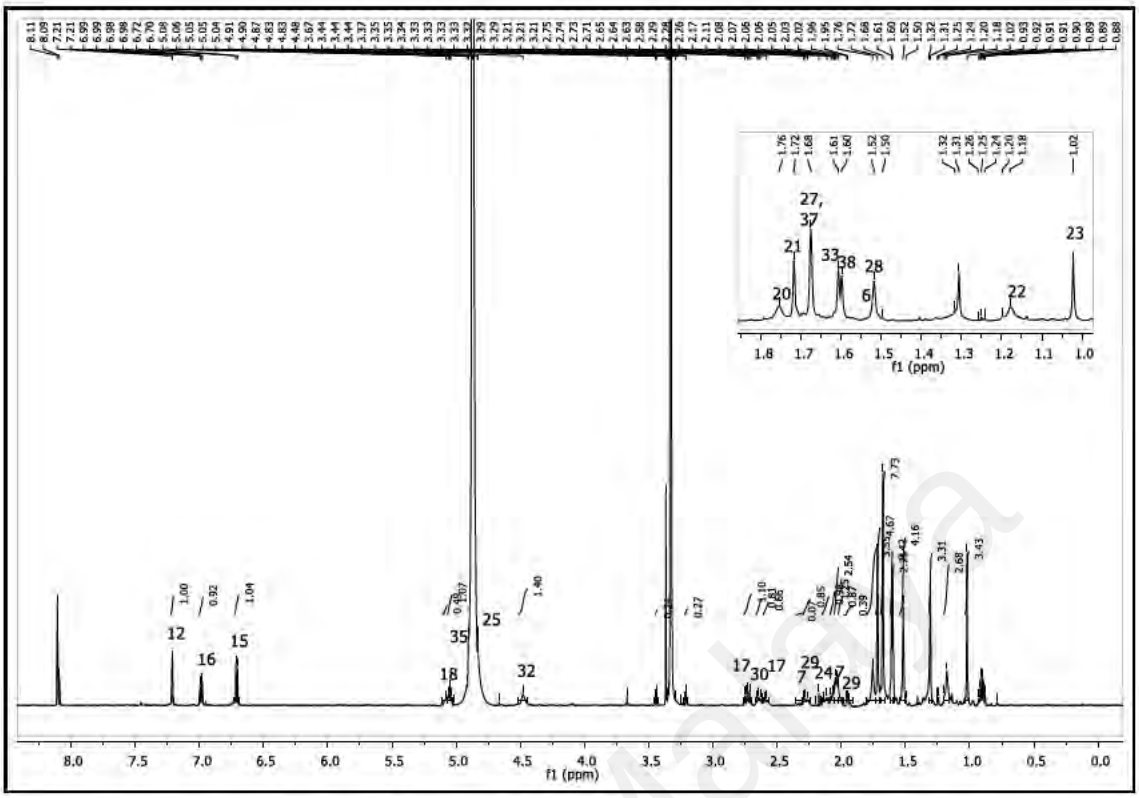

Figure 4.45: ^{1}H-NMR of (+)-camboginol 253.

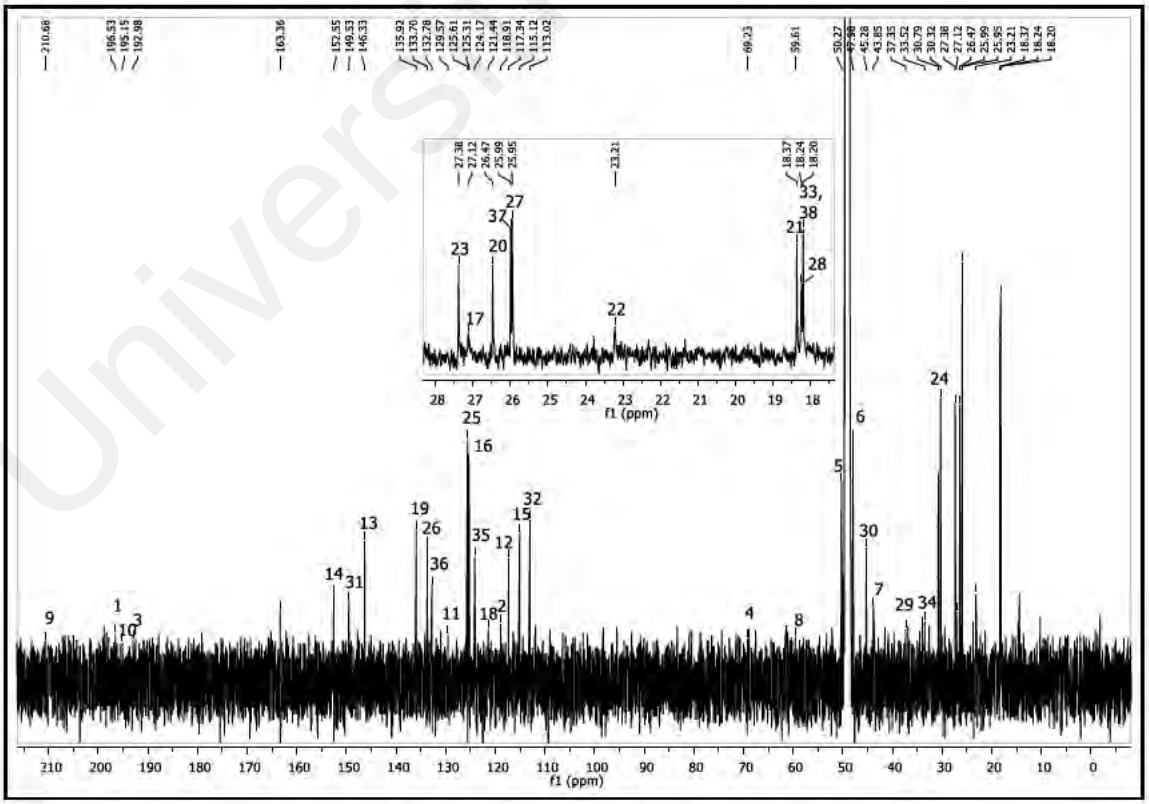

Figure 4.46: ^{13}C-NMR of (+)-camboginol 253.

4.2.2.2 Xanthochymol 270

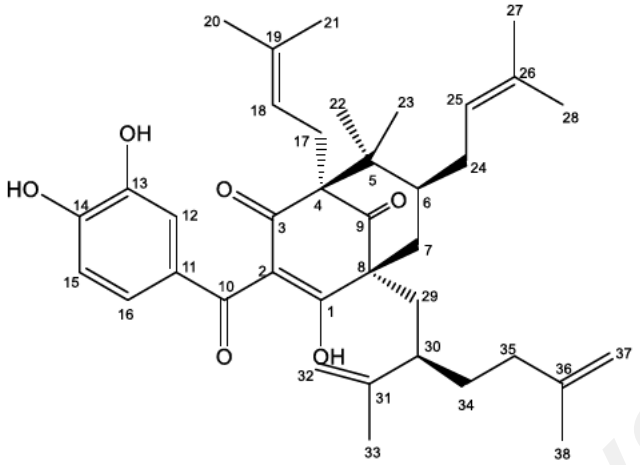

Xanthochymol **270** with $[\alpha]_D^{25}$ as +162.5° (c 0.048, $CHCl_3$) was isolated as yellow amorphous. The LCMS-IT-TOF spectrum displayed a pseudomolecular ion peak at $[M+H]^+$ 603.3672, indicated the molecular formula of $C_{38}H_{50}O_6$ (calcd 602.3607). The IR spectrum revealed signals at υ_{max} 3397, 2971, 2930, 1647, 1444, 1375, and 1145 cm^{-1}. Besides, the UV absorption of xanthochymol **270** was detected at wavelength 274 and 230 nm, corresponding to PPAPs type.

The ^{1}H-NMR spectrum (Figure 4.47) of xanthochymol **270** showed the presence of three aromatic protons characteristic of 3,4-dihydroxybenzoyl group [(δ_H 7.21, *d*, *J*=2.1 Hz, H-12), (6.73, *d*, *J*= 8.3 Hz, H-15), (7.00, *dd*, *J*= 8.3, 2.1 Hz, H-16)], two prenylated groups derived at [δ_H 2.57 and 2.73 (*m*, H-17), 5.05 (*m*, H-18), and two singlets at δ_H 1,71 and 1,68 (*s*, H-20 and H-21) as well as 2.06 (*m*, H-24), 4.87 (*m*, H-25), two singlets at δ_H 1.75 and 1.52 (H-27 and H-28 respectively)], an isolavandulyl group shown at two broad singlet of 2H at δ_H 4.65 (H-32) and 4.67 (H-37), and 2 singlets of methyls at δ_H 1.63 (H-33) and 1.68 (H-37), in addition of methylene and methine protons which showed a complex protons within the range δ_H 1.44-2.55 and two methyl groups (singlets on δ_H 1.18 and 1.02, corresponding to H-22 and H-23 respectively) on a saturated carbon. The significant difference in the ^{1}H-NMR spectrum of xanthochymol **270** and (+)-camboginol

is the presence of two terminal methylene in the former while there is only one in the latter structure.

From the ^{13}C (Figure 4.48) and DEPT-NMR spectra, a total of 38 carbons were determined. eight methyls, eight methylenes, seven methines and fifteen quaternary carbons were discovered from the spectra. The ^{13}C-NMR spectrum showed characteristic resonances for six aromatic carbons (δ_C 129.6, 117.3, 146.3, 152.5, 115.1, and 125.2) and a bicyclo [3.3.1] nonane-2,4,9-trione moiety in evidence of three quaternary carbons (δ_C 69.8, 50.2, and 60.1), a methine (δ_C 47.9), a methylene (δ_C 43.7), an unconjugated ketone (δ_C 210.7), and an enolized 1,3-diketone (δ_C 195.8, 117.9, and 194.5).

The study of the NMR spectra and the comparison with the literature values confirmed the structure as xanthochymol **270** (Table 4.29).

Table 4.29: ^{1}H and ^{13}C-NMR spectral data of xanthochymol 270 in CD_3OD+0.1 % TFA.

Position	Experimental (CD_3OD+0.1% TFA)		Reference (CD_3OD+0.1% TFA) (Roux et al., 2000)	
	δ_H, *J* (Hz)	δ_C	δ_H, *J* (Hz)	δ_C
1	-	195.82	-	195.7
2	-	117.93	-	117.9
3	-	194.46	-	194.4
4	-	69.78	-	69.8
5	-	50.21	-	50.4
6	1.49, *m*	47.92	1.51, *m*	48.1
7	2.12, *m*	43.72	2.05, *m*	43.9
	2.27, *m*		2.26, *m*	
8	-	60.13	-	59.9
9	-	210.70	-	209.8
10	-	197.47	-	196.4
11	-	129.63	-	129.5
12	7.21, *d* (2.1)	117.33	7.21, *d* (2.1)	117.5
13	-	146.98	-	147.0
14	-	152.50	-	152.5
15	6.73, *d* (8.3)	115.09	6.72, *d* (8.0)	115.2
16	7.00, *dd* (8.3, 2.1)	125.18	7.00, *dd* (8.0, 2.1)	125.3
17	2.57, *m*	27.05	2.51, *m*	27.2
	2.73, *m*		2.77, *m*	
18	5.05, *m*	121.32	5.07, *m*	121.4
19	-	135.86	-	136.0
20	1.71, *s*	26.40	1.74, *s*	26.6
21	1.68, *s*	18.33	1.69, *s*	18.5
22	1.18, *s*	23.18	1.17, *s*	23.3
23	1.02, *s*	27.33	1.01, *s*	27.5
24	2.06, *m*	30.74	2.03, *m*	30.4
25	4.87, *m*	125.56	4.88, *m*	125.7
26	-	133.65	-	133.7
27	1.75, *m*	25.95	1.67, *s*	26.1
28	1.52, *s*	18.16	1.50, *s*	18.4
29	1.96, *m*	37.67	1.93, *m*	37.8
	2.02, *m*		2.02, *m*	
30	2.55, *m*	44.69	2.51, *m*	44.8
31	-	148.93	-	149.0
32	4.65, *br s*	113.52	4.53, *br s*	113.7
33	1.63, *s*	17.76	1.59, *s*	17.9
34	1.44, *m*	33.05	1.46, *m*	32.9
35	1.84, *m*	36.76	1.85, *m*	36.9
36	-	146.28	-	149.5
37	4.67, *br s*	110.44	4.65, *br s*	110.6
38	1.68, *s*	22.76	1.69, *s*	23.0

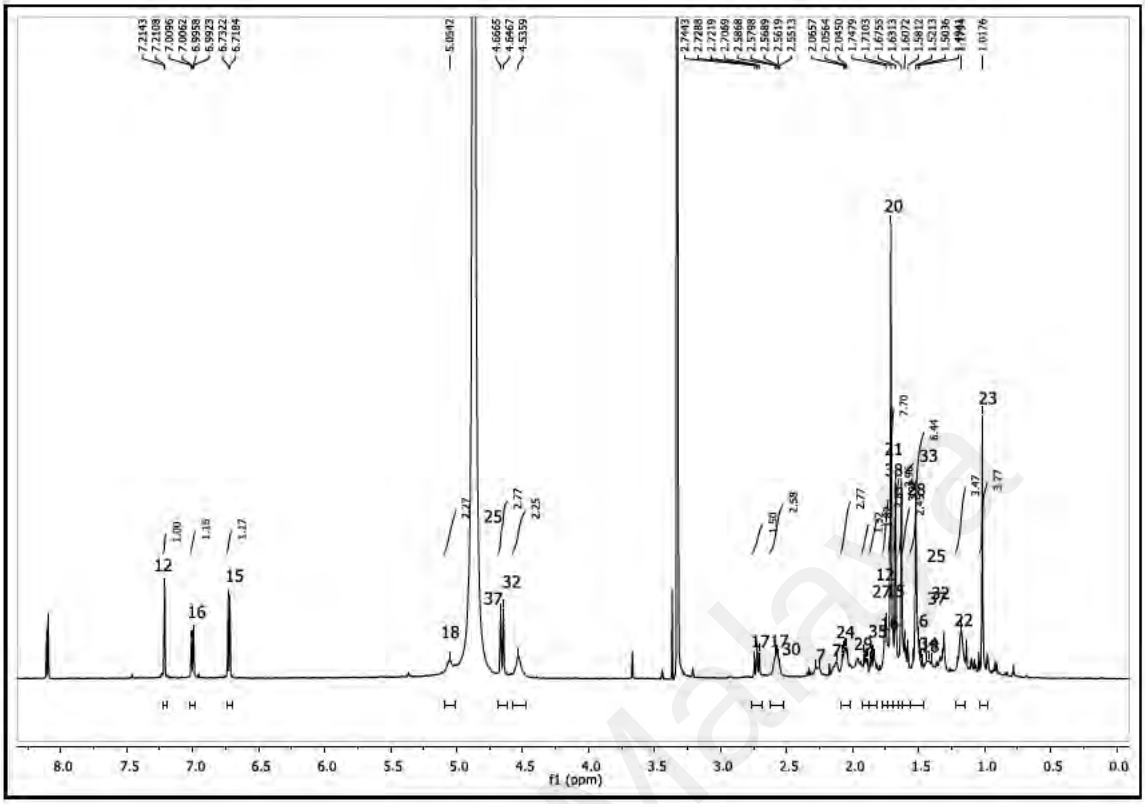

Figure 4.47: ^{1}H-NMR of xanthochymol 270.

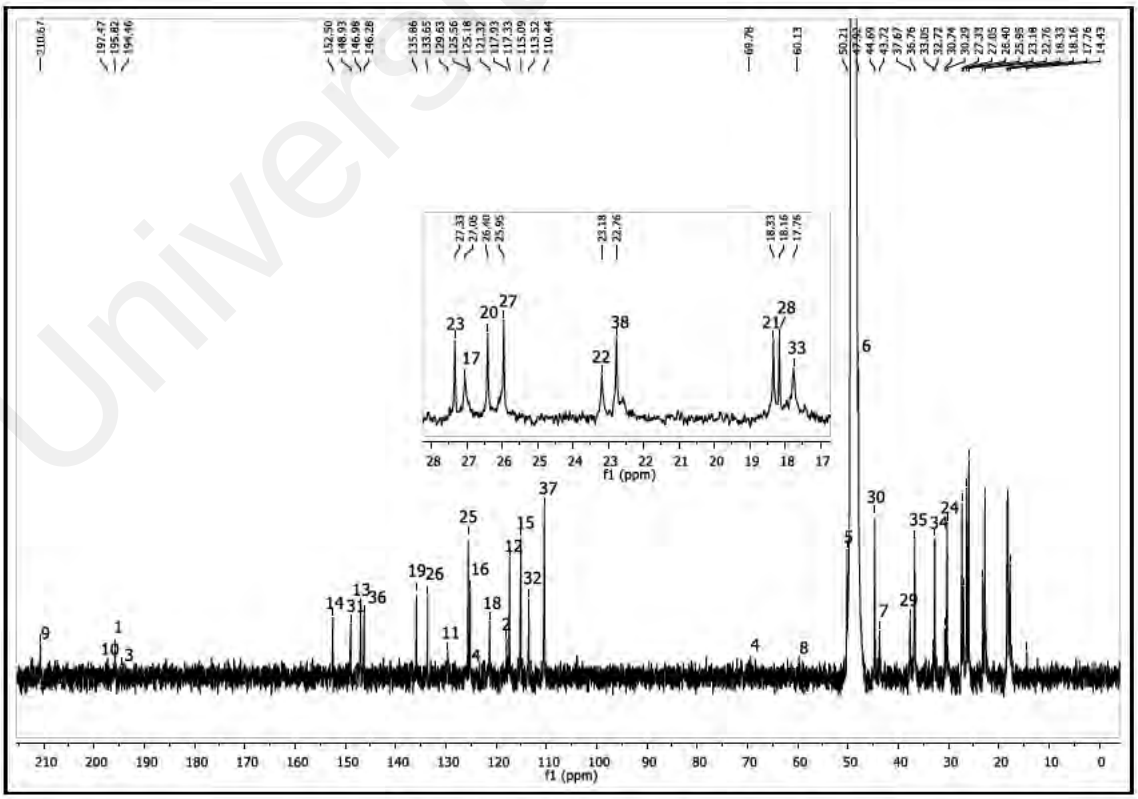

Figure 4.48: ^{13}C-NMR of xanthochymol 270.

4.2.2.3 Isoxanthochymol 248

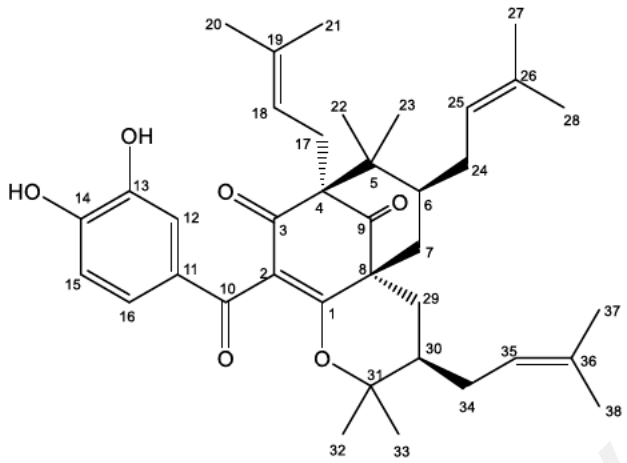

Isoxanthochymol **248** was obtained as a yellow amorphous with the $[\alpha]_D^{25}$ of +183.3° (c 0.09, $CHCl_3$). The HRESIMS measurement revealed an $[M+H]^+$ ion peak at m/z 603.3682 (calcd 603.3607), which corresponded to the molecular formula of $C_{38}H_{50}O_6$. The UV absorptions at λ_{max} 273 and 234 nm indicated the pattern of PPAPs. The IR spectrum showed the absorptions at υ_{max} 3359 (OH), 1718 (six-membered cyclic C=O), 1678, 1592 (conjugated C=O), 1382, 1296, and 1120 cm^{-1}.

The proton NMR (Figure 4.49) showed the presence of three aromatic protons characteristic of 3,4-dihydroxybenzoyl group at δ_H 7.04 (H-16, *dd*, *J*= 8.3, 2.0 Hz); 6.75 (H-15, *d*; *J*=8.3 Hz), 7.26 (H-12, *d*, *J*= 2.0 Hz). Besides, three prenylated groups were observed; [δ_H 2.45 (H-17, *dd*, *J*= 13.3, 4.5 Hz) and 2.65 (H-17, *dd*, *J*= 13.4, 8.4 Hz), 4.94 (*m*, H-18), and two singlets at δ_H 1.60 and 1.59 (*s*, H-20 and H-21)], [δ_H 2.13 (*m*, H-24) and 2.67 (*m*, H-24), 4.94 (*m*, H-25), and two singlets at δ_H 1.68 and 1.65 (*s*, H-27 and H-28)] as well as [δ_H 1.84 (*m*, H-34) and 2.05 (*m*, H-34), 5.22 (*m*, H-35), and two singlets at δ_H 1.80 and 1.70 (*s*, H-37 and H-38). Four methyls were found to be attached to two saturated carbons [two on C-5 (δ_H 1.16, 1.00, *s*, H-22, and H-23) as well as two on C-31 (0.91, 1.27, *s*, H-32 and H-33) respectively]. The doublet of doublet at δ_H 1.06 (*J*=14.0,

14.0 Hz) and 3.04 (*J*=14.0, 3.6 Hz) revealed the presence of methylene group at position 29.

The ^{13}C (Figure 4.50) and DEPT-NMR spectra revealed ten methyls, five methylenes, eight methines and fifteen quaternary carbons, which make a sum of 38 carbons. 1, 3-diketo-5-enol moiety was in evidence on the ^{13}C-NMR spectra of isoxanthochymol **248** at δ_C 208 (C-9), 196.3 (C-3), 173.7 (C-1), 52.6 (C-8), and 69.5 (C-4). The carbonyl of the phenone (C-10) was observed at δ_C 194.and the six aromatic carbons were revealed at C-11 to C-16 (δ_C 131.2, 116.2, 146.6, 152.5, 115.6, and 124.4 respectively).

On comparison with spectra data from literature, the structure ascribed as being a substituted acylphloroglucinol derivative, isoxanthochymol **248** (Table 4.30).

Table 4.30: ^{1}H and ^{13}C-NMR spectral data of isoxanthochymol 248 in CD_3OD+0.1 % TFA.

Position	Experimental (CD_3OD+0.1% TFA)		Reference (CD_3OD+0.1% TFA) (Fuller et al., 1999)	
	δ_H, *J* (Hz)	δ_C	δ_H, *J* (Hz)	δ_C
1	-	173.69	-	173.9
2	-	126.53	-	110.2
3	-	196.31	-	196.3
4	-	69.46	-	69.6
5	-	47.04	-	46.7
6	1.52, *m*	47.49	1.50, *m*	47.5
7	2.04 pro-*S*, *dd* (14.9, 7.6) 2.30 pro-*R*, *d* (14.7)	40.09	2.02 pro-*S*, *dd* (14.5, 7.4) 2.28 pro-*R*, *d* (14.0)	40.0
8	-	52.60	-	52.6
9	-	207.97	-	208.0
10	-	194.27	-	194.3
11	-	131.17	-	131.2
12	7.26, *d* (2.0)	116.22	7.24, *d* (2.0)	116.3
13	-	146.58	-	146.8
14	-	152.58	-	152.5
15	6.75, *d* (8.3)	115.65	6.73, *d* (8.0)	115.6
16	7.04, *dd* (8.3, 2.0)	124.32	7.02, *dd* (8.0, 2.0)	124.4
17	2.45 pro-*S*, *dd* (13.3, 4.5) 2.65 pro- *R*, *dd* (13.4, 8.4)	26.63	2.43 pro-*S*, *dd* (13.5, 5.0) 2.63 pro-*R*, *dd* (13.8, 8.0)	26.5
18	4.94, *m*	121.17	4.91, *m*	121.1
19	-	135.44	-	135.3
20	1.60, *s*	26.49	1.58, *s*	26.3
21	1.59, *s*	18.25	1.57, *s*	18.2
22	1.16, *s*	22.87	1.14, *s*	22.8
23	1.00, *s*	27.05	0.98, *s*	27.0
24	2.13 pro-*R*, *m* 2.67 pro-*S*, *m*	30.55	2.12 pro-*R*, *m* 2.67 pro-*S*, *m*	30.5
25	4.94, *m*	126.34	4.91, *m*	126.2
26	-	134.00	-	133.5
27	1.68, *s*	26.11	1.68, *s*	26.1
28	1.65, *s*	18.61	1.66, *s*	18.5
29	1.06 pro-*S*, *dd* (14.0, 14.0) 3.04 pro-*R*, *dd* (14.0, 3.6)	29.03	1.01 pro-*S, dd* (14, 14) 3.02 pro-*R*, *dd* (14, 3)	29.0
30	1.39, *m*	44.58	1.36, *m*	44.7
31	-	88.22	-	88.1
32	0.91, *s*	29.20	0.90, *s*	29.0
33	1.27, *s*	21.58	1.25, *s*	21.3
34	1.84 pro-*R*, *m* 2.05 pro-*S*, *m*	30.55	1.83 pro-*R*, *m* 2.05 pro-*S*, *m*	30.5
35	5.22, *m*	122.93	5.20, *m*	122.8
36	-	134.65	-	134.6
37	1.80, *s*	25.99	1.78, *s*	26.1
38	1.70, *s*	18.05	1.63, *s*	17.8

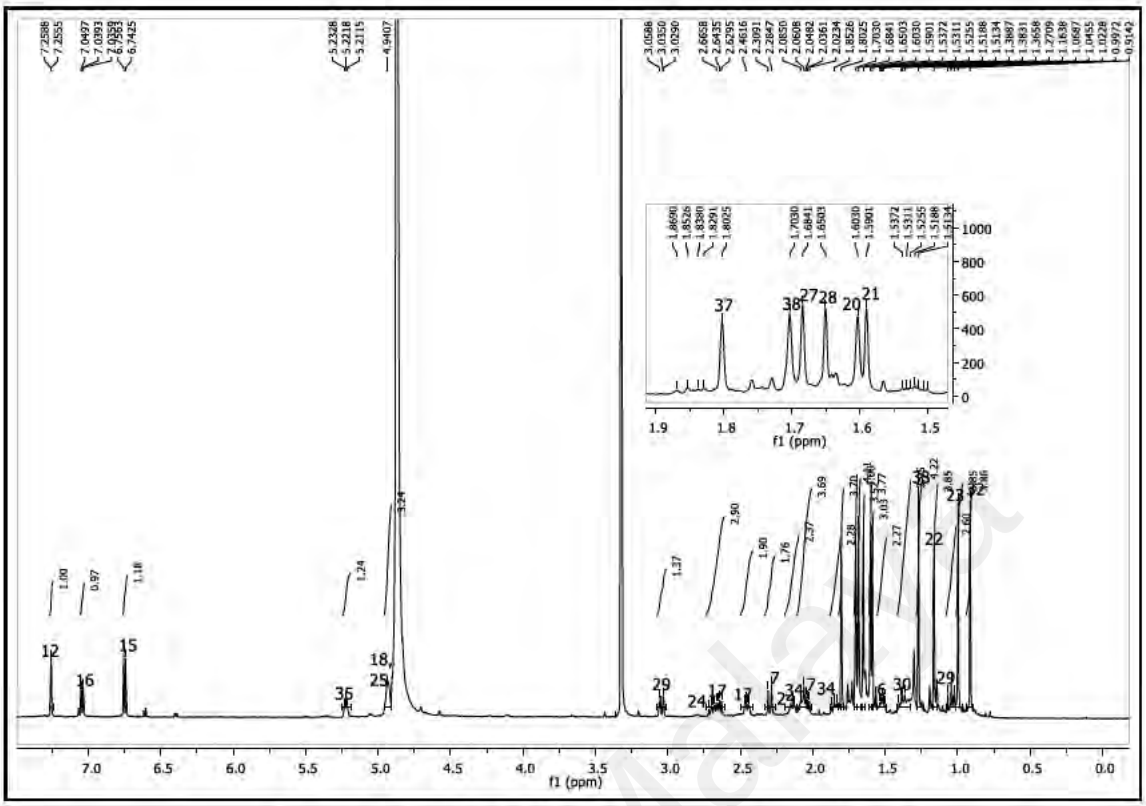

Figure 4.49: ^{1}H-NMR of isoxanthochymol 248.

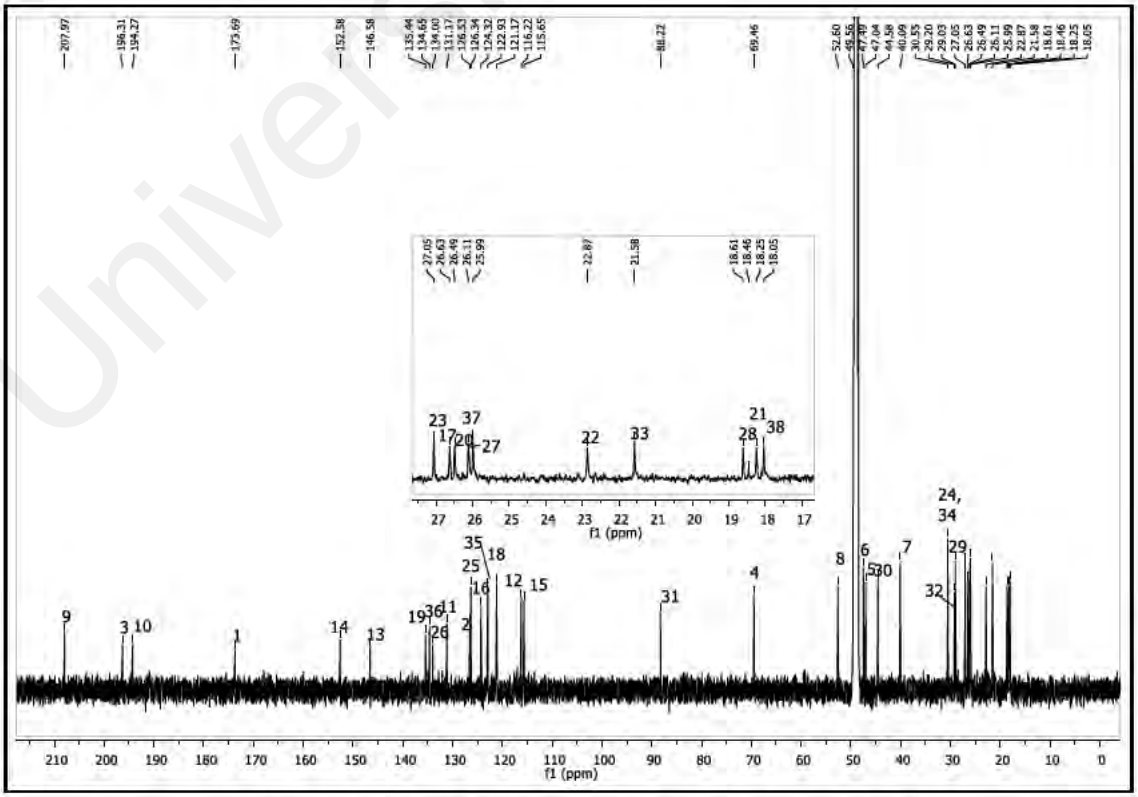

Figure 4.50: ^{13}C-NMR of isoxanthochymol 248.

4.2.2.4 Identification of enantiomer (+)-camboginol 253, (+)-isoxanthochymol 248, (+)-xanthochymol 270, and (+)-cycloxanthochymol 252

Through ^{13}C-NMR dereplication, enantiomers (±)-cycloxanthochymol **252/453**, (±)-camboginol **253/254**, (+)-isoxanthochymol **248**/ (−)-isogarcinol **310** were identified. However, the absolute configuration is not possible to confirm through ^{13}C-NMR dereplication.

Therefore, the isolation and purification work were executed, and the optical rotations were measured. The optical rotations values obtained for the three (3) isolated PPAPs were the same, (+)-. Hence, the three (3) PPAPs were identified as (+)-camboginol **253**, (+)-isoxanthochymol **248**, and (+)-xanthochymol **270** after the comparison of spectra data and optical rotations values with literature. These three (3) compounds were known compounds, and the absolute configurations were reported in literature. The reported absolute configurations were shown in Figure 4.51. As similar configurations were shown by the three isolated PPAPs, cycloxanthochymol **252** was suggested to have the same optical rotation nature, which is (+).

In summary, the identified structures were (+)-camboginol **253**, (+)-cycloxanthochymol **252**, (+)-isoxanthochymol **248**, (−)-xanthochymol **270**, garcimultiflorone D **262** and parvifoliol F **492**. All the structures were shown in Figure 4.51.

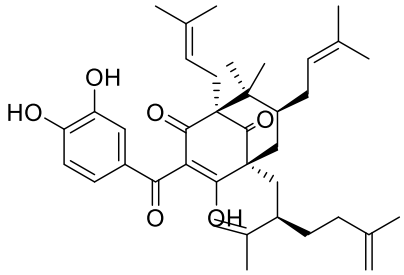

Xanthochymol **270**

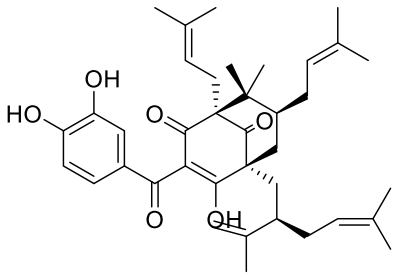

(+)-camboginol **253**

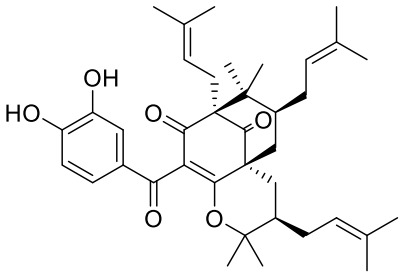

Isoxanthochymol **248**

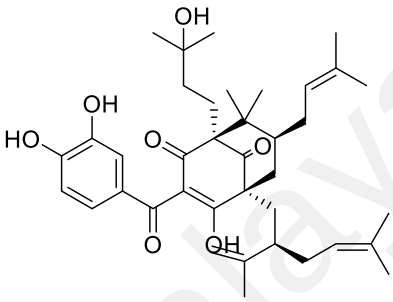

Garcimultiflorone D **262**

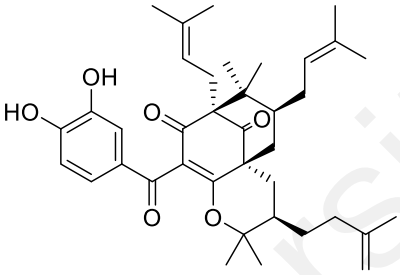

(+)-cycloxanthochymol **252**

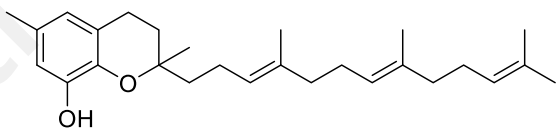

Parvifoliol F **492**

Figure 4.51: The metabolites identified from *G. griffithii* leaves.

4.2.3 Cholinesterase inhibitory activities of *G. griffithii*

A cholinesterase inhibitory activities screening was done on the DGG leaves. The result showed 88.10% and 94.07% inhibition at 200 µg/ml on AChE and BChE respectively. Therefore, the isolation process was proceeded and three PPAPs; (+)-camboginol **253**, xanthochymol **270**, and isoxanthochymol **248** were obtained.

However, the activities result of the three isolated compounds was beyond expectation. All the three isolated compounds showed mild AChE and BChE inhibition (Table 4.31), except xanthochymol **270** and isoxanthochymol **248** displayed moderate BChE inhibition

with the IC_{50} values of 110.63±13.14 and 75.17±8.21 µM respectively. The details were recorded in Table 4.31.

Table 4.31: Cholinesterase inhibitory activities of *G griffithii* extracts and isolated compounds.

	AChE		**BChE**	
	% Inhibition at 100 µg/ml	IC_{50} (µM)	% Inhibition at 100 µg/ml	IC_{50} (µM)
(+)-camboginol **253**	38.25	-	46.41	-
Xanthochymol **270**	24.22	-	50.07	110.63±13.14
Isoxanthochymol **248**	27.73	-	50.88	75.17±8.21
Galantamine (standard)	-	2.92±0.23	-	6.98±0.06

CHAPTER 5: CONCLUSION

Two plants, *M. lepidota* (Calophyllaceae) and *G. griffithii* (Clusiaceae) were investigated in this study. The first plant, *M. lepidota,* was investigated because it exhibited potent BChE activity. BChE is an enzyme that plays a crucial role in compensating for AChE's inadequate hydrolysis of ACh, thereby preserving normal cholinergic pathways. Additionally, BChE's correlation with β-amyloid deposition implies it might be a target for slowing the progression of AD. This study was done with the aid of ^{13}C-NMR dereplication and isolation using bioassay guided strategy on the HML bark.

The dereplication technique using MixONat allowed the identification of several major known compounds: sitosterol **174,** stigmasterol **173**, α-amyrin **194**, friedelin **186**, 3β-friedelinol **189**, betulinic acid **177**, lepidotol A **70**, and lepidotol B **71.** Furthermore, through a bioassay guided isolation process, seven (7) compounds were successfully isolated from the three most potent BChE inhibition fractions. The isolated compounds were identified as lepidotol A **70**, lepidotol B **71**, lepidotol E **86**, lepidotin A **88**, lepidotin B **89**, pyranojacareubin **164** as well as a new coumarin, lepidotin C **490**. Lepidotol A **70** was reported as the major constituents from the fruits of *M. lepidota* by Rouger *et al.*, while for the study, triterpenes were the compounds with higher percentage of yield, and lepidotol B **71** was the major coumarins from the bark of *M. lepidota*.

The structure of lepidotin C **490** was similar to lepidotin B **89**. The difference was on the positioning of methyl groups at C-2" and C-3". The *gem*-dimethyl group of lepidotin C **490** was attached to C-2" which is vicinal to the electronegative oxygen atom whereas in lepidotin B **89**, the *gem*-dimethyl is attached to C-3" which is not directly vicinal to the oxygen atom. Therefore, the chemical shift of the quartenary carbon, C-2" in lepidotin C **490** (δ_C 93.39) is more deshielded than C-3" in lepidotin B **89** (δ_C 43.6). This hypothesis

was substantiated by the proposed biosynthesis pathway (Chamberlain et al., 1969) on the occurrence of 1,1- to 1,2-dimethylallyl derivatives which further lead to the formation of lepidotin C **490**. Besides, lepidotin C **490**, with the IC_{50} value of 1.79±0.07 μM was threefold more potent BChE inhibitor compared to the standard, galantamine (IC_{50} value of 6.98±0.06 μM).

The most potent compound, lepidotin B **89** exhibited threefold higher BChE inhibition compared to the natural therapeutic agent, galantamine (standard). The combined application of molecular docking and molecular dynamics simulations on lepidotin B **89** has indicated that its potency might stem from its robust interaction with all five key regions: the peripheral anionic site (PAS) residues (Asp70 and Tyr332), the acyl hydrophobic pocket marked by Leu286, the catalytic triad residues Ser198 and His438, the oxyanion hole (OH) residues Gly116, and the choline binding site residue Trp82. This binding was characterized by a binding free energy of -37.65 ± 0.14 kcal/mol. The intricate interaction was facilitated through multiple forces, encompassing van der Waals interactions, hydrogen bonding, π-alkyl interactions, π-π stacking, and π-π T-shaped interactions. Thus, lepidotin B **89** which possesses hydrofuran ring and *sec*-butyl acyl group could be a potential lead compound in future drug discovery studies for the treatment of AD. This work demonstrated that ^{13}C-NMR dereplication technique coupled with bioassay guided isolation can accelerate the investigation of bioactive natural mixtures.

G. griffithii, the second plant, was chosen for study due to the compound of interest, PPAPs, commonly found in *Garcinia* species. PPAPs, with highly oxygenated acylphloroglucinol-derived cores (a bicyclo [3.3.1] nonane-2,4,9-trione or bicyclo [3.2.1] octane-2,4,8-trione (Richard et al., 2012)) decorated with isoprenyl, geranyl or more highly substituted side chains, is an intriguing skeleton. ^{13}C-NMR dereplication was also

applied on this second plant, resulting in the identification of six (6) compounds from this study, namely xanthochmol **270**, (+)-cycloxanthchymol **253**, isoxanthochymol **248**, (+)-camboginol **253**, garcimultiflorone D **262**, and parvifoliol F **492**, in which xanthochymol **270**, isoxanthochymol **248** and (+)-camboginol **253** were successfully isolated. Nevertheless, there is no significant cholinesterase inhibitory activity exhibited from the three (3) isolated compounds.

Based on the aforementioned study, it is evident that ^{13}C-NMR dereplication significantly aids in streamlining tedious laboratory work during the isolation Nevertheless, this kind of ^{13}C-NMR dereplication technique has some limitations*, i.e.*,

(i) Minor compounds are hard to identify as some of the chemical shifts (especially quaternary δ_C) may not appear on the spectrum.

(ii) The deuterated solvent used in the research must be the same as used in the literature.

(iii) Enantiomer cannot be identified as they are having the same ^{13}C-NMR spectra data.

(iv) Cannot identify new compounds.

(v) Over-dependence on the tool and misused may occur over time.

The constraint can be enhanced by either employing a more sensitive NMR spectrometer or conducting the same experiments using various deuterated solvents. Furthermore, ^{13}C-NMR dereplication analysis using MixONat facilitates the identification of compounds present in complex extracts/mixtures. MixONat can also be used to identify targeted compounds, whether the target is the type of structure or bioactive compounds. Besides, the amount of work and time consumed can be reduced with the aid of MixONat in NPs studies. The dereplication method is environmentally

friendly too because less chemicals are used during research and isolation work will only be proceeded if necessary.

In conclusion, the prospects for advancing NPs research through the aid of ^{13}C-NMR dereplication on *M. lepidota* and *G. griffithii* are highly promising. The exploration of potential compounds can be broadened by incorporating diverse dereplication methodologies, such as molecular networking, which can enhance the recognition of known entities while also shedding light on new bioactive molecules. Furthermore, the avenue of in vivo testing, encompassing cytotoxicity evaluations and neuroprotective assays, emerges as a crucial next step. These tests offer the opportunity to gain deeper insights into the therapeutic potential of the identified compounds, thus fostering the evolution of pharmaceutical practices. In this holistic manner, the amalgamation of advanced analytical techniques and biological assessments paves the way for comprehensive and impactful contributions to the field of NPs research.

REFERENCES

Abdul Rashid, S., Ab. Ghani, P., Daud, N., Ab Ghani Hilmi, Z., Nor Azemi, S. N. A., Syed Wahid, S. N., et al. (2016). Malaysia's ageing population trends. In M. A. Abdullah, W. K. Yahya, N. Ramli, S. R. Mohamed, & B. E. Ahmad, *Regional Conference on Science, Technology and Social Sciences (RCSTSS 2014)* Singapore.

Abdul Wahab, S. M., Sivasothy, Y., Liew, S. Y., Litaudon, M., Mohamad, J., & Awang, K. (2016). Natural cholinesterase inhibitors from *Myristica cinnamomea* King. *Bioorganic & Medicinal Chemistry Letters*, *26*(15), 3785-3792.

ACD/Labs. (2011). NMR spectroscopy software. In: ACD/Labs Canada.

Adams, K. L., Qiu, Y.-L., Stoutemyer, M., & Palmer, J. D. (2002). Punctuated evolution of mitochondrial gene content: High and variable rates of mitochondrial gene loss and transfer to the nucleus during angiosperm evolution. *Proceedings of the National Academy of Sciences*, *99*(15), 9905-9912.

Adriano Rutz, M. S., Galgonek;, J., Mietchen;, D., Willighagen;, E., Gaudry;, A., Graham;, J. G., et al. (2022). *The LOTUS initiative for open knowledge management in natural products research* LOTUS. https://doi.org/https://doi.org/10.7554/eLife.70780

Ahmed, T., & Gilani, A.-H. (2009). Inhibitory effect of curcuminoids on acetylcholinesterase activity and attenuation of scopolamine-induced amnesia may explain medicinal use of turmeric in Alzheimer's disease. *Pharmacology Biochemistry and Behavior*, *91*(4), 554-559.

Alam, M. S., Jain, N., Kamil, M., & Ilyas, M. (1987). Mesuein-A novel flavanone glycoside from *Mesua Ferrea*. *Chemistry & Industry*(16), 565-566.

Alfonso, L., Ai, G., Spitale, R. C., & Bhat, G. J. (2014). Molecular targets of aspirin and cancer prevention. *British Journal of Cancer*, *111*(1), 61-67.

Anand, R., Gill, K. D., & Mahdi, A. A. (2014). Therapeutics of Alzheimer's disease: Past, present and future. *Neuropharmacology*, *76*, 27-50.

Association, A. s. (2019). *2019 Alzheimer's disease facts and figures* (1552-5260). http://www.sciencedirect.com/science/article/pii/S1552526019300317

Atri, A. (2019). Current and future treatments in Alzheimer's disease. *Seminars in Neurology*, *39*(02), 227-240.

Attinger, P. (2008). *La médecine mésopotamienne*. Azugal.

Awang, K., Chan, G., Litaudon, M., Ismail, N. H., Martin, M. T., & Gueritte, F. (2010). 4-Phenylcoumarins from *Mesua elegans* with acetylcholinesterase inhibitory activity. *Bioorganic & Medicinal Chemistry*, *18*(22), 7873-7877.

Azmi, M. N., Péresse, T., Remeur, C., Chan, G., Roussi, F., Litaudon, M., et al. (2016). Kingianins O–Q: Pentacyclic polyketides from *Endiandra kingiana* as inhibitor of Mcl-1/Bid interaction. *Fitoterapia*, *109*, 190-195.

Azonwade, F., Mabanza-Banza, B. B., Le Ray, A.-M., Bréard, D., Blanchard, P., Goubalan, E., et al. (2023). Chemodiversity of propolis samples collected in various areas of Benin and Congo: Chromatographic profiling and chemical characterization guided by ^{13}C NMR dereplication. *Phytochemical Analysis*, *34*(4), 461 - 475.

Bakiri, A., Hubert, J., Reynaud, R., Lanthony, S., Harakat, D., Renault, J.-H., et al. (2017). Computer-aided ^{13}C NMR chemical profiling of crude natural extracts without fractionation. *Journal of Natural Products*, *80*(5), 1387-1396.

Bala, K. R., & Seshadri, T. R. (1971). Isolation and synthesis of some coumarin components of *Mesua ferrea* seed oil. *Phytochemistry*, *10*(5), 1131-1134.

Bandaranayake, W. M., Selliah, S. S., Sultanbawa, M. U. S., & Games, D. E. (1975). Xanthones and 4-phenylcoumarins of *Mesua thwaitesii*. *Phytochemistry*, *14*(1), 265-269.

Barbalho, S. M., Direito, R., Laurindo, L. F., Marton, L. T., Guiguer, E. L., Goulart, R. d. A., et al. (2022). *Ginkgo biloba* in the aging process: A narrative review. *Antioxidants*, *11*(3), 525.

Bertoncello, K. T., Aguiar, G. P. S., Oliveira, J. V., & Siebel, A. M. (2018). Micronization potentiates curcumin's anti-seizure effect and brings an important advance in epilepsy treatment. *Scientific Reports*, *8*(1), 2645.

Beutler, J. A. (2009). Natural products as a foundation for drug discovery. *Current Protocols in Pharmacology*, *46*(1), 9.11.11-19.11.21.

Bhattacharyya, P., Chakrabartty, P., & Chowdhuty, B. K. (1988). Mesuarin - a new 4-phenyl coumarin from *Mesua ferrea* L. *Chemistry & Industry*(7), 239-240.

Biodiversity of flora in Malaysia. Global Information Hub on Integrated Medicine (Globinmed). Retrieved 4 November 2020 from

https://www.globinmed.com/index.php?option=com_content&view=article&id=104182:biodiversity-of-flora-2&catid=268&limitstart=3&Itemid=319

Blount, J. F., & Williams, T. H. (1976). Revised structure by xanthochymol. *Tetrahedron Letters*, *17*(34), 2921-2924.

Bruguiére, A. (2019). *Mise au point d'une méthode d'analyse déréplicative par RMN du carbone 13* Université D'Angers].

Bruguière, A., Derbré, S., Coste, C., Le Bot, M., Siegler, B., Leong, S. T., et al. (2018). ^{13}C-NMR dereplication of *Garcinia* extracts: Predicted chemical shifts as reliable databases. *Fitoterapia*, *131*, 59-64.

Bruguière, A., Derbré, S., Dietsch, J., Leguy, J., Rahier, V., Pottier, Q., et al. (2020). MixONat, a software for the dereplication of mixtures based on ^{13}C NMR spectroscopy. *Analytical Chemistry*, *92*, 8793-8801.

Bui, T. T., & Nguyen, T. H. (2017). Natural product for the treatment of Alzheimer's disease. *Journal of Basic and Clinical Physiology and Pharmacology*, *28*(5), 413-423.

Byrne, C., Parnell, J. A. N., & Chayamarit, K. (2018). Systematics of the Thai Calophyllaceae and Hypericaceae with comments on the Kielmeyeroidae (Clusiaceae). *Thai Forest Bulletin (Botany)*, *46*(2), 162-216.

Calixto, J. B. (2019). The role of natural products in modern drug discovery. *Anais da Academia Brasileira de Ciências*, *91*.

Carletti, E., Aurbek, N., Gillon, E., Loiodice, M., Nicolet, Y., Fontecilla-Camps, J.-C., et al. (2009). Structure–activity analysis of aging and reactivation of human butyrylcholinesterase inhibited by analogues of tabun. *Biochemical Journal*, *421*(1), 97-106.

CAS. SciFinder. https://doi.org/https://www.cas.org/products/scifinder

Cechinel Filho, V., Meyre-Silva, C., & Niero, R. (2009). Chemical and pharmacological aspects of the genus *Calophyllum*. *Chemistry and Biodiversity*, *6*(3), 313-327.

Chahar, M. K., Sanjaykumar, D., & Lokesh, T. (2012). Anti-nociceptive and anti-inflammatory activity of mesuol isolated from *Mesua ferrea* L. seed oil. *International Journal of Current Pharmaceutical Research*, *4*(1), 51-54.

Chaithanya, K. K., Gopalakrishnan, V., Hagos, Z., & Kamalakararao, K. (2018). In vitro antioxidant activities of bioactive flavonoid mesuaferrin-A from stem bark ethyl acetate extract of *Mesua ferrea* L. *Drug Invention Today*, *10*(7), 1234-1237.

Chakraborty, D., & Bose, P. (1960). On the constitution of mesuol. The bitter antibiotic principle of *Mesua Ferrea* Linn. Part I *Proceedings of the National Institute of Sciences of India*, *26*, 1-11.

Chakraborty, D. P., & Chatterji, D. (1969). Structure of mesuagin, a new 4-phenylcoumarin *The Journal of Organic Chemistry*, *34*(12), 3784-3786.

Chakthong, S., Chukaew, A., Saithong, S., Chusri, S., Limsuwan, S., & Voravuthikunchai, S. P. (2020). Xanthones and coumarins from the twigs of *Mesua ferrea* L. *Progress in Applied Science and Technology*.

Chamberlain, T., Collins, J., & Grundon, M. (1969). Claisen rearrangements in the biosynthesis of 1, 1-and 1, 2-dimethylallyl derivatives. The biosynthesis of the quinoline alkaloid, ravenoline. *Journal of the Chemical Society D: Chemical Communications*(21), 1269b-1270.

Chan, G. (2015). *Bioactive 4-phenylcoumarins from Mesua elegans and Mesua kunstleri* University of Malaya].

Chase, M. W., Christenhusz, M. J. M., Fay, M. F., Byng, J. W., Judd, W. S., Soltis, D. E., et al. (2016). An update of the Angiosperm Phylogeny Group classification for the orders and families of flowering plants: APG IV. *Botanical Journal of the Linnean Society*, *181*(1), 1-20.

Chatterji, D. (1968). *Studies on naturally occurring heterocyclic compounds* University of Calcutta]. http://hdl.handle.net/10603/164761

Chaturonrutsamee, S., Kuhakarn, C., Surawatanawong, P., Prabpai, S., Kongsaeree, P., Jaipetch, T., et al. (2018). Polycyclic polyprenylated acylphloroglucinols and biphenyl derivatives from the roots of *Garcinia nuntasaenii* Ngerns. & Suddee. *Phytochemistry*, *146*, 63-74.

Chaturvedula, V. S. P., Schilling, J. K., & Kingston, D. G. I. (2002). New cytotoxic coumarins and prenylated benzophenone derivatives from the bark of *Ochrocarpos punctatus* from the Madagascar rainforest. *Journal of Natural Products*, *65*(7), 965-972.

ChemNetBase. (2015). *Dictionary of natural products 26.2*

Chen, X., Liu, Z., Zhong, B., Zhu, M., Yao, H., Chen, X., et al. (2022). Cytotoxic 4-phenylcoumarins from the flowering buds of *Mesua ferrea*. *Natural Product Research*, 1-10.

Chen, Y., Gan, F., Jin, S., Liu, H., Wu, S., Yang, W., et al. (2017). Adamantyl derivatives and rearranged benzophenones from *Garcinia xanthochymus* fruits. *RSC Advances*, *7*(28), 17289-17296.

Chen, Y., Ma, Z., Teng, H., Gan, F., Xiong, H., Mei, Z., et al. (2019a). Adamantyl and homoadamantyl derivatives from *Garcinia multiflora* fruits. *RSC Advances*, *9*(22), 12291-12299.

Chen, Y., Ma, Z., Teng, H., Gan, F., Xiong, H., Mei, Z., et al. (2019b). Four intricately caged polycyclic polyprenylated acylphloroglucinols from *Garcinia multiflora* fruits. *Organic Chemistry Frontiers*, *6*(17), 3085-3092.

Chen, Y., Xue, Q., Teng, H., Qin, R., Liu, H., Xu, J., et al. (2020). Acylphloroglucinol derivatives with a tricyclo-[4.4.1.11,4]dodecane skeleton from *Garcinia bracteata* fruits. *The Journal of Organic Chemistry*, *85*(10), 6620-6625.

Cheng, H.-C., Wang, L.-T., Khalil, A. T., Chang, Y.-T., Lin, Y.-C., & Shen, Y.-C. (2004). Pyranoxanthones from *Calophyllum Inophyllum*. *Journal of the Chinese Chemical Society*, *51*(2), 431-435.

Cheng, L. Y., Chen, C. L., Kuo, Y. H., Chang, T. H., Lin, I. W., Wang, S. W., et al. (2018). Polyprenylated polycyclic acylphloroglucinol: Angiogenesis inhibitor from *Garcinia multiflora*. *Bioorganic & Medicinal Chemistry Letters*, *28*(10), 1860-1863.

Chow, Y. L., & Quon, H. H. (1968). Chemical constituents of the heartwood of *Mesua ferrea*. *Phytochemistry*, *7*(10), 1871-1874.

Chukaew, A., Saithong, S., Chusri, S., Limsuwan, S., Watanapokasin, R., Voravuthikunchai, S. P., et al. (2019). Cytotoxic xanthones from the roots of *Mesua ferrea* L. *Phytochemistry*, *157*, 64-70.

Ciochina, R., & Grossman, R. B. (2006). Polycyclic polyprenylated acylphloroglucinols. *Chemical Reviews*, *106*(9), 3963-3986.

Çokuğraş, A. N. (2003). Butyrylcholinesterase: structure and physiological importance. *Turkish Journal of Biochemistry*, *28*(2), 54-61.

Colovic, M. B., Krstic, D. Z., Lazarevic-Pasti, T. D., Bondzic, A. M., & Vasic, V. M. (2013). Acetylcholinesterase inhibitors: Pharmacology and toxicology. *Current Neuropharmacology*, *11*(3), 315-335.

Crepet, W., & Nixon, K. (1998). Fossil Clusiaceae from the late Cretaceous (Turonian) of New Jersey and implications regarding the history of bee pollination. *American Journal of Botany*, *85*(8), 1122.

Crombie, L., Games, D. E., & McCormick, A. (1966). Isolation and structure of Mammea B/BA, B/BB, B/BC and C/BB: A group of 4-n-propyl- and 4-n-amyl-coumarin extractives of *Mammea americana* L. *Tetrahedron Letters*, *7*(2), 151-156.

Crombie, L., Jones, R. C. F., & Palmer, C. J. (1987). Synthesis of the *Mammea* coumarins. Part 1. The coumarins of the mammea A, B, and C series. *Journal of the Chemical Society, Perkin Transactions 1*(0), 317-331.

D.A. Case, H.M. Aktulga, K. Belfon, I.Y. Ben-Shalom, J.T. Berryman, S.R. Brozell, et al. (2023). *Amber 2023*. In

Dang, B. T., Guitton, Y., Freuze, I., Grovel, O., Litaudon, M., Richomme, P., et al. (2015). Dereplication of *Mammea neurophylla* metabolites to isolate original 4-phenylcoumarins. *Phytochemistry Letters*, *11*, 61-68.

Dar, R. A., Shahnawaz, M., Rasool, S., & Qazi, P. H. (2017). Natural product medicines: A literature update. *The Journal of Phytopharmacology*, *6*(6), 340-342.

David, B., Wolfender, J.-L., & Dias, D. A. (2015). The pharmaceutical industry and natural products: historical status and new trends. *Phytochemistry Reviews*, *14*(2), 299-315.

Davis, C. C., Latvis, M., Nickrent, D. L., Wurdack, K. J., & Baum, D. A. (2007). Floral gigantism in Rafflesiaceae. *Science*, *315*(5820), 1812-1812.

de Andrade Teles, R. B., Diniz, T. C., Costa Pinto, T. C., de Oliveira Júnior, R. G., Gama e Silva, M., de Lavor, É. M., et al. (2018). Flavonoids as therapeutic agents in Alzheimer's and Parkinson's diseases: A systematic review of preclinical evidences. *Oxidative Medicine and Cellular Longevity*, *2018*, 7043213.

De Boer, D., Nguyen, N., Mao, J., Moore, J., & Sorin, E. J. (2021). A comprehensive review of cholinesterase modeling and simulation. *Biomolecules*, *11*(4), 580.

de Souza, L. G., Rennó, M. N., & Figueroa-Villar, J. D. (2016). Coumarins as cholinesterase inhibitors: A review. *Chemico-Biological Interactions*, *254*, 11-23.

Dementia cases set to rise 312 per cent by 2050: Is Malaysia prepared? . Retrieved 3 April 2023 from https://adfm.org.my/dementia-cases-set-to-rise-312-per-cent-by-2050-is-malaysia-prepared/

Dennis, T. J., Kumar, K. A., & Srimannarayana, G. (1988). A new cyclo hexadione from *Mesua ferrea*. *Phytochemistry*, *27*(7), 2325-2327.

Dietz, A. A., Rubinstein, H. M., & Lubrano, T. (1973). Colorimetric determination of serum cholinesterase and its genetic variants by the propionylthiocholine—dithiobis (nitrobenzoic Acid) procedure. *Clinical chemistry*, *19*(11), 1309-1313.

Ee, G. C., Lim, C. K., Rahmat, A., & Lee, H. L. (2005). Cytotoxic activities of chemical constituents from *Mesua daphnifolia*. *Tropical Biomedicine*, *22*(2), 99-102.

Ee, G. C. L., Teh, S. S., Kwong, H. C., Mah, S. H., Lim, Y. M., & Rahmani, M. (2012). A new benzophenone from *Mesua congestiflora,* an inhibitor against human B lymphocyte cancer cell line. *Phytochemistry Letters*, *5*(3), 545-548.

Ee, G. C. L., Teh, S. S., Mah, S. H., Rahmani, M., Taufiq-Yap, Y. H., & Awang, K. (2011). A novel cyclodione coumarin from the stem bark of *Mesua beccariana*. *Molecules*, *16*(9), 7249-7255.

Ee, G. C. L., Teh, S. S., Rahmani, M., Taufiq-Yap, Y. H., Go, R., & Mah, S. H. (2012). A new furanoxanthone from the root bark of *Mesua ferrea*. *Letters in Organic Chemistry*, *9*(6), 457-459.

Ekins, S. (2016). The next era: Deep learning in pharmaceutical research. *Pharmaceutical Research*, *33*(11), 2594-2603.

El-Seedi, H. R., El-Barbary, M., El-Ghorab, D., Bohlin, L., Borg-Karlson, A.-K., Goransson, U., et al. (2010). Recent insights into the biosynthesis and biological activities of natural xanthones. *Current Medicinal Chemistry*, *17*(9), 854-901.

Elfita, E., Muharni, M., Latief, M., Darwati, D., Widiyantoro, A., Supriyatna, S., et al. (2009). Antiplasmodial and other constituents from four Indonesian *Garcinia* spp. *Phytochemistry*, *70*(7), 907-912.

Ellman, G. L., Courtney, K. D., Andres, V., & Featherstone, R. M. (1961). A new and rapid colorimetric determination of acetylcholinesterase activity. *Biochemical Pharmacology*, *7*(2), 88-95.

Escobedo-Martínez, C., Concepción Lozada, M., Hernández-Ortega, S., Villarreal, M. L., Gnecco, D., Enríquez, R. G., et al. (2012). ^{1}H and ^{13}C NMR characterization of

new cycloartane triterpenes from *Mangifera indica*. *Magnetic Resonance in Chemistry*, *50*(1), 52-57.

Fan, Y. M., Yi, P., Li, Y., Yan, C., Huang, T., Gu, W., et al. (2015). Two unusual polycyclic polyprenylated acylphloroglucinols, including a pair of enantiomers from *Garcinia multiflora*. *Organic Letters*, *17*(9), 2066-2069.

Fang, Z., Tang, Y., Ying, J., Tang, C., & Wang, Q. (2020). Traditional Chinese medicine for anti-Alzheimer's disease: berberine and evodiamine from *Evodia rutaecarpa*. *Chinese Medicine*, *15*(1), 82.

Ferchichi, L., Derbré, S., Mahmood, K., Touré, K., Guilet, D., Litaudon, M., et al. (2012). Bioguided fractionation and isolation of natural inhibitors of advanced glycation end-products (AGEs) from *Calophyllum flavoramulum*. *Phytochemistry*, *78*, 98-106.

Flora and Fauna. (2016). The Government of Malaysia Retrieved 30 October 2020 from https://www.malaysia.gov.my/portal/content/143

Fotso, G. W., Ntumy, A. N., Ngachussi, E., Dube, M., Mapitse, R., Kapche, G. D. W. F., et al. (2014). Epunctanone, a new benzophenone, and further secondary metabolites from *Garcinia epunctata* Stapf (Guttiferae). *Helvetica Chimica Acta*, *97*(7), 957-964.

Fu, W., Wu, M., Zhu, L., Lao, Y., Wang, L., Tan, H., et al. (2015). Prenylated benzoylphloroglucinols and biphenyl derivatives from the leaves of *Garcinia multiflora* Champ. *RSC Advances*, *5*(95), 78259-78267.

Fuller, R. W., Blunt, J. W., Boswell, J. L., Cardellina, J. H., & Boyd, M. R. (1999). Guttiferone F, the first prenylated benzophenone from *Allanblackia stuhlmannii*. *Journal of Natural Products*, *62*(1), 130-132.

Gao, X.-M., Yu, T., Lai, F. S. F., Pu, J.-X., Qiao, C.-F., Zhou, Y., et al. (2010). Novel polyisoprenylated benzophenone derivatives from *Garcinia paucinervis*. *Tetrahedron Letters*, *51*(18), 2442-2446.

Gao, Y.-L., Wang, Y.-J., Chung, H.-H., Chen, K.-C., Shen, T.-L., & Hsu, C.-C. (2020). Molecular networking as a dereplication strategy for monitoring metabolites of natural product treated cancer cells. *Rapid Communications in Mass Spectrometry*, *34*(S1), e8549.

Gautier, J., Cave, A., Kunesch, G., & Polonsky, J. (1972). On the biosynthesis of neoflavanoids. *Experientia*, *28*(7), 759-761.

Ghazali, S. A. I. S. M., & Izaddin, S. A. (2006). *Phytochemical studies of Mesua corneri (Linn.) and Garcinia mangostana (Linn.) and their biological activities* Universiti Putra Malaysia].

Ghosh, S. (2017). Triterpene structural diversification by plant cytochrome P450 enzymes. *Frontiers in Plant Science*, *8*(1886).

Gogoi, B. (2018). Anti-cancerous potentiality of coumarins of *Mesua assamica* (King & Prain) Kosterm.–An endemic plant of Assam. *International Journal of Pharmacognosy & Phytochemical Research*, *9*(7), 939-942.

Govindachari, T. R., Pai, B. R., Subramaniam, P. S., Ramdas Rao, U., & Muthukumaraswamy, N. (1967). Constituents of *Mesua ferrea* L.—II: : Ferruol A, a new 4-alkylcoumarin. *Tetrahedron*, *23*(10), 4161-4165.

Govindachari, T. R., Pai, B. R., Subramaniam, P. S., Rao, U. R., & Muthukumaraswamy, N. (1967). Constituents of *Mesua ferrea* L.—I : Mesuaxanthone A and mesuaxanthone B. *Tetrahedron*, *23*(1), 243-248.

Grantham, C., & Geerts, H. (2002). The rationale behind cholinergic drug treatment for dementia related to cerebrovascular disease. *Journal of the Neurological Sciences*, *203-204*, 131-136.

Grossman, R. B., & Yang, X.-W. (2020). Structural revision of garcinielliptin oxide and garcinielliptone E. *Journal of Natural Products*, *83*(6), 2041-2044.

GROUP, T. A. P. (2009). An update of the Angiosperm Phylogeny Group classification for the orders and families of flowering plants: APG III. *Botanical Journal of the Linnean Society*, *161*(2), 105-121.

Grunwald, C. (1975). Plant Sterols. *Annual Review of Plant Physiology*, *26*(1), 209-236.

Guilet, D., Hélesbeux, J.-J., Séraphin, D., Sévenet, T., Richomme, P., & Bruneton, J. (2001). Novel cytotoxic 4-phenylfuranocoumarins from *Calophyllum dispar*. *Journal of Natural Products*, *64*(5), 563-568.

Gunasekera, S. P., Ramachandran, S., Selliah, S., & Sultanbawa, M. U. S. (1975). Chemical investigation of ceylonese plants. Part XVII. Isolation and structures of the xanthones in the extractives of *Mesua ferrea* L. (form *M. salicina* Pl. and Tr.)(Guttiferae). *Journal of the Chemical Society, Perkin Transactions 1*(23), 2447-2450.

Gunasekera, S. P., & Sultanbawa, M. U. S. (1977). Chemical investigation of Ceylonese plants. Part 20. Extractives of *Mesua myrtifolia*. Isolation and structure of a new

triterpene hydroxy-acid, myrtifolic acid. *Journal of the Chemical Society, Perkin Transactions 1*(1), 6-10.

Gunatilleke, N., Pethiyagoda, R., & Gunatilleke, S. (2017). Biodiversity of Sri Lanka. *Journal of the National Science Foundation of Sri Lanka*, *36*, 25-62.

Gustafson, K. R., Blunt, J. W., Munro, M. H. G., Fuller, R. W., McKee, T. C., Cardellina, J. H., et al. (1992). The guttiferones, HIV-inhibitory benzophenones from *Symphonia globulifera*, *Garcinia livingstonei*, *Garcinia ovalifolia* and *Clusia rosea*. *Tetrahedron*, *48*(46), 10093-10102.

Gutiérrez-Mellado, M.-C., Edwards, R., Tena, M., Cabello, F., Serghini, K., & Jorrín, J. (1996). The production of coumarin phytoalexins in different plant organs of sunflower (*Helianthus annuus* L.). *Journal of Plant Physiology*, *149*(3), 261-266.

Harvey, A. L., Edrada-Ebel, R., & Quinn, R. J. (2015). The re-emergence of natural products for drug discovery in the genomics era. *Nature Reviews Drug Discovery*, *14*, 111.

He, W., Goodkind, D., & Kowal, P. R. (2016). An aging world: 2015. In: United States Census Bureau Washington, DC.

Hill, R. A., & Connolly, J. D. (2017). Triterpenoids. *Natural Product Reports*, *34*(1), 90-122.

Hogan, D. B., & Patterson, C. (2002). Progress in clinical neurosciences: Treatment of Alzheimer's disease and other dementias - Review and comparison of the cholinesterase inhibitors. *Canadian Journal of Neurological Sciences / Journal Canadien des Sciences Neurologiques*, *29*(4), 306-314.

Holas, O., Musilek, K., Pohanka, M., & Kuca, K. (2012). The progress in the cholinesterase quantification methods. *Expert Opinion on Drug Discovery*, *7*(12), 1207-1223.

Huang, T., Chen, P., Liu, B., Li, X., Lv, X., & Hu, K. (2020). NPid: an automatic approach to rapid identification of known natural products in the crude extract of crabapple based on 2D ^{1}H–^{13}C heteronuclear correlation spectra of the extract mixture. *Analytical Chemistry*, *92*(16), 10996-11006.

Ignatushchenko, M. V., Winter, R. W., & Riscoe, M. (2000). Xanthones as antimalarial agents: stage specificity. *The American journal of tropical medicine and hygiene*, *62*(1), 77-81.

Iinuma, M., Tosa, H., Tanaka, T., & Riswan, S. (1996). Two new dimeric xanthones in *Mesua ferrea*. *Heterocycles*, *43*(9), 1999-2004.

Jamila, N., Khairuddean, M., Yeong, K. K., Osman, H., & Murugaiyah, V. (2015). Cholinesterase inhibitory triterpenoids from the bark of *Garcinia hombroniana*. *J Enzyme Inhib Med Chem*, *30*(1), 133-139.

Jean, B. (2008). *Pharmacognosy, Phytochemistry, Medicinal Plants (2e ed.-retirage broch")*. Lavoisier.

Jiang, N., Li, S.-Y., Xie, S.-S., Li, Z.-R., Wang, K. D. G., Wang, X.-B., et al. (2014). Design, synthesis and evaluation of multifunctional salphen derivatives for the treatment of Alzheimer's disease. *European Journal of Medicinal Chemistry*, *87*, 540-551.

Jin, S., Wang, W., Gan, F., Xie, W., Xu, J., Chen, Y., et al. (2021). Discovery of novel polycyclic oolyprenylated acylphloroglucinols from the fruits of *Garcinia xanthochymus* as antitumor agents by suppressing the STAT3 signaling. *International Journal of Molecular Sciences*, *22*(19), 10365.

Kaennakam, S., Sukandar, E. R., Rassamee, K., Siripong, P., & Santi, T.-p. (2022). Cytotoxic polyprenylated benzoylphloroglucinol derivatives from the branches of *Garcinia schomburgkiana*. *Planta medica*, *89*(05), 508-515.

Kantarci, K., Weigand, S. D., Przybelski, S. A., Shiung, M. M., Whitwell, J. L., Negash, S., et al. (2009). Risk of dementia in MCI- combined effect of cerebrovascular disease, volumetric MRI, and ^{1}H MRS. *Neurology*, *72*(17), 1519-1525.

Karunakaran, T., Ee, G. C., Teh, S. S., Daud, S., Mah, S. H., Lim, C. K., et al. (2016). A new coumarin from stem bark of *Mesua hexapetala*. *Natural Product Research*, *30*(14), 1591-1597.

Karunakaran, T., Ee, G. C. L., Tee, K. H., Ismail, I. S., Zamakshshari, N. H., & Peter, W. M. (2016). Cytotoxic prenylated xanthone and coumarin derivatives from Malaysian *Mesua beccariana*. *Phytochemistry Letters*, *17*, 131-134.

Kaufmann, D., Kaur Dogra, A., Tahrani, A., Herrmann, F., & Wink, M. (2016). Extracts from Traditional Chinese Medicinal plants inhibit acetylcholinesterase, a known Alzheimer's disease target. *Molecules*, *21*(9), 1161.

Kaur, R., Vasudev, P. G., & Chattopadhyay, S. K. (2012). (1S,5R,7R,30S)-14-de-oxy-isogarcinol. *Acta Crystallographica Section E Structure Reports Online*, *68*(Pt 6), o1861-1862.

Keawsa-Ard, S., Liawruangrath, B., & Kongtaweelert, S. (2015). Bioactive compounds from *Mesua ferrea* stems. *Chiang Mai Journal of Science*, *42*(1), 186-196.

Khaw, K. Y., Choi, S. B., Tan, S. C., Wahab, H. A., Chan, K. L., & Murugaiyah, V. (2014). Prenylated xanthones from mangosteen as promising cholinesterase inhibitors and their molecular docking studies. *Phytomedicine*, *21*(11), 1303-1309.

Kim, K. H., Lee, D., Lee, H. L., Kim, C.-E., Jung, K., & Kang, K. S. (2018). Beneficial effects of Panax ginseng for the treatment and prevention of neurodegenerative diseases: past findings and future directions. *Journal of Ginseng Research*, *42*(3), 239-247.

Kitagawa, D. A. S., Cavalcante, S. F. d. A., de Paula, R. L., Rodrigues, R. B., Bernardo, L. B., da Silva, M. C. J., et al. (2019). In vitro evaluation of neutral aryloximes as reactivators for *Electrophorus* eel acetylcholinesterase inhibited by paraoxon. *Biomolecules*, *9*(10), 583.

Knestrick, M. A., Tawfik, R., Shaw, L. N., & Baker, B. J. (2019). Chromatographic editing enhances natural product discovery. *Journal of Pharmaceutical and Biomedical Analysis*, *176*, 112831.

Krishna Chaithanya, K., Gopalakrishnan, V. K., Hagos, Z., Kamalakararao, K., Noyola, P. P., John Dogulas, P., et al. (2019). Isolation and structural characterization of bioactive anti-inflammatory compound mesuaferrin-A from *M. Ferrea*. *Analytical Chemistry Letters*, *9*(1), 74-85.

Lannang, A. M., Louh, G. N., Biloa, B. M., Komguem, J., Mbazoa, C. D., Sondengam, B. L., et al. (2010). Cytotoxicity of natural compounds isolated from the seeds of *Garcinia afzelii*. *Planta medica*, *76*(7), 708-712.

Le, D. H., Nishimura, K., Takenaka, Y., Mizushina, Y., & Tanahashi, T. (2016). Polyprenylated benzoylphloroglucinols with DNA polymerase inhibitory activity from the fruits of *Garcinia schomburgkiana*. *Journal of Natural Products*, *79*(7), 1798-1807.

Leiro, J., Arranz, J. A., Yáñez, M., Ubeira, F. M., Sanmartín, M. L., & Orallo, F. (2004). Expression profiles of genes involved in the mouse nuclear factor-kappa B signal transduction pathway are modulated by mangiferin. *International immunopharmacology*, *4*(6), 763-778.

Lesch, B., & Braese, S. (2004). A short, atom ‐ Economical entry to tetrahydroxanthenones. *Angewandte Chemie International Edition*, *43*(1), 115-118.

Li, Q., Yang, H., Chen, Y., & Sun, H. (2017). Recent progress in the identification of selective butyrylcholinesterase inhibitors for Alzheimer's disease. *European Journal of Medicinal Chemistry*, *132*, 294-309.

Liaw, C.-C., Chang, J.-L., Wang, B.-W., Chen, P.-L., Weng, J.-R., Lin, K.-W., et al. (2019). Discovering a racemate polycyclic prenylated acylphloroglucinol with unprecedented skeleton by an ESI-LCMS analytical approach. *Organic Letters*, *21*(4), 857-861.

Lin, K. W., Huang, A. M., Tu, H. Y., Lee, L. Y., Wu, C. C., Hour, T. C., et al. (2011). Xanthine oxidase inhibitory triterpenoid and phloroglucinol from guttiferaceous plants inhibit growth and induced apoptosis in human NTUB1 cells through a ROS-dependent mechanism. *Journal of Agricultural and Food Chemistry*, *59*(1), 407-414.

Lin, K. W., Huang, A. M., Yang, S. C., Weng, J. R., Hour, T. C., Pu, Y. S., et al. (2012). Cytotoxic and antioxidant constituents from *Garcinia subelliptica*. *Food Chemistry*, *135*(2), 851-859.

Liu, H., Gan, F., Jin, S., Li, J., Chen, Y., & Yang, G. (2017). Acylphloroglucinol and tocotrienol derivatives from the fruits of *Garcinia multiflora*. *RSC Advances*, *7*(47), 29295-29301.

Liu, X., Yu, T., Gao, X. M., Zhou, Y., Qiao, C. F., Peng, Y., et al. (2010). Apoptotic effects of polyprenylated benzoylphloroglucinol derivatives from the twigs of *Garcinia multiflora*. *Journal of Natural Products*, *73*(8), 1355-1359.

Lopez, O. L. (2013). Mild cognitive impairment. *Continuum (Minneapolis, Minn.)*, *19*(2 Dementia), 411-424.

Majumdar, S. (1979). *Studies on the naturally occurring heterocyclic compounds* University of Calcutta].

Manse, Y., Sakamoto, Y., Miyachi, T., Nire, M., Hashimoto, Y., Chaipech, S., et al. (2022). Antiallergic properties of biflavonoids isolated from the flowers of *Mesua ferrea* Linn. *Separations*, *9*(5), 127.

Masters, K.-S., & Br se, S. (2012). Xanthones from fungi, lichens, and bacteria: the natural products and their synthesis. *Chemical Reviews*, *112*(7), 3717-3776.

Masullo, M., Bassarello, C., Bifulco, G., & Piacente, S. (2010). Polyisoprenylated benzophenone derivatives from the fruits of *Garcinia cambogia* and their absolute configuration by quantum chemical circular dichroism calculations. *Tetrahedron*, *66*(1), 139-145.

Matern, M. P. J. H. U. (2010). Biosynthesis of phenylpropanoids and related compounds. In M. Wink (Ed.), *Annual Plant Reviews Volume 40: Biochemistry of Plant Secondary Metabolism* (Vol. 40, pp. 182-257).

Meunier, M., Bréard, D., Awang, K., Boisard, S., Guilet, D., Richomme, P., et al. (2023). Matrix free laser desorption ionization assisted by ^{13}C NMR dereplication: A complementary approach to LC-MS^2 based chemometrics. *Talanta*, *253*, 123998.

Miller, B. R., III, McGee, T. D., Jr., Swails, J. M., Homeyer, N., Gohlke, H., & Roitberg, A. E. (2012). MMPBSA.py: An efficient program for end-state free energy calculations. *Journal of Chemical Theory and Computation*, *8*(9), 3314-3321.

MixONat. Retrieved June 2020 from http://sourceforge.net/projects/mixonat

Morel, C., Dartiguelongue, C., Youhana, T., Oger, J.-M., Séraphin, D., Duval, O., et al. (1999). New coumarins from *Mesua racemosa*: Isolation and synthesis. *Heterocycles-Sendai Institute of Heterocyclic Chemistry*, *51*(9), 2183-2192.

Morel, C., Guilet, D., Oger, J.-M., Séraphin, D., Sévenet, T., Wiart, C., et al. (1999). 6-Acylcoumarins from *Mesua racemosa*. *Phytochemistry*, *50*(7), 1243-1247.

Morris, G. M., Goodsell, D. S., Halliday, R. S., Huey, R., Hart, W. E., Belew, R. K., et al. (1998). Automated docking using a Lamarckian genetic algorithm and an empirical binding free energy function. *Journal of Computational Chemistry*, *19*(14), 1639-1662.

Murray, R. D. H. (1978). Naturally occurring plant coumarins. In W. Herz, H. Grisebach, & G. W. Kirby (Eds.), *Fortschritte der Chemie Organischer Naturstoffe / Progress in the Chemistry of Organic Natural Products* (pp. 199-429). Springer Vienna.

Negi, J., Bisht, V., Singh, P., Rawat, M., & Joshi, G. (2013). Naturally occurring xanthones: chemistry and biology. *Journal of Applied Chemistry*, *2013*(9).

Negi, J. S., Singh, P., & Rawat, B. (2011). Chemical constituents and biological importance of Swertia: a review. *Current Research in Chemical Biology*, *3*(1), 1-15.

Nguyen, H. D., Trinh, B. T. D., & Nguyen, L.-H. D. (2011). Guttiferones Q-S, cytotoxic polyisoprenylated benzophenones from the pericarp of *Garcinia cochinchinensis*. *Phytochemistry Letters*, *4*(2), 129-133.

Nguyen, L. H., Venkatraman, G., Sim, K. Y., & Harrison, L. J. (2005). Xanthones and benzophenones from *Garcinia griffithii* and *Garcinia mangostana*. *Phytochemistry*, *66*(14), 1718-1723.

Nuzillard, J.-M. (2021). Taxonomy focused natural product databases for carbon-13 NMR-based dereplication. *Analytica*, *2*(3), 50-56.

Oladoye, S. O., Ayodele, E. T., Abdul-Hammed, M., & Idowu, O. T. (2015). Characterisation and identification of taraxerol and taraxer-14-en-3-one from *Jatropha tanjorensis* (Ellis and Saroja) leaves. *Pakistan Journal of Scientific and Industrial Research Series A: Physical Sciences*, *58*(1), 46-50.

Ortiz Villamizar, M. C., Puerto Galvis, C. E., Vargas Méndez, L. Y., & Kouznetsov, V. V. (2018). Chapter 5 - Coumarin-based molecules as suitable models for developing new neuroprotective agents through structural modification. In G. Brahmachari (Ed.), *Discovery and Development of Neuroprotective Agents from Natural Products* (pp. 149-235). Elsevier.

Panthong, K., & Boonsri, S. (2018). Triterpenes from the Twigs of *Mesua kunstleri*. *Burapha Science Journal 23*(1), 364-376.

Peres, V., Nagem, T. J., & de Oliveira, F. F. (2000). Tetraoxygenated naturally occurring xanthones. *Phytochemistry*, *55*(7), 683-710.

Perry, E., Walker, M., Grace, J., & Perry, R. (1999). Acetylcholine in mind: a neurotransmitter correlate of consciousness? *Trends in Neurosciences*, *22*(6), 273-280.

Pinto, M., Sousa, M., & Nascimento, M. (2005). Xanthone derivatives: new insights in biological activities. *Current Medicinal Chemistry*, *12*(21), 2517-2538.

Plant of the world online. (n.d.). Royal Botanical Gardens Kew Science. Retrieved 18 January 2020 from http://powo.science.kew.org/taxon/19345-1#other-data

Raad, I., Terreux, R., Richomme, P., Matera, E.-L., Dumontet, C., Raynaud, J., et al. (2006). Structure–activity relationship of natural and synthetic coumarins inhibiting the multidrug transporter P-glycoprotein. *Bioorganic and Medicinal Chemistry*, *14*(20), 6979-6987.

Raina, R., Mondhe, D. M., Malik, J. K., & Gupta, R. C. (2016). Chapter 48 - *Garcinia cambogia*. In R. C. Gupta (Ed.), *Nutraceuticals* (pp. 669-680). Academic Press.

Raja, V. J., Lim, K.-H., Leong, C.-O., Kam, T.-S., & Bradshaw, T. D. (2014). Novel antitumour indole alkaloid, Jerantinine A, evokes potent G2/M cell cycle arrest targeting microtubules. *Investigational New Drugs*, *32*(5), 838-850.

Rajaonarivelo, M., Rakotonandrasana, O. L., Martin, M.-T., Dumontet, V., & Rasoanaivo, P. (2016). A new polycyclic polyprenylated scylphloroglucinol derivative from *Garcinia verrucosa*. *Natural Product Communications*, *11*(7), 1934578X1601100734.

Raju, M. S., Srimannarayana, G., Rao, N. V. S., Bala, K. R., & Seshadri, T. R. (1976). Structure of mesuaferrone-b a new biflavanone from the stamens of *Mesua ferrea* linn. *Tetrahedron Letters*, *17*(49), 4509-4512.

Ramiandrasoa, F., Kunesch, N., Poisson, J., & Kunesch, G. (1983). Le calofloride, intermédiaire d'un type nouveau de la biogenèse des néoflavonoïdes. *Tetrahedron*, *39*(23), 3923-3928.

Rasol, N. E., Naz, H., Awang, K., Ridhwan, M. J. M., Choy, Y. K., & Ismail, N. H. (2017). Isomeric polycyclic polyprenylated acylphloroglucinols from the bark of *Mesua ferrea* (Clusiaceae). *Natural Product Communications*, *12*(8), 1934578X1701200834.

Richard, J.-A., Pouwer, R. H., & Chen, D. Y.-K. (2012). The Chemistry of the polycyclic polyprenylated acylphloroglucinols. *Angewandte Chemie International Edition*, *51*(19), 4536-4561.

Ridwan Islam, I. A., Al Sikder, Mohammad Rashedul Haque, Abdullah Al-Mansur, Mansoor Ahmed, Munawar Rasheed, Mohammad A. Rashid. (2014). Chemical investigation of *Mesua nagassarium* (Burm. f.) Kosterm. *Journal of Basic & Applied Sciences*, *10*, 124-128.

Roberts, R., & Knopman, D. S. (2013). Classification and epidemiology of MCI. *Clinics in Geriatric Medicine*, *29*(4), 753-772.

Rost, B., Radivojac, P., & Bromberg, Y. (2016). Protein function in precision medicine: deep understanding with machine learning. *FEBS Letters*, *590*(15), 2327-2341.

Rouger, C. (2015). *Activité pharmacologique de dérivés polyphénoliques isolés de Clusiaceae et de Calophyllaceae malaisiennes: effets régulateurs sur des marqueurs endothéliaux de l'inflammation et de l'immunité* Université d'Angers].

Rouger, C., Derbré, S., Charreau, B., Pabois, A., Cauchy, T., Litaudon, M., et al. (2015). Lepidotol A from *Mesua lepidota* inhibits inflammatory and immune mediators in human endothelial cells. *Journal of Natural Products*, *78*(9), 2187-2197.

Rouger, C., Derbré, S., & Richomme, P. (2018). *Mesua* sp.: chemical aspects and pharmacological relevance of prenylated polyphenols. *Phytochemistry Reviews*, *18*, 317-342.

Roux, D., Hadi, H. A., Thoret, S., Guenard, D., Thoison, O., Pais, M., et al. (2000). Structure-activity relationship of polyisoprenyl benzophenones from *Garcinia pyrifera* on the tubulin/microtubule system. *Journal of Natural Products*, *63*(8), 1070-1076.

Roy, S. K., Kumari, N., Pahwa, S., Agrahari, U. C., Bhutani, K. K., Jachak, S. M., et al. (2013). NorA efflux pump inhibitory activity of coumarins from *Mesua ferrea*. *Fitoterapia*, *90*, 140-150.

Ruhfel, B. R., Bittrich, V., Bove, C. P., Gustafsson, M. H., Philbrick, C. T., Rutishauser, R., et al. (2011). Phylogeny of the clusioid clade (Malpighiales): evidence from the plastid and mitochondrial genomes. *American Journal of Botany*, *98*(2), 306-325.

Rukachaisirikul, V., Naklue, W., Phongpaichit, S., Towatana, N. H., & Maneenoon, K. (2006). Phloroglucinols, depsidones and xanthones from the twigs of *Garcinia parvifolia*. *Tetrahedron*, *62*(36), 8578-8585.

Rushdey El-Seedi †, H. (2005). Antimicrobial triterpenes from *Poulsenia armata* miq. standl. *Natural Product Research*, *19*(2), 197-202.

Saenkham, A., Jaratrungtawee, A., Siriwattanasathien, Y., Boonsri, P., Chainok, K., Suksamrarn, A., et al. (2020). Highly potent cholinesterase inhibition of geranylated xanthones from *Garcinia fusca* and molecular docking studies. *Fitoterapia*, *146*, 104637.

Sakunpak, A., & Panichayupakaranant, P. (2012). Antibacterial activity of Thai edible plants against gastrointestinal pathogenic bacteria and isolation of a new broad spectrum antibacterial polyisoprenylated benzophenone, chamuangone. *Food Chemistry*, *130*(4), 826-831.

Sarker, S. D., & Nahar, L. (2017). Progress in the Chemistry of naturally occurring coumarins. In A. D. Kinghorn, H. Falk, S. Gibbons, & J. i. Kobayashi (Eds.), *Progress in the Chemistry of Organic Natural Products 106* (pp. 241-304). Springer International Publishing.

Seethapathy, G. S., Tadesse, M., Urumarudappa, S. K. J., V. Gunaga, S., Vasudeva, R., Malterud, K. E., et al. (2018). Authentication of *Garcinia* fruits and food supplements using DNA barcoding and NMR spectroscopy. *Scientific Reports*, *8*(1), 10561.

Seo, E.-J., Fischer, N., & Efferth, T. (2018). Phytochemicals as inhibitors of NF-κB for treatment of Alzheimer's disease. *Pharmacological Research*, *129*, 262-273.

Seo, S., Tomita, Y., & Tori, K. (1975). Carbon-13 NMR spectra of urs-12-enes and application to structural assignments of components of *Isodon japonicus* hara tissue cultures. *Tetrahedron Letters*, *16*(1), 7-10.

Shal, B., Ding, W., Ali, H., Kim, Y. S., & Khan, S. (2018). Anti-neuroinflammatory potential of natural products in attenuation of Alzheimer's disease. *Frontiers in Pharmacology*, *9*(548).

Shan, T., Ma, Q., Guo, K., Liu, J., Li, W., Wang, F., et al. (2011). Xanthones from mangosteen extracts as natural chemopreventive agents: potential anticancer drugs. *Current molecular medicine*, *11*(8), 666-677.

Shan, W.-G., Lin, T.-S., Yu, H.-N., Chen, Y., & Zhan, Z.-J. (2012). Polyprenylated xanthones and benzophenones from the bark of *Garcinia oblongifolia*. *Helvetica Chimica Acta*, *95*(8), 1442-1448.

Sharifi-Rad, M., Lankatillake, C., Dias, D. A., Docea, A. O., Mahomoodally, M. F., Lobine, D., et al. (2020). Impact of natural compounds on neurodegenerative disorders: from preclinical to pharmacotherapeutics. *Journal of Clinical Medicine*, *9*(4), 1061.

Sharma, P., Gupta, Y. K., Sharma, M., & Dobhal, M. (2010). Two new compounds from the stem of *Nerium oleander*. *Indian Journal of Chemistry*, *49B*, 374-378.

Silva-Castro, L. F., Derbré, S., Le Ray, A. M., Richomme, P., García-Sosa, K., & Peña-Rodriguez, L. M. (2021). Using ^{13}C-NMR dereplication to aid in the identification of xanthones present in the stem bark extract of *Calophyllum brasiliense*. *Phytochemical Analysis*, *32*(6), 1102-1109.

Singh, S., Gray, A. I., & Waterman, P. G. (1993). Mesuabixanthone-A and mesuabixanthone-B: Novel bis-xanthones from the stem bark of *Mesua ferrea* (Guttiferae). *Natural Product Letters*, *3*(1), 53-58.

Soine, T. O. (1964). Naturally occurring coumarins and related physiological activities. *Journal of Pharmaceutical Sciences*, *53*(3), 231-264.

Sousa, M. E., & Pinto, M. M. M. (2005). Synthesis of xanthones: An overview. *Current Medicinal Chemistry*, *12*(21), 2447-2479.

Sriyatep, T., Andersen, R. J., Patrick, B. O., Pyne, S. G., Muanprasat, C., Seemakhan, S., et al. (2017). Scalemic caged xanthones isolated from the stem bark extract of *Garcinia propinqua*. *Journal of Natural Products*, *80*(5), 1658-1667.

Sriyatep, T., Maneerat, W., Sripisut, T., Cheenpracha, S., Machan, T., Phakhodee, W., et al. (2014). Cowabenzophenones A and B, two new tetracyclo [7.3.3.3.0]tetradecane-2,12,14-trione derivatives, from ripe fruits of *Garcinia cowa*. *Fitoterapia*, *92*, 285-289.

Stepankova, S., & Komers, K. (2008). Cholinesterases and cholinesterase inhibitors. *Current Enzyme Inhibition*, *4*(4), 160-171.

Stevens, P. F. (2007). Hypericaceae. In K. Kubitzki (Ed.), *Flowering Plants · Eudicots: Berberidopsidales, Buxales, Crossosomatales, Fabales p.p., Geraniales, Gunnerales, Myrtales p.p., Proteales, Saxifragales, Vitales, Zygophyllales, Clusiaceae Alliance, Passifloraceae Alliance, Dilleniaceae, Huaceae, Picramniaceae, Sabiaceae* (pp. 194-201). Springer Berlin Heidelberg.

Suhandi, A. S. A., Dessy Effendi, Elfian , Perbatakusuma, E. A., Meyers, K. J. M., & Wiratno. (2002). *Final report feasibility study of conservation concession reconciliatory effort between the demand of increasing local revenue and ecosystem protection in the process of power devolution.* (A case study from Siberut Island, Sumatra. Jakarta. Published on the Internet., Issue. https://adriawanperbatakusuma.wordpress.com/

Sukandar, E. R., Kaennakam, S., Aree, T., Nöst, X., Rassamee, K., Bauer, R., et al. (2020). Picrorhizones A–H, polyprenylated benzoylphloroglucinols from the stem bark of *Garcinia picrorhiza*. *Journal of Natural Products*, *83*(7), 2102-2111.

Sukumaran, S. D., Faraj, F. L., Lee, V. S., Othman, R., & Buckle, M. J. (2018). 2-Aryl-3-(arylideneamino)-1, 2-dihydroquinazoline-4 (3 H)-ones as inhibitors of cholinesterases and self-induced β-amyloid (Aβ) aggregation: biological evaluations and mechanistic insights from molecular dynamics simulations. *RSC Advances*, *8*(14), 7818-7831.

Suresh, C., Chandra, T. R., Meeta, K., & Deep, K. G. (2014). Nagakesara (*Mesua ferrea* Linn.) -A gift for git, skin and bleeding disorders. *International Journal of Ayurveda & Alternative Medicine*, *2*(4), 48-53.

Tan, W. N., Khairuddean, M., Wong, K. C., Khaw, K. Y., & Vikneswaran, M. (2014). New cholinesterase inhibitors from *Garcinia atroviridis*. *Fitoterapia*, *97*, 261-267.

Tan, X., Zhong, F., Teng, H., Li, Q., Li, Y., Mei, Z., et al. (2020). Acylphloroglucinol and tocotrienol derivatives from the fruits of *Garcinia paucinervis*. *Fitoterapia*, *146*, 104688.

Tang, Z., Lu, L., Zhou, X., Shen, J., Song, W., Tang, Y., et al. (2020). A new cytotoxic polycyclic polyprenylated acylphloroglucinol from *Garcinia nujiangensis* screened by the LC-PDA and LC-MS. *Natural Product Research*, *34*(17), 2448-2455.

Tanjung, M., Rachmadiarti, F., Saputri, R. D., & Tjahjandarie, T. S. (2018). Mesucalophylloidin, a new isoprenylated 4-phenylcoumarin from *Mesua calophylloides* (Ridl.) Kosterm. *Natural Product Research*, *32*(9), 1062-1067.

Tanjung, M., Saputri, R. D., Fitriati, F. F., & Tjahjandarie, T. S. (2016). Antimalarial and antioxidant activities of isoprenylated coumarins from the stem bark of *Mesua borneensis* L. *Journal of Biologically Active Products from Nature*, *6*(2), 95-100.

Tantapakul, C., Phakhodee, W., Ritthiwigrom, T., Cheenpracha, S., Prawat, U., Deachathai, S., et al. (2012). Rearranged benzophenones and prenylated xanthones from *Garcinia propinqua* twigs. *Journal of Natural Products*, *75*(9), 1660-1664.

Tanzi, R. E. (2021). FDA approval of Aduhelm paves a new path for Alzheimer's disease. *ACS Chemical Neuroscience*, *12*(15), 2714-2715.

Teh, S. S., Ee, G. C. L., & Mah, S. H. (2013). Chemical constituents and new xanthone derivatives from *Mesua ferrea* and *Mesua congestiflora*. *Asian Journal of Chemistry*, *25*(15), 8780-8784.

Teh, S. S., Ee, G. C. L., Mah, S. H., & Ahmad, Z. (2016). Structure–activity relationship study of secondary metabolites from *Mesua beccariana*, *Mesua ferrea* and *Mesua congestiflora* for anti-cholinesterase activity. *Medicinal Chemistry Research*, *25*(5), 819-823.

Teh, S. S., Ee, G. C. L., Mah, S. H., Lim, Y. M., & Rahmani, M. (2012). *Mesua beccariana* (Clusiaceae), a source of potential anti-cancer lead compounds in drug discovery. *Molecules*, *17*(9), 10791-10800.

Teh, S. S., Ee, G. C. L., Rahmani, M., Sim, W. C., Mah, S. H., & Teo, S. H. (2010). Two new pyranoxanthones from *Mesua beccariana* (Guttiferae). *Molecules*, *15*(10), 6733-6742.

Teh, S. S., Ee, G. C. L., Rahmani, M., Taufiq-Yap, Y. H., Go, R., & Mah, S. H. (2011). Pyranoxanthones from *Mesua ferrea*. *Molecules*, *16*(7), 5647-5654.

Teng, H., Li, Q., Ma, Z., Li, X., Xie, W., Chen, Y., et al. (2021). Polyprenylated acylphloroglucinols with different carbon skeletons from the fruits of *Garcinia multiflora*. *Frontiers in Chemistry*, *9*.

Teng, H., Ma, Z., Teng, H., Du, Y., Chen, X., Chen, Y., et al. (2020). Two novel cyclohexanone-monocyclic polycyclic polyprenylated acylphloroglucinols from *Garcinia multiflora* fruits. *Natural Product Research*, 1-7.

Teng, H., Ren, Y., Ma, Z., Tan, X., Xu, J., Chen, Y., et al. (2019). Homoadamantane polycyclic polyprenylated acylphloroglucinols from the fruits of *Garcinia multiflora*. *Fitoterapia*, *137*, 104245.

Thimmappa, R., Geisler, K., Louveau, T., O'Maille, P., & Osbourn, A. (2014). Triterpene biosynthesis in plants. *Annual Review of Plant Biology*, *65*(1), 225-257.

Tian, D. S., Yi, P., Xia, L., Xiao, X., Fan, Y. M., Gu, W., et al. (2016). Garmultins A-G, biogenetically related polycyclic acylphloroglucinols from *Garcinia multiflora*. *Organic Letters*, *18*(22), 5904-5907.

Ting, C.-W., Hwang, T.-L., Chen, I.-S., Cheng, M.-J., Sung, P.-J., Yen, M.-H., et al. (2014). Garcimultiflorone G, a novel benzoylphloroglucinol derivative from *Garcinia multiflora* with inhibitory activity on neutrophil pro-inflammatory responses. *Chemistry and Biodiversity*, *11*(5), 819-824.

Ting, C. W., Hwang, T. L., Chen, I. S., Yen, M. H., & Chen, J. J. (2012). A new benzoylphloroglucinol derivative with an adamantyl skeleton and other constituents from *Garcinia multiflora*: effects on neutrophil pro-inflammatory responses. *Chemistry and Biodiversity*, *9*(1), 99-105.

Trinh, B. T. D., Nguyen, N.-T. T., Ngo, N. T. N., Tran, P. T., Nguyen, L.-T. T., & Nguyen, L.-H. D. (2013). Polyisoprenylated benzophenone and xanthone constituents of the bark of *Garcinia cochinchinensis*. *Phytochemistry Letters*, *6*(2), 224-227.

Trisuwan, K., & Ritthiwigrom, T. (2012). Benzophenone and xanthone derivatives from the inflorescences of *Garcinia cowa*. *Archives of pharmacal research*, *35*(10), 1733-1738.

Verotta, L., Lovaglio, E., Vidari, G., Finzi, P. V., Neri, M. G., Raimondi, A., et al. (2004). 4-Alkyl- and 4-phenylcoumarins from *Mesua ferrea* as promising multidrug resistant antibacterials. *Phytochemistry*, *65*(21), 2867-2879.

Vieira, L. M. M., & Kijjoa, A. (2005). Naturally-occurring xanthones: Recent developments. *Current Medicinal Chemistry*, *12*(21), 2413-2446.

Walia, S., & Mukerjee, S. K. (1984). Ferrxanthone, a 1,3,5,6-tetraoxygenated xanthone from *Mesua ferrea*. *Phytochemistry*, *23*(8), 1816-1817.

Wan Othman, W. N. N., Liew, S. Y., Khaw, K. Y., Murugaiyah, V., Litaudon, M., & Awang, K. (2016). Cholinesterase inhibitory activity of isoquinoline alkaloids from three *Cryptocarya* species (Lauraceae). *Bioorganic & Medicinal Chemistry*, *24*(18), 4464-4469.

Wang, S.-Y., Wang, Y.-X., Guo, Y.-P., Huang, J., Wang, J.-H., Xiao, W., et al. (2020). New cytotoxic 4-alkyl-dihydroxyfuran coumarins from *Mesua ferrea*. *Phytochemistry Letters*, *38*, 121-127.

Wang, S., Guo, Y., Yao, D., Liu, L., Duan, H., Meng, L., et al. (2019). 4-Alkyl-5,7-dihydroxycoumarins from the flowering buds of *Mesua ferrea*. *Fitoterapia*, *138*, 104192.

Wang, Y.-L., Ye, Y.-S., Fu, W.-W., Wu, R., Xiang, Q., Lao, Y.-Z., et al. (2019). Garsubelone A, the first dimeric polycyclic polyprenylated acylphloroglucinols with complicated heptacyclic architecture from *Garcinia subelliptica*. *Organic Letters*, *21*(5), 1534-1537.

Wang, Z.-Q., Li, X.-Y., Hu, D.-B., & Long, C.-L. (2018). Cytotoxic garcimultiflorones K–Q, lavandulyl benzophenones from *Garcinia multiflora* branches. *Phytochemistry*, *152*, 82-90.

WFO. (2022a). *Calophyllaceae J.Agardh*. http://www.worldfloraonline.org/taxon/wfo-7000000101

WFO. (2022b). *Clusiaceae Lindl.* Retrieved 15 June 2023 from http://www.worldfloraonline.org/taxon/wfo-7000000141.

WFO. (2022c). *Garcinia L.* Retrieved 16 June 2023 from https://wfoplantlist.org/plant-list/taxon/wfo-4000015318-2022-12?page=1

WFO. (2022d). *Mesua L.* Retrieved 15 June 2023 from https://wfoplantlist.org/plant-list/taxon/wfo-4000023881-2022-12?page=1

WHO. (2019). *WHO global report on traditional and complementary medicine 2019* (9241515430).

Wightman, E. L. (2017). Potential benefits of phytochemicals against Alzheimer's disease. *Proceedings of the Nutrition Society*, *76*(2), 106-112.

Wu, Z., Dai, X., Wang, W., Zhang, X., Chen, J., Liu, J., et al. (2022). Polyprenylated benzophenones and tocotrienol derivatives from the edible fruits of *Garcinia oblongifolia* Champ. ex Benth. and their cytotoxicity activity. *Journal of Agricultural and Food Chemistry*, *70*(34), 10506-10520.

Wurdack, K. J., & Davis, C. C. (2009). Malpighiales phylogenetics: Gaining ground on one of the most recalcitrant clades in the angiosperm tree of life. *American Journal of Botany*, *96*(8), 1551-1570.

Xia, Z. X., Zhang, D. D., Liang, S., Lao, Y. Z., Zhang, H., Tan, H. S., et al. (2012). Bioassay-guided isolation of prenylated xanthones and polycyclic acylphloroglucinols from the leaves of *Garcinia nujiangensis*. *Journal of Natural Products*, *75*(8), 1459-1464.

Xu, G., Kan, W. L., Zhou, Y., Song, J. Z., Han, Q. B., Qiao, C. F., et al. (2010). Cytotoxic acylphloroglucinol derivatives from the twigs of *Garcinia cowa*. *Journal of Natural Products*, *73*(2), 104-108.

Xu, Z.-H., Grossman, R. B., Qiu, Y.-F., Luo, Y., Lan, T., & Yang, X.-W. (2022). Polycyclic polyprenylated acylphloroglucinols bearing a lavandulyl-derived substituent from *Garcinia xanthochymus* fruits. *Journal of Natural Products*, *85*(12), 2845-2855.

Xue, Q., Chen, Y., Yin, H., Teng, H., Qin, R., Liu, H., et al. (2020). Prenylated xanthones and benzophenones from the fruits of *Garcinia bracteata* and their potential antiproliferative and anti-inflammatory activities. *Bioorganic Chemistry*, *104*, 104339.

Yamada, M., Marui, Y., Hayashi, C., Miki, Y., & Takemura, S. (2001). New thiocholine ester substrates for the assay of human serum cholinesterase. *Clinical chemistry*, *47*(11), 1962-1966.

Yan, F.-L., Wang, A.-X., & Jia, Z.-J. (2004). Pentacyclic triterpenoids from *Aster ageratoides* var. pilosus. *Die Pharmazie - An International Journal of Pharmaceutical Sciences*, *59*(11), 882-884.

Yang, H., Tian, D., Zeng, Y., Huang, L., Gu, W., Hao, X., et al. (2020). Phenolic derivatives from *Garcinia multiflora* Champion ex Bentham and their chemotaxonomic significance. *Biochemical Systematics and Ecology*, *88*, 103981.

Yang, X.-W., Grossman, R. B., & Xu, G. (2018). Research progress of polycyclic polyprenylated acylphloroglucinols. *Chemical Reviews*, *118*(7), 3508-3558.

Yang;, X.-W., Grossman;, R. B., & Xu, G. *Table of PPAPs* https://doi.org/http://www.uky.edu/~rbgros1/PPAPs/allPPAPs.html

Yin, T., Yu, Y., Liu, Q., Zhu, G., Bai, L., Zhang, W., et al. (2023). ^{13}C-NMR-based MixONat strategy coupled with 2D NMR for rapid dereplication and identification of new secondary metabolites from Aloe vera. *Journal of Food Composition and Analysis*, *115*, 104975.

Yu, L., Cao, R., Yi, W., Yan, Q., Chen, Z., Ma, L., et al. (2010). Synthesis of 4-[(diethylamino)methyl]-phenol derivatives as novel cholinesterase inhibitors with selectivity towards butyrylcholinesterase. *Bioorganic & Medicinal Chemistry Letters*, *20*(11), 3254-3258.

Yücel, Y. Y., Tacal, Ö., & Özer, I. (2008). Comparative effects of cationic triarylmethane, phenoxazine and phenothiazine dyes on horse serum butyrylcholinesterase. *Archives of Biochemistry and Biophysics*, *478*(2), 201-205.

Zanforlin, E., Zagotto, G., & Ribaudo, G. (2017). The medicinal Chemistry of natural and semisynthetic compounds against Parkinson's and Huntington's diseases. *ACS Chemical Neuroscience*, *8*(11), 2356-2368.

Zar Wynn Myint, K., Kido, T., Kusakari, K., Prasad Devkota, H., Kawahara, T., & Watanabe, T. (2019). Rhusflavanone and mesuaferrone B: tyrosinase and elastase inhibitory biflavonoids extracted from the stamens of *Mesua ferrea* L. *Natural Product Research*, 1-5.

Zhang, H., Dan, Z., Ding, Z. J., Lao, Y. Z., Tan, H. S., & Xu, H. X. (2016). UPLC-PDA-QTOFMS-guided isolation of prenylated xanthones and benzoylphloroglucinols from the leaves of *Garcinia oblongifolia* and their migration-inhibitory activity. *Scientific Reports*, *6*, 35789.

Zhang, H., Tao, L., Fu, W. W., Liang, S., Yang, Y. F., Yuan, Q. H., et al. (2014). Prenylated benzoylphloroglucinols and xanthones from the leaves of *Garcinia oblongifolia* with antienteroviral activity. *Journal of Natural Products*, *77*(4), 1037-1046.

Zhang, H., Zhang, D. D., Lao, Y. Z., Fu, W. W., Liang, S., Yuan, Q. H., et al. (2014). Cytotoxic and anti-inflammatory prenylated benzoylphloroglucinols and xanthones from the twigs of *Garcinia esculenta*. *Journal of Natural Products*, *77*(7), 1700-1707.

Zhang, L. J., Chiou, C. T., Cheng, J. J., Huang, H. C., Kuo, L. M., Liao, C. C., et al. (2010). Cytotoxic polyisoprenyl benzophenonoids from *Garcinia subelliptica*. *Journal of Natural Products*, *73*(4), 557-562.

Zhang, X.-C., Yang, X.-F., Gu, T.-Z., Cao, Y.-F., & Lu, C.-H. (2020). Antimicrobial polycyclic polyprenylated acylphoroglucinols from *Mesua ferrea* flower. *Phytochemistry Letters*, *40*, 84-88.

Zhang, X., Gao, R., Liu, Y., Cong, Y., Zhang, D., Zhang, Y., et al. (2019). Anti-virulence activities of biflavonoids from *Mesua ferrea* L. flower. *Drug Discoveries and Therapeutics*, *13*(4), 222-227.

Zheng, B. C. (1988). The earliest monograph on pharmaceutics in China. *Journal of Traditional Chinese Medicine 8*(1), 75-76.

Zheng, D., Chen, Y., Wan, S., Jiang, J., Chen, S., Zheng, C., et al. (2021). Polycyclic polyprenylated acylphloroglucinol congeners from *Garcinia yunnanensis* Hu with inhibitory effect on α-hemolysin production in *Staphylococcus aureus*. *Bioorganic Chemistry*, *114*, 105074.

Zheng, D., Jiang, J.-M., Chen, S.-M., Wan, S.-J., Ren, H.-G., Chen, G., et al. (2021). Structural revision of guttiferone F and 30-*ep*i-cambogin. *Journal of Natural Products*, *84*(4), 1397-1402.

Zhou, F., Huang, R., Cao, T., Liu, J., Yang, W., Li, F., et al. (2022). 4-Phenylcoumarins from *Mesua ferrea* with selective CYP1B1 inhibitory activity. *Medicinal Chemistry Research*, *31*(12), 2172-2181.

Zhou, Y., Lee, S., Choi, F. F., Xu, G., Liu, X., Song, J. Z., et al. (2010). Qualitative and quantitative analysis of polycyclic polyprenylated acylphloroglucinols from *Garcinia* species using ultra performance liquid chromatography coupled with electrospray ionization quadrupole time-of-flight tandem mass spectrometry. *Analytica Chimica Acta*, *678*(1), 96-107.

Zueva, I., Dias, J., Lushchekina, S., Semenov, V., Mukhamedyarov, M., Pashirova, T., et al. (2019). New evidence for dual binding site inhibitors of acetylcholinesterase as improved drugs for treatment of Alzheimer's disease. *Neuropharmacology*, *155*, 131-141.